Ministry of Water Resources

Bangladesh Water Development Board

Coastal Embankment Improvement Project, Phase-I (CEIP-I)

Long Term Monitoring, Research and Analysis of Bangladesh Coastal Zone (Sustainable Polders Adapted to Coastal Dynamics)

Macro scale morphology current situation - interim report

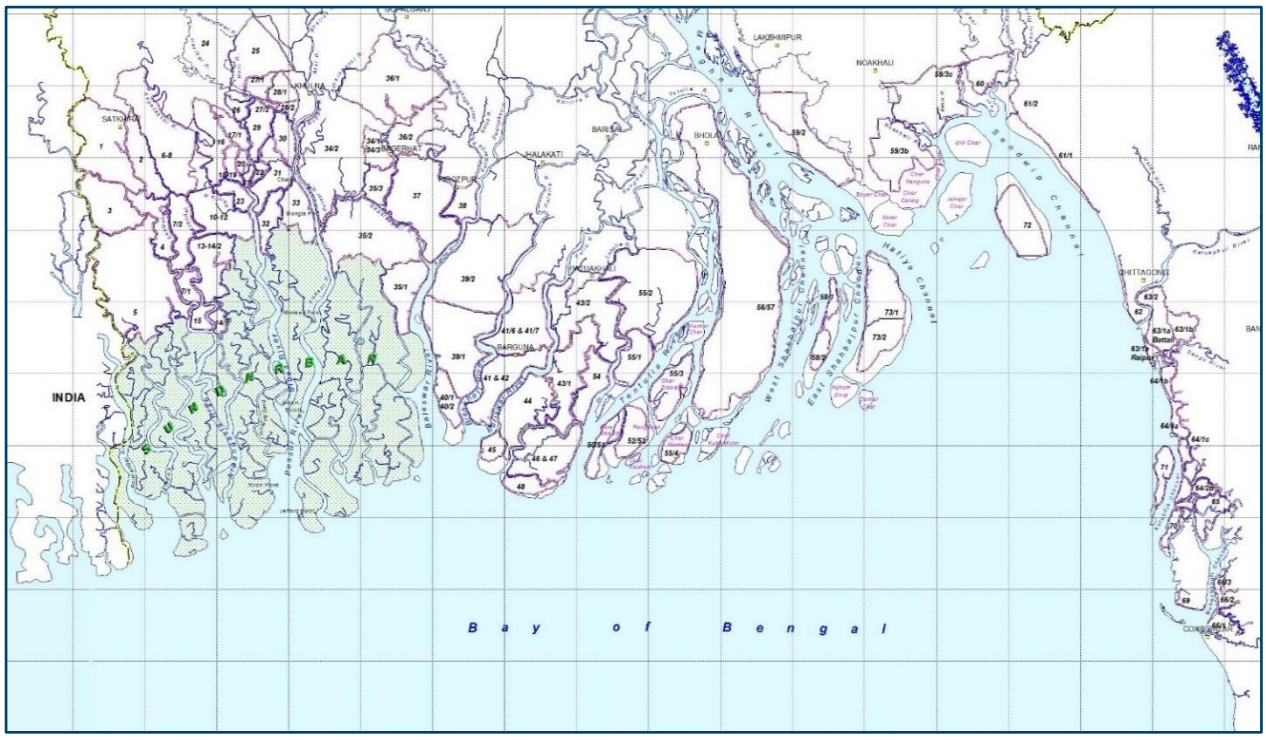

Joint Venture of DHI The expert in WATER ENVIRONMENTS & Deltares Enabling Delta Life in association with IWM, Bangladesh and University of Colorado, Boulder and Columbia University

November 2020

Ministry of Water Resources

Bangladesh Water Development Board

Coastal Embankment Improvement Project, Phase-I (CEIP-I)

Long Term Monitoring, Research and Analysis of Bangladesh Coastal Zone (Sustainable Polders Adapted to Coastal Dynamics)

Macro scale morphology current situation - interim report

November 2020

Joint Venture of DHI & Deltares Enabling Delta Life

The expert in WATER ENVIRONMENTS

in association with IWM Water Environment & Climate

University of Colorado, Boulder, USA
Columbia University, USA

Contents

1 Introduction 10
1.1 Background and project context 10
1.2 Objectives 11
1.2.1 Basin hydrology model (Hydrotrend) 12
1.2.2 River branch model (Delft3D-FM 1D) 12
1.2.3 Coastal model (Delft3D-FM 2D) 13
1.3 Outline of the report 14

2 Macro scale delta dynamics 15
2.1 Introduction 15
2.2 Sediment dynamics 16
2.2.1 River Sediment 16
2.2.2 Sediment transport forcing 17
2.3 Morphodynamics 18
2.4 Previous modelling efforts 19
2.5 A synthesis – motivation for the modelling approach 19

3 Data 22
3.1 Coordinate systems 22
3.1.1 Horizontal reference system 22
3.1.2 Vertical datum 23
3.2 Morphology 23
3.2.1 Bathymetry 23
3.2.2 Topography 24
3.3 Hydrodynamics 25
3.3.1 Water levels 25
3.3.2 Discharge 31
3.3.3 Waves 32
3.4 Meteorology 32

4 Development basin hydrology model (HydroTrend) 33
4.1 Introduction 33
4.2 Conceptual description 33
4.3 Input data 34
4.4 Model set-up 34
4.5 Model calibration 35
4.5.1 Calibration approach 35
4.5.2 Results of reference scenario: Data-model comparison 36
4.6 Results 40
4.6.1 Ganges basin 40
4.6.2 Brahmaputra basin 41
4.6.3 Comparison with existing GBM sediment load observations and estimates 44

5 Development river model (Delft3D-FM 1D) 46
5.1 Introduction 46
5.2 Numerical network 46
5.3 Cross-sectional profiles 49
5.3.1 Bathymetric dataset 49
5.3.2 Profile types 49
5.3.3 Measured profiles 49

5.3.4 Hybrid profiles 51
5.4 Friction 55
5.5 Sediment model 55
5.6 Boundary conditions 55
5.6.1 Upstream 55
5.6.2 Downstream 56
5.7 Initial conditions 57
5.8 Model experiments 57
5.9 Calibration of hydrodynamics 58
5.9.1 Water levels 58
5.9.2 Discharge 64
5.10 Model application and validation 67
5.10.1 Flow budget 67
5.10.2 Suspended sediment budget 70

6 Development coastal model (Delft3D-FM 2D) 72
6.1 Introduction 72
6.2 Grid and bathymetry 73
6.2.1 Automated grid generation 73
6.2.2 Bathymetry 75
6.3 Hydrodynamic calibration: tidal propagation 78
6.3.1 Boundary conditions 78
6.3.2 Tuning bathymetry and roughness 78
6.3.3 Results stage 1 model 79
6.3.4 Results stage 3 model 81
6.4 Hydrodynamic calibration: modelled vs. observed discharges 86
6.4.1 EDP 2009/2010 86
6.4.2 Pussur-Sibsa 2011 88
6.5 Sediment model 90
6.5.1 Sediment Data 90
6.5.2 Model sediment settings 90
6.5.3 Bed composition 91
6.5.4 Morphology 92
6.6 Sediment transport boundary conditions 92
6.7 Sediment transport calibration 93
6.8 Morphodynamic model setup 93
6.8.1 Method 93
6.8.2 Domain and initial bathymetry 94
6.8.3 Boundary conditions 95
6.8.4 Sediment settings 99
6.8.5 Morphological settings 105
6.8.6 Calibration 106
6.8.7 Sensitivity analysis 110
6.9 Present-day analysis 110
6.9.1 Distribution of surface sediment 110
6.9.2 Sediment fluxes 111
6.9.3 Volume balance 113
6.9.4 Detailed sedimentation/erosion maps 116
6.10 Conclusions 120
6.11 Recommendations 120

7 Discussion 121
7.1 Performance of the models 121
7.2 Lessons learned from the model results and future applications 122

8 Conclusions 124

9 References 125

A Summary statistics Hydrotrend results 129

B Hypsometric curves of schematized profiles 133

C Automatic grid generation based on distance to bank lines 141

FIGURES

Figure 1.1 Cascade of modelling scales, the macro-scale is studied in this report. 11
Figure 1.2 Macro-scale morphology model domains (left) and zoomed in on Bangladesh (right). 14
Figure 2.1 Names of the major river branches in the GBM delta. 15
Figure 2.2 Sediment transport modes defined from sediment origin and transport mechanism (Jansen et al., 1979) 16
Figure 2.3 Changes of the delta in the period 1985-2016 according to Aqua Monitor. Green area became from water to land and blue area became from land to water. 19
Figure 2.4 The GBM delta divided into the sub-areas, from east to west: Active delta (with delta forming estuaries), Polder area, Sundarbans, and sub-aqueous delta 21
Figure 2.5 Conceptual model of sediment transport pathways in the GBM delta (Wilson and Goodbred, 2015). 21
Figure 3.1 Spatial coverage of all in-situ bathymetry observations available (see colours and text boxes for name and date of bathymetry data surveys). 24
Figure 3.2 Satellite derived digital elevation model (DEM) for the Bangladesh coastal zone. Elevation shown in millimetres. 25
Figure 3.3 Overview of BWDB water level gauges. 27
Figure 3.4 Overview of BIWTA water level gauges. 27
Figure 3.5 Availability of the BIWTA data. 28
Figure 3.6 Observations (blue dots) and constructed signal using tidal analysis (red lines) for Hiron Point (left) and Mongla (right). 29
Figure 3.7 Observations (blue dots) and constructed signal using tidal analysis (red lines) for Chandpur (left) and for Chitalkhali (right). 29
Figure 3.8 Mean tidal range (top) and M2 tidal amplitude in the delta. 30
Figure 3.9 Spatial distribution of amplitude and phase of the M2 primary tidal constituent through the Bay of Bengal. 31
Figure 3.10 Time-series of discharge for all locations showing the complete time-series available (top) and a zoom-in of the year 2001 (bottom), and a map showing the locations of the stations. 32
Figure 4.1 Observed vs. simulated mean and maximum water discharge for the A) Ganges river and B) Brahmaputra river. Percent error values are written as percentages next to error bars. Average and maximum observed water discharge are written to the left of the dotted lines and are reported in units of m3/s. 37
Figure 4.2 Observed vs. simulated mean annual daily water discharge for the A) Ganges river and B) Brahmaputra river. Discharge data were trimmed from the initial reference time period of 1976-2006 to 1976-2004 for the Ganges and 2002 for the Brahmaputra, since the observed discharge records were missing a considerable number of values at the tail end of their respective records. 38
Figure 4.3 Observed vs. simulated mean annual water discharge, averaged over the reference scenario time period of 1976-2004 for the Ganges River (A) and 1976-2002 for the Brahmaputra River (B). 40
Figure 4.4 Projected water discharge, sediment discharge, bedload discharge, and suspended sediment concentration for the Ganges river driven by climate representative of the years 2020, 2040, 2060, and 2080 under the RCP4.5 emission scenario (A-D) and RCP8.5 emission scenario (E-H). Data for the reference scenario representative of the year 2000 are included in the line plots to amplify trends and to extend the analysis timeframe. 42
Figure 4.5 Projected water discharge, sediment discharge, bedload discharge, and suspended sediment concentration for the Brahmaputra River driven by climate representative of the years 2020, 2040, 2060, and 2080 under the RCP4.5 emission scenario (A-D) and RCP8.5 emission scenario (E-H). Climate hindcasts for the reference scenario representative of the year 2000 are included in the line plots to amplify trends and to extend the analysis timeframe. 43
Figure 5.1 Interpolation scheme of the Delft3D-FM 1D model. 46
Figure 5.2 Schematization of the major river branches in a network for the 1D GBM model, including locations where boundary conditions are forces and observation points used for model-data comparison. 48
Figure 5.3 Examples of a few selected profiles (dataset shown in figure titles). 50

Figure 5.4 Map of the GBM delta with the model network (blue), the topo-bathymetric observations (gray dots), and the polygons (red) defining sub areas of the river branches for schematization of the hybrid profiles. 52
Figure 5.5 Example of methodology to derive an area and river length based on a tightly data-fitting polygon (red), which is found by the definition of manually defined outer polygons (blue). 53
Figure 5.6 Methodology of schematizing cross-sectional profiles, illustrated for the downstream part of the Brahmaputra: a) histogram of the gridded topo-bathymetric observations within the sub area defined by the polygon; b) hypsometric curve derived from the histogram, c) schematized cross-sectional profile constructed from the hypsometric curve and the river width; d) positioning of the cross-sectional profile on to the model network. 53
Figure 5.7 Morphological characteristics of the Jamuna (non-tidal) and Pussur (tidal) rivers derived from observed profiles (blue) and schematized hybrid profiles (red). Figures shows river width (a), cross-sectional area (b), and mean and minimum bed level of the profiles (c). 54
Figure 5.8 Spatially varying roughness field (Manning's n) imposed on the 1D model. 55
Figure 5.9 Timeseries of discharge from 1975 up till 2012 at the three measurement locations (Hardinge, Bahadurabad & Bhairab) used to force the model at the upstream boundaries. 56
Figure 5.10 Target diagram of the BIAS and RMSE between model results and observations on water levels, for the model with measured (left) and hybrid (right) profiles. River systems are indicated by the colours. 59
Figure 5.11 Map overview of the BIAS (left) and RMSE (right) between the model with measured (top) and hybrid (bottom) cross-sections and observations. 60
Figure 5.12 Timeseries of the modelled and observed water levels in the Ganges from upstream (Hardinge Bridge) to the downstream confluence of the Ganges and Jamuna in to Padma. 61
Figure 5.13 Timeseries of the modelled and observed water levels in the Gorai-Madhumati river from upstream (bifurcation of Ganges) to the downstream bifurcation towards the Baleshawr (upstream of Khulna). 62
Figure 5.14 Cross-sectional profile in the Jamuna, showing observed values (red) and char sections which are filled in by interpolation (blue). 63
Figure 5.15 Scatter plot of the observed and modelled tidal range for the model with measured (left) and hybrid (right) cross-sectional profiles. 64
Figure 5.16 Timeseries of the modelled and observed discharge at Baruria (upstream of Padma) and the Gorai (Gorai Railway Bridge). Figures are zoomed-in on a two-year period to highlight the monsoon-drive discharge fluctuations. 65
Figure 5.17 Scatter plots of the modelled and observed discharge for the confluence of Ganges and Jamuna (Baruria, left) and the bifurcation of the Gorai (right), for both model variants. 66
Figure 5.18 Time-series and scatter plot of the observed discharge at Baruria and the combined discharge from the observations of Bahadurabad, Hardinge with the Gorai substracted. 67
Figure 5.19 Mean and peak annual discharge budget for the upstream (non-tidal) rivers in the GBM delta. Vertical dotted lines indicate connecting tributaries. Values on top of the bars show the value of the bar multiplied by 1 * 10^3 (m^3/s). 68
Figure 5.20 Discharge division for the three most important bifurcations in the upstream part of the GBM delta. Absolute values (top panel) and percentages (bottom panel). 69
Figure 5.21 Division of the tidal prism for downstream bifurcations in absolute values (top panel) and percentages (bottom panel). Colours indicate the first (blue) and second (red) river system indicated in the labels on the horizontal axis (see Figure 5.2 for names of the river systems). ..70
Figure 5.22 Mean annual suspended sediment budget at the boundaries of the model (apex of the delta). ..71
Figure 5.23 Mean annual suspended sediment budget for upstream part of the GBM delta. Vertical dotted lines indicate connecting tributaries. Values on top of the bars show the value of the bar multiplied by 1 * 10^3 (m^3/s). 71
Figure 6.1 Overall mesh (top panel) and detail of delta (lower panel) for stage 1 model. 74
Figure 6.2 Overall mesh (top panel) and detail of delta (bottom panel), stage 3 model. 75
Figure 6.3 Comparison between MIKE21-FM Bay of Bengal storm surge bathymetry (left panels) and the representation in Delft3D-FM large-scale morphological model (right panels). Top panels: overview of coastal areas; Bottom panels: zoom area in Sundarbans. 76
Figure 6.4 Comparison between MIKE21-FM Bay of Bengal storm surge model elevation (left panels) and the representation in Delft3D-FM large-scale morphological model (right panels). 77

Figure 6.5 Bathymetry interpolation procedure for river reaches. (a) curvilinear grid and sample set in geographic space; (b) Sample set in curvilinear space; (c) Interpolated bathymetry in curvilinear space; (d) Back transformed bathymetry in geographic space. The channel now smoothly follows the correct thalweg even though only sparse cross-sections are given. 77
Figure 6.6 Example manning roughness map distinguishing sea (cyan), estuaries (blue) and Meghna//Padma (brown) 79
Figure 6.7 Observed (top panels) and simulated (bottom panels) mean tidal range (left panels) and M2 amplitude (right panels). 80
Figure 6.8 Simulated vs. observed M2 amplitude in points shown in Figure 6.7. (rmse = root mean square error, mae = mean average error, corr = correlation coefficient) 80
Figure 6.9 Observed and modelled mean tidal range (left panels) and M2 amplitude (right panels) for calibration run 19. 82
Figure 6.10 Ratio of modelled vs. observed M2 tidal amplitude, run 19. 83
Figure 6.11 Modelled vs. observed M2 tidal amplitude, run 19. 83
Figure 6.12 Spatial Chezy roughness distribution. 84
Figure 6.13 Observed and modelled mean tidal range (left panels) and M2 amplitude (right panels) for calibration run 20. 85
Figure 6.14 Modelled vs. observed M2 tidal amplitude, run 20 85
Figure 6.15 Location map of 13-hrs measurements during EDP programme 86
Figure 6.16 Calibration of discharges in Lower Meghna area. Top: with settings as in run 19; bottom: with roughness distribution as in Figure 6.12 (run 20). Dry period. 87
Figure 6.17 Calibration of discharges in Lower Meghna area. Top: with settings as in run 19; bottom: with roughness distribution as in Figure 6.12 (run 20). Monsoon season. 87
Figure 6.18 Representation of all 13-hrs measurements in stage 3 model 88
Figure 6.19 Comparison model – observations for Pussur-Sibsa area, dry period 88
Figure 6.20 Comparison model – observations for Pussur-Sibsa area, monsoon period. Top panels: with schematized hydrograph; bottom panels: with measured discharges at upstream boundaries. 89
Figure 6.21 Comparison modelled (black) and observed (blue) water levels at Hardinge Bridge, monsoon period. Settings as in run 20. 89
Figure 6.22 Conceptual multi-fraction bed layer model under conditions of (a) erosion of finer fractions (b) deposition of finer fractions. Darker colours indicate the presence of more, coarser fractions. 92
Figure 6.23 Erosion and sedimentation patterns for Run Sq1 after 1 year (upper panel) and Run Sq26 after 14 days (lower panel). 94
Figure 6.24 Morphodynamic model domain and bathymetry. (a) Bathymetry for runs starting in 2000; (b) Bathymetry for runs starting in 2012 94
Figure 6.25 Observed river discharges of the main three rivers, 1974-2012. Blue lines: observed actual discharges. Yellow lines: multi-year average discharge curve based on days before/after peak 95
Figure 6.26 Observed peak discharges and yearday on which peak discharge took place, for Hardinge, Bahadurabad and Bhairab Bazar. 96
Figure 6.27 Monthly wind climatology for the Bay of Bengal, derived from 30 years of ERA5 data 98
Figure 6.28 Monthly wave climatology at the 85m depth contour offshore of the Meghna estuary, derived from 30 years of ERA5 data 99
Figure 6.29 Behaviour of sediment concentration and bottom change as a function of sediment parameters; left panel: typical Deltares settings with no critical shear stress for deposition; right panel: typical DHI setting with critical shear stress for deposition 101
Figure 6.30 Time series of sediment concentration at Hardinge, Rupsha and Mongla. 103
Figure 6.31 Time-averaged sediment concentration pattern in delta; left: without wind and wave forcing, right: with wind and wave forcing. 104
Figure 6.32 Standard deviation of sediment concentration pattern in delta; left: wind and wave forcing, right: with wind and wave forcing. 104
Figure 6.33 Sedimentation/erosion pattern over period 2000-2009 in lower Meghna area, and volume balance areas applied in EDP study (2009). Left panel: simulation without wind and waves; right panel: simulation with realistic time series of wind and waves. 106
Figure 6.34 Volume and hypsometry change 2000- 2009; left: without and right: with wind and waves; Area 1. 107

Figure 6.35 Volume and hypsometry change 2000- 2009; left: without and right: with wind and waves; Area 2. 107
Figure 6.36 Volume and hypsometry change 2000- 2009; left: without and right: with wind and waves; Area 3. 107
Figure 6.37 Volume and hypsometry change 2000- 2009; left: without and right: with wind and waves; Area 4. 108
Figure 6.38 Volume and hypsometry change 2000- 2009; left: without and right: with wind and waves; Area 5. 108
Figure 6.39 Volume and hypsometry change 2000- 2009; left: without and right: with wind and waves; Area 6. 108
Figure 6.40 Volume and hypsometry change 2000- 2009; left: without and right: with wind and waves; Area 7. 109
Figure 6.41 Computed vs. observed erosion (red), sedimentation (green) and net volume change (black) in the period 2000-2009, for a simulation without (left) and with (right) wind and waves. 109
Figure 6.42 Mud volume percentage in upper bed layer after 15 years. The remaining percentage consists of sand....111
Figure 6.43 Yearly cumulative mud transports (left pane) and sand transports (right pane), mind the different vector scales 112
Figure 6.44 Yearly cumulative mud transports with amounts per cross-section 112
Figure 6.45 Yearly cumulative mud transports, details of Figure 6.44 (mind the different vector scales). Left panels are for mud. Top panels are with waves and wind. Lower panels are without waves and wind. 113
Figure 6.46 Bathymetry volume balance over 25 years, with waves and wind 114
Figure 6.47 Cumulative sediment volume change over time for different areas. Without waves. 115
Figure 6.48 Cumulative sediment volume change over time for different areas, where 'c' refers to the coastal areas, ‘m’ to the middle range of ocean cells and 'o' refers to the most ocean directed areas. Numbers increase from west to east. Without waves. 116
Figure 6.49 Simulated sedimentation-erosion pattern, Meghna estuary, 2000-2009 117
Figure 6.50 Observed sedimentation-erosion pattern, Meghna estuary, 2000-2009....117
Figure 6.51 Simulated bed level changes, 2000-2019 118
Figure 6.52 Observed land to water (blue) and water to land (green) changes, 2000-2019 (Source: Aqua Monitor) 119
Figure 6.53 Simulated bed level changes, 2000-2019; left panel: bed level 2000; right panel: bed level 2019. 119

ACRONYMS AND ABBREVIATIONS

BIWTA	Bangladesh Inland Water Transport Authority
BoB	Bay of Bengal
BWDB	Bangladesh Water Development Board
CEGIS	Centre for Environmental and Geographic Information Services
CEIP	Coastal Embankment Improvement Project
DEM	Digital Elevation Model
GBM	Ganges Brahmaputra Meghna
IWM	Institute of Water Modelling
MES	Meghna Estuary Study
SLR	Sea Level Rise
SOB	Survey of Bangladesh
SSC	Suspended Sediment Concentration
SWRM	South West Region Model
TBM	Temporary Bench Mark
TRM	Tidal River Management
ToR	Terms of Reference

1 Introduction

1.1 Background and project context

The main objective of the “long-term monitoring, research and analysis of the Bangladesh coastal zone” project is to create a framework for polder design, based on understanding of the long-term and large-scale dynamics of the delta and sustainable polder concepts. The modelling work within the project is carried out to improve our understanding of the long-term and large-scale dynamics of the Ganges-Brahmaputra-Meghna (GBM) delta. There is insufficient knowledge about sediment budget in the delta involving sediment transport within the estuaries, sediment sources and sediment distribution into the river system. Sediment and tidal dynamics are important for river and coastal erosion, land reclamation, and delta development. The knowledge on sediment dynamics, distribution, erosion-deposition processes and sediment management at present and in the future under climate change, land use changes and proposed interventions in the upstream reaches of the Ganges-Brahmaputra river systems are essential for the framework of polder design.

The time scales associated with the driving processes for the morphological changes range from hours (tides) to decades or even longer (climate change). Similar, the morphological responses encompass a large range of spatial scales, from thousands of kilometres (e.g. basin scale) to a few meters (e.g. internal polder drainage and siltation of peripheral rivers). Making long-term (~25-50-100y) predictions for this system is therefore particularly challenging and will be based on a cascade of process-based morphodynamic models (see the Inception report).

The cascade of models considers three different spatial and temporal scales (see Figure 1.1):

- Macro-scale: annual sediment balance of the Bengal part of the GBM delta, and long-term morphodynamics. This scale is necessary to get a comprehensive understanding on how the system functions as a whole and to estimate the impact of climate change and anthropogenic works in a general context.
- Meso-scale: regional river and estuary dynamics, driven by seasonal fluctuations in forcing conditions. This scale will highlight meandering and other dynamics of main estuarine branches and how they respond to major changes in tidal volumes, translating the macro scale findings into relevant impacts on local polder level.
- Micro-scale: water-logging and polder management. This scale is necessary to provide a detailed and local reference of (future) boundary conditions for dedicated polder design and management.

This report focusses on the macro-scale morphodynamic processes in the GBM delta. The report describes the development of models covering the larger domain of the GBM basin and coastal zone. The area of interest of the models is the Bengal part of the Delta. The models are utilized to enhance our understanding of the morphodynamic processes most important for the present GBM delta. In a next phase the models will be used to project potential future changes in boundary conditions on the GBM delta, and to study the relevance for its macro-scale morphodynamics.

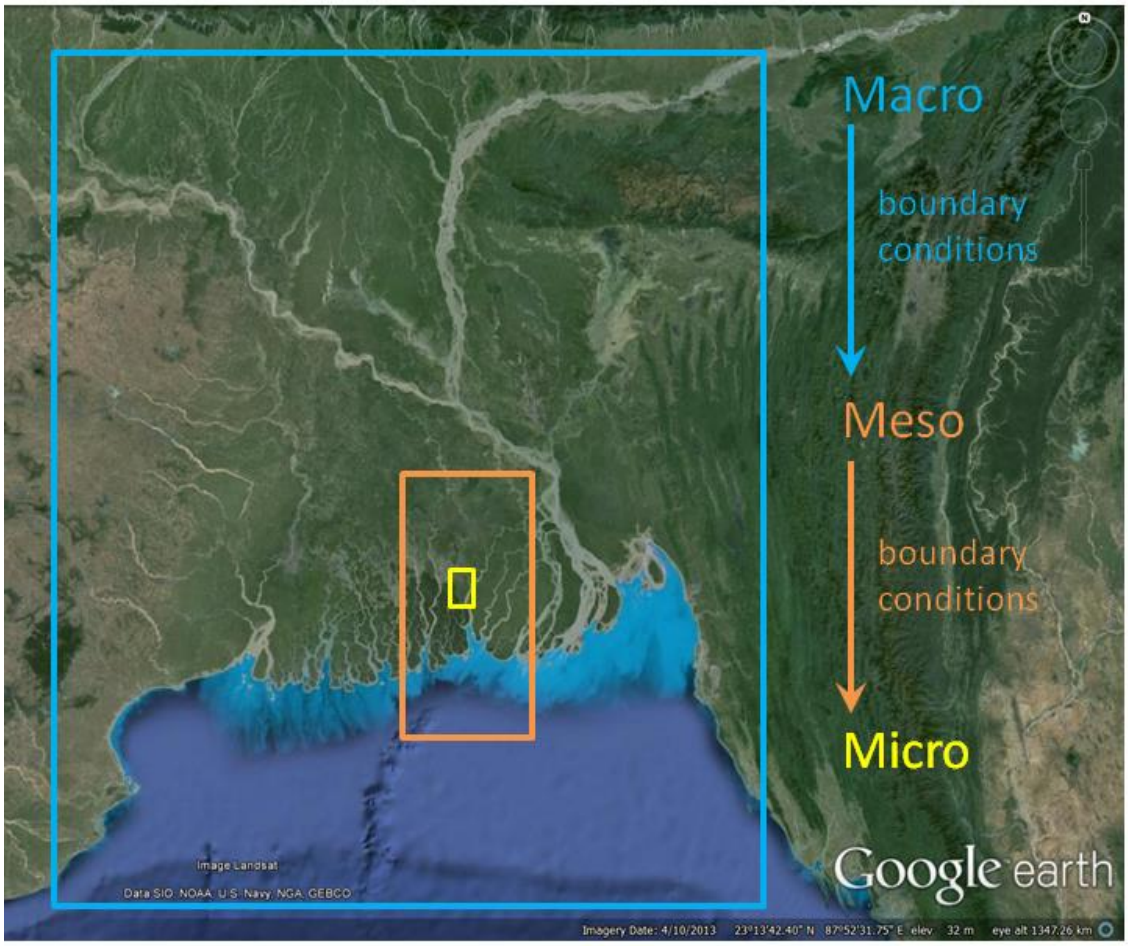

Figure 1.1 Cascade of modelling scales, the macro-scale is studied in this report.

1.2 Objectives

The macro-scale morphology topic described in this report is the first component in a cascade of spatial and temporal scales that are studied. The purpose of this first part is to:

- Understand the large-scale annual sediment dynamics and long-term morphodynamics of the GBM delta;
- Predict responses to changes in external forcing conditions (due to climate change and anthropogenic activity) and their consequences for the morphodynamics of the GBM delta.

The developed models described in this report provide the tools to study sediment transport patterns in the delta (including sources and sinks) and assess the effect of changing boundary conditions on the sediment budget and the morphological development. The macro-scale morphological models are used to translate these effects to high-resolution meso-scale models (on the scale of an individual river or estuary) for their boundary conditions. This multi-scale model approach allows for a quantitative understanding on the effect of changes in external drivers on polder sustainability and its associated design criteria.

The models are subsequently applied to establish an understanding of the long-term and large-scale sediment dynamics of the GBM delta and, based on the understanding of the current situation (this interim report), identify drivers of future developments and quantify the effect of future changes in the external forcing mechanisms (extension of this report). To reach the objectives, three types of models are set up and applied, each of them having a specific task in describing the governing processes. These models are:

1. A catchment hydrology model (HydroTrend); the model quantifies the incoming sediment fluxes for the GBM delta, based on the catchment characteristics (i.e. drainage basin morphology and biophysical properties).
2. A river branch model (Delft3D-FM 1D); the model quantifies the distribution of incoming flow and sediment fluxes over the major river branches of the GBM delta, based on the cross-sectionally averaged river bed properties (i.e. geometry, flow resistance, sediment composition).
3. A coastal model (Delft3D-FM 2D); the model quantifies the distribution of incoming flow and sediment fluxes and the morphological changes that are the result of gradients in the sediment redistribution.

The following sections describe each of these models in more detail, specifying their function within the study and their basic approach including their strengths and weaknesses.

1.2.1 Basin hydrology model (Hydrotrend)

HydroTrend is an empirical climate-driven, hydrological water balance and transport model that simulates water discharge and sediment load at a river outlet. Hydrotrend uses topographical drainage basin characteristics, like contributing basin area, glacial coverage and relief, as well as climatological parameters, like temperature and rainfall to estimate daily river dynamics (Kettner et al., 2008). The empirical basis of HydroTrend makes it an extremely fast and flexible model environment, limiting computational effort. The empirical set-up however, limits the results of the model to fluxes at the river outlets.

The aim is to use the catchment hydrology model to:

- estimate incoming total annual water and sediment fluxes for each of the upstream basins of the Ganges and Brahmaputra rivers, which then can be propagated into the macro-scale morphodynamics delta models (Delft3D).
- estimate daily dynamics and analyse variability of suspended sediment fluxes for each of the Ganges and Brahmaputra rivers.
- estimate future water and sediment fluxes under projections of a changing climate and upstream dam engineering for each of the Ganges and Brahmaputra rivers.

The model can be set up for unique contributing river basins and requires a suite of input parameters to be specified for each basin. This project models the Ganges and Brahmaputra rivers as separate basins, since their basin properties and climatic conditions are distinctly different.

In this phase of the project HydroTrend will be used to hindcast discharge dynamics for calibration, and forecast future sediment loads of the Ganges-Brahmaputra on a daily timescale with use of downscaled regional Earth System Models. The forecast results will be used to force the GBM scale (process-based) models in the following phase of the project. In this next phase a database of engineering measures proposed by the Indian Interlinkages River Project will be analysed as well to assess the effect of proposed anthropogenic activities (Darby et al., 2015, Rahman et al., 2018, Higgins et al., 2018).

1.2.2 River branch model (Delft3D-FM 1D)

The river branch model provides information on the distribution of flow and suspended sediment transport over the major rivers of the GBM delta. The main objectives are:

- To derive a sediment budget for the GBM Delta, covering the largest part (major rivers) of Bangladesh.
- To assess the large-scale distribution of different sediment fractions (coarse and fine sediment).
- To apply the sediment budget model to assess the effect of scenarios of changing boundary conditions (downstream and upstream), climate change and land use adaptation, and

- to provide boundary conditions to meso-scale models.

The river branch model of the GBM delta is based on the Delft3D-Flexible Mesh (FM) software, which can integrate 1D, 2D and 3D meshes for hydrodynamics, sediment transport, and morphodynamics. Here, a 1D approach is preferred for computational effort reasons. The numerical network of the Delft3D-FM software is fully unstructured, which allows for easy adjustment of network resolution and domain extent.

The model domain covers the Bangladeshi part of the GBM delta, from upstream of the three major rivers to the very downstream part of the large number of major estuaries bifurcating in the delta. The bathymetric representation of the model is set-up in two-fold; consisting of an approach with traditional cross-sectional profiles derived directly from observations, and an approach that involves constructing hybrid cross-sectional profiles to derive characteristic conditions which are more suitable for long-term calculations. The traditional model-setup will serve as a bench-mark model for hydrodynamic modelling, and the model-setup with hybrid profiles will be used, after model calibration, to achieve the main objectives.

The strength of the one-dimensional approach is the computationally efficient model set-up which allows for long-term calculations without the constraint of applying any input reduction scheme (schematization of boundary conditions). In this way the long-term effect of the interaction of tides and river discharge on the sediment distribution is studied using (real-time) boundary information that resembles actual conditions. The obvious weakness of a 1D model is the assumption that the governing processes can be described by cross-sectionally averaged parameters.

1.2.3 Coastal model (Delft3D-FM 2D)

The coastal model provides information on the internal sediment distribution as a result of fluvial and tidal forcing, and information on the gross morphodynamic trends that results from gradients in the sediment transport pathways. The main objectives are:

- To study the large-scale tidal propagation and flow distribution, and how this is expected to change in the future
- To study the coarse and fine sediment distribution, and how the distribution is affected by human interventions and climate change
- To define pathways for fine sediment
- To study the morphology of major channels on decadal scales;
- To provide boundary conditions in terms of large-scale bed elevation change and sediment concentrations to meso-scale models.

The coastal model of the GBM delta is based on the Delft3D-Flexible Mesh (FM) software and set-up as a 2D (depth-averaged) model. The strength of this approach is that it allows to study all scales of hydrodynamic and morphodynamic processes, forced by the seasonal and long-term fluctuations in fluvial, tidal, and climatic conditions. A more detailed 3D approach, however, is not preferred because the increase in computational effort would make the model unsuitable for long-term morphological simulations. Consequently, weaknesses of the 2D approach are neglecting any 3D processes (although considered less important for the long-term morphodynamics) and the constraint in using only schematized boundary conditions (due to the need for input reduction on the boundary information) for long-term simulations.

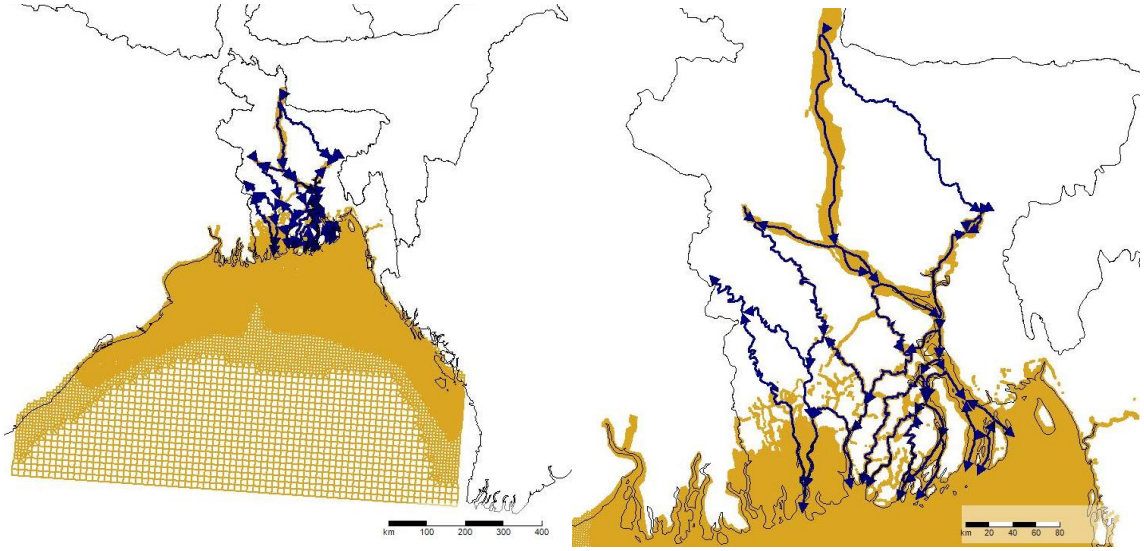

Figure 1.2 Macro-scale morphology model domains (left) and zoomed in on Bangladesh (right).

1.3 Outline of the report

The report starts in the previous section with the objectives of the macro-scale morphology component and the approach (methods) adopted. Chapter 2 outlines the knowledge background by providing a description on the governing hydrodynamics, sediment dynamics and historical morphological changes in the GBM delta. Previous modelling efforts done to study these delta dynamics are discussed as well. The following chapter (Chapter 3) gives an overview on the availability of measurement data. These data are used in the subsequent chapters, which describe the development and calibration/validation of the models used to study the macro-scale morphology. At first, an overview of the development of the basin-scale hydrology model is given (Chapter 4). Subsequently, Chapter 0 describes the development of a one-dimensional (1D) river branch model that covers all the major rivers in the GBM delta. The model development focusses in detail on the approach to derive characteristic profiles to set-up a cross-sectionally averaged model suited for long-term sediment dynamics. Chapter 6 describes the development of a two-dimensional (2D) model that covers the larger part of the GBM delta and coastal zone. The chapter describes specifically the novel approach of automatic grid generation, developed within the project. The results of model application, addressing the objectives of the study, are integrally discussed in Chapter 7. The report finalizes with conclusions in Chapter 8.

2 Macro scale delta dynamics

2.1 Introduction

Setting up a numerical model requires an abundance of choices to be made such as modelling platform, spatial and temporal resolution and extent, physical processes to be included, etc. It is essential to have a thorough knowledge and understanding of the physical system (conceptual model), model limitations, and lessons learnt from previous modelling efforts in order to make substantiated choices. This chapter summarizes the knowledge of the system and associated assessment to derive a well-defined foundation for the modelling work to be executed. The chapter frequently refers to the names of the major river branches in the GBM delta. Therefore, an overview is presented in Figure 2.1.

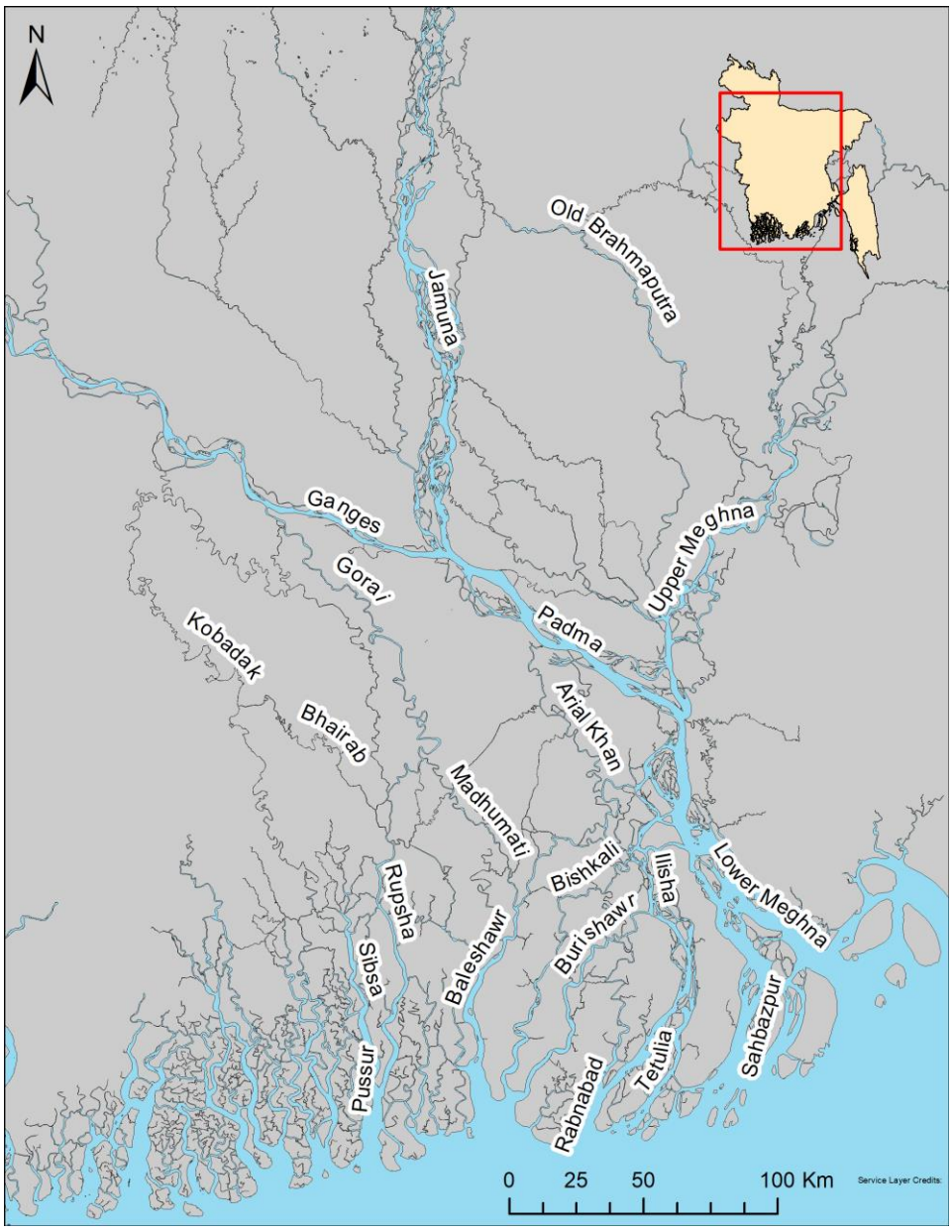

Figure 2.1 Names of the major river branches in the GBM delta.

2.2 Sediment dynamics

2.2.1 River Sediment

The concentration and distribution of sediment in the river channels are important controls on delta morphology. Understanding sediment composition across different transport mechanisms also provides insight into the reworking and accretion of material across the delta. Estimates of suspended sediment concentration (SSC) and grain size distributions have been collected across the entire GBM delta system, from the upstream portion in India, to the coastal shelf. Both in situ measurements (e.g. Kuehl et al., 1989; Barua et al., 1994; Datta and Subramanian, 1997; Singh et al., 2007) and remote sensing (Islam et al., 2001) methods have been used to make these estimates. In addition to estimates of concentration, the mineralogy of sediment samples is also recorded for the Ganga River in India (Chakrapani et al., 1995) and the Ganges, Padma, Jamuna and Meghna rivers in Bangladesh (Datta and Subramanian, 1997). Generally, the sediment of the GBM delta is dominated by grain sizes ranging from fine sands to clays, with seasonal variability in transport due to monsoons. More detailed results from these analyses for suspended and bed load transport are summarized in the following.

Suspended Load

Like many fluvial systems, most of the sediment in the GBM delta is transported as suspended load of which a part is wash load and the remaining part belongs to bed material load (Jansen et al., 1979, see Figure 2.2). Wash load is defined as very fine sediment, which remains in near-constant suspension, even when velocities are negligible or there is slack water. This means that wash load does not participate in the exchange between water column and bed, and thus does not cause bed level change. Therefore, wash load is often ignored in morphological studies (of mostly rivers). However, for the present study it is required to consider the full suspended load including wash load because of various reasons. First, the distinction between wash load and bed material load is not everywhere the same but spatially variable. Wash load in the upstream rivers can become bed material load in the downstream estuary as the sediment settles eventually either in spatial or temporal context. This means that even the fine clay fraction of sediment does take part in the morphological changes of the GBM delta. Second, in systems with relatively high sediment concentrations like the GBM delta the influence of (total) sediment concentration on the hydrodynamics is important (Winterwerp et al., 2009, Wang et al., 2014). Considering the full suspended load without defining and excluding wash load has the consequence that more than one sediment fractions of sediment (i.e. graded sediment) will need to be simulated in the morphodynamic models.

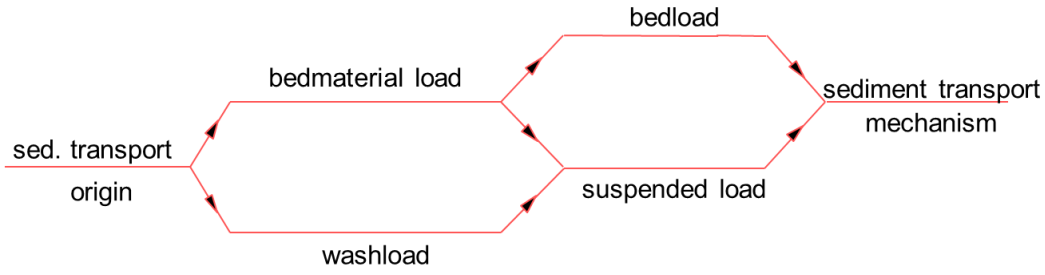

Figure 2.2 Sediment transport modes defined from sediment origin and transport mechanism (Jansen et al., 1979)

Suspended sediment concentration (SSC) have been assessed for several of the large rivers. Dry season estimates of SSC using Thematic Mapper (TM) and Advanced very-high-resolution radiometer (AVHRR) data resulted in average concentrations of 750 mg/L for the Brahmaputra and 500 mg/L for the Ganges River. During the monsoon season, average SSC increased to 1100 mg/L and 1250 mg/L, respectively (Islam et al., 2001). The authors argue that the increase in Ganges wet season SSC is tied to bank erosion and deposition during peak flooding. This increase in concentration can also be seen in sediment yields of the Padma River, where yields increase four-fold from 50 Mt/yr in the dry season to 200 Mt/yr during the monsoon (Barua et al., 1994). Other estimates for suspended sediment load of the Brahmaputra (or Jamuna) River include 332 Mt/yr

(Sarker et al., 2014), and 106 Mt/yr for the combined system (Datta and Subramanian, 1997). Sediment moves seaward by fluvial forcing, and westward by tidal forcing (Barua et al., 1994).

In the Ganga River in India, suspended sediments range from very fine sands to medium silts (Chakrapani et al., 1995; Singh et al., 2007). Suspended sediment in the main rivers of the GBM delta is finer, with predominantly fine silts and clays. Textural analysis by Datta and Subramanian (1997) showed fine silts and clays in the Ganges, Meghna, Jamuna and Padma Rivers. In their estimation, the grain size of more than 95% of the suspended material is fine silt and clays (≤16 microns). Median grain sizes sampled in the Meghna Estuary are similarly fine, ranging from 13.8 to 25 microns, or fine to medium silts (Kuehl et al. 1989, Barua et al., 1994).

The mineralogy of these suspended sediments has also been reported. Mineral constituents in suspended sediment samples throughout the GBM delta were predominantly quartz, followed by illite, kaolinite and feldspars (Datta and Subramanian, 1997). Trace amounts of chlorite, carbonates and montmorillonite were present at most sampling locations. Chakrapani et al. (1995) looked at the mineralogy upstream of the GBM delta system in India and noted changes in the mineral abundance moving downstream towards Bangladesh. Upstream, a high percentage of micas was noted. Towards the Bay of Bengal, smectite abundance increases, exceeding the mica abundance. In addition, samples also contain low levels of chlorites, vermis and kaolinites (Chakrapani et al., 1995).

Bed Load

Coarse sediment in fluvial systems is transported by rolling, sliding or saltating (bouncing) along the channel bed. Bed load transport is initiated when velocities near the bed are high enough to surpass a threshold for motion. In general, bed load makes up a smaller proportion of sediment load than suspended material.

Each of the major rivers of the GBM delta has sandy bed material (Sarker et al., 2014). Estimates for sediment transport of bed load are unknown, although previous work supposes it may be as high as suspended transport rates (Garzanti et al., 2010). The mineralogy of the bed load is similar to that of the suspended load. Sediments are quartz-dominated, with the presence of feldspars and clays (Datta and Subramanian, 1997).

Bed load sediments are coarser than the suspended load. Upstream of the GBM delta in India, bed load sediment is primarily fine sands (~60%) to very fine sands (~20%), with the remaining material being coarser sands, silts and clays (Singh et al., 2007). Moving into the GBM delta, bed sediment samples were 76% fine to very fine sands, with silt-sized grains making up the remaining bed layer (Datta and Subramanian, 1997). Downstream of the junction of the Ganges and Brahmaputra rivers, bed sediments are even finer. Grain sizes in that reach are very coarse silts (Singh et al., 2007). In the coastal region, samples showed the dominant size classes were also fine to very fine sands (Stummeyer et al., 2002).

2.2.2 Sediment transport forcing

Fluvial forcing

The three main rivers of the GBM delta, the Ganges, Brahmaputra, and Meghna, deliver a total of 1 trillion (10^{12}) m^3 of water and 1 billion (10^9) ton sediment per year to the Bay of Bengal through the Lower Meghna River (Akter et al., 2016). There are two other smaller branches, the Gorai River and the Arial Khan River, each delivering about 30 billion m^3 of water to the bay annually (EGIS, 2001), with 30 and 25 million ton of sediment respectively (Table 2.1).

Table 2.1 Annual discharge and sediment load of the various rivers of the GBM delta (from: Akter et al., 2016).

River	Discharge (m^3/s)			Annual sediment load (10^6 ton/yr)
	Mean	Peak	Minimum	
Jamuna	20,200	70,000	4,250	590
Ganges	11,300	52,000	600	550
Padma	32,000	95,000	4,800	1,000
Upper Meghna	-	13,700	-	-
Gorai	1,000	-	-	30
Arial Khan	1,000	-	-	25

Marine forcing

Tides along the coast of the Bengal delta (including the Indian part) are semidiurnal, with a slight diurnal inequality. The average tidal range varies from 1.5 m in the west to more than 4 m at the NE tip of the Meghna estuary (Akter et al., 2016). The Meghna estuary, the main delta forming estuary, is a mesotidal estuary, where the tidal range varies between 2 and 4 m (MES II, 2001).

2.3 Morphodynamics

The studies on the morphological development of the GBM delta on a geological time scale, carried out by Allison et al. (2003), Fergusson (1863), Goodbred & Kuehl (2000a, 2000b), Kuehl et al. (2005), Umitsu (1985, 1993), Williams (1919) and Morgan & McIntire (1959), have been summarized by Akter et al. (2016). They concluded that changes to the courses of the Ganges and Brahmaputra rivers were a consequence of the delta building process, which was itself driven by abundant sediment input from erosion of the Himalayas, conditioned by sustained sea-level rise (SLR) that began during the late Quaternary and modified internally by regional tectonics within the Bengal Basin.

On the century-scale the most important event concerns the Brahmaputra avulsion north of Madhupur Tract (where Dhaka is located). Before the avulsion the Brahmaputra was flowing east of Madhupur Tract and after the avulsion the river now flows west of Madhupur Tract forming the present Jamuna River. Before the avulsion the two branches of Ganges had their own delta forming estuaries, separated from the one of Brahmaputra and Meghna together. The two branches Gorai and Padma were about equal in importance. After the avulsion the Padma River increased in importance because of the confluence of Jamuna. This has as consequence that the rivers come together with one combined delta forming estuary. After its formation the combined delta forming estuary has been shifting westwards. It is also remarked that the delta forming estuaries at present have a south-west facing orientation. This is probably due to the fact that the tidal wave in the Bengal Bay is propagating from west to east. In general, estuaries have the tendency of facing to the direction where the tidal wave comes from.

On decadal timescale Akter et al. (2016) noted the changes of various bifurcations. The reported developments suggest that the western branches of bifurcations in de delta increased in dominance over eastern bifurcations. An example is that the Gorai River is now mainly discharging through the Nabaganga River.

Figure 2.3 shows the (decadal) morphological development of the delta based on satellite images between 1985 and 2016, according to Aqua Monitor developed by Deltares (Donchyts et al., 2016). According to Akter et al. (2016) the Shabazpur Channel is at present the main channel of the delta building estuary. However, the satellite images show that in the last years (approx. since 2009) the Hatiya Channel is increasing in importance and it seems to be the main channel in 2017.

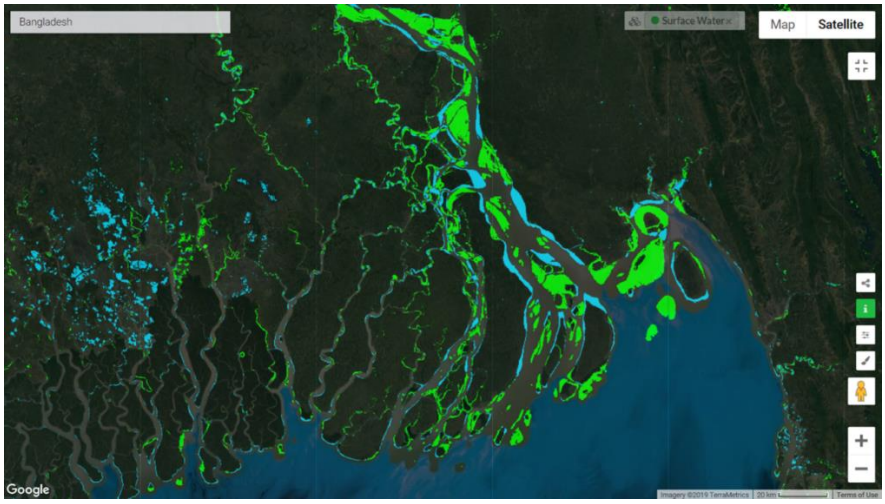

Figure 2.3 Changes of the delta in the period 1985-2016 according to Aqua Monitor. Green area became from water to land and blue area became from land to water.

2.4 Previous modelling efforts

Process-based models of the GBM delta exist, and most models are based on the MIKE[1] modelling platform. Existing 1D models like the General Model and the Super model can supply useful information for setting up the present GBM 1D model. Experience and lessons learnt from the studies using these models are valuable for the set-up and application of the GBM delta models. An example is the study by Galappatti et al. (1996) who carried out a 1D morphodynamic modelling study for the main (upstream) rivers in Bangladesh. They showed that the rivers are morphologically very active. Consequently, the measured cross-sectional profiles may be less suitable for a 1D model than schematised cross-sectional profiles. Due to the propagation of dunes and sand waves in the river, observed cross-sections at a certain location may fluctuate substantially depending on when the measurements are carried out. The results may vary greatly depending if the top or the trough of a sand wave is passing the measurement location at the time of observations.

Additionally, the experience using Delft3D for long-term morphodynamic simulations within projects carried out by the Consortium will be used and lessons learnt from this will be applied (e.g. need to include floodplains in predictions, necessity to let the sediment distribution spin-up before starting morphology, morphodynamic upscaling strategies).

2.5 A synthesis – motivation for the modelling approach

The GBM delta is formed by sediment. The large scale morphodynamics of the delta is a matter of sediment supply and sediment distribution on the one hand, and relative sea-level rise on the other hand.

At the macro-scale of the whole delta (Figure 1.1), fluvial input is the only sediment source. At present this sediment supply is about 1 billion ton per year (Table 2.1).

If the bulk density of sediment is 1.3 ton/m^3 this sediment supply is sufficient to heighten the whole delta area of about 150,000 km^2 with about 5 mm/year. Considering that a large part of the delta cannot or does not need to be heightened by sedimentation, this is sufficient to compensate a quite high relative sea-level rise if the sediment can be properly distributed within the delta. However, change of the fluvial sediment supply due to climate change and human activities in the upstream

[1] https://www.mikepoweredbydhi.com/products

river basins will directly influence the future development of the delta. Therefore, the Hydrotrend model will be set up and applied to predict the future development of the river discharge and sediment load.

At the macro-scale, the GBM delta can be divided in different areas, see e.g. Figure 2.4 in which four areas are distinguished: active delta with the delta forming estuaries, polder area, Sundarbans and finally the subaqueous delta. In each of these areas the sedimentation depends on sediment supply, accommodation space and sediment transport capacity. Each of these three factors can form a limitation to the sedimentation rate:

- Sediment supply limited: Sediment source is not sufficient for fulfilling the sediment demand. As an example, if future sediment transport from the rivers to the delta will decrease or sea-level rise will accelerate, the delta as a whole will then become sediment supply limited when the sediment transported is less than what is needed for the delta in terms of sedimentation to keep pace with sea-level rise.
- Accommodation space depends on areas where sediment can accumulate and it increases with sea level rise (with a rate equal to the water area multiplied with sea level rise rate). In accommodation space limited areas sedimentation supply is is higher than required to grow the area in line with sea level rise. Transport capacity limited: This is the case when there is sufficient sediment supply but accommodation space cannot be filled because the sediment transport capacity between the sediment source and the area with accommodation space is too low.

Which limitation applies is important for how the area/system will respond to changing river sediment input and/or accelerating sea level rise, see Wang et al. (2018) who used this conceptual model for projecting the response of the Dutch Wadden Sea to future sea level rise scenarios.

The active delta is located in the eastern part of the overall delta, with the Lower Meghna being the main delta forming estuary. This area receives the major part of the sediment supply from the rivers. The sediment supply is thus ample, and the flow driven by river and tide provides sufficient sediment transport capacity to redistribute the sediment. The sedimentation rate here is limited by accommodation space (sediment supply is much more than needed for the area to grow with the rising sea level). As consequence the delta is extending seawards and a part of the sediment is transported further offshore.

The polder area is west of the active delta and east and north of the Sundarbans. Sediment supply to this area is partly via the (2^{nd} and 3^{rd} order) river tributaries from upstream and partly by the tidal flow from the coastal zone. Sedimentation within the polders is transport capacity limited because sediment exchange with the river / estuary branches is practically blocked. When this blockage is removed by e.g. tidal river management (TRM) the question then arises if the sedimentation will become sediment supply limited or transport capacity limited. The river branches / channels between the polders are probably accommodation space limited at present.

For the Sundarbans the sediment supply is also partly fluvial and partly marine. At present the sedimentation seems to be accommodation space limited as the area can keep up with sea-level rise. For the future scenarios with faster sea-level rise it is the question if it will become sediment supply limited or transport capacity limited.

The marine sediment redistributed to the polder area and Sundarbans is actually sediment from the delta forming estuaries. The remaining sediment from the delta forming estuaries is contributing to the subaqueous delta further seawards where the sedimentation is per definition supply limited. This conceptual model of sediment transport pathways is summarized and visualized in Figure 2.5.

In the conceptual model for the macro-scale development of the GBM delta described above and shown in Figure 2.5 the development of the polder area and the Sundarbans depends very much on how the fluvial sediment supply is distributed via the river tributaries and how the sediment out of the delta forming estuaries is transported along the coast and landwards via the tidal estuaries. The design of sediment management measures like TRM will also rely on the understanding of this sediment distribution. Therefore, a 1D river network model and a 2D depth-averaged (2DH) model are set up for simulating the present and future macro-scale sediment distribution in and morphological development of the delta. The 1D model mainly focusses on the distribution via the river tributaries whereas the 2DH model also covers the sediment transport along the coast.

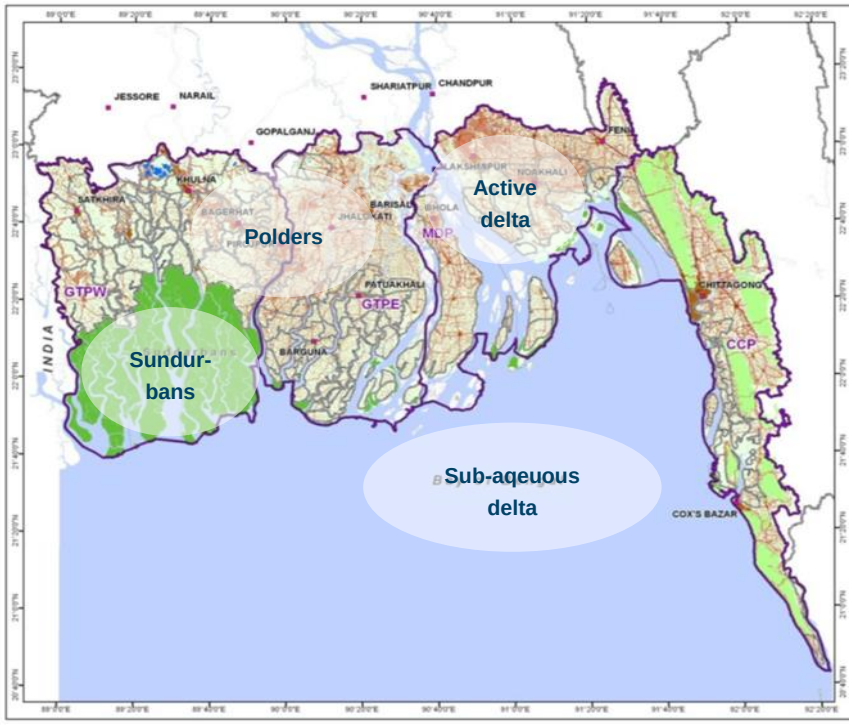

Figure 2.4 The GBM delta divided into the sub-areas, from east to west: Active delta (with delta forming estuaries), Polder area, Sundarbans, and sub-aqueous delta

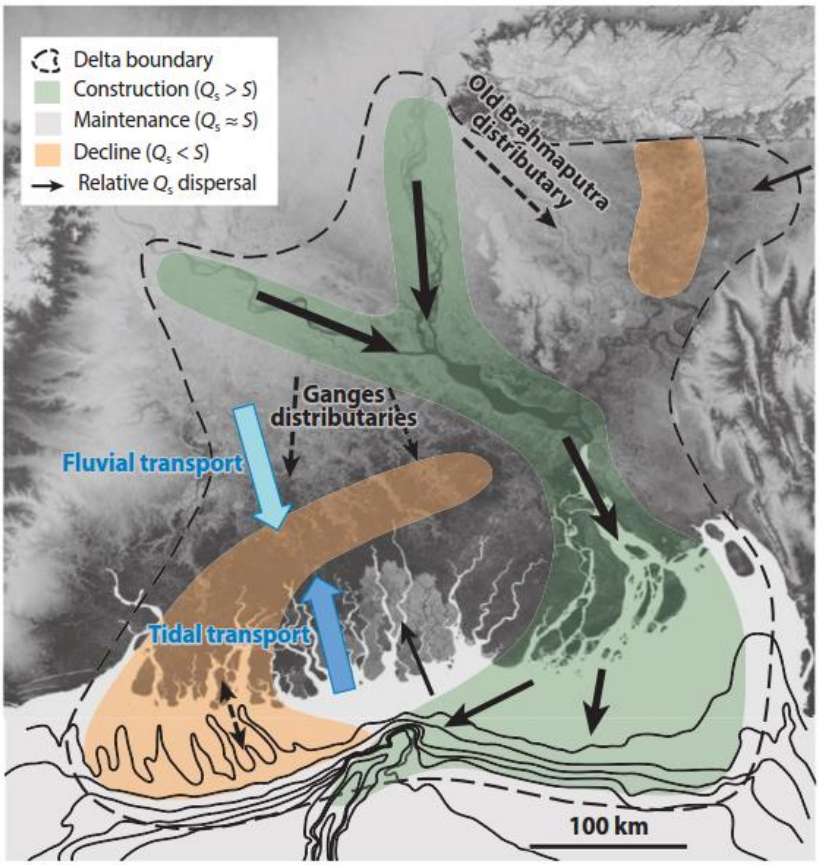

Figure 2.5 Conceptual model of sediment transport pathways in the GBM delta (Wilson and Goodbred, 2015).

3 Data

The macro-scale models cover a vast area of the GBM delta, and consequently, require an enormous amount of data (in-situ and remote sensed observations) of the various physical properties to force the model and to compare with model output. In this chapter all data used for the analysis, model input, and validation is described. For a more in-depth description of all data, however, reference is made to the data report of the project.

3.1 Coordinate systems

3.1.1 Horizontal reference system

All data and models in this report are using the Bangladesh Universal Transverse Mercator (BTM) horizontal coordinate system. The BTM datum is a local projected coordinate system, which has the advantage over a global geographic system that the units are given in linear measurements (e.g. meters) rather than angular degrees. Usually, the globally available Universal Transverse Mercator (UTM) grid can be used for this purpose. The country of Bangladesh, however, is covered by two UTM tiles (UTM45N and UTM46N) which makes usage impractical. To overcome this problem a new horizontal reference system was developed in the Flood Action Plan 19 (FAP 19) in May 1992[2]. Since then this reference system is used for official cartography. The projection parameters of the BTM system and transformation parameters from the global WGS84 system to BTM are shown in Table 3.1.

Table 3.1 Projection parameters of the BTM coordinate system and conversion parameters from WGS84.

Parameter	Value
Projection parameters	
Ellipsoid	Everest Modified Bangladesh
Projection method	Transverse Mercator
Latitude of origin	0° N
Central meridian	90°
False Northing, Easting	-2,000,000 m, 500,000 m
Scale factor	0.9996
Datum transformation parameters	
Semi-major axis	6,377,298.52400
Semi-minor axis	6,356,097.52000
Inverse Flattening 1/F	300.80170000
Rotation X, Y, Z	0, 0, 0
Translation X, Y ,Z	-288.000m, -735.000m, -255.000m

The BTM coordinate system is not documented in the online registry of the official EPGS Geodetic Parameter Dataset (the database for coordinate reference systems and transformation parameters), thus does not have a unique EPSG code assigned to it. The Gulshan 303 coordinate system however has a unique EPSG code assigned to it: 3106[3], and the BTM system is equal to the Gulshan 303 but comprises a false northing of 2,000 km (see Table 3.1).

[2] http://socolzahid-en.blogspot.com/2012/07/bangladesh-transverse-mercator-btm.html

[3] https://epsg.io/3106

3.1.2 Vertical datum

The vertical reference system used throughout the report (data and models) is the Public Works Department datum (PWD). This national vertical reference datum is maintained by the Survey of Bangladesh (SoB) through 465 benchmark stations covering the larger part of Bangladesh[4]. The PWD reference system is related to Mean Sea Level (MSL) which is established at Rangadia, Chittagong in 1992. The conversion from MSL to PWD is a fixed level difference, indicated as 1.5 ft (= 0.4572 m) below the MSL level[5]. However, throughout literature the following conversion is more established and is used in this study:

(1) PWD = MSL + 0.46

3.2 Morphology

3.2.1 Bathymetry

Most of the bathymetric information on the rivers in the GBM delta and the coastal zone is available on cross-sectional transects gathered via Single Beam Echo Sounding (SBES). In-situ measurements with full spatial coverage (e.g. through Multibeam Echo Sounding, MBES) are scarce and are not used in this study. The available observations are gathered on project basis during the past decades and were merged into a single database during the present project. Therefore, data in rivers that are monitored less frequently can be outdated while data in the most important rivers is more recent and more frequently available. Furthermore, during the project new surveys have been performed. Figure 3.1 shows the spatial coverage (enveloping polygons) of the observations available.

[4] http://www.sob.gov.bd/site/page/2e0fd063-09e4-4512-a470-a5fbd3668c71/Geodetic-

[5] http://www.ffwc.gov.bd/index.php/definitions

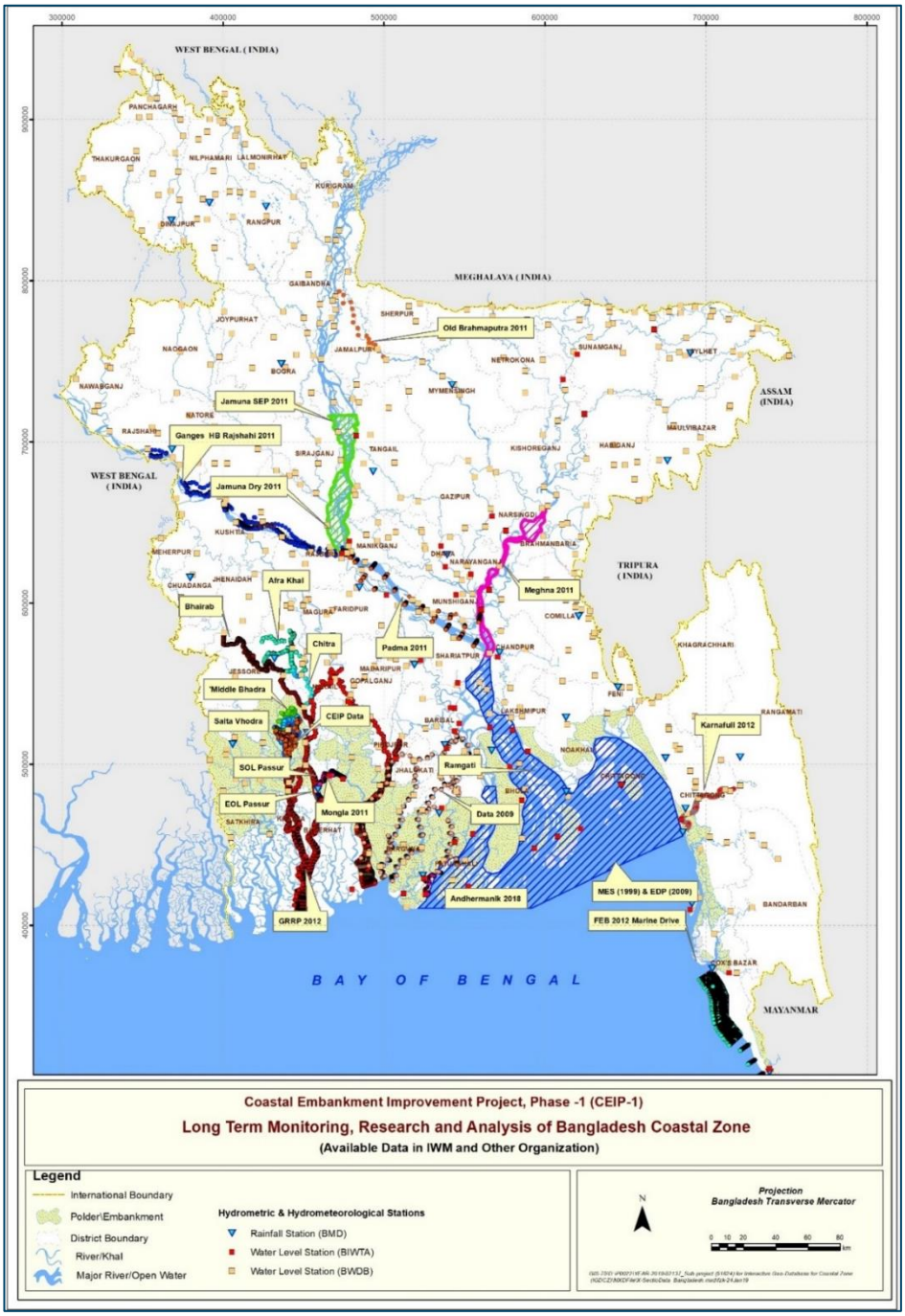

Figure 3.1 Spatial coverage of all in-situ bathymetry observations available (see colours and text boxes for name and date of bathymetry data surveys).

Besides the in-situ observations shown in Figure 3.1 a complete bathymetric dataset of the GBM delta is available from the MIKE21 Bay of Bengal (BoB) model (Uddin et al., 2014). This dataset is, besides the observations, used in the development of the coastal model (see Section 6.2.2).

3.2.2 Topography

The bed level of the dry land area is available through RTK-GPS observations; however, these data are sparsely populated and therefore not suitable for input in models. A dataset that delivers full coverage of the topography of the coastal zone of Bangladesh is a satellite derived digital elevation model (DEM). This dataset was acquired by FINNMAP (a Finnish consultancy firm) in 1991 and

updated by IWM in 2009 (IWM, 2009) using Google images from 2006-2007 to correct the data and to delineate the Sundarbans Forest (Payo et al, 2016). After this update the dataset has been updated regularly by IWM with land surveys executed for different projects across the delta. The dataset available for this project provides topography information on a 30 m resolution grid of the Bangladesh coastal zone (Figure 3.2). Because this dataset is acquired by remote sensing the reliability of the data must be considered carefully. It is, for example, not known if the data provides the vertical level of the land or the top of the canopy in densely vegetated areas (e.g. the Sundarbans).

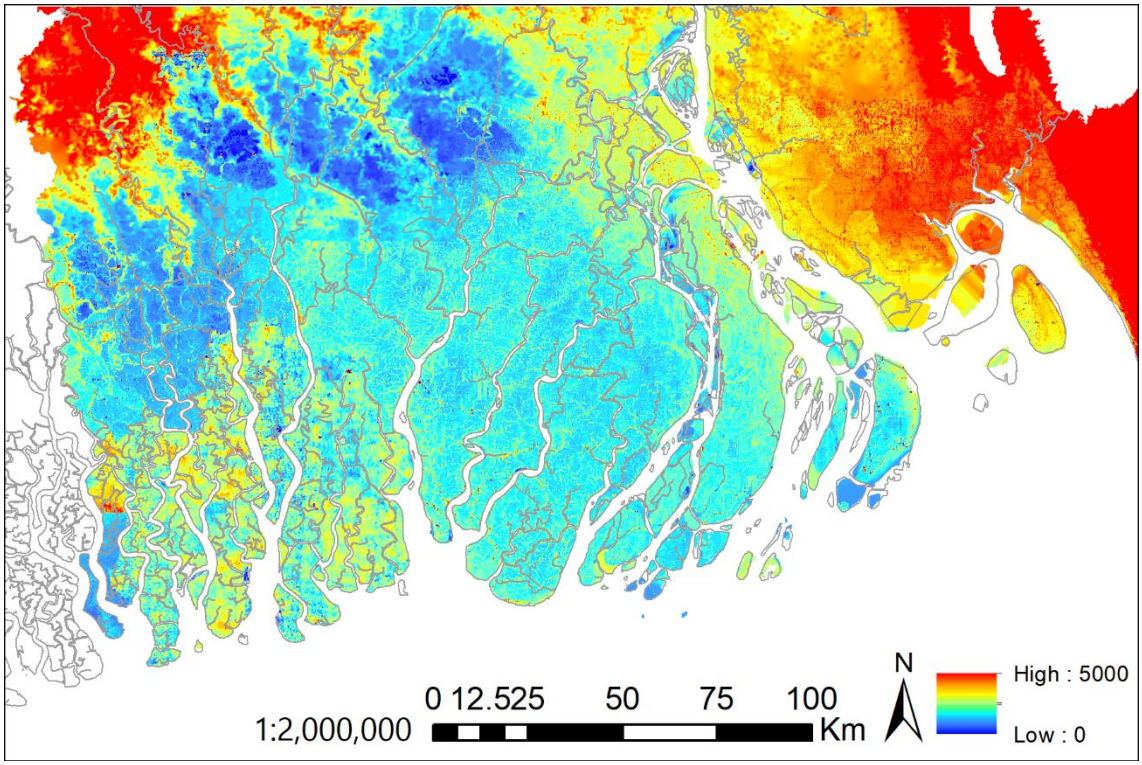

Figure 3.2 Satellite derived digital elevation model (DEM) for the Bangladesh coastal zone. Elevation shown in millimetres.

3.3 Hydrodynamics

3.3.1 Water levels

3.3.1.1 Time-series

In-situ observations of the free surface elevation (water levels) are available at numerous stations in Bangladesh from two primary sources: data from the Bangladesh Water Development Board (BWBD) and Bangladesh Inland Water Transport Authority (BIWTA) monitoring stations.

The BWBD monitoring stations (Figure 3.3) are manually operated staff gauges where water levels are read and reported on 3-hour intervals, excluding the nights. A photograph showing such a staff gauge is shown in Photograph 3.1. The main purpose of these monitoring stations is to monitor monsoonal flood discharge waves and to serve as a flood early warning indicator. Therefore, the maintained 3-hour interval is sufficient. The data is, however, less suited to derive tidal properties in the tidally influenced zone as the 3-hour time-resolution is not frequent enough for a proper representation of the tidal curve. Furthermore, because the staff gauges are often constructed from bamboo material which is positioned directly into the bed sediment, and because these constructions are relocated along the banks throughout the year to be accessible, the vertical referencing of these

measurements is highly uncertain. The BWBD data was made available at the start of the project for the time period 2011-2015 on most of the monitoring stations shown in Figure 3.3. In a later stage of the project the Interactive Geo-Database for the Coastal Zone[6] was set-up, where the BWBD data can be downloaded for long time periods.

Data from the monitoring stations of the BIWTA (Figure 3.4) focus on the coastal zone, is collected automatically (using pressure sensors), and reported on varying frequencies (mostly 30-minute intervals), making it more suitable for deriving tidal properties. The availability of the BIWTA data, however, is variable and includes “no-data” gaps. Figure 3.5 shows the temporal availability of the BIWTA data for each monitoring gauge.

Photograph 3.1 BWBD staff gauge along the Padma river.

[6] *https://gis.iwmbd.com/ceip/home*

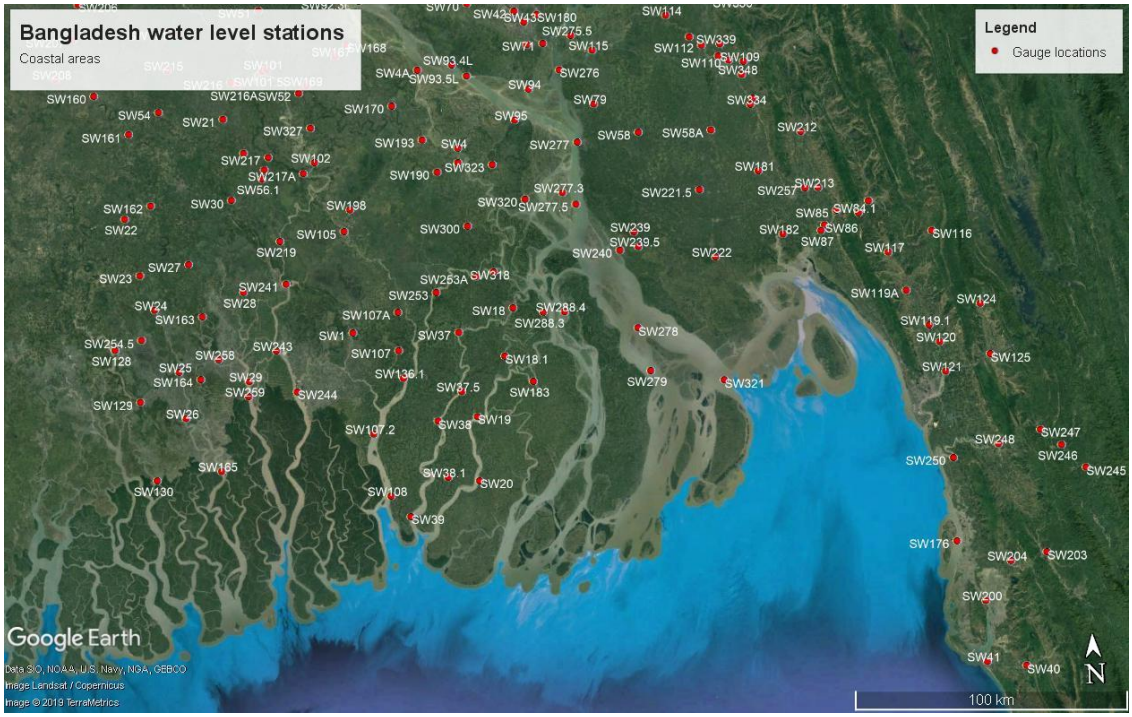

Figure 3.3 Overview of BWDB water level gauges.

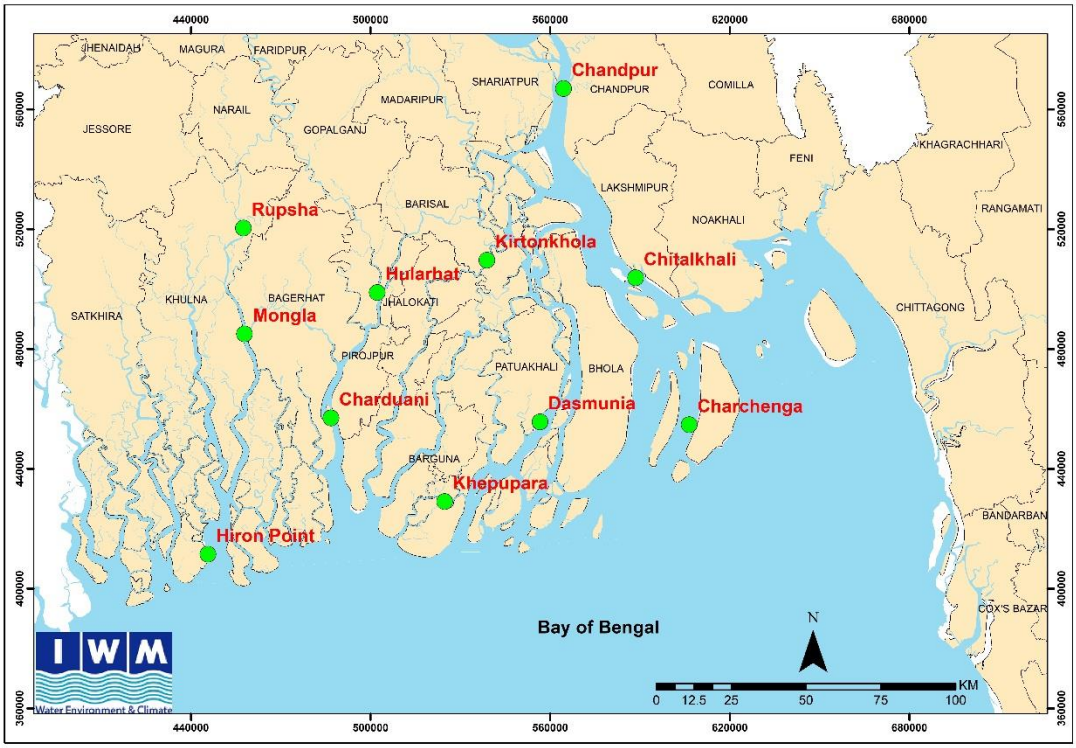

Figure 3.4 Overview of BIWTA water level gauges.

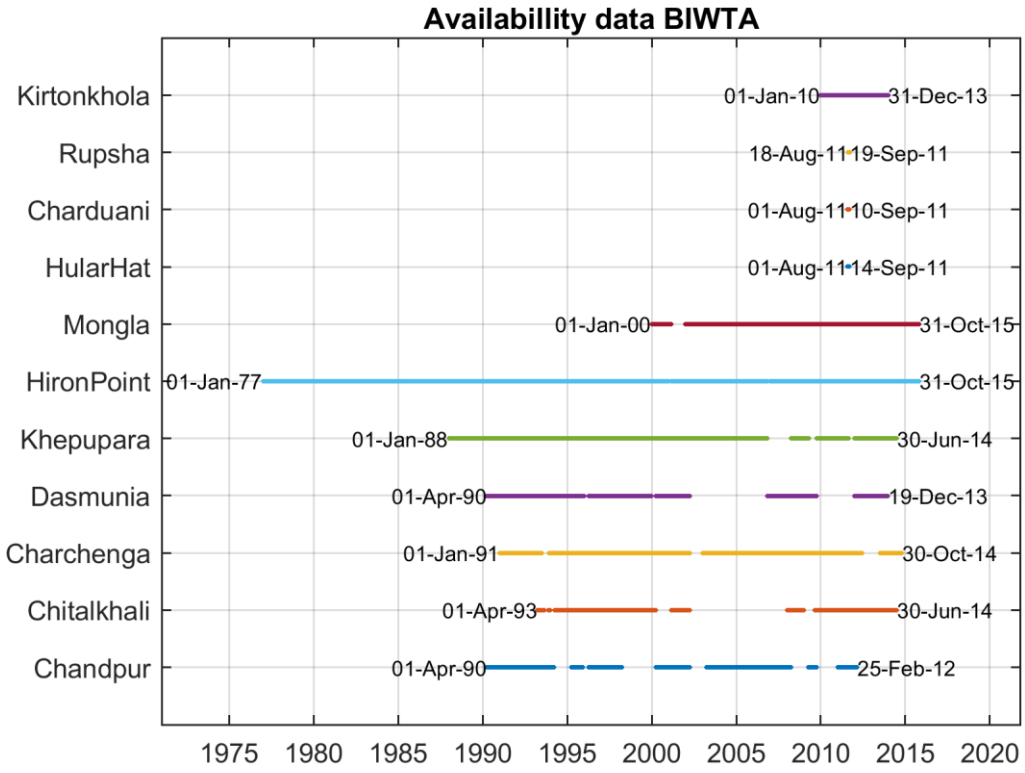

Figure 3.5 Availability of the BIWTA data.

3.3.1.2 Tide in the delta

The primary use of the water level time-series data in this study is model calibration and validation, which is mainly done on the main tidal constituents, particularly M2, throughout the delta. However, performing tidal analysis on these timeseries with coarse temporal resolution, varying sampling frequency, and including data gaps, is not straightforward. Furthermore, using long timeseries (e.g. one-year duration), creates problems in areas where the tide is strongly modulated by the discharge (e.g. the Padma river), which gives rise to a highly non-stationary tidal signal. After trying various configurations, it has been chosen to perform an analysis on 28 days in January 2012 for all stations and selecting only those stations for which the root-mean-squared (rms) error between the reconstructed signal from tidal analysis and the observations was less than 16% of the mean tidal range.

Tidal analysis was carried out using the open-source Matlab function *tidalfit* and associated *tidalval* prediction. The tidal components that could be resolved in the 28-day series were M2, M4, S2, N2, K2, O1, K1, and P1. Examples of the reconstructed signal where the input data was of good quality are shown in Figure 3.6. More problematic - but still acceptable - examples are shown in Figure 3.7 for stations Chandpur and Chitalkhali. For Chandpur, on the confluence of Upper Meghna and Padma into Lower Meghna, some discrepancy arises from mean water level variations with higher than normal values around the 11th of January and lower than normal around the 19th of January. Values of the mean tidal range and the estimated M2 tidal amplitude (used for model calibration) is shown in Figure 3.8.

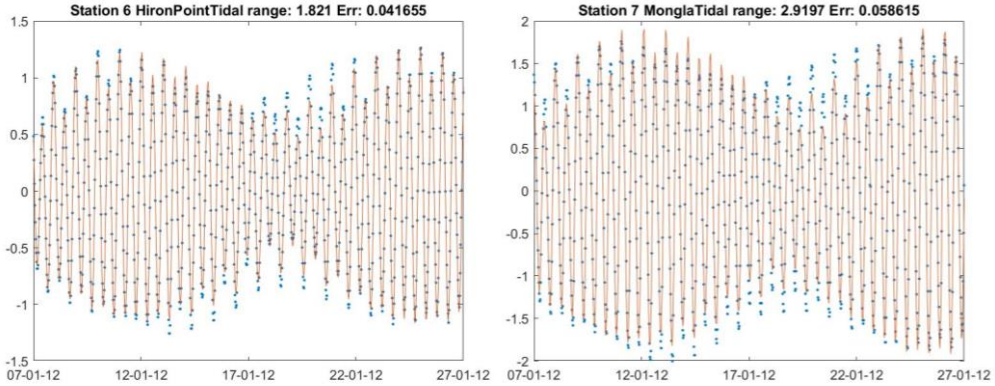

Figure 3.6 Observations (blue dots) and constructed signal using tidal analysis (red lines) for Hiron Point (left) and Mongla (right).

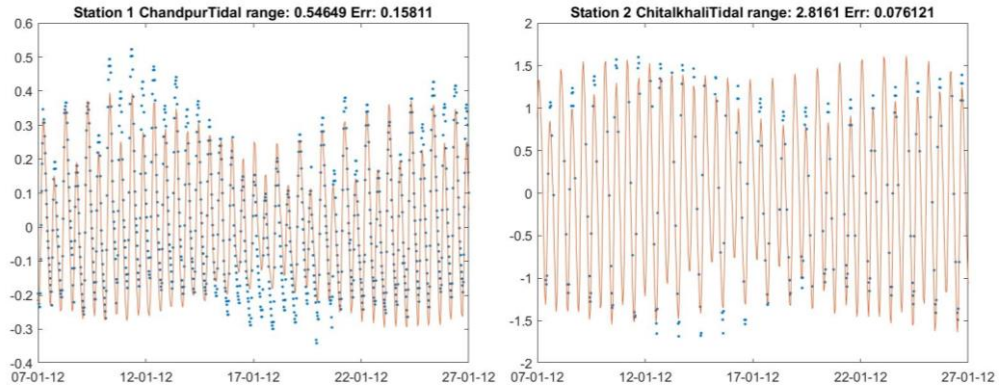

Figure 3.7 Observations (blue dots) and constructed signal using tidal analysis (red lines) for Chandpur (left) and for Chitalkhali (right).

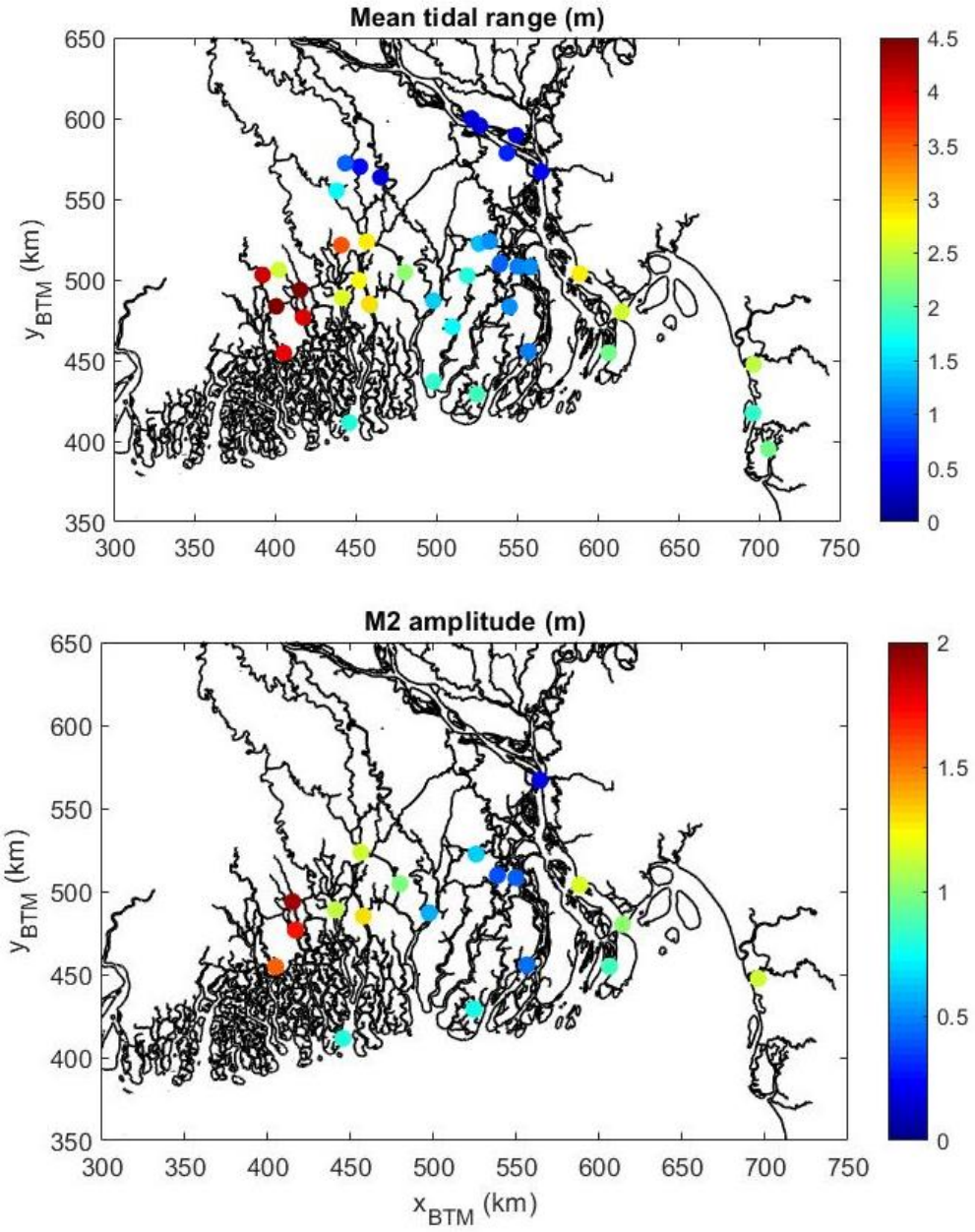

Figure 3.8 Mean tidal range (top) and M2 tidal amplitude in the delta.

3.3.1.3 Offshore tide

The offshore tidal environment is known from global tide models and can be used to force large scale regional models. The TPXO global tide inverse model (Egbert and Erofeeva, 2002) was used to derive offshore amplitudes and phases of the primary tidal components. The spatial distribution of the M2 tidal amplitude and phase over the Bay of Bengal is shown in Figure 3.5.

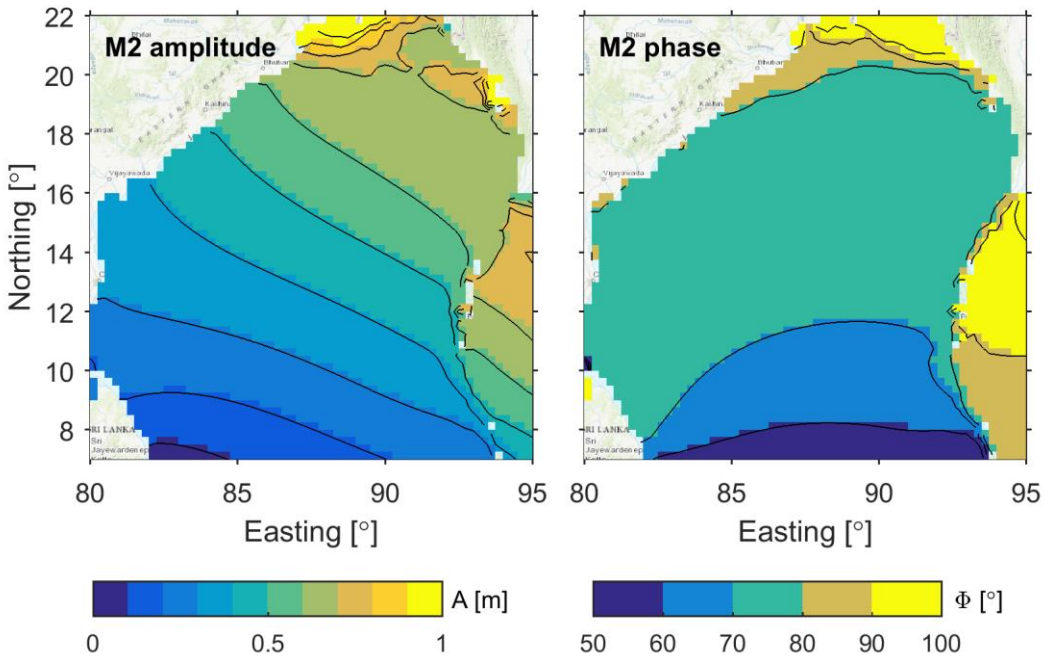

Figure 3.9 Spatial distribution of amplitude and phase of the M2 primary tidal constituent through the Bay of Bengal.

3.3.2 Discharge

The river discharge is measured at several strategic locations at the upstream reaches of the GBM delta (see the map in Figure 3.10). At these locations, the BWDB estimates the instantaneous discharge using stage-discharge relationships (or rating curves). These relationships are empirically derived functions that relate the water level at a point to the corresponding discharge. After such a relationship is established discharge can be monitored continuously by simply measuring the free surface elevation (water level stage). This method provides a simple and low-cost measure to derive continuous discharge time-series. It is, however, less accurate than deriving discharge from in-situ velocity observations. The discharge time-series available for the study are shown in Figure 3.10 for the complete time-series (top of sub-panels) and a zoom-in of the year 2001 (bottom of sub-panels). The figures show clearly that the discharge is highly variable throughout the year, with a minimum in the dry-monsoon period (Dec-Mar) and a maximum in the monsoon season (Jul-Sep).

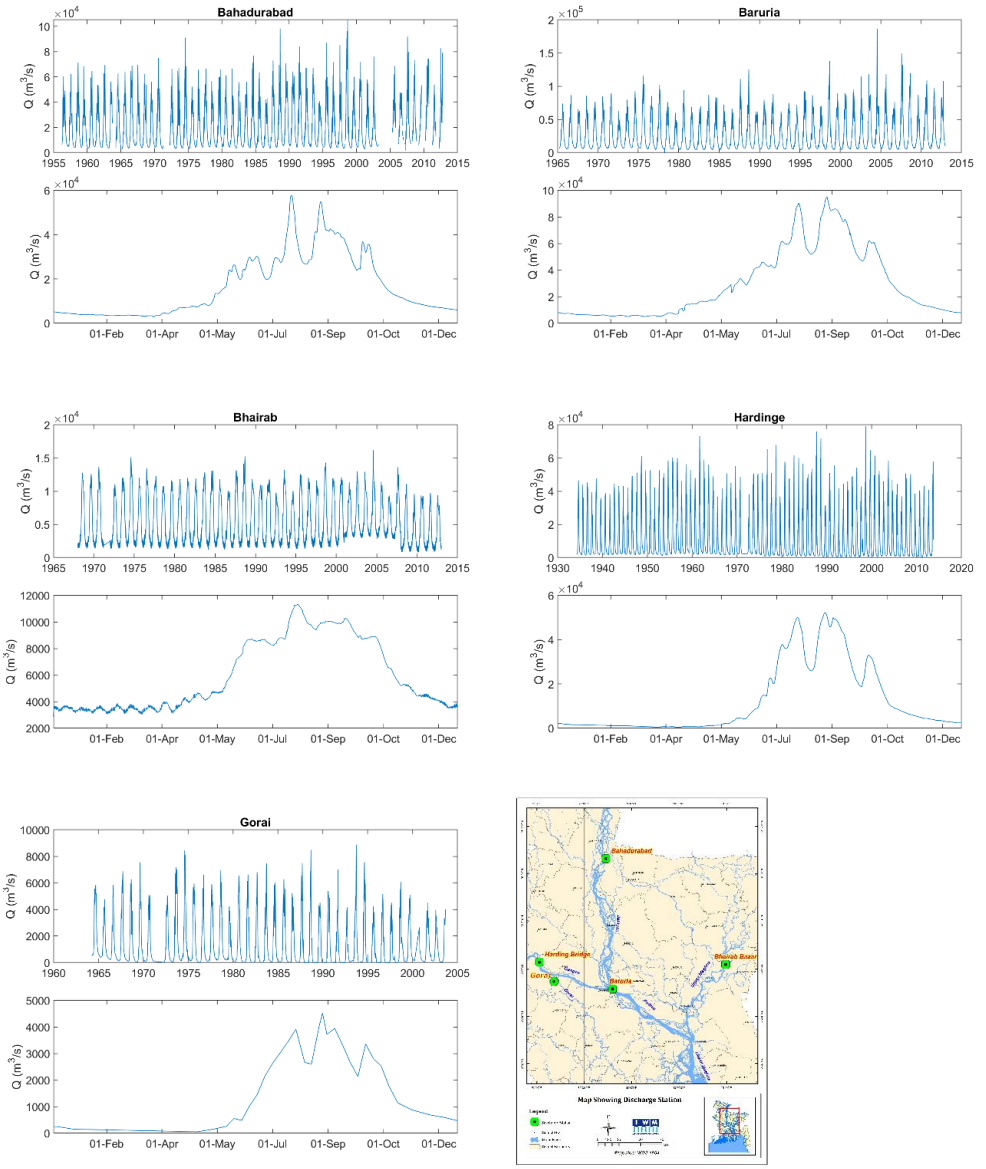

Figure 3.10 Time-series of discharge for all locations showing the complete time-series available (top) and a zoom-in of the year 2001 (bottom), and a map showing the locations of the stations.

3.3.3 Waves

Wave information was obtained in the offshore part of the Bay of Bengal (~20 m water depth) from the ERA5 re-analysis (Hersbach et al., 2020). Wave information is used in the morphological coastal model.

3.4 Meteorology

Wind and pressure field can be derived for the complete study area from global meteorological models. In this study the data from the ERA5 re-analysis (Hersbach et al., 2020) is used to acquire monthly spatially varying fields of wind velocity and direction, and pressure. The meteorological information is used in the morphological coastal model.

4 Development basin hydrology model (HydroTrend)

4.1 Introduction

The following sections describe the development and application of the basin hydrology (HydroTrend) model. First, a conceptual description of the governing equations is provided (Section 1.1). Second, the data sources used for model input are briefly described (Section 1.1). Third, the development of the model is shown by presenting the model setup (Section 1.1) and calibration procedure (Section 1.1). Finally, the model is applied for the current objectives (see Section 1.2.1) and results are discussed (Section 1.1).

4.2 Conceptual description

HydroTrend is an empirical model that provides suspended sediment estimates as a basin-averaged outflux. Therefore, it requires a thorough vetting of simulation results against real-world data. With careful validation the HydroTrend model has proven to be reliable in a variety of settings: smaller high sediment yield basins (Taiwan, New Zealand (Kettner et al., 2007)), complex continental-scale river basins (MacKenzie River), tropical basins with natural and intense deforestation and intensive land-use (Magdalena River (Kettner et al., 2010)) and many more.

The main processes captured in HydroTrend define a hydrological water balance. The model incorporates a budget of basin-wide rainfall (Q_r), snow (Q_n) and glacier ice melt (Q_{ice}), evapotranspiration (Q_{Ev}) and shallow groundwater contributions (Q_g), the sum of which controls water discharge at the river mouth (Q in m^3/s):

(2) $$Q = Qr + Qn + Qice – QEv \pm Qg$$

An empirical relationship originates from multiple regression analysis of a global dataset of >400 rivers comprising long-term water discharge and suspended sediment load (Syvitski and Milliman, 2008). Long-term suspended sediment load, Qs, is estimated at the river mouth (kg/s) for a basin with a mean annual temperature $T \geq 2°C$ as follows:

(3) $$Qs = \omega\, B\, Q^{0.31} A^{0.5} R\, T$$

Main controls of sediment flux include the drainage basin area, A (km^2) the total water discharge at the delta apex, Q (m^3/s), the basin relief R (m), and the basin-averaged mean annual temperature, T (°C). Additional impacts are captured in the B-factor, including the importance of lithology, L, reservoir trapping in the drainage basin, Te, and human controlled erosion and land-use practices, Eh:

(4) $$B = L\,(1 – Te)\,Eh$$

Daily suspended sediment load at the river mouth (kg/s) (Morehead et al., 2003):

(5) $$(Qs[i])\ /Qs) = \Psi[i]\,(Q[i] / Q)Ca$$

In which the Psi and C-factors accounts for individual daily measurement or modeled deviation off of the power function defined by a rating curve. This term thus introduces the day-to-day log-normal variability typically observed around a sediment rating curve. Data comparison in found that this daily variability, e.g. due to hysteresis over a flood season, is relatively modest in large basins. The factors

are empirically set based on basin geometry A, and climate (more detailed equations are listed in Morehead 2003).

Finally, daily bedload at the river mouth (kg/s) when $u \geq u_{cr}$:

(6) $$Qb[i] = (\rho s / \rho s - \rho) * (\rho\ g\ Q[i]\ \beta\ S\ eb) / (g \tan \lambda)$$

In this modified Bagnold equation, the bedload is modelled as dependent on the grain and water densities, the river water discharge at the modelled outlet of the basin Q (m^3/s) and the local channel reach slope S (-). The latter is importantly approximated from the slope of the digital elevation model at the delta apex, or specified if known from river bathymetric surveys.

4.3 Input data

Topographical information is extracted from the HydroSheds[9] DEM to specify each basin total area, hypsometry, slopes, river length and relief. HydroTrend defines a hydrological water balance by incorporating a budget of averaged basin-wide rainfall, snow and glacier ice melt, evapotranspiration and shallow groundwater contributions, the sum of which controls water discharge at the river mouth. Temperature and precipitation parameters are being derived from World Meteorological Organization (WMO) Climate Stations[10] and a variety of regional and global databases.

4.4 Model set-up

HydroTrend was set up to run simulations for the Ganges and Brahmaputra basins separately in order to incorporate each basins' unique properties into the present modelling exercise. The Meghna river is the only major tributary supplying additional water and sediment to the GBM system, but it was not included in the present analysis due to its negligible contribution to the GBM's total flow volume (~1%; (Coleman, 1969; Darby, 2015). Model setup and parameterization for this project were modified after Darby et al. (2015). The locations of the respective catchment outlets were designated at the Farakka Barrage (at 24.80°N 87.93°E) in eastern India for the Ganges, and at the confluence of the Jamuna (Brahmaputra) River with the Ganges in Bangladesh (at 23.82°N 89.75°E). These locations were chosen as they are considered key boundary nodes for simulating the influx of water and sediment from the main river channels into the GBM delta.

Three input files are required to run HydroTrend. The first input file is the main input file (HYDRO.IN), which describes general drainage basin properties and physical parameters. The main input file is also used to specify simulation time period and averaging interval (days in this case). Physical parameters requiring specification for the main input file include river base flow, glacier equilibrium line altitude and change per year, lapse rate to calculate freezing line, river basin length, and presence/absence of reservoirs. River length and floodplain gradient upstream of the basin outlets were derived from catchment DEMS using ArcGIS standard topographic data and catchment delineation tools (Darby et al., 2015). Lapse rate (°C/km), used to calculate daily temperatures in altitude bins, and initial equilibrium line altitude, the starting glacier equilibrium line altitude (m), were deemed identical for the two catchments. Their values were chosen with reference to the International Civil Aviation Organization standard and Ya-feng et al. (1980), respectively. Base flow for each catchment was calculated as the mean annual flow minima estimated from hydrological records for the gauging stations located at Hardinge Bridge (period of record 1973-1995) on the Ganges river and Bahadurabad Bridge (1973-1995) on the Brahmaputra river (Darby et al., 2015). The Farakka Barrage on the Ganges was the only significant large reservoir specified under "reservoir storage capacity" in the input file setup (Lehner et al., 2001, Lehner et al., 2011).

Hypsometric curves represent the topography of each of the respective drainage basins upstream of their catchment outlets and define the drainage areas. The second input file to the model describes

[9] https://www.hydrosheds.org/

[10] http://www.wmo.int/pages/prog/wcp/wcdmp/CON_3.php

this basin hypsometry (HYDRO0.HYPS). In this file, the total number of hypsometric bins are specified, followed by two columns containing values for altitude (m) and associated cumulative drainage area (km^2). This data represents the topography of the drainage basins upstream of their catchment outlets and define the drainage area encompassed within a series of elevation bins (spaced at 25 m intervals). The Advanced Spaceborne Thermal Emission and Reflection Radiometer (ASTER) Global Digital Elevation Model (GDEM) product was used to calculate and model the Ganges and Brahmaputra's hypsometric curves, while drainage basin area in each elevation bin was derived using the ArcGIS toolbox (following Darby et al., 2015).

The third input file contains climate data (HYDRO.CLIMATE). This file specifies the number of rows of input values, followed by two columns containing total precipitation (mm) and average temperature (°C) data. Climate projections used for the present project were developed from five climate models: GFDL-ESM2M, HadGEM2, IPSL-CM5A, MIROC_ESM_CHEM, and NORESM-M. From each model, the climate data was gathered for the following three periods: reference scenario (time period 1951-2005), RCP4.5 global warming emission scenario (time period 2006-2099), and RCP8.5 global warming emission scenario (time period 2006-2099). The following time periods are considered: 1976-2006 (reference scenario), 2006-2035 (representative for the climate of the year 2020), 2026-2055 (representative for the climate of the year 2040), 2046-2075 (representative for the climate of the year 2060), and 2066-2095 (representative for the climate of the year 2080). Temporal resolution was set to one day (daily data).

The HydroTrend model is originally coded in C, but this version was made accessible through the Python Modelling Tool (pymt), an Open Source Python package developed by the Community Surface Dynamics Modelling System (CSDMS). The Jupyter Notebook application was used to run HydroTrend through the pymt package. Separate Jupyter notebooks were run for each 30-year simulation for each basin, emission scenario, climate model, and time period, for a total of 90 HydroTrend simulations. 30-year simulations were conducted over the period 1976-2099 rather than a single century-long simulation to prevent a timing offset associated with leap year, which cannot be resolved by HydroTrend itself. Output ASCII files were generated with daily data for each model run. A summary statistics csv file was also written for each model run, which computed statistics averaged over each simulation time period (30 years), allowing for easy data analysis and comparison between model runs.

4.5 Model calibration

4.5.1 Calibration approach

HydroTrend model outputs from the reference scenario (1976-2006) simulations were compared with observed records in order to calibrate and validate the HydroTrend model setup. Climate hindcast data from five climate models (GFDL-ESM2M, HadGEM2, IPSL-CM5A, MIROC_ESM_CHEM, and NORESM-M) were used to drive the reference scenario simulations. Observed data were provided by the Institute of Water Modelling (IWM). Observed records consist of water discharge values for the Ganges river at Hardinge Bridge and the Brahmaputra river at Bahadurabad. Rated discharge values were utilized for comparison with simulated values. Observed (rated) daily discharge values at Hardinge Bridge range from January 1934 to October 2004 and at Bahadurabad from January 1956 to July 2002.

The observed (rated) sediment load for the Ganges and Brahmaputra rivers were calculated using sediment-rating curves, since direct sediment measurements from the rivers are lacking. Sediment-rating curves from Higgins et al., 2018 were utilized. Curves were established using Ganges river water discharge data from Hardinge Bridge over the period 1980-1995 (Islam et al., 1999) and Brahmaputra river discharge data from Bahadurabad Gauging Station over the period 1989-1994 (Islam et al., 1999). The sediment-rating curve equation for the Ganges river is $Qs = 0.007 \times Q^{1.51}$ ($R^2 = 0.68$) and for the Brahmaputra river is $Qs = 0.005 \times Q^{1.56}$ ($R^2 = 0.78$), with units of kg/s for Qs and m^3/s for Q. The observed sediment record was not used extensively for calibration and validation purposes since this dataset does not encapsulate direct sediment measurements; however, the

observed sediment discharge record will be used for evaluating the timing of annual peak sediment discharge, which will be discussed in more detail in the following sections.

4.5.2 Results of reference scenario: Data-model comparison

Reference scenario (1976-2006) model outputs forced by five climate models (GFDL-ESM2M, HadGEM2, IPSL-CM5A, MIROC_ESM_CHEM, and NORESM-M) were compared with observed water discharge records from the Ganges and Brahmaputra rivers. Figure 4.1 portrays HydroTrend model performance by comparing mean and maximum simulated water discharge values with observed records. Overall, HydroTrend simulated mean water discharge well for both rivers. Percent error between observed and simulated values for mean water discharge for the Ganges river ranged from 1.8% (MIROC-ESM-CHEM) to 29.5% (IPSL_CM5A). The largest water discharge that was simulated during each 30-yearlong model run is hereby referred to as the maximum water discharge. Percent error for maximum water discharge ranged between 28.1% (MIROC-ESM-CHEM) and 149.2% (IPSL_CM5A). For the Brahmaputra river, mean water discharge ranged from -7.1% (MIROC-ESM-CHEM) to -12.5% (HadGEM2). Percent error for maximum water discharge ranged between -0.2% (HadGEM2) and 16.7% (IPSL_CM5A).

Observed and simulated mean annual daily discharge were also assessed to see how well HydroTrend simulated the rivers' hydrographs over the reference scenario (Figure 4.2). HydroTrend performed well in this regard considering the reduced complexity of this model, particularly in simulating the Brahmaputra rivers' annual flow regime (Figure 4.2B). The averaging interval was trimmed by 2 and 4 years for the Ganges and Brahmaputra rivers, respectively, depending on the comprehensiveness of the observed discharge record. Table 4.1 reports how the timing of peak flow compares to observed and simulated values over the reference scenario. Differences in timing are to be expected for a basin-averaged precipitation in a 1D model. First, timing may be inaccurate because precipitation is not uniformly distributed throughout the basin and the timing of monsoonal arrival may already be off in the primary climate simulations. This is illustrated by the fact that the different models have different delays (Table 4.1) Then, the basin-wide 1D model takes into account a lag between input precipitation and arrival of high discharge for long rivers (approximated by a simplified shockwave dampening approach). In reality there could be distinct spatial variations in delay of the river runoff routing due to for example irrigation management or reservoir storage at the small farm pond scale, thus timing at the daily timescale can be complex to resolve. Simulations are calibrated to optimize to capture the peak discharge instead of the most accurate timing. This strategy was deliberately chosen to most accurately represent peak input flow dynamics and peak potential sediment transport characteristics for the macroscale model, but it compromises some of the precision in timing of daily predictions.

Finally, observed and simulated mean annual water discharge data were assessed to complete the model-data comparison. The purpose of this task was to investigate how mean water discharge varied in reality, compared to simulated discharge. Figure 4.3 portrays mean annual water discharge from the five climate-model-hindcasts compared with observed discharge records over the reference scenario. The Ganges and Brahmaputra basins show different trends in inter-annual variability of water discharge for both modelled and observed data (Figure 4.3). For the Ganges basin, the model results illustrate large inter-annual variabilities compared to observed discharge. The IPSL-CM5A model generated about twice as much variability than the other four models. In addition, between the other four models, variability is larger than the observed differences in annual mean water discharge. Hence, the IPSL-CM5A model is an outlier with respect to water discharge, which is largely controlled by its predictions of annual and monsoonal rainfall. The IPSL-CM5A model shows outliers on both the high and low ends of water discharge (Figure 4.3A).

The large differences in inter-annual variability between climate models are not consistent over the entire GBM basin. For example, in Figure 4.3B, the modelled discharge in the Brahmaputra basin shows similar intra-annual variability to the observed water discharge record. Also, the variation from

the mean in the Brahmaputra basin is less than the variation from the mean in the Ganges basin – especially for the IPSL-CM5A model. This can be explained by the fact that mean annual precipitation is lower in the western part of the GBM basin, where the Ganges basin is located. In turn, the variation in the Ganges basin is substantially larger than the variation in the Brahmaputra basin, which is located in the eastern part of the GBM basin. This discussion is supported by takeaways from Section 4.3 of the Climate Change Scenarios report (Deliverable D-4D).

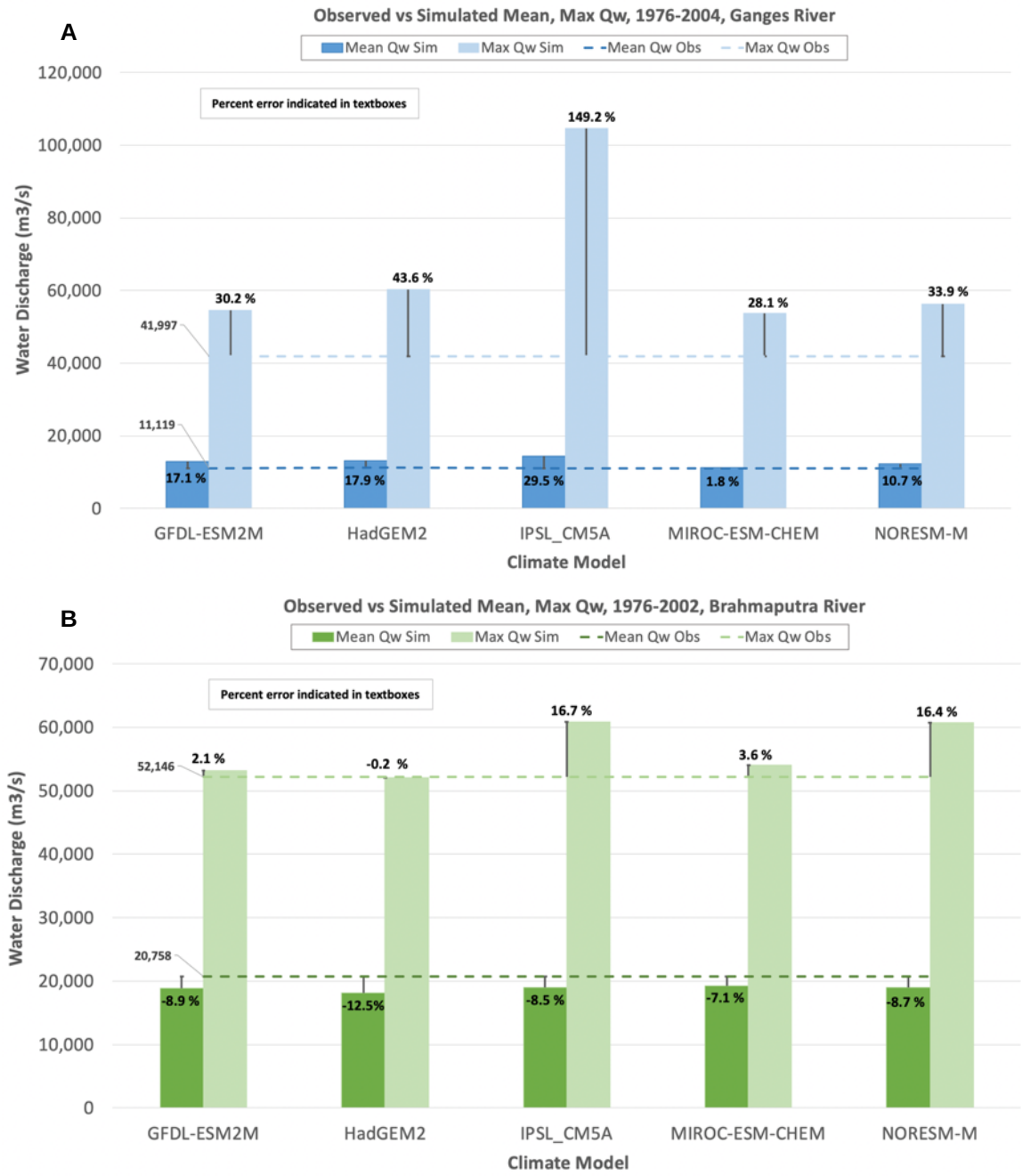

Figure 4.1 Observed vs. simulated mean and maximum water discharge for the A) Ganges river and B) Brahmaputra river. Percent error values are written as percentages next to error bars. Average and maximum observed water discharge are written to the left of the dotted lines and are reported in units of m3/s.

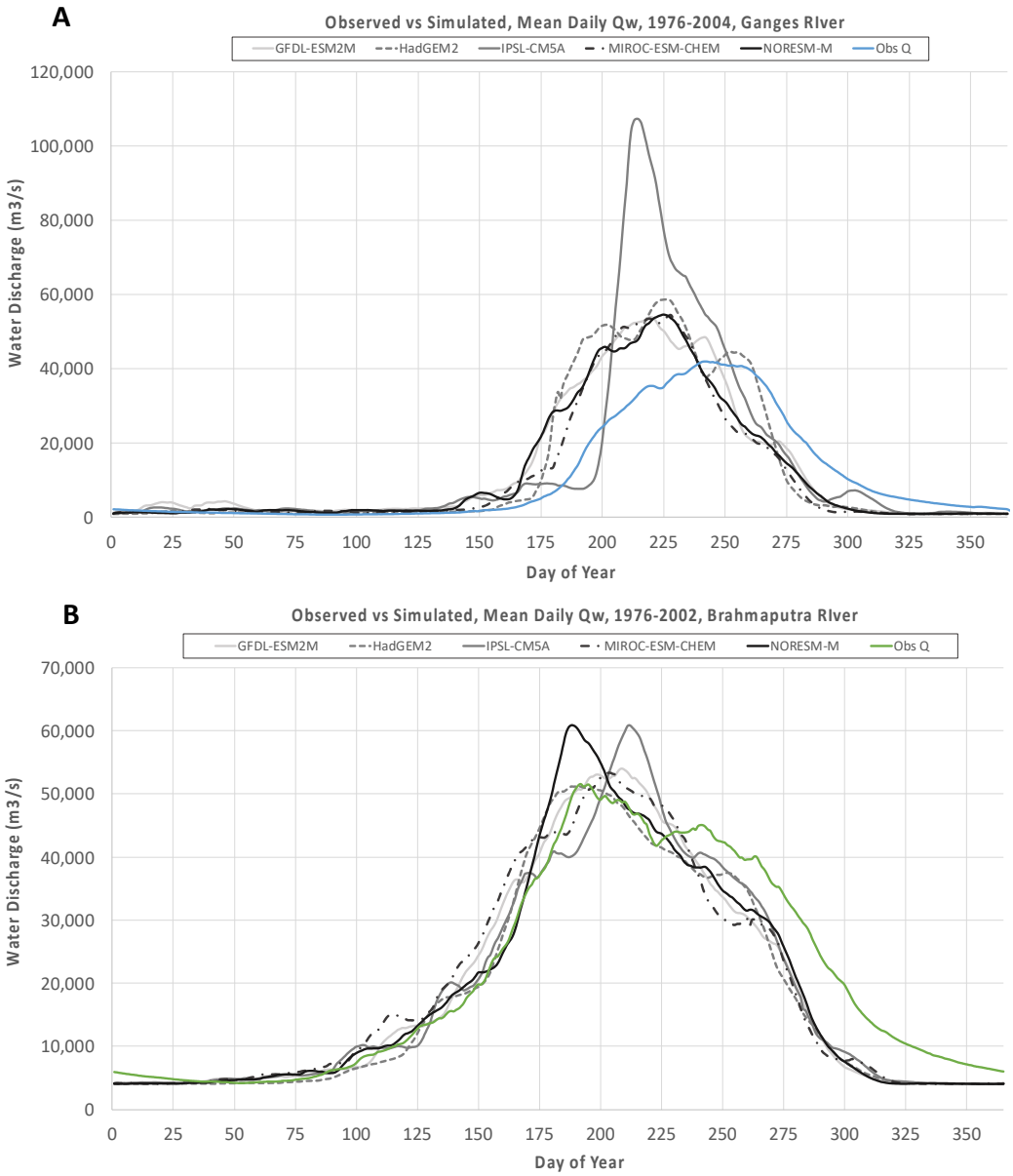

Figure 4.2 Observed vs. simulated mean annual daily water discharge for the A) Ganges river and B) Brahmaputra river. Discharge data were trimmed from the initial reference time period of 1976-2006 to 1976-2004 for the Ganges and 2002 for the Brahmaputra, since the observed discharge records were missing a considerable number of values at the tail end of their respective records.

Table 4.1 A comparison of the timing of peak flow between observed and simulated records averaged over the reference scenario (1976-2006) for the Ganges and Brahmaputra rivers. Values are reported as days of the calendar year (Julien day). The "difference" column represents the difference, in days, between observed and simulated peak flow. A positive difference indicates that simulated timing of peak flow occurred later in time than was observed, and a negative difference indicates that peak flow occurred earlier in time than was observed.

Day of Year of Peak Qw						
	Brahmaputra			**Ganges**		
Climate Model	**Observed**	**Simulated**	**Difference**	**Observed**	**Simulated**	**Difference**
GFDL-ESM2M	200	200	0	244	220	+24
HadGEM2	200	192	+8	244	227	+17
IPSL_CM5A	200	214	-14	244	216	+28
MIROC-ESM-CHEM	200	206	-6	244	227	+17
NORESM-M	200	190	+10	244	228	+16
Day of Year of Peak Qs						
GFDL-ESM2M	200	202	-2	259	217	+42
HadGEM2	200	184	+16	259	228	+31
IPSL_CM5A	200	213	-13	259	217	+42
MIROC-ESM-CHEM	200	203	-3	259	228	+31
NORESM-M	200	201	-1	259	217	+42

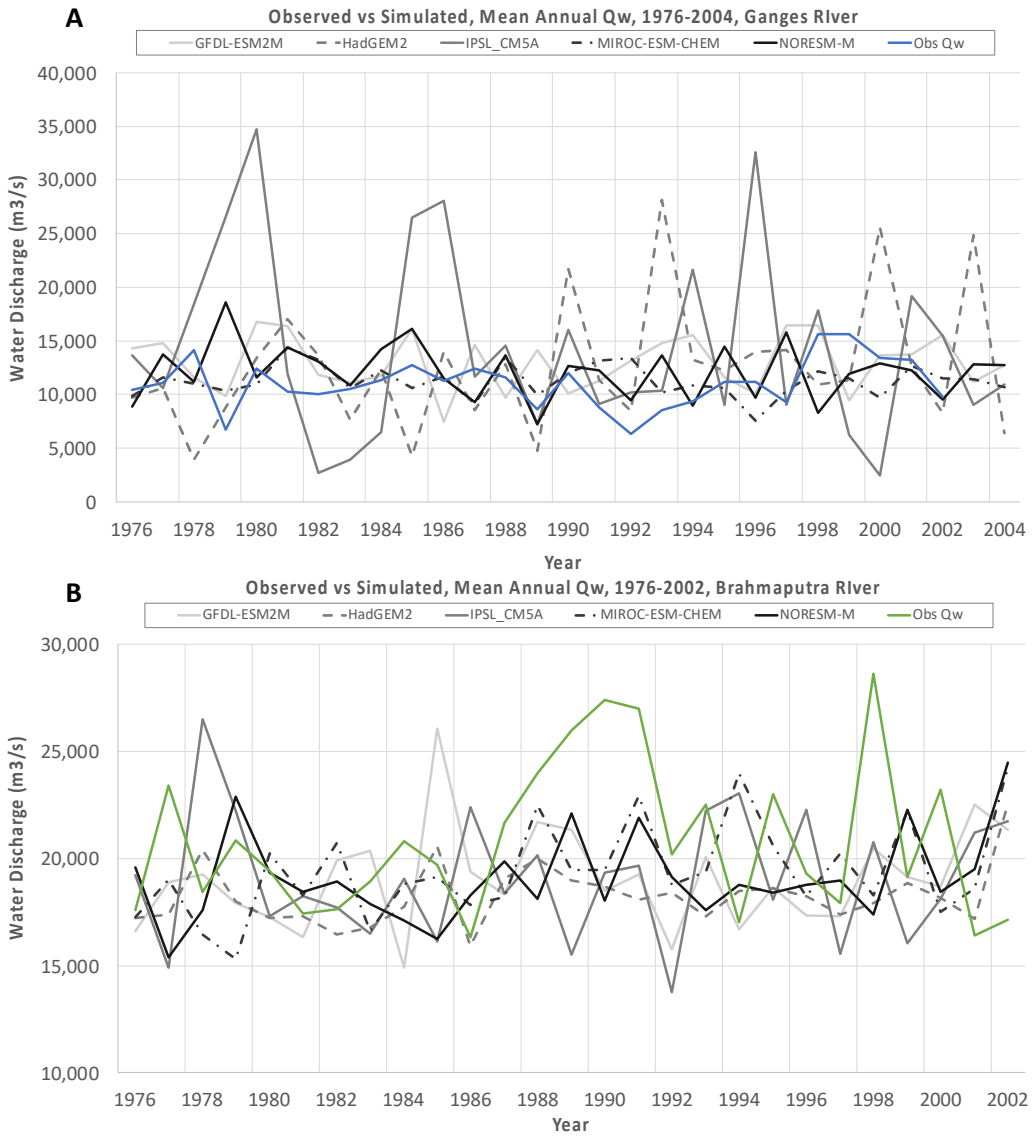

Figure 4.3 Observed vs. simulated mean annual water discharge, averaged over the reference scenario time period of 1976-2004 for the Ganges River (A) and 1976-2002 for the Brahmaputra River (B).

4.6 Results

The HydroTrend model has been run for the Ganges and Brahmaputra rivers for the time period from 1976-2099 for the two global climate change scenarios, RCP4.5 and RCP8.5. Hence, this section evaluates potential changes in water and sediment discharge in the Ganges and Brahmaputra basins due to predicted future climate change scenarios. The results are presented per basin in the following chapters.

4.6.1 Ganges basin

HydroTrend model results for the Ganges basin (Figure 4.4 and TableApx A.1) show both water discharge and sediment discharge increasing in the Ganges river from 1976-2099. Mean water discharge (averaged across all climate models) for the RCP4.5 emission scenario increased by 37% over the simulation, while mean sediment discharge increased by 29%. For the RCP8.5 emission scenario, mean water discharge increased by 46% and sediment discharge increased by 45%. Bedload discharge also increased over the simulation time period by 37% (RCP4.5) and 46%

(RCP8.5) (Details are listed in). Suspended sediment concentration increases less dramatically, with a percent increase of 17% (RCP4.5) and 3% (RCP8.5). portrays average simulated water discharge, sediment discharge, bedload discharge, and suspended sediment concentration as average values over the time periods representative of the years 2020, 2040, 2060, and 2080. Climate hindcasts from the reference scenario are also included in the line plots to amplify trends and to extend the analysis timeframe. Simulated values averaged over each time period are also reported numerically in . Percent change calculations reported were calculated by subtracting the statistic/value from the year 2000 statistic/value by the year 2080 statistic/value, dividing by the year 2000 statistic/value, and multiplying by 100; this simple calculation illustrates how discharge and other parameters changed from the reference time period (1976-2006) to the end of 20th century time period (2066-2099) of the simulation timeframe.

Maximum annual water discharge (peak flow) shifted earlier in time in the Ganges river as the simulations progressed through time. For example, the MIROC-ESM-CHEM climate model under the RCP4.5 emission scenario generated a peak flow on the 227th day of the year in 2020, whereas peak flow occurred on the 202nd day of the year in 2080, equivalent to a 25-day shift earlier in time (nearly a month). Averaged across climate models, peak flow occurred earlier in time in the Ganges basin by 3% and 5% for RCP4.5 and RCP8.5, which is equivalent to 12 and 17 days, respectively.

4.6.2 Brahmaputra basin

Similar to the Ganges basin, model results for the Brahmaputra basin (Figure 4.5 and TableApx A.2) show both water discharge and sediment discharge in the Brahmaputra river increasing from 1976-2099. Mean water discharge (averaged across all climate models) for the RCP4.5 emission scenario increased by 21% over the simulation time period, while mean sediment discharge increased by 52%. For the RCP8.5 emission scenario, mean water discharge increased by 29% and mean sediment discharge increased drastically by 88%. Bedload discharge also increased over the simulation time period by 21% (RCP4.5) and 29% (RCP8.5). Finally, suspended sediment concentration increased by 15% (RCP4.5) and 16% (RCP8.5). shows average simulated water discharge, sediment discharge, bedload discharge, suspended sediment concentration as averaged values representative of the years 2020, 2040, 2060, and 2080. Climate hindcasts from the reference scenario were included in the line plots to amplify trends and to extend the analysis timeframe. Simulated values averaged over each time period are also numerically reported in .

Maximum annual water discharge (peak flow) shifted earlier in time in the Brahmaputra river under the RCP8.5 emission scenario but did not shift significantly for the RCP4.5 scenario. The day of peak flow for the RCP4.5 scenario (averaged across climate models) shifted slightly later in time with a percent change of 0.2%, equivalent to ¾ of a day. Contrastingly, for the RCP8.5 emission scenario, peak flow shifted earlier in time by 4%, equivalent to 14 days.

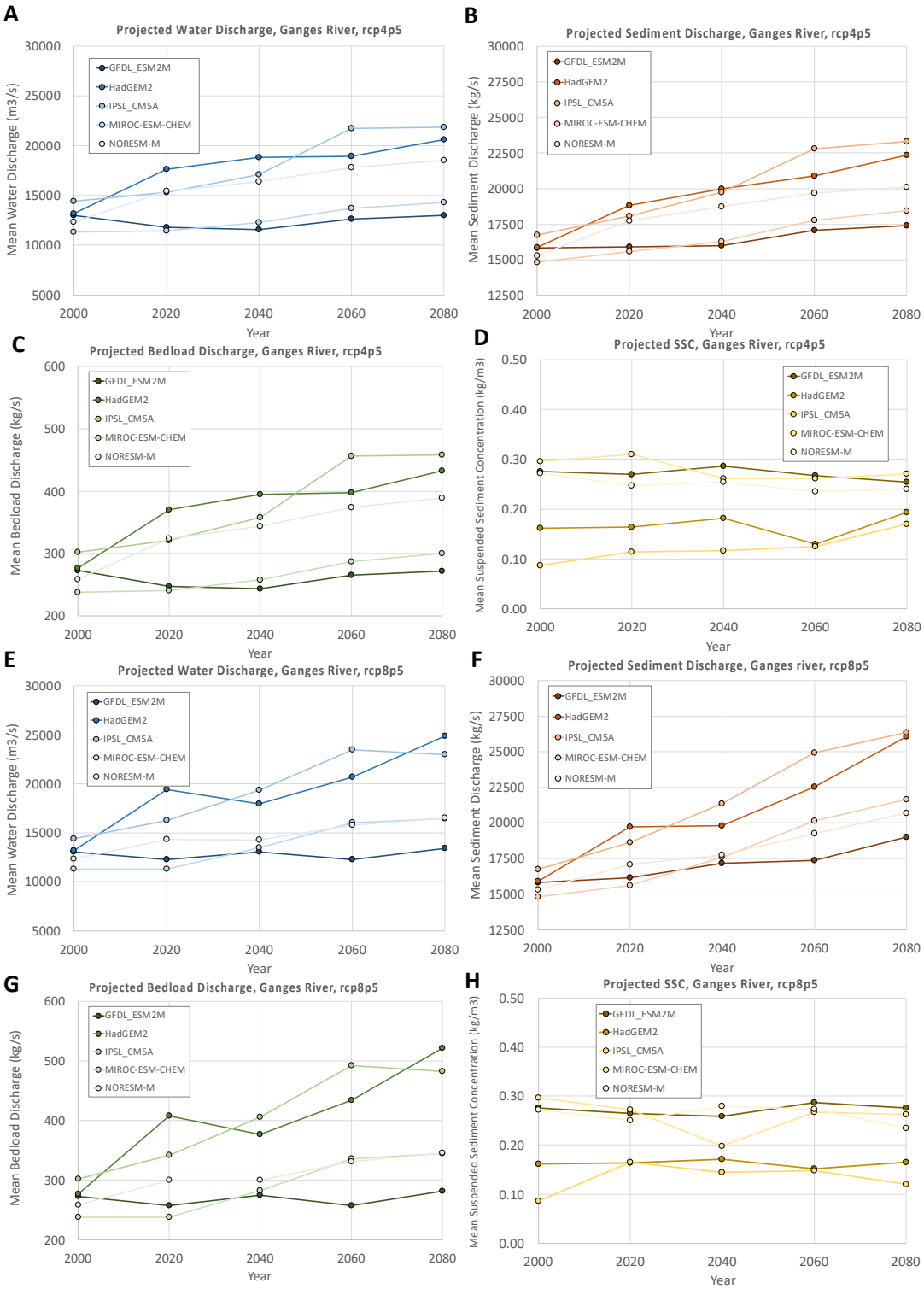

Figure 4.4 Projected water discharge, sediment discharge, bedload discharge, and suspended sediment concentration for the Ganges river driven by climate representative of the years 2020, 2040, 2060, and 2080 under the RCP4.5 emission scenario (A-D) and RCP8.5 emission scenario (E-H). Data for the reference scenario representative of the year 2000 are included in the line plots to amplify trends and to extend the analysis timeframe.

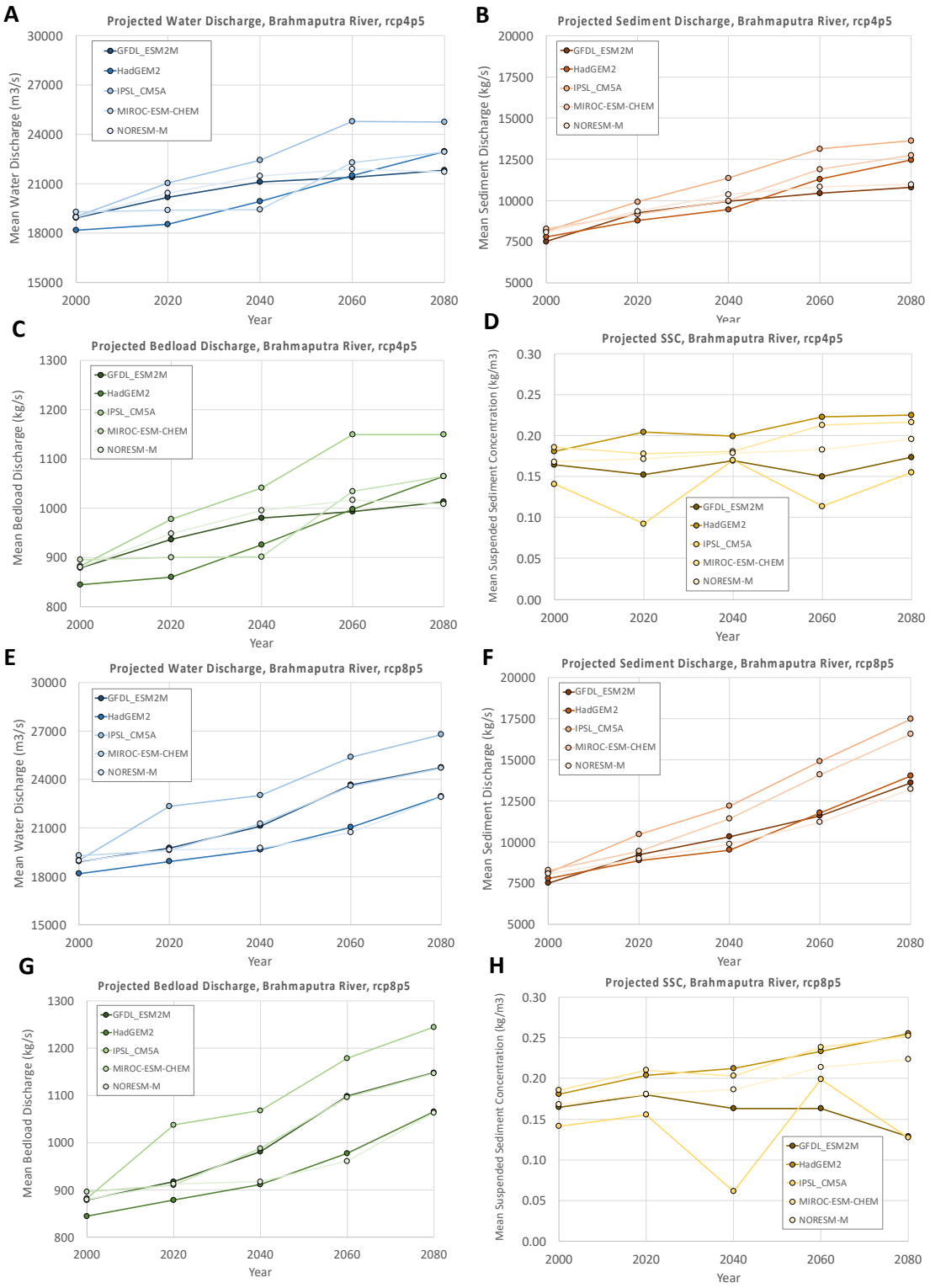

Figure 4.5 Projected water discharge, sediment discharge, bedload discharge, and suspended sediment concentration for the Brahmaputra River driven by climate representative of the years 2020, 2040, 2060, and 2080 under the RCP4.5 emission scenario (A-D) and RCP8.5 emission scenario (E-H). Climate hindcasts for the reference scenario representative of the year 2000 are included in the line plots to amplify trends and to extend the analysis timeframe.

4.6.3 Comparison with existing GBM sediment load observations and estimates

The simulated results shown in and TableApx A.2 and TableApx A.2, and presented visually in Figure 4.4 and Figure 4.5, allow for the calculation of annual sediment discharge for the Ganges and Brahmaputra basins. In this section, only sediment discharge calculated over the reference scenario (1976-2006) is reported, since simulated data over this time period can be directly compared with observations. The HydroTrend simulations, averaged over the five climate models, simulated an annual sediment discharge of 496 MT/year for the Ganges basin and 251 MT/year for the Brahmaputra basin. Together, these values sum up to 747 MT/year for the entire GBM basin.

The simulated sediment discharge for the Ganges basin is close to values predicted from previous work. The current report (Chapter 2) presents an annual sediment discharge for the Ganges basin of 550 MT/year, which is close to the 496 MT/year that the HydroTrend model runs estimated. However, the simulated annual sediment discharge for the Brahmaputra basin is much lower than has been previously estimated in past work. In this report, annual sediment discharge for the Brahmaputra basin is documented at 590 MT/year, which is more than twice as much as HydroTrend simulated in the present modeling exercise, which estimates an annual sediment discharge of 251 MT/year.

The underestimation of sediment discharge at the Brahmaputra basin outlet can be explained by a few possible reasons. First, large uncertainties in the hindcasted precipitation data exist, which in turn produces a large uncertainty in the sediment load estimates. Another potential explanation is that previous work overestimated the annual sediment discharge in the Brahmaputra river. This is possible since sediment discharge estimates for the Brahmaputra basin are not commonly found in the literature, and among previously published work, estimates for annual sediment discharge are highly variable. Future work will attempt to better constrain the sediment discharge in the Brahmaputra basin, both through detailed observations and modeling efforts. The figure below (Figure 4.6) places the presently estimated annual sediment discharge values for the Ganges and Brahmaputra basins in the context of previous estimations.

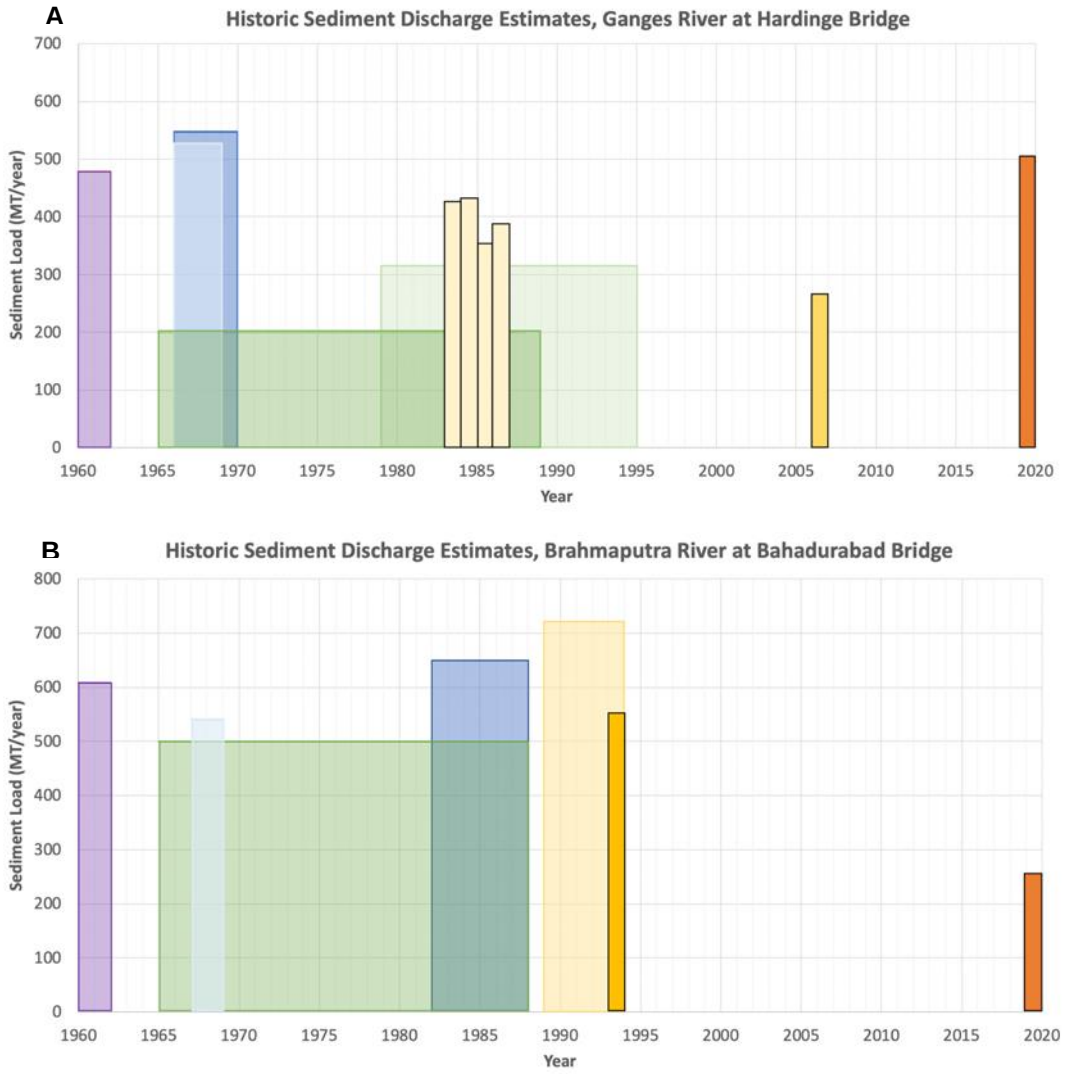

Figure 4.6. Historic annual sediment discharge estimates from published work. A) Ganges river evaluated at Hardinge Bridge, and B) Brahmaputra river evaluated at Bahadurabad Bridge. References from left to right (A): Coleman, 1969 (purple); FAP24, 1996 (dark blue); BWDB, 1972, in Islam et al., 1999 (light blue); Islam et al., 1999 (dark green); CBJET, 1991 (light green); Hossain, 1992 (yellow); Rice, 2010 (dark yellow), present study (orangey red). References from left to right (B): Coleman, 1969 (purple); CBJET, 1991 (green); BWDB, 1972, in Islam et al., 1999 (light blue); Hossain, 1992 (dark blue); Islam et al., 1999 (light yellow); Kabir and Ahmed, 1996 (dark yellow); present study (orangey red).

5 Development river model (Delft3D-FM 1D)

5.1 Introduction

The following sections of this chapter discuss all aspect of the development of the river branch model. The model set-up is discussed in Section 5.2 through Section 5.8. The procedure can roughly be summarized as:

- Setting up a numerical network that covers the most important river branches of the GBM delta
- Constructing cross-sectional profiles to give a proper representation of the dimensions of the channels
- Imposing boundary conditions of hydrodynamics and sediment input

Subsequently hydrodynamic calibration of the model is shown in Section 5.9 and the validity of the derived sediment balance is discussed in Section 5.10.

5.2 Numerical network

The numerical domain of Delft3D-FM consists of a fully unstructured network (Kernkamp et al., 2011). In the 1D (alpha release) mode the network can be expressed as a set of converging and diverging lines, representing for example river branches including confluences and bifurcations. In Figure 5.1 a schematic diagram of a simplified 1D numerical network is shown. The physical properties (e.g. bed level, water depth) are specified and calculated at the net nodes of the network, which are linked through 1D net links (connections) with a uniform spatial discretization. The net links that are located between net nodes joining more than two net links (a junction) make up a (river) branch. The cross-sectional area and base level at the net nodes is specified by user-defined profiles. To reduce the required input, these profiles do not have to be specified for each net node in a network. The cross-sectional area and base level are interpolated (between profiles) or duplicated (between a profile and junction) from neighbouring profiles within a single branch. In the default case, interpolation is not continued along connecting branches at a junction (net link code = 1). However, the user can continue the interpolation (net link code = 6) along a junction so that the cross-sectional profile and base level change smoothly over the course of the main branch (e.g. in case of a confluence of a large and a smaller river). In the model set-up of the 1D GBM delta model, both these options will be used.

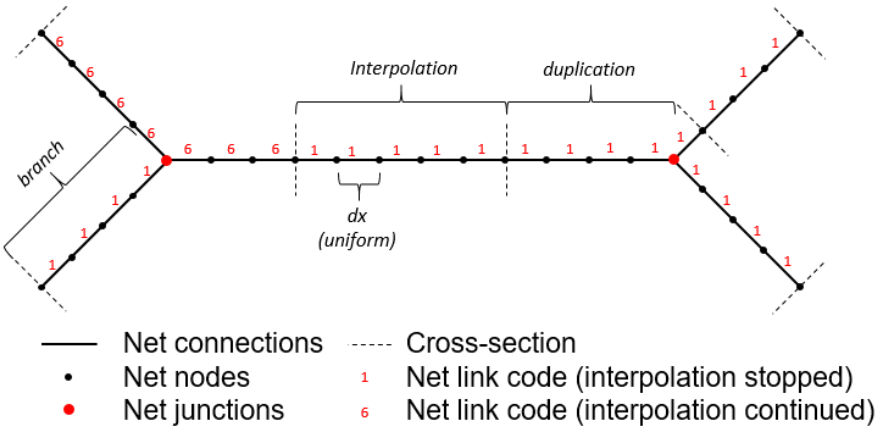

Figure 5.1 Interpolation scheme of the Delft3D-FM 1D model.

The GBM delta is schematized in a 1D network from the upstream part of the three major rivers (Ganges, Brahmaputra, and Meghna) up to the seaward limit of the major estuaries (Arpangachi, Pussur, Baleshawr, Bishkali, Burishawr, Galachipa, Tetulia, Sahpazpur, and the main branch of the

Lower Meghna). The network is schematized using GIS software and the choice for the extent of the model (i.e. which branches to include) is based on experience and local knowledge (pers. comm. IWM). The schematization is converted to a numerical network suitable for the modelling suite using the embedded RGFGRID tools. In this procedure a spatial discretization of 1500 m is used for the spatially uniform distance between net nodes. The spatial interval is chosen as a compromise between accuracy of the river branch geometries and computational efficiency. The network is shown with the names of the rivers in Figure 5.2.

Properties of the numerical network are shown in Table 5.1. Although Delft3D-FM calculates a maximum allowed computational time step during the simulation based on the Courant-Friedrichs-Lewy (CFL) number, a couple of other time steps need to be set and are network (grid) dependent. The initial time step (dtini) specifies the time step for the very first computational step which is needed because no model results are available yet to calculate the CFL conditions (this value should be small). The user time step (dtuser) specifies the time step used for updating the boundary conditions, and the maximum time step (dtmax) specifies a maximum limit during the simulation (irrespective of CFL conditions).

Table 5.1 Parameters of the 1D GBM model network.

Property	**Values**
Coordinate system	Bangladesh Transverse Mercator (BTM)
Extent of domain	x_1 = 276017, y_1 = 448780 x_2 = 807850, y_2 = 696230
Vertical datum	Public Works Datum (PWD)
Number of net nodes	2108
dx	1500 m
dt_{ini}	1 s
dt_{user}	30 s
dt_{max}	30 s

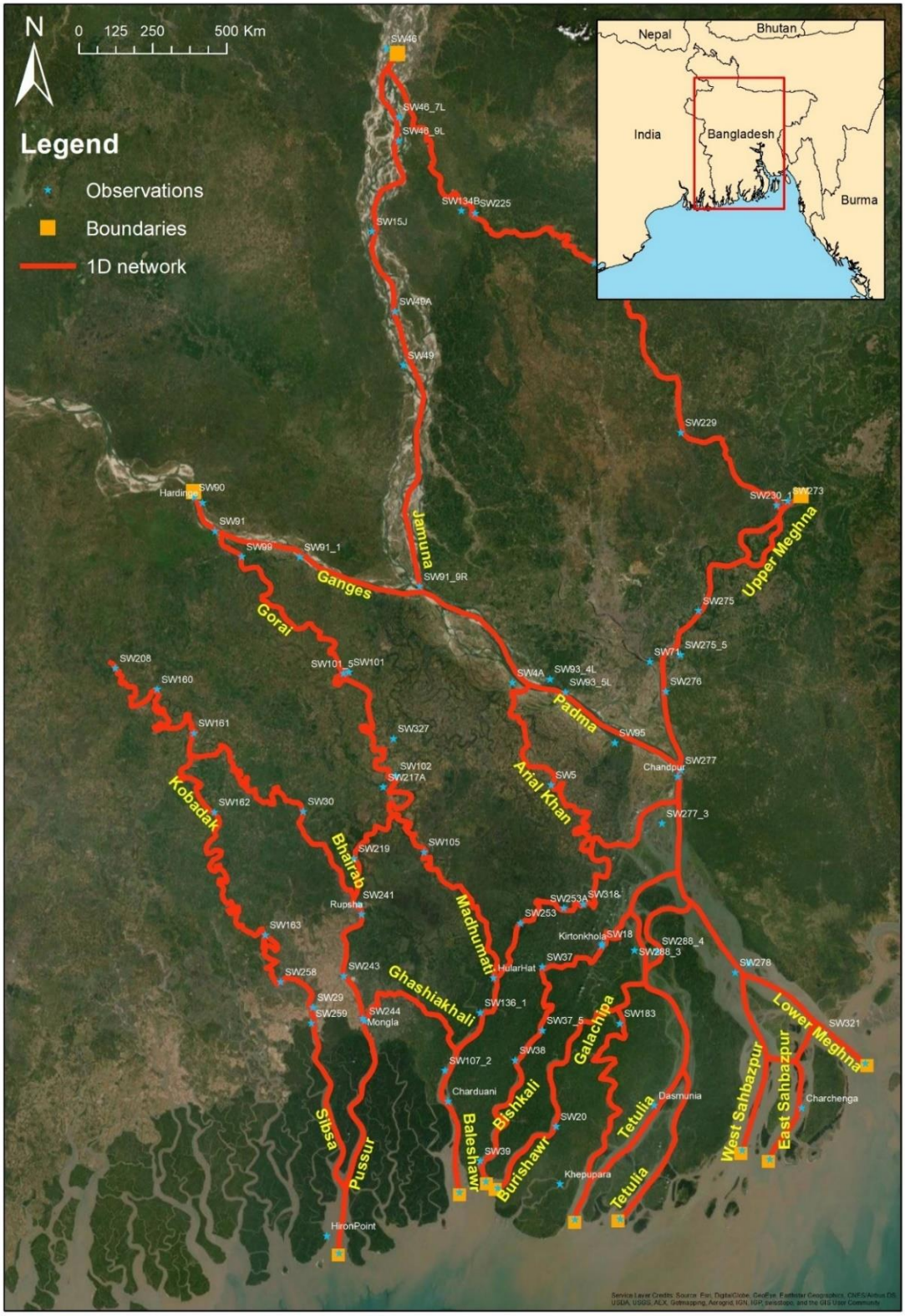

Figure 5.2 Schematization of the major river branches in a network for the 1D GBM model, including locations where boundary conditions are forces and observation points used for model-data comparison.

5.3 Cross-sectional profiles

5.3.1 Bathymetric dataset

The 1D GBM model covers a vast area of the Bangladeshi part of the delta, and as such, an extensive dataset of bathymetric measurements is used to define the cross-sectional profiles. The data is described in Section 3.2.1.

5.3.2 Profile types

In Delft3D-FM 1D (river branch) models the cross-sectional area and base level in the model environment are provided by the geometry of profiles specified at branches in the network. The cross-sectional profiles can be schematised and prescribed to the model in different ways. In all cases it is essential to know that a 1D model uses the model input to calculate storage and conveyance. The storage width is represented by the total width at the water surface, and the conveyance is represented by two parameters, viz. the flow-carrying cross-sectional area and the hydraulic radius:

(7) $$R = A/P$$

Here, *A* is the flow-carrying cross-sectional area and *P* is the wetted perimeter. This means that any way of schematisation of the cross-sectional profiles can be used as long as these parameters are correctly represented. It should further be noted that these parameters vary spatially (along a branch) and temporarily (with the varying water level due to tidal motion or river discharge variation). Thus, the specified cross-sectional profiles for a branch in the river network need to represent the variations in these parameters along the branch at any possible water level.

In this study two alternative types of profiles are used:

- Measured
- Hybrid (schematized from bathymetric observations)

5.3.3 Measured profiles

The model set-up with measured profiles uses the most recent dataset of each river if the spatial coverage of this dataset is sufficient, otherwise an older dataset is used. The selection of the profiles is done using GIS software and the shapefiles of the datasets, shown in Figure 5.2. The original profiles filtered out of the datasets consist of very high-resolution data (i.e. several measurements in one-meter length). Forcing the model with such an enormous amount of data is unnecessary. The spatial resolution of the profiles is therefore reduced to a 10 m resolution for profile with widths less than 500 m and 50 m resolution for profiles with widths more than 500 m. Showing figures of all profiles would be excessive, therefore a few examples are shown in Figure 5.3.

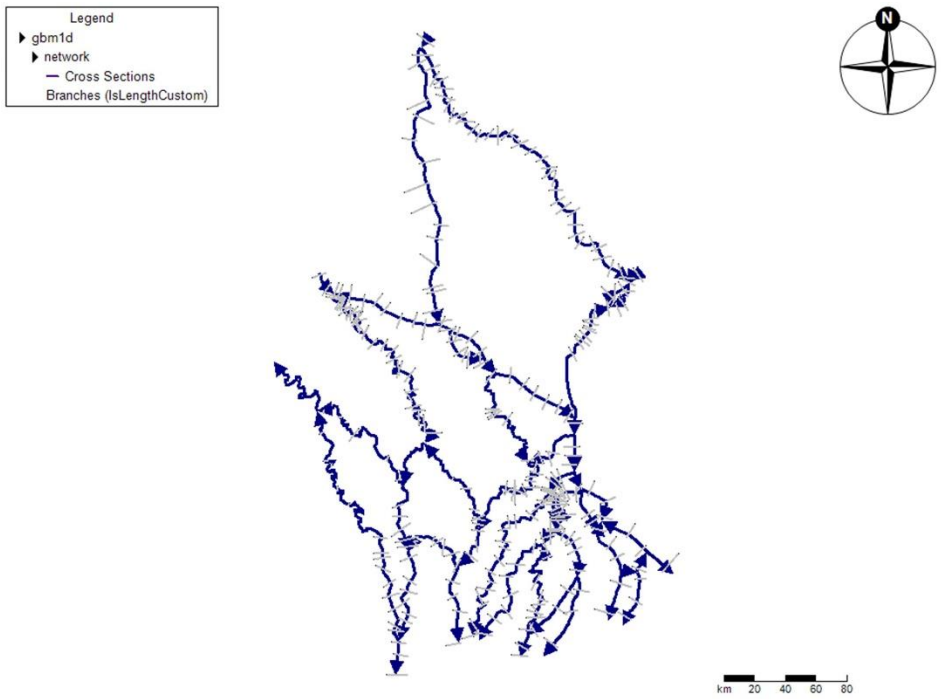

Figure 5.2 Map showing the selection of measured profiles.

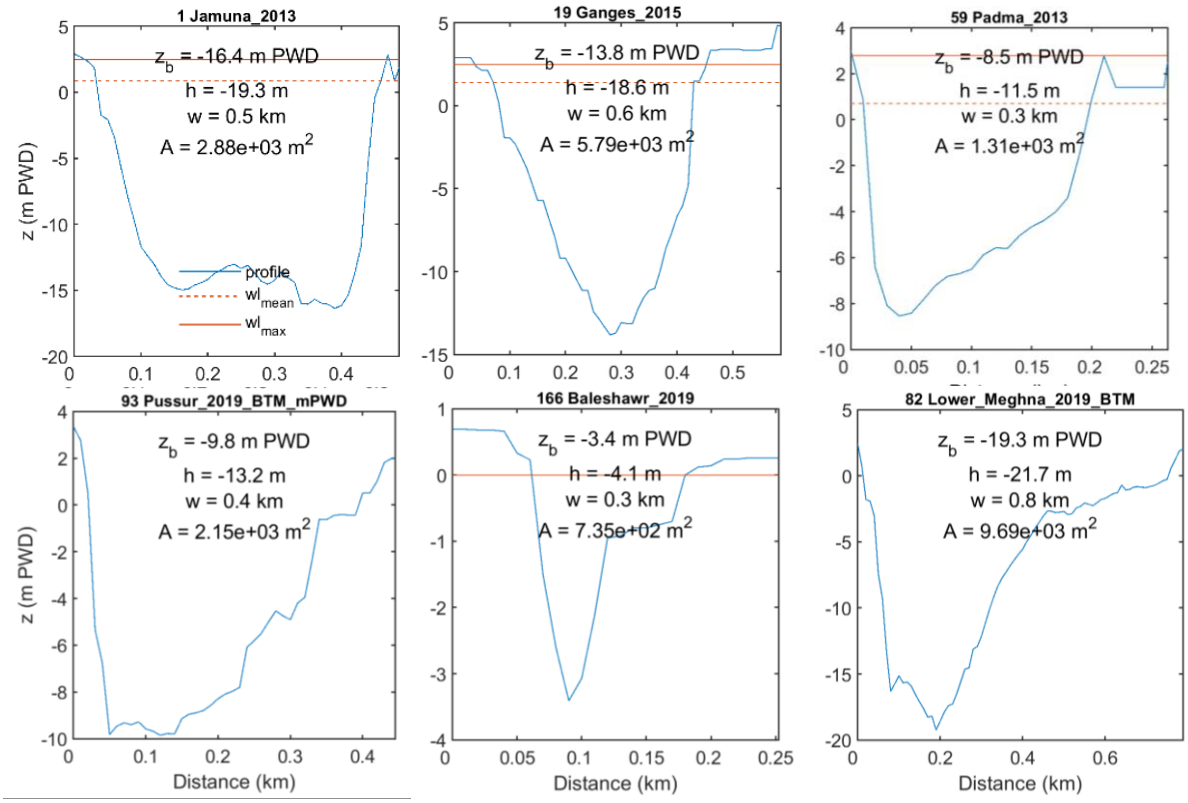

Figure 5.3 Examples of a few selected profiles (dataset shown in figure titles).

5.3.4 Hybrid profiles

The model set-up with hybrid profiles has the advantage over the measured profiles that the measurements of several profiles (in time as well in space) can be used to derive a characteristic cross-sectional profile for a section of a river branch. The hybrid profiles are constructed from subsets of the bathymetric dataset. The selection of the subsets is done by (manually defined) polygons that cover a part of a river branch (Figure 5.4). The size of the polygons depends on the change in geometric properties of the river and data availability. The size should not be too small as the geometry of the constructed 'characteristic' profile will resemble the geometry of an actual observed profile (reducing the advantage of the schematization) and not too large as longitudinal variations will be discarded.

The subsets of the bathymetric dataset are used to create a tightly fitting polygon on the data (inner polygon in Figure 5.5). This polygon is used to set-up a local mesh grid where the values of the grid cells are determined by the median of all samples that fall within a grid cell. From the gridded dataset the following properties are calculated:

- The total area of grid cells that contain data,
- The distribution in elevation (histogram) of the subset of the data.

Grid cells with no data coverage are not taken into account. The distribution in elevation is schematized by establishing a probability density histogram (Figure 5.6a) on the height level of the gridded topo-bathymetric observations (the width of the bins is determined via an automated algorithm). Subsequently, a hypsometric curve is established based on the total area of the grid cells and the values of the binned dataset of elevation (Figure 5.6b).

To set-up a schematized profile, the width of the river should be known as well. In other (e.g. SOBEK) type of 1D river branch models this is an easy procedure as the length of a river branch is known from the model architecture. Because the Delft3D-FM 1D model network is fully unstructured, this quantity is hard to derive, and the river width is therefore inserted as manual input for each manually defined polygon. With the information on the width of the river section and the hypsometric curve, a characteristic and symmetric profile can be established (Figure 5.6c). Finally this profile is defined in x,y,z coordinates and positioned at the net node closest to the centre of the boundary fitted polygon (Figure 5.6d).

The result of the schematization is shown for all polygons in Appendix B, shown as the established hypsometric curves (FigureApx B.1 - FigureApx B.8). The validity (correctness) of the schematization procedure is studied by comparing the morphological characteristics of the river from the hybrid profiles with respect to these properties derived directly from the observed profiles (Figure 5.7). The figure shows that mean and maximum bed level of the hybrid profiles compare very well to the observed profiles (Figure 5.7c), both for a tidal and non-tidal river. The width is manually inserted and, therefore logically, compares well to the data as well, leading to a proper presentation of the cross-sectional area in the schematized profiles.

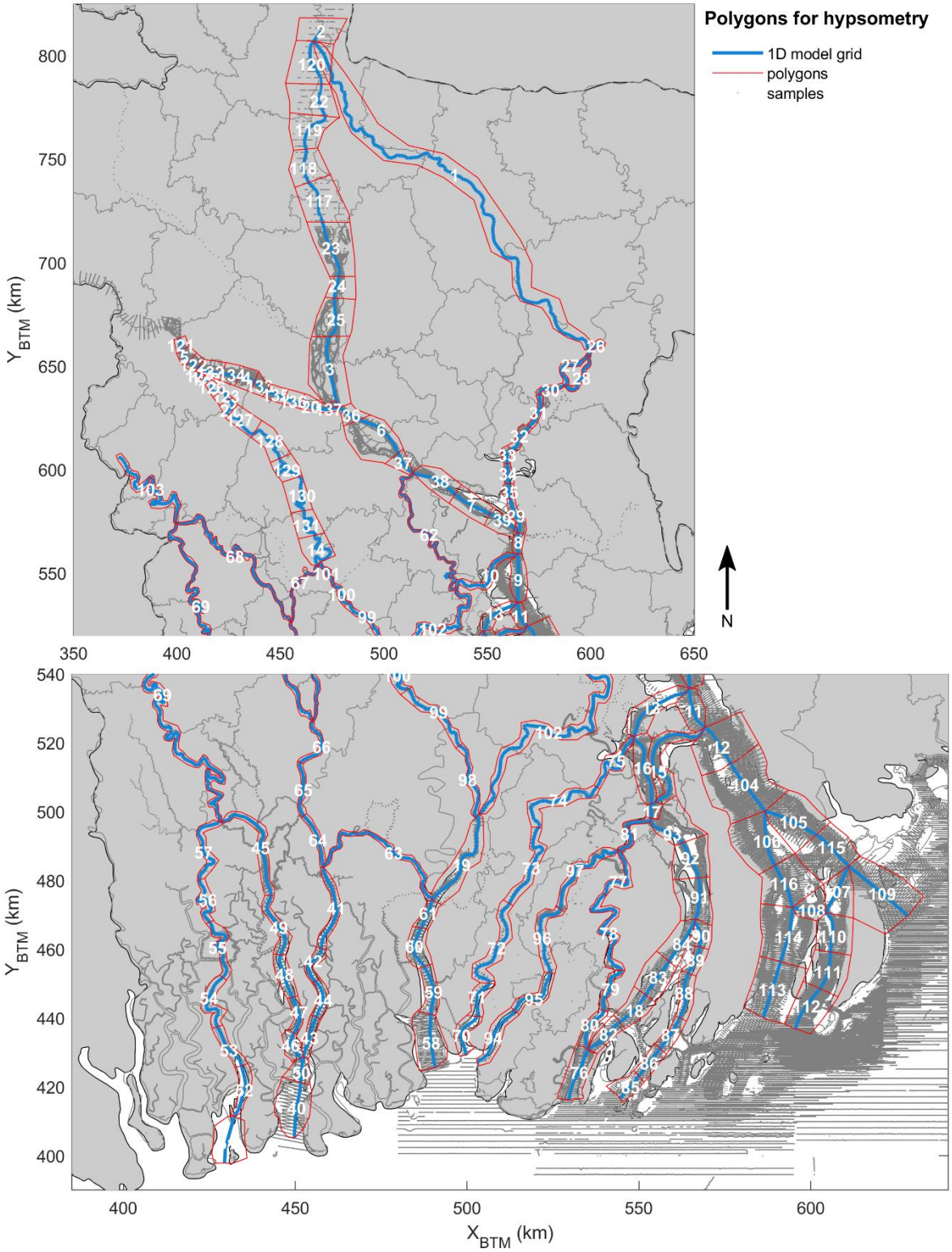

Figure 5.4 Map of the GBM delta with the model network (blue), the topo-bathymetric observations (gray dots), and the polygons (red) defining sub areas of the river branches for schematization of the hybrid profiles.

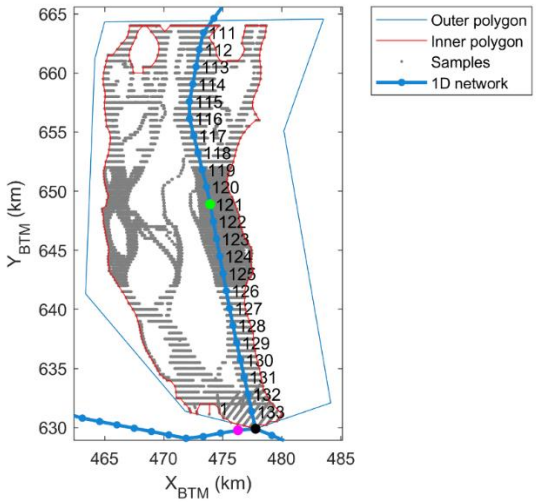

Figure 5.5 Example of methodology to derive an area and river length based on a tightly data-fitting polygon (red), which is found by the definition of manually defined outer polygons (blue).

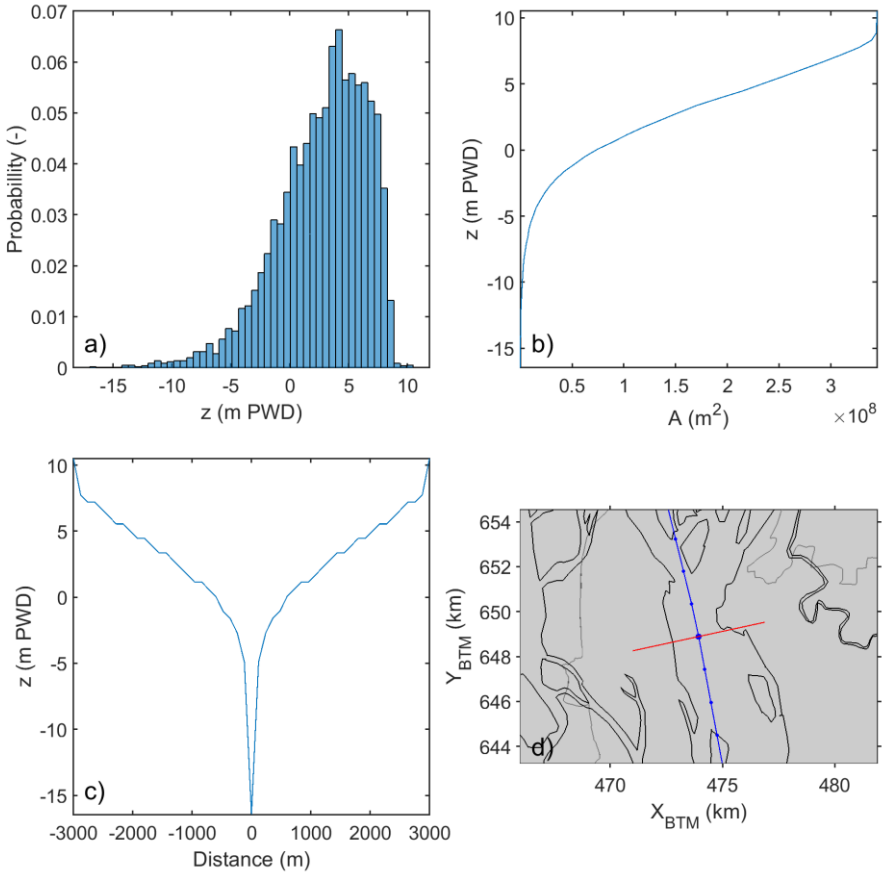

Figure 5.6 Methodology of schematizing cross-sectional profiles, illustrated for the downstream part of the Brahmaputra: a) histogram of the gridded topo-bathymetric observations within the sub area defined by the polygon; b) hypsometric curve derived from the histogram, c) schematized cross-sectional profile constructed from the hypsometric curve and the river width; d) positioning of the cross-sectional profile on to the model network.

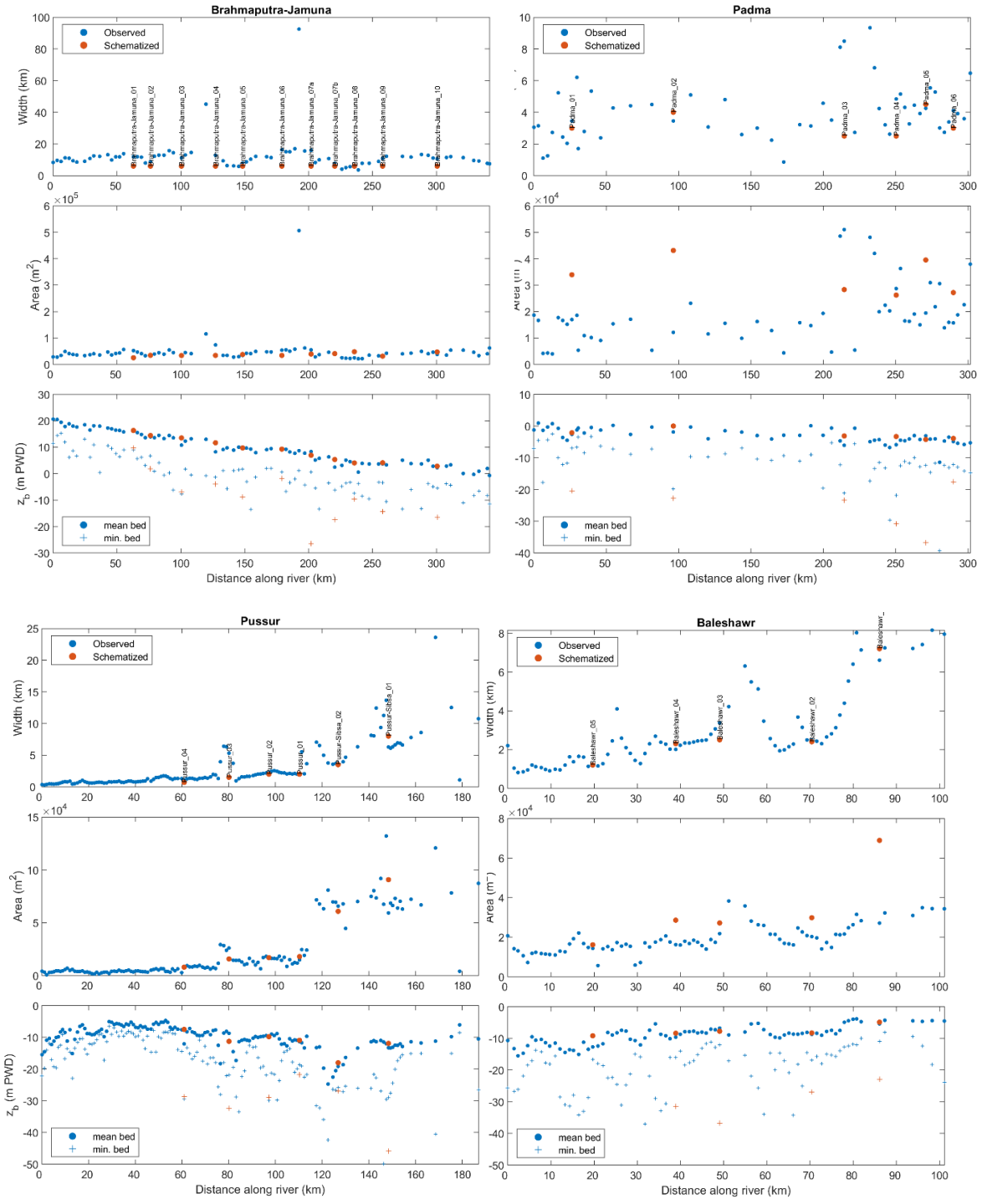

Figure 5.7 Morphological characteristics of the Jamuna (non-tidal) and Pussur (tidal) rivers derived from observed profiles (blue) and schematized hybrid profiles (red). Figures shows river width (a), cross-sectional area (b), and mean and minimum bed level of the profiles (c).

5.4 Friction

A spatially varying Manning's coefficient (Manning's n) is imposed on the model as roughness coefficient. The values are shown on the map in Figure 5.8, for each polygon specifying a certain area of the model domain. Areas not enclosed by a polygon have a value of 0.020 $s^{1/3}/m$.

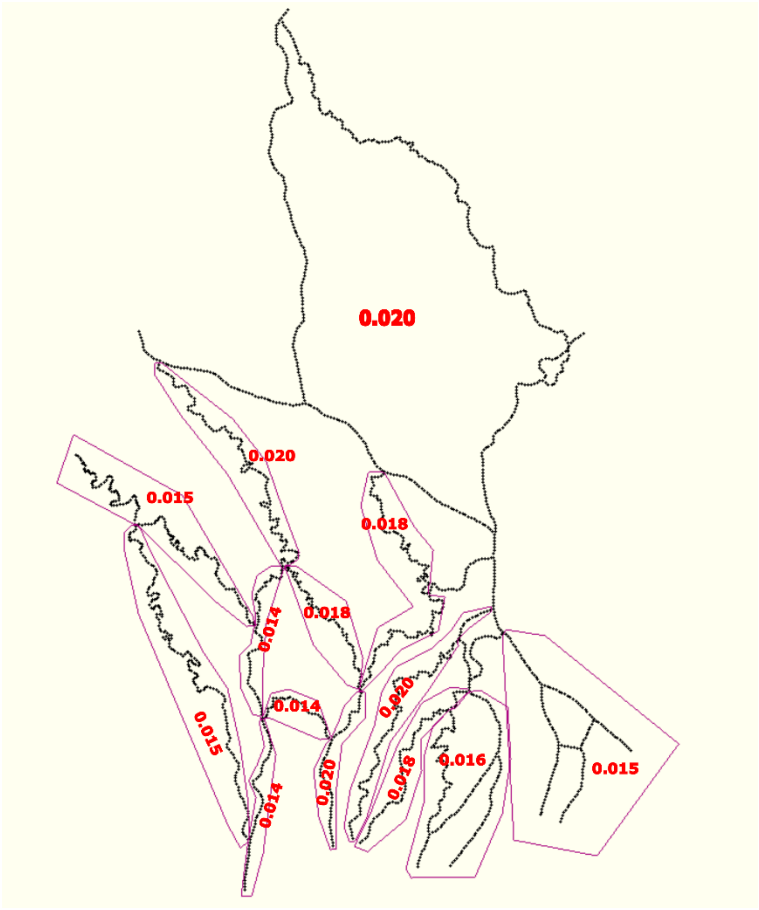

Figure 5.8 Spatially varying roughness field (Manning's n) imposed on the 1D model.

5.5 Sediment model

Sediment is modelled via built-in sediment transport formulations that are coupled online (updated every computational time-step) to the hydrodynamics. A cohesive (mud) and non-cohesive (sand) sediment fraction is modelled. The transport formulations and the associated parameter values are identical to the sediment model used for the (2D) coastal model, and is described in Section 6.5.

5.6 Boundary conditions

5.6.1 Upstream

The upstream open model boundaries are situated at the three major rivers (from west to east) Ganges, Brahmaputra, and Meghna (Figure 5.2). Due to the availability of long-term discharge observations at Hardinge Bridge (Ganges), Bahadurabad (Brahmaputra), and Bhairab Bazar (Meghna) (see Section 3.3.2) the open boundaries are situated exactly at these locations (and not at

Bangladesh' national border). At these upstream boundaries the model is forced hydrodynamically with measured discharge time series (Figure 5.9) for calibration and validation purposes. For model application (see Section 5.8) the model is forced by a hydrograph that resembles the mean annual discharge variation. The construction of this hydrograph is described in the set-up of the coastal model (see Section 6.3.1).

Suspended sediment concentrations are derived from literature (see Section 2.2.2) and are prescribed as mean annual values. For non-cohesive sediment an equilibrium concentration is prescribed and for cohesive sediment constant values of 900 mg/l (Jamuna and Ganges) and 100 mg/l (Upper Meghna) are included in the model (similar to the coastal model).

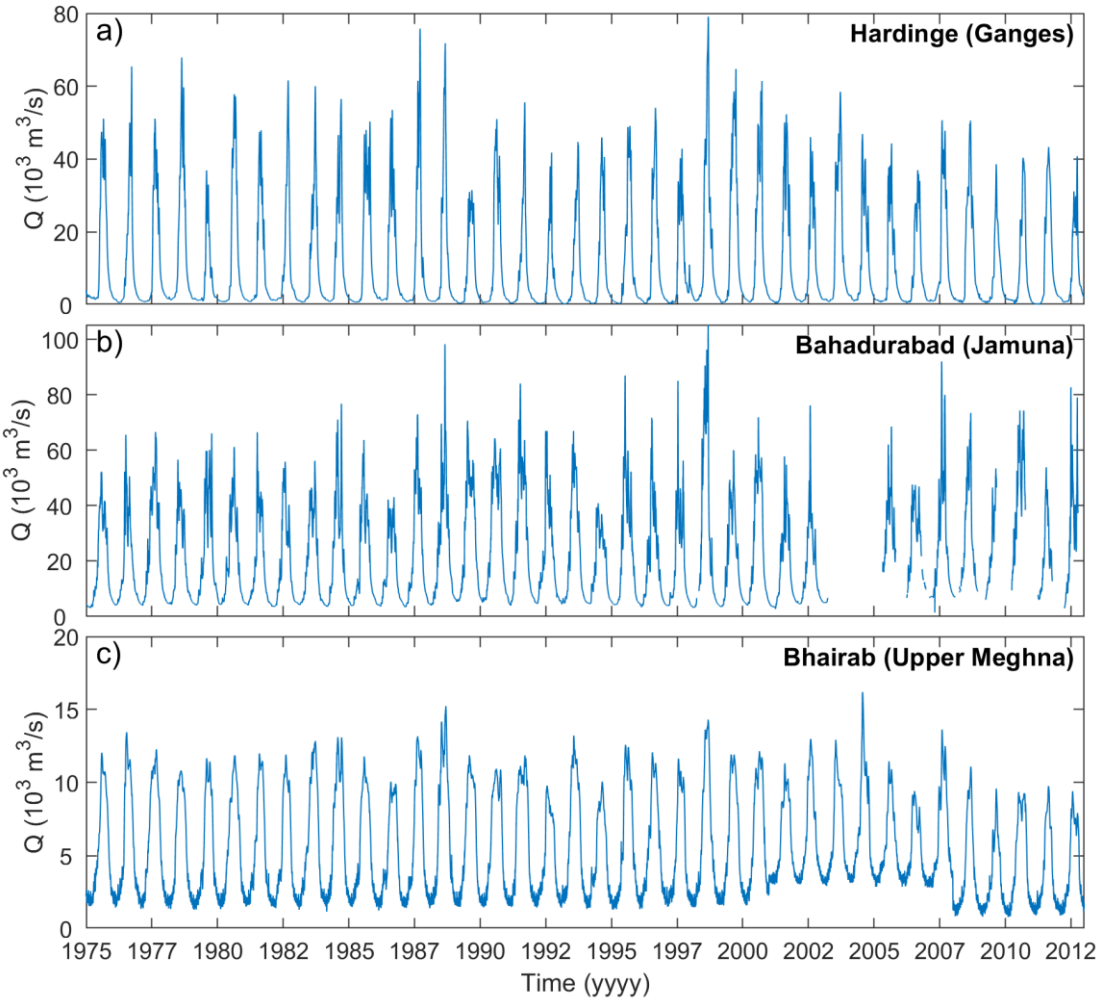

Figure 5.9 Timeseries of discharge from 1975 up till 2012 at the three measurement locations (Hardinge, Bahadurabad & Bhairab) used to force the model at the upstream boundaries.

5.6.2 Downstream

The downstream boundary conditions are imposed at the seaward boundaries of the estuaries (Figure 5.2). The hydrodynamic boundary conditions consist of astronomical tidal constituents, prescribing the amplitude and phase of the tidally induced water level fluctuations. The constituents are derived from the MIKE21 Bay of Bengal model (Uddin et al., 2014) and include all tidal constituents that could be solved from the one-year model results.

5.7 Initial conditions

To reduce the spin-up time of the model – and to avoid numerical instabilities in the initial stage of the model simulation – initial conditions are imposed on the model. The initial water level is derived from the observations and interpolated to the model net nodes. Second, a new initial conditions file is created from the output of a previous model simulation to deliver the best spatially varying conditions. The initial bed composition is spatially uniform and equal to the coastal model (see Chapter 7).

5.8 Model experiments

The boundary conditions imposed on the model for the current situation (this report) allow to simulate any time period within the availability of the discharge data (see Figure 5.2). Two time periods were chosen to serve the following purposes: a short time period that overlaps with the availability of data for water level comparison, and a long time period that allows for a proper comparison of the model with discharge measurements. Subsequently, the model is applied to study the annual flow and sediment dynamics in the GBM delta. In Table 5.2 the settings and the purpose of the model calibration and validation exercise are summarized.

Table 5.2 Simulation types with the period modelled and the purpose of the simulation.

Simulation type	Time period	Purpose	Section
Calibration	1 Apr 2012 – 7 Oct 2012	Comparison to observations (several months) of water levels	0
	1 Jan 1975 - 1 Jan 2000	Comparison to long-term observations (25 years) of discharge	5.9.2
Validation	1 Jan 1975 - 1 Jan 2000	Annual flow and sediment dynamics	5.10

5.9 Calibration of hydrodynamics

This section describes the results of the calibrated models with measured and hybrid profiles. The model features used to calibrate the models mainly constitute the bed level; i.e. the method of embedding the measured bed level profiles in to the model. A 1D model is most sensitive to (errors in) the cross-sectional profiles. Most of the calibration effort has been put in an appropriate choice of representative profiles and constructing hypsometric curves from these measurements. Variations in spatially varying roughness values were tested to optimize model outcomes.

5.9.1 Water levels

The model variants with measured and hybrid profiles are both run for a short period (several months) to directly compare to observations of water levels. First, a time-series analysis is made and secondly performance of the model is evaluated in the tide-dominated part of the GBM delta using harmonic analysis.

5.9.1.1 Time-series

Figure 5.10 shows for both models target-diagrams of the error statistics BIAS and Root Mean Squared Error (RMSE);

(8) $$BIAS = \frac{1}{n}\sum(X_{sim} - X_{obs})$$

(9) $$RMSE = \sqrt{\frac{1}{n}\sum(X_{sim} - X_{obs})^2}$$

subdivided per river system as indicated by the colouring. The figure shows that model results for both measured and hybrid profiles cluster near small error values for both statistics but clearly perform less for specific river systems. Figure 5.11 shows the spatial distribution of the error statistics. The figure shows that the Kobadak river performs poor in both models, which is mainly due to a lack of bathymetry measurements to construct realistic cross-sectional profiles. Therefore, the Kobadak river will not be considered in this study. The hybrid model shows, contrary to the measured model variant, that it is not performing well for the upstream (non-tidal) rivers (dark blue colours). Timeseries plots of the (mainly) non-tidal rivers Ganges (Figure 5.12) and Padma (Figure 5.13) show that both model variants perform well in dry-season (April-May) and perform less in monsoon-season (after July). This model mismatch in the monsoon season is the worst for the hybrid model variant.

The reason for the model mismatch is the availability of bathymetry measurement on the floodplains (chars) in the upstream rivers. In the monsoon season, the floodplains become part of the flow-carrying cross-section of the river and hence, a detailed description of the hypsometry of the floodplains is required. Bathymetry measurements are scarce at the floodplains which means they are not represented well in the hybrid model variant. In the measured model variant, this effect is present as well but reduced because the hypsometry of the floodplains (gaps in the cross-sections) is estimated using linear interpolation (Figure 5.14).

The downstream stations in the Padma (Figure 5.13) show a similar performance of both models in the tide-dominated part. The reproduction of tidal properties is evaluated in the next section.

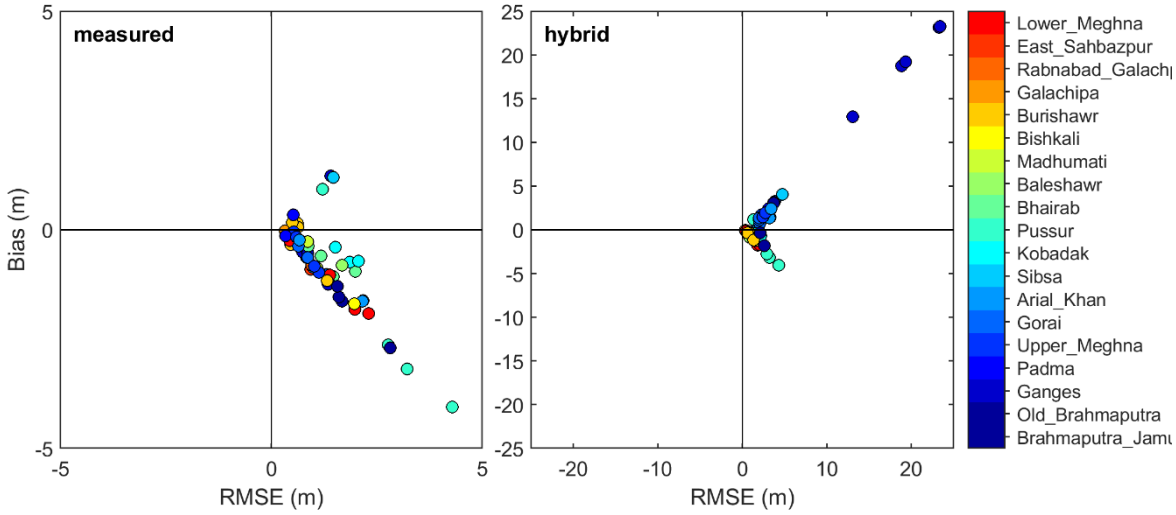

Figure 5.10 Target diagram of the BIAS and RMSE between model results and observations on water levels, for the model with measured (left) and hybrid (right) profiles. River systems are indicated by the colours.

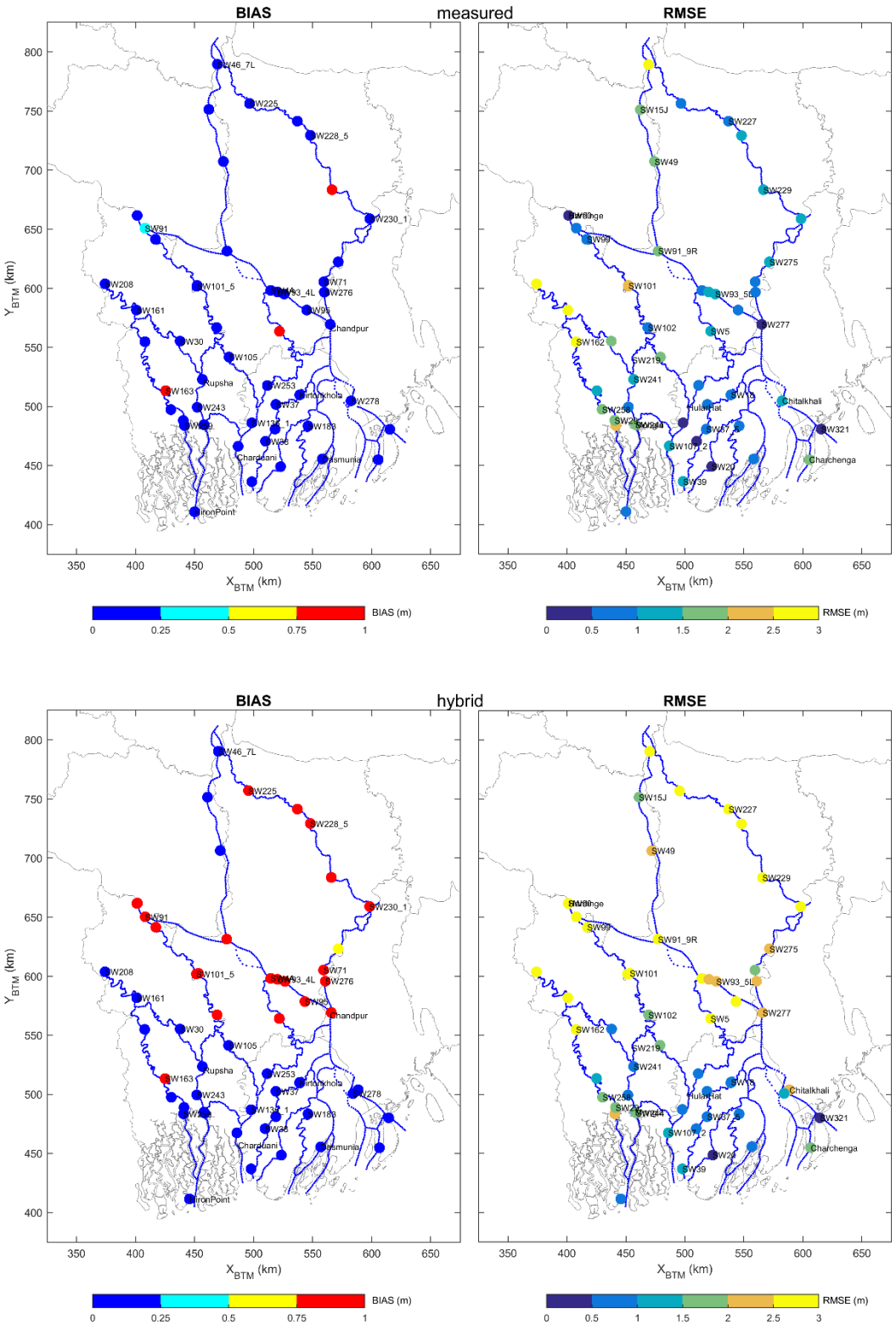

Figure 5.11 Map overview of the BIAS (left) and RMSE (right) between the model with measured (top) and hybrid (bottom) cross-sections and observations.

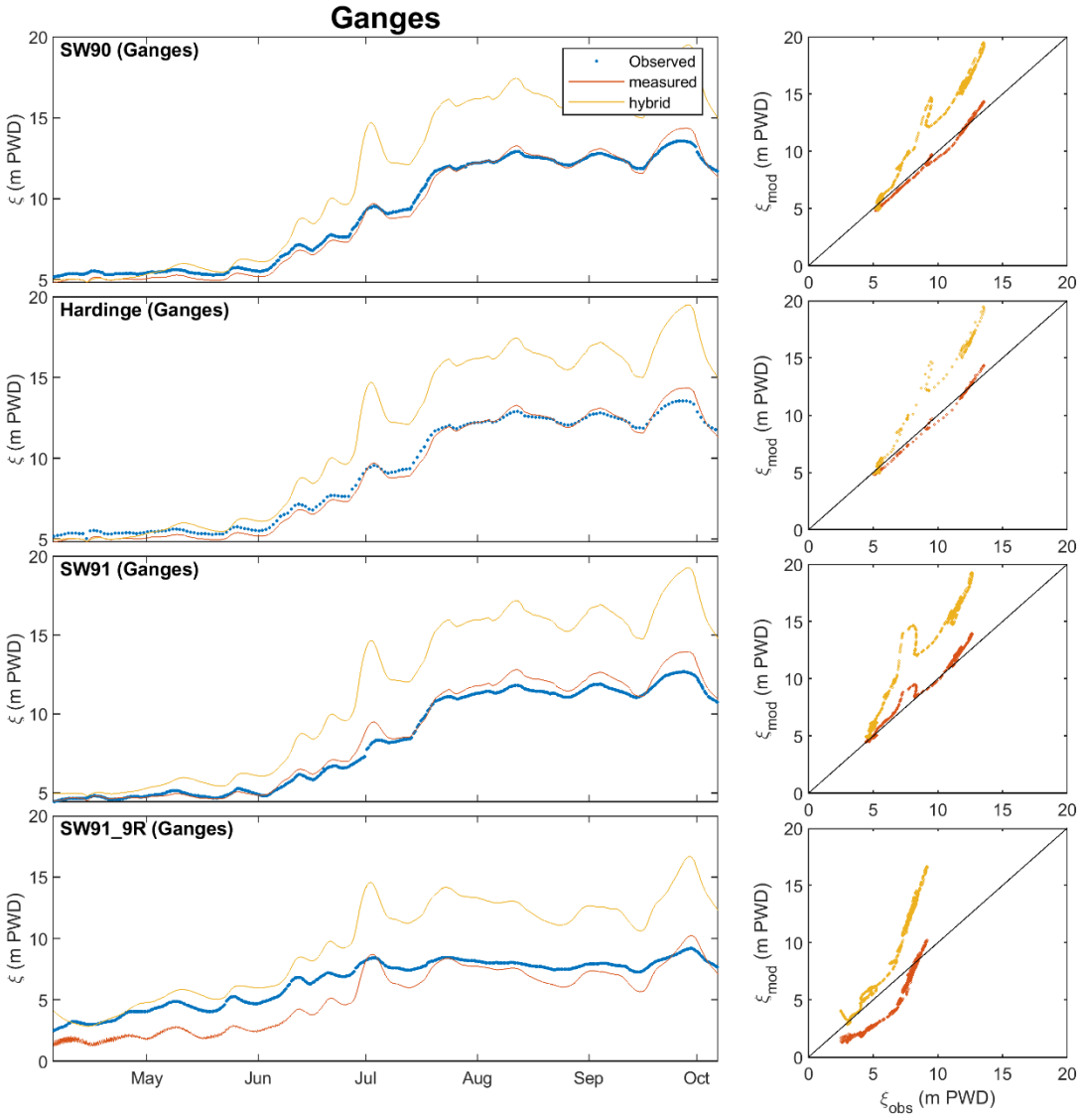

Figure 5.12 Timeseries of the modelled and observed water levels in the Ganges from upstream (Hardinge Bridge) to the downstream confluence of the Ganges and Jamuna in to Padma.

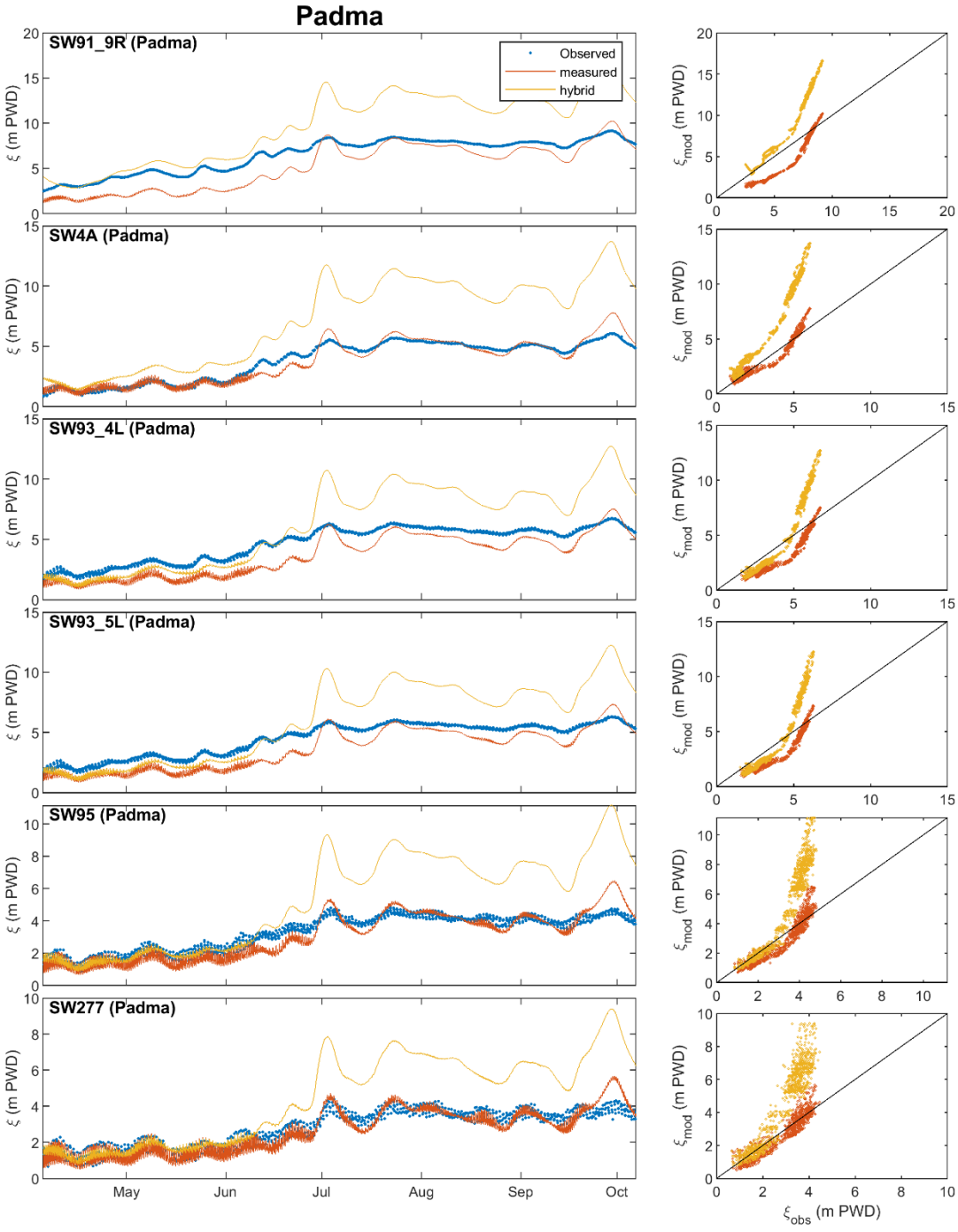

Figure 5.13 Timeseries of the modelled and observed water levels in the Gorai-Madhumati river from upstream (bifurcation of Ganges) to the downstream bifurcation towards the Baleshawr (upstream of Khulna).

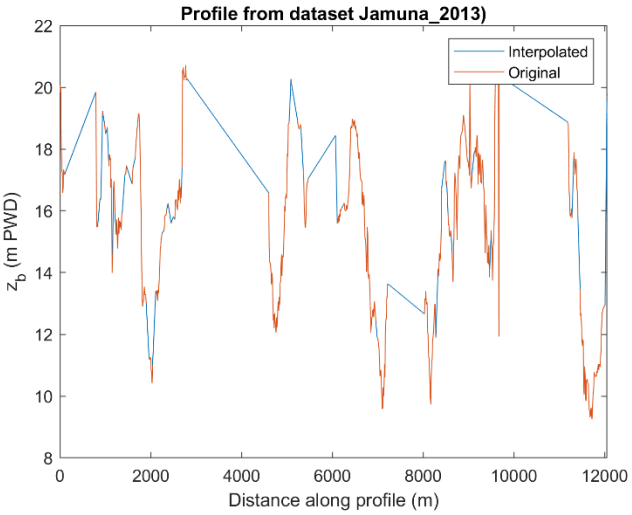

Figure 5.14 Cross-sectional profile in the Jamuna, showing observed values (red) and char sections which are filled in by interpolation (blue).

5.9.1.2 Tide

The harmonic analysis described in Section 3.3.1.2 is a powerful way to analyse tidal propagation in the GBM delta and provides a good measure for model comparison. However, as explained in Chapter 3, harmonic analysis on the available data is not straightforward as tidal signals are highly non-stationary and the coarse temporal resolution hampers the analysis. The consequence is that this analysis can only be done for the 30-min data from the BIWTA, the 3-hr interval data from the BWDB is omitted. Therefore, the analysis here compares the model with the observed values by the mean tidal range estimated from the first month (dry season) of the simulation. The values from the BWDB dataset (with the SW code) should be considered carefully, as the 3-hr interval challenges the calculation of a mean tidal range.

The observed and mean tidal range is plotted for all observation stations in the tide-dominated rivers (Figure 5.15) for stations where the mean tidal range is larger than 0.2 m The figure shows that both model variants perform reasonably well for all the rivers in the GBM delta. As expected, the model variant with the measured profiles performs slightly better than the model variant with the schematized profiles. The measured model variant performs slightly better hydrodynamically because the cross-sectional profiles imposed on the model resemble the situation of the river bed as it was during the water level measurements. The cross-sectional profiles imposed on the hybrid model variant are basically a smoothed bathymetry.

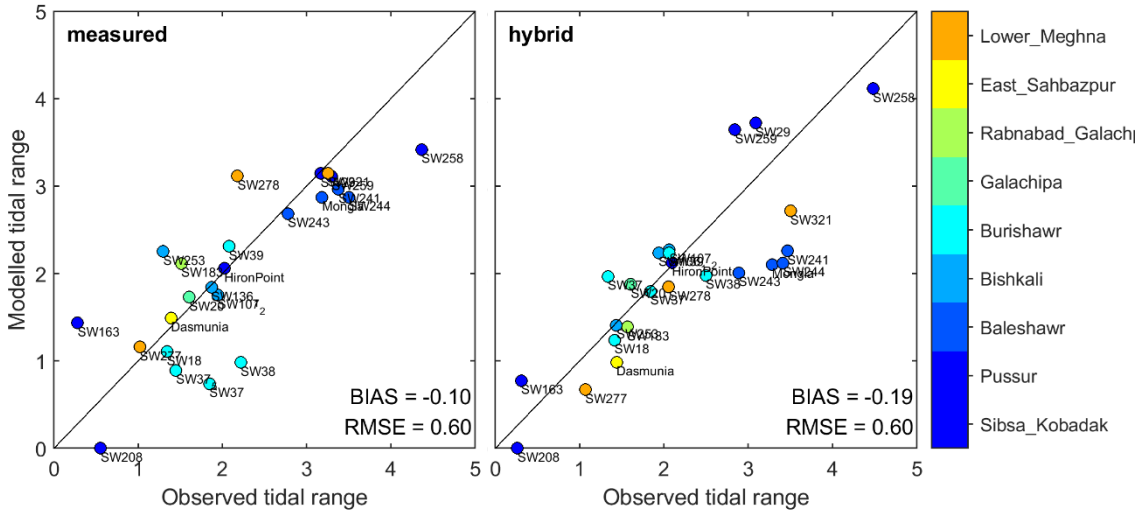

Figure 5.15 Scatter plot of the observed and modelled tidal range for the model with measured (left) and hybrid (right) cross-sectional profiles.

5.9.2 Discharge

Both model variants are run for a time period of 25 years to allow for a good comparison with long-term discharge data available at the confluence of the Ganges and the Jamuna (Baruria) and the bifurcation of the Gorai (Gorai Railway Bridge). The performance of the models is visualized in timeseries (Figure 5.16), scatter plots (Figure 5.17), and a table with error statistics (Table 5.3). These figures and tables show that both models perform quite well in distributing the discharge and that the distribution is modelled well at the Gorai bifurcation during the monsoonal fluctuation. The model-data comparison is also nearly perfect in the Gorai, but at Baruria both model variants show an over-estimation of the discharge for most of the modelled period. The over-estimation is smaller for the model with the measured profiles.

To get a better understanding on the over-estimation of the models at Baruria, the discharge at Baruria is plotted with a discharge that is calculated by adding the contributions from Jamuna and Ganges and subtracting the contribution from the Gorai. These time-series and scatterplot (Figure 5.18) explain the model-data mismatch observed: part of the discharge from the Jamuna and Ganges is flowing towards locations elsewhere and does not flow to Baruria. These locations can be smaller distributaries, but also overland flooding, water-intake, and evaporation (etc.). These processes are not included in the present set-up of the 1D model (the model results present a closed flow budget, but the data does not). Another source of data-model mismatch can be attributed to the accuracy of the stage-discharge derived measurements (see Chapter 3).

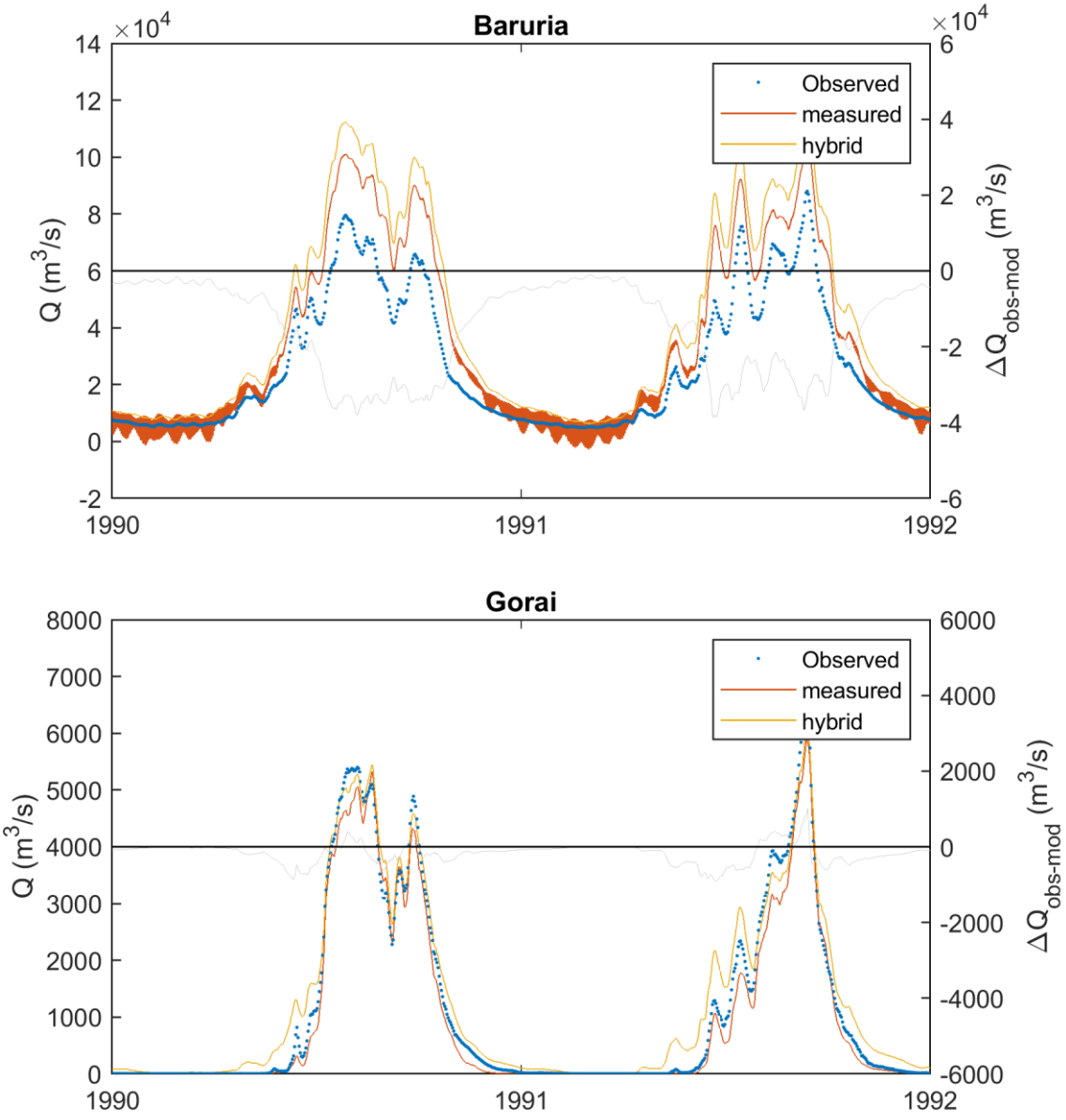

Figure 5.16 Timeseries of the modelled and observed discharge at Baruria (upstream of Padma) and the Gorai (Gorai Railway Bridge). Figures are zoomed-in on a two-year period to highlight the monsoon-drive discharge fluctuations.

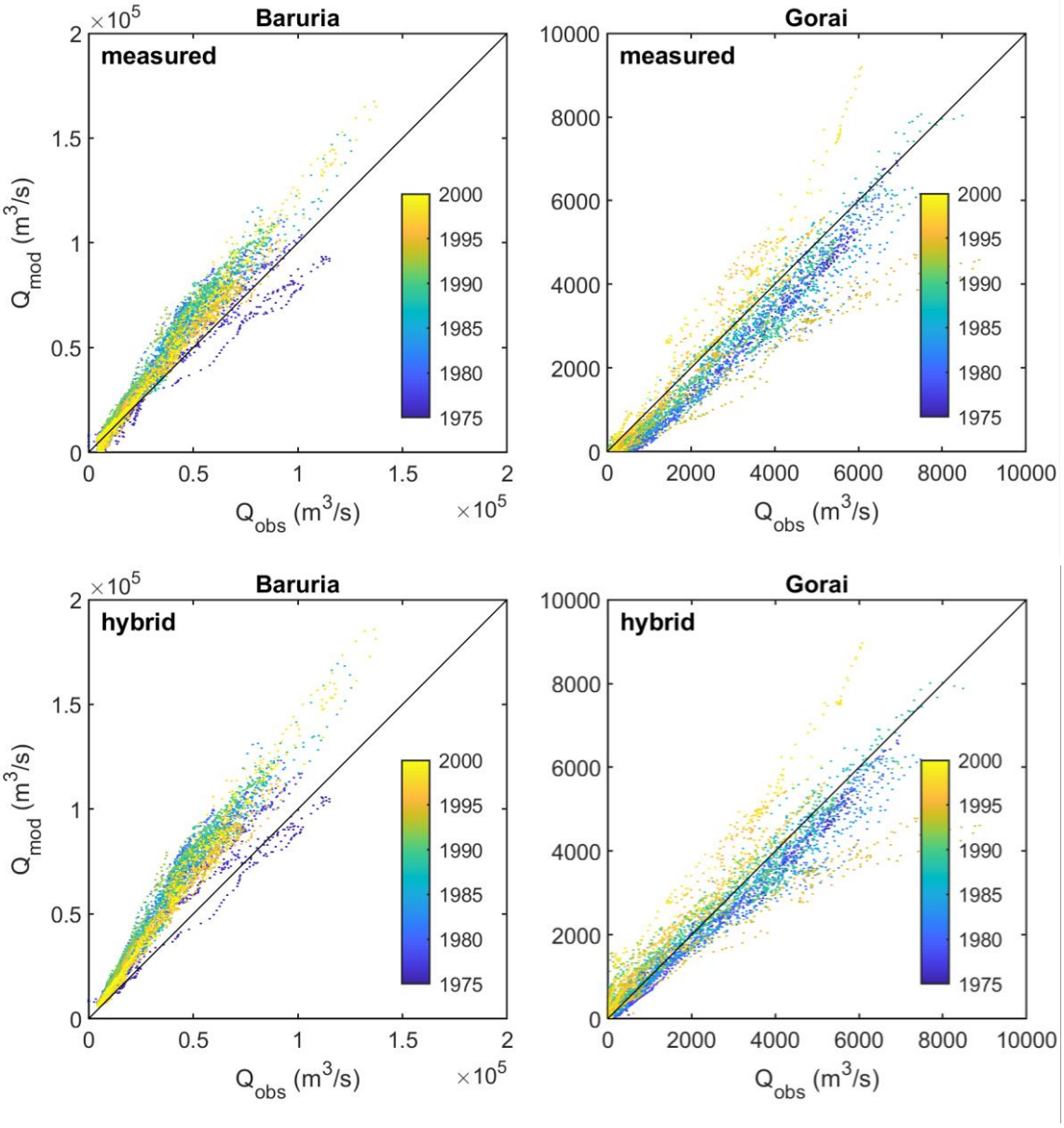

Figure 5.17 Scatter plots of the modelled and observed discharge for the confluence of Ganges and Jamuna (Baruria, left) and the bifurcation of the Gorai (right), for both model variants.

Table 5.3 Error statistics of the measured and modelled discharge.

Model	Station	Bias (m^3/s)	RMSE (m^3/s)	Corr. Coeff. (R)
Measured profiles	Baruria	4850	8989	0.98
	Gorai	-251	534	0.97
Hybrid profiles	Baruria	10629	14060	0.98
	Gorai	-8	472	0.97

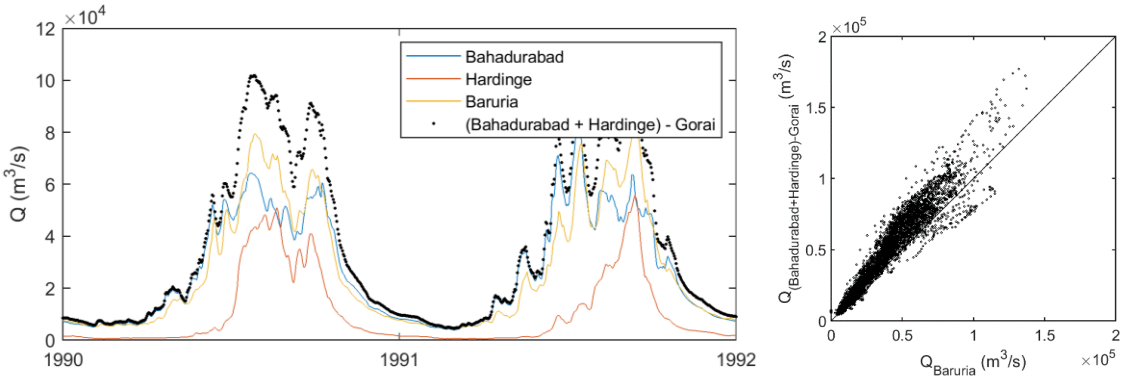

Figure 5.18 Time-series and scatter plot of the observed discharge at Baruria and the combined discharge from the observations of Bahadurabad, Hardinge with the Gorai substracted.

5.10 Model application and validation

The analysis of water levels shows that the model variants with measured and hybrid profiles perform similar in the tide-dominated part of the GBM delta, and that the model with measured profiles performs better in the upstream fluvial dominated part. The key property to simulate with the 1D model is the distribution of discharge and suspended sediment load over the river tributaries. The discharge analysis shows that the model with measured profiles performs best. Therefore, the model variant with measured profiles is used for the scenario-analysis. The following sections show the results of the 'measured' model variant which is run for a period of 25 years (see Table 5.2). The annual flow and sediment dynamics are analysed and, if possible, compared to literature as an aggregated form of validation.

5.10.1 Flow budget

Upstream

The mean and peak annual discharge is shown for the upstream (non-tidal) rivers in Figure 5.19. The figure shows in the Gorai tributary a mean annual discharge of ~1,000 m^3/s. At the confluence of the Jamuna and Ganges, flowing into the Padma, the figure shows a mean annual discharge of ~30,000 m^3/s and peak annual discharge ~100,000 of m^3/s. These values compare well to the values in (Table 2.1).

For the other branches there is no quantitative comparison available. However, it is apparent from the figure that the ratio between mean and peak annual discharge is approximately 1:3 – 1:4 in the upstream (non-tidal) branches of the GBM delta.

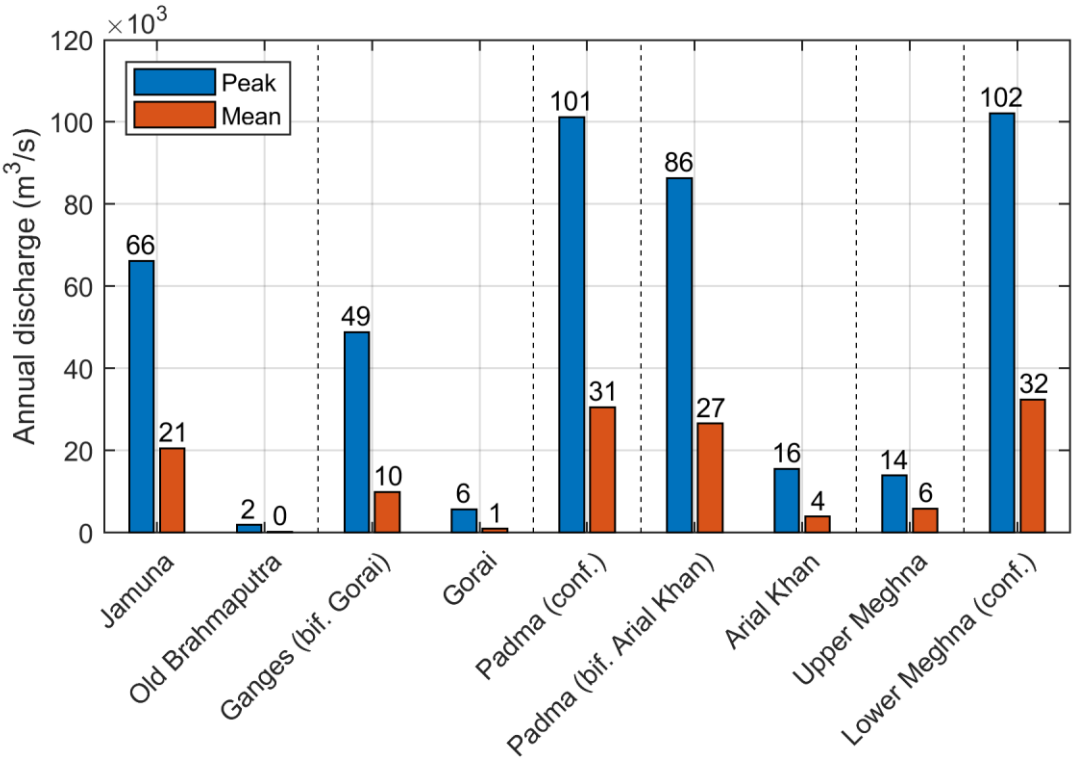

Figure 5.19 Mean and peak annual discharge budget for the upstream (non-tidal) rivers in the GBM delta. Vertical dotted lines indicate connecting tributaries. Values on top of the bars show the value of the bar multiplied by 1 * 10^3 (m^3/s).

In Figure 5.20 the division of mean annual discharge is shown for the most important bifurcations in the upstream part of the delta. The figure shows the discharge flowing towards the primary branch (blue) and to the secondary (bifurcating) branch (red), in absolute values (top panel) and percentages (bottom panel). The figure shows the largest part of the mean annual discharge is flowing towards the Padma (and subsequently the Lower Meghna) and that the Gorai and Arial Khan roughly receive the same amount of discharge annually. The amount of the annual discharge flowing from the Gorai river in to the Madhumati is ~13%. This is sligthly smaller than the known distribution of ~20% (pers. comm. IWM) but is at least in the same order of magnitude. Given the uncertainties in these values these results can be qualified as reasonable.

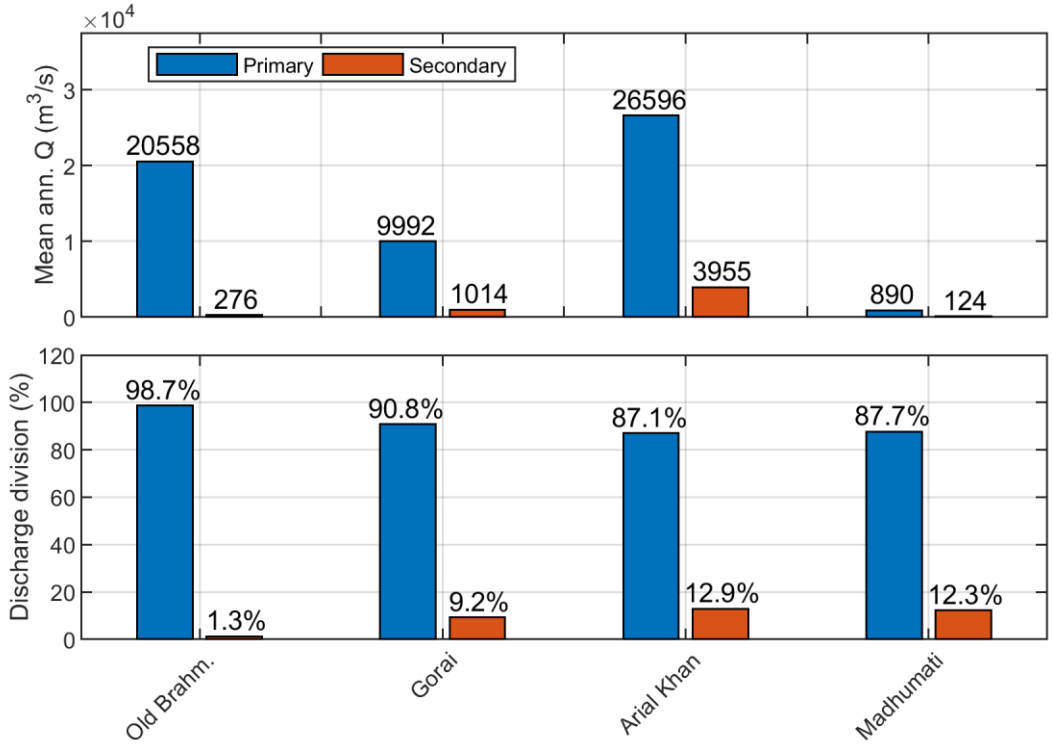

Figure 5.20 Discharge division for the three most important bifurcations in the upstream part of the GBM delta. Absolute values (top panel) and percentages (bottom panel).

Downstream

For the downstream bifurcations, the tidal prism is calculated as the volume of water entering a river branch during the flood period of the tide (averaged over the simulation period). The tidal prism is shown in Figure 5.21 for the most important bifurcations in the downstream part of the GBM delta. The figure shows that ~65% of the tidal prism flows into the Sibsa river.

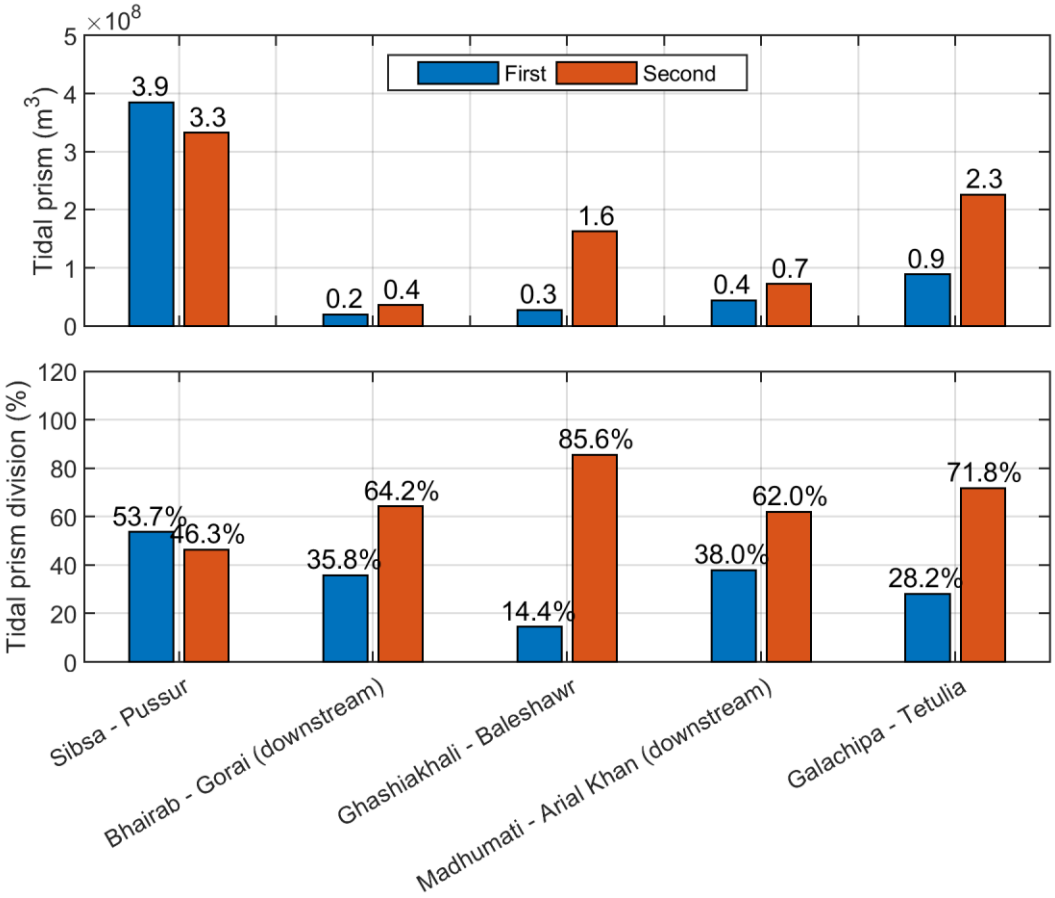

Figure 5.21 Division of the tidal prism for downstream bifurcations in absolute values (top panel) and percentages (bottom panel). Colours indicate the first (blue) and second (red) river system indicated in the labels on the horizontal axis (see Figure 5.2 for names of the river systems).

5.10.2 Suspended sediment budget

The suspended sediment load distributed over the tributaries in the upstream part of the GBM delta is calculated as a mean annual value over the 25 years that are simulated.

Figure 5.22 shows the mean annual suspended sediment load at the boundaries. Compared to Table 2.1 the suspended sediment load on the Jamuna river is 20% larger, and in the Ganges 25% smaller. In the next phase[11] of the project the boundary conditions will be improved by imposing the time-varying results from the HydroTrend model instead of the mean annual suspended sediment concentration used here.

In Figure 5.23 the distribution of the suspended sediment load is shown for the most important distributaries. The figure shows a load of 40 Mt/yr and 31 Mt/yr for the Gorai and Arial Khan tributaries, respectively. This is ~25% larger than the values shown in Table 2.1. In the Lower Meghna the total suspend load constitutes up to ~900 Mt/yr, which is smaller than the ~1000 Mt/yr given in literature but lies in the same order of magnitude.

[11] Macro scale morphology - future situation – deliverable D-4A-1:4

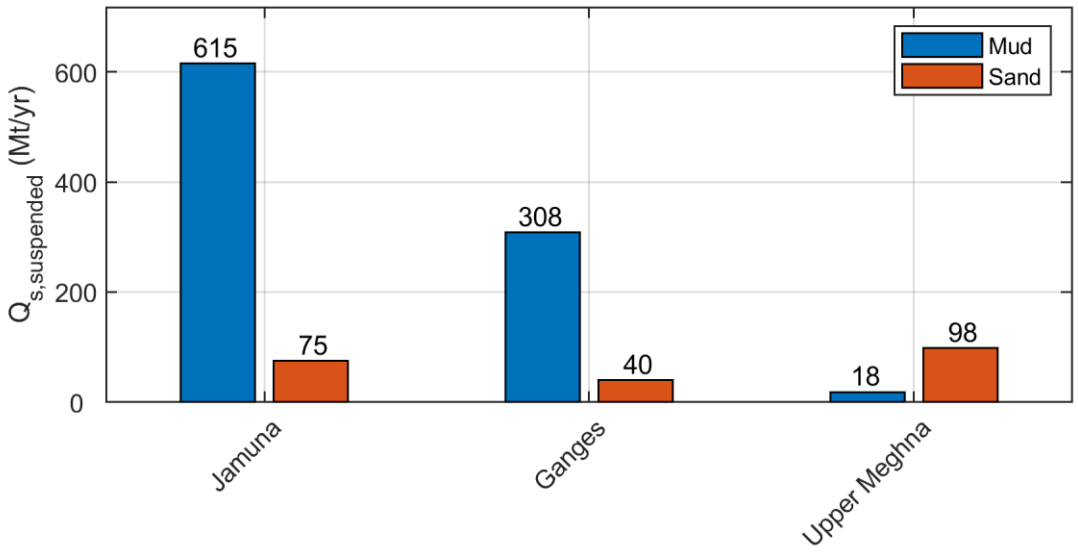

Figure 5.22 Mean annual suspended sediment budget at the boundaries of the model (apex of the delta).

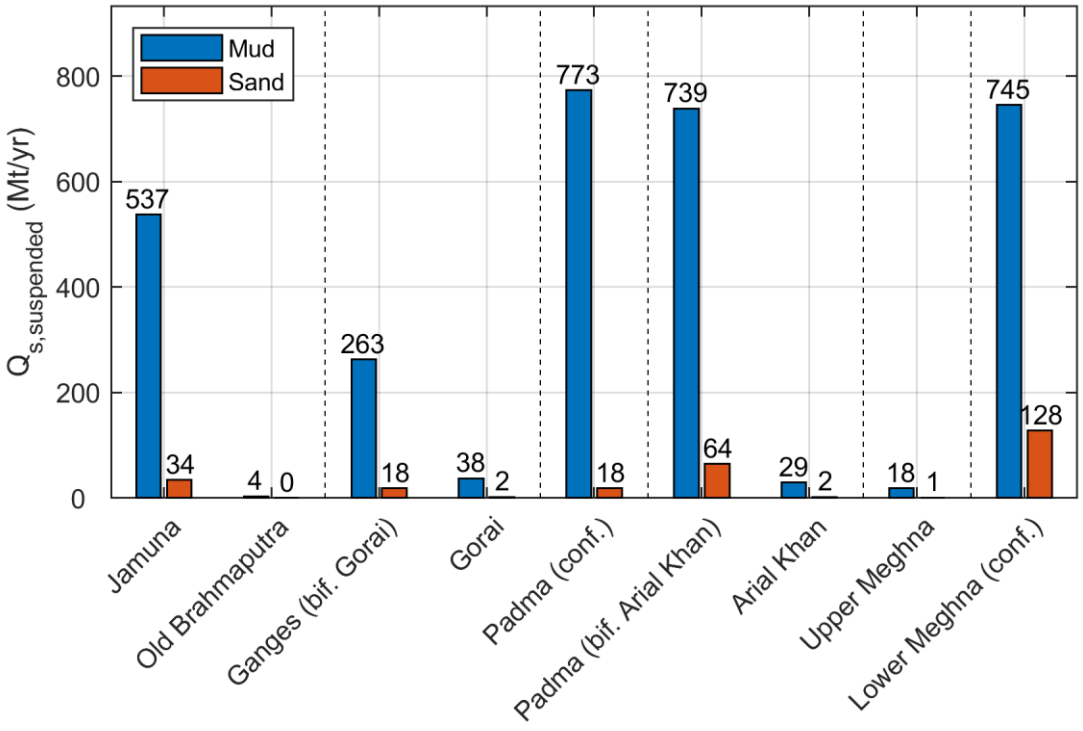

Figure 5.23 Mean annual suspended sediment budget for upstream part of the GBM delta. Vertical dotted lines indicate connecting tributaries. Values on top of the bars show the value of the bar multiplied by 1 * 10^3 (m^3/s).

6 Development coastal model (Delft3D-FM 2D)

6.1 Introduction

The development of the 2D coastal model is described in the following sections. A synoptic overview of the procedure is as follows:

- Construct an unstructured-grid model of the entire GBM delta and a large part of the Bay of Bengal, covering the main rivers and estuaries with widths greater than 500 m, in a mesh of which the cell sizes range from 8 km to 500 m, with rectangular grid cells except where areas of different resolution are connected by triangles.
- Run and calibrate the model hydrodynamically with realistic boundary conditions for river flow of the three main rivers and full astronomical boundaries at the sea boundary. The calibration focuses on reproducing the M2 amplitude variations throughout the delta, in comparison with data from a large number of tidal stations, for each of which a limited tidal analysis is carried out.
- Verify the discharges through a number of cross-sections, mainly in the Meghna and the Pussur-Sibsa system and where necessary adjust the calibration.
- The main variables in the calibration are the bathymetry, ensuring the continuity of channels in the relatively coarse grid, and the roughness, which is varied only on a very large scale (e.g. different values for sea –estuaries – rivers).
- The model has been developed in three stages:
    - In the first stage, up to the confluence of Jamuna and Ganges at Baruria;
    - In the second stage the Ganges and Jamuna up to Hardinge Bridge resp. Bahadurabad were included. In the Meghna the model runs up to Bhairab Bazar.
    - The (so far) final stage includes the Gorai River as it was seen as an important source of sediment to the Pussur-Sibsa system. It is included as a curvilinear grid section connected to the overall grid using triangles and quadrilaterals.
- Two types of morphodynamic simulations are carried out:
    - Short-term (~ 1 year) runs with realistic time series boundaries and full astronomical sea boundary components;
    - Long-term (5-100 year) runs with schematized *representative* boundary conditions for the river discharges and simplified *representative* tidal components, combined with a *morphological factor* approach to accelerate the morphodynamic simulations.
- Calibration of the sediment model on the shorter time scale is carried out using available sediment concentration measurements, for selected periods where bathymetric, hydrodynamic and sediment concentration measurements are available.
- Calibration of the decadal-scale morphological development is carried out using the accelerated approach.

It must be noted that having a good calibration for sediment concentrations on the short term is no guarantee that the same settings will lead to good morphological behaviour. This is in part because the longer-term evolution is influenced by parameters that have little influence on short time-scales, but also because there are different paths towards a reasonable concentration distribution that may have quite different resulting sedimentation/erosion patterns.

Therefore, our approach in calibrating the sediment and morphology behaviour consists of trying to **reconcile** the settings for both types of simulations, rather than taking the settings resulting from the sediment calibration and assuming them to be equally valid for the morphological runs.

6.2 Grid and bathymetry

6.2.1 Automated grid generation

Given the objectives of the model as outlined in section 1.2.3, the generated grid must fulfil the following requirements:

1. Boundary conditions far from the region of interest and allowing both effects of sea level rise and changes in upstream flow and sediment discharges to be accounted for;
2. Grid resolution fine enough to represent the major river system but coarse enough to allow long-term simulations in acceptable runtime;
3. Grid covering recent channel areas, potentially flooded areas and areas prone to erosion;

Given these requirements a model domain was selected covering the Bay of Bengal up to the seaward limit of the MIKE21 storm surge model and up to the confluence of Ganges and Jamuna (for initial model calibration) and up to Hardinge Bridge on the Ganges and Bahadurabad on the Jamuna; in all cases up to Bhairab Bazar on the Meghna.

Rather than constructing a complicated mesh consisting of curvilinear and triangular elements, a 'quadtree' type approach was opted for with rectangular grid cells that can locally be refined by a factor of two in both directions. The connections between such areas are made of triangles. This approach can be automated to a large extent and guarantees that no small grid cells are generated that may reduce the time step, and does not lead to preferential orientation of channels. Besides, the resulting grids are perfectly orthogonal.

The basis for generating the grid is a rectangular grid with cells of 16x16km^2, aligned at the seaward boundary with the Bay of Bengal Mike21-FM grid. The parameters for this overall grid are:

Table 6.1 Parameters of base grid from which quad grid is developed

Property	Value	Property	Value
X origin	-320 km	Grid size x	16 km
Y origin	-150 km	Grid size y	16 km
Orientation	-40	Number of cells x	81
		Number of cells y	72

Next, the grid was automatically refined based on a combination of distance to the nearest bankline and water depth. Areas that are not expected to ever flood are excluded by taking out entire grid cells, based on polygons. Details of the procedure are given in Appendix C, and the resulting grid is shown in Figure 6.1.

Since the automated procedure based on a combination of distance to banklines and depth was rather complicated and could still lead to some areas with rather deviating shapes, the procedure for the final stage of the model was simplified to one where successive two by two refinement was carried out using user-defined polygons, which gave more and easier control over the resolution and the removing from areas that are certain not to flood. The exact procedure is described in Appendix C and has also been the basis for several meso-scale model setups. The resulting mesh is shown in Figure 6.2.

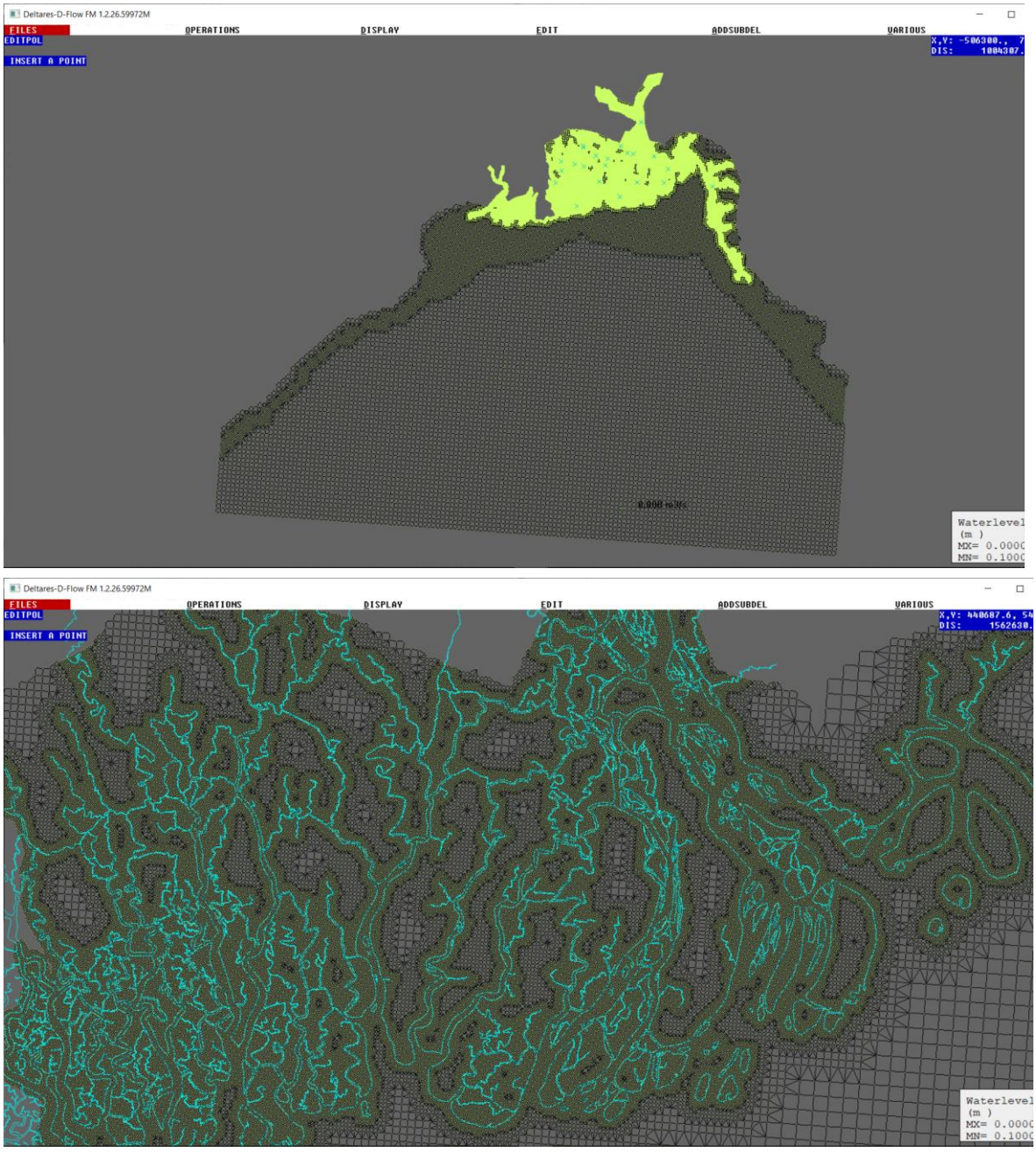

Figure 6.1 Overall mesh (top panel) and detail of delta (lower panel) for stage 1 model.

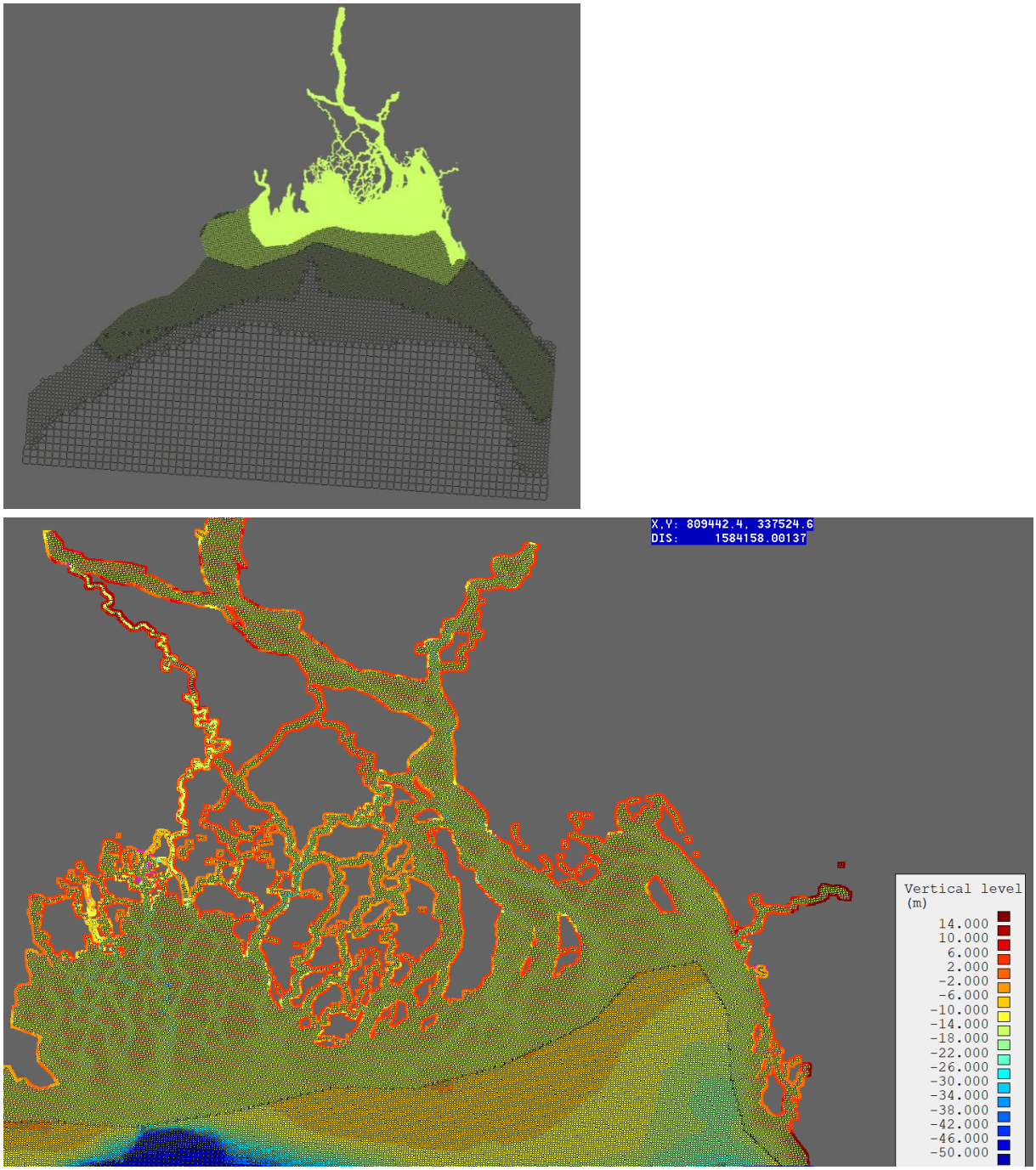

Figure 6.2 Overall mesh (top panel) and detail of delta (bottom panel), stage 3 model.

6.2.2 Bathymetry

The bathymetry for the macro 2D hydrodynamic model was initially based on that of the validated MIKE21-FM Bay of Bengal model (IWM, 2010), which generally has a finer grid size than the current model. It is based on bathymetric datasets close to the reference year 2010.

Additionally, several datasets exist for different parts of the system and during different periods. These were used to generate up-to-date initial bathymetric sample sets for morphological calibration/validation runs, in the following manner: if bathymetric surveys for a given area exist for times T1 and T2, then the overall model bathymetry will be initialised as much as possible with data from time T1. For river branches where the available datasets only contain cross-sections that are

sparsely distributed in space, the methodology of Vo et al. (2020) has been applied to generate comprehensive sample sets with bathymetric information: construct a curvilinear grid of the river reach under consideration and apply a coordinate transformation of the cross-sectional data to the curvilinear grid administration. The actual interpolation happens in the curvilinear coordinate space, after which the data is transformed back to real world geographical space. This process is illustrated in Figure 6.5.

A full overview of all available bathymetries is available in the data inventory and is not repeated here.

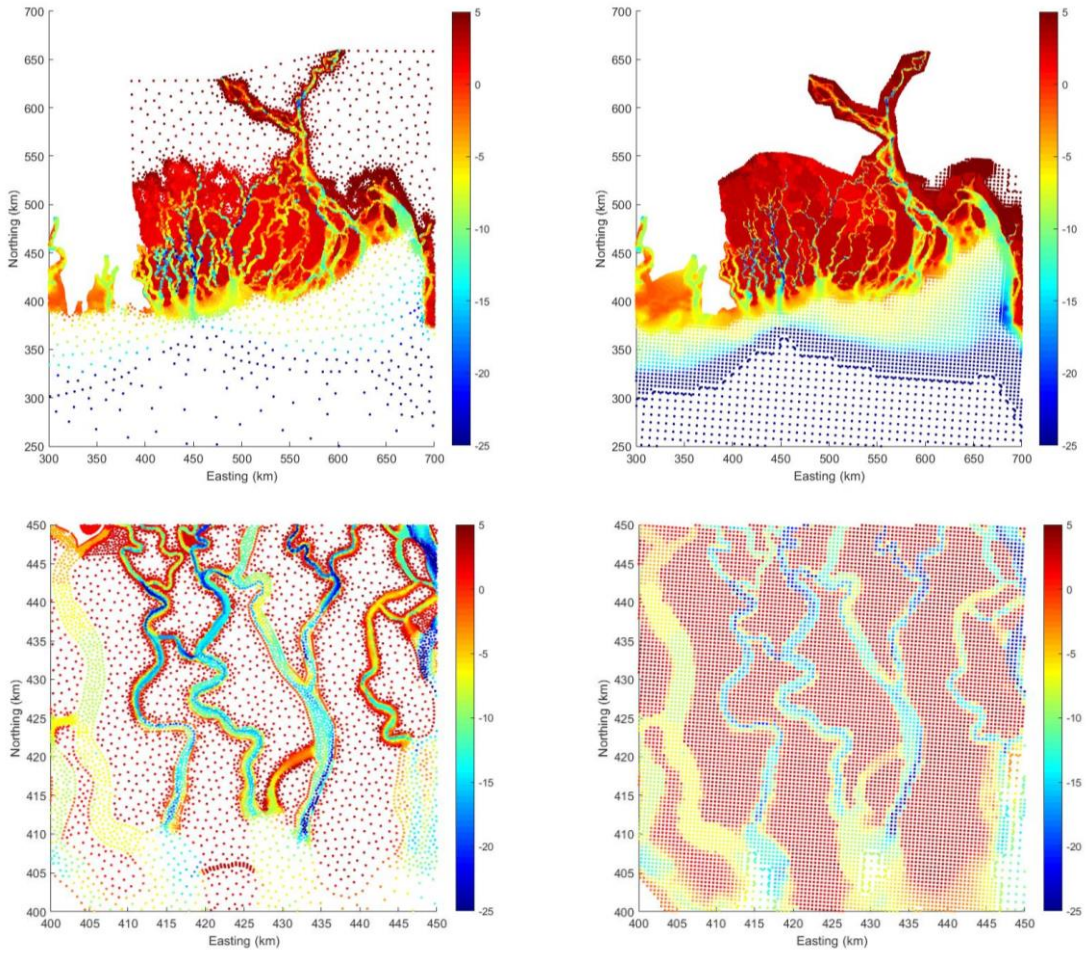

Figure 6.3 Comparison between MIKE21-FM Bay of Bengal storm surge bathymetry (left panels) and the representation in Delft3D-FM large-scale morphological model (right panels). Top panels: overview of coastal areas; Bottom panels: zoom area in Sundarbans.

The DEM of the non-poldered areas, mostly in the Sundarbans, was taken over from the MIKE21-FM Bay of Bengal storm surge model as these areas may be inundated during regularly occurring events. The poldered areas were put at a level of +3m, preventing inundation under normal circumstances. A comparison between the MIKE21-FM model representation of the DEM and that in the Delft3D-FM morphological model is given in Figure 6.4.

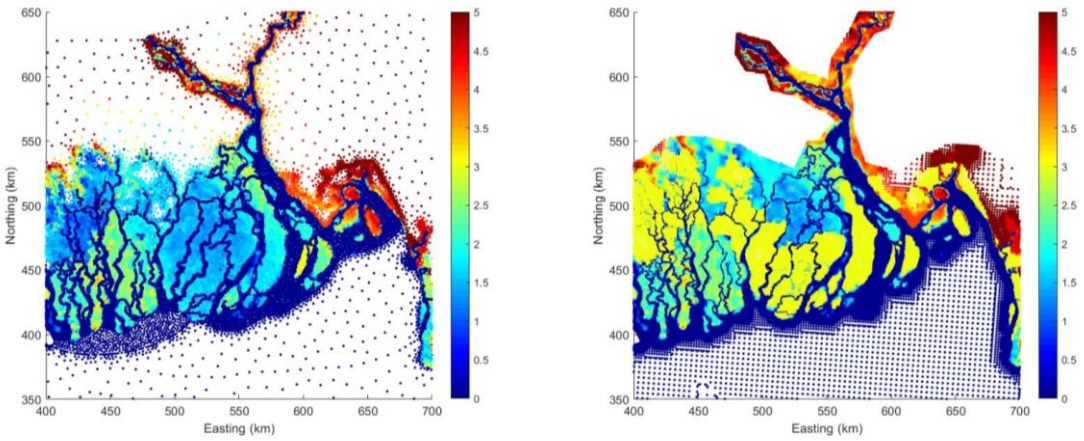

Figure 6.4 Comparison between MIKE21-FM Bay of Bengal storm surge model elevation (left panels) and the representation in Delft3D-FM large-scale morphological model (right panels).

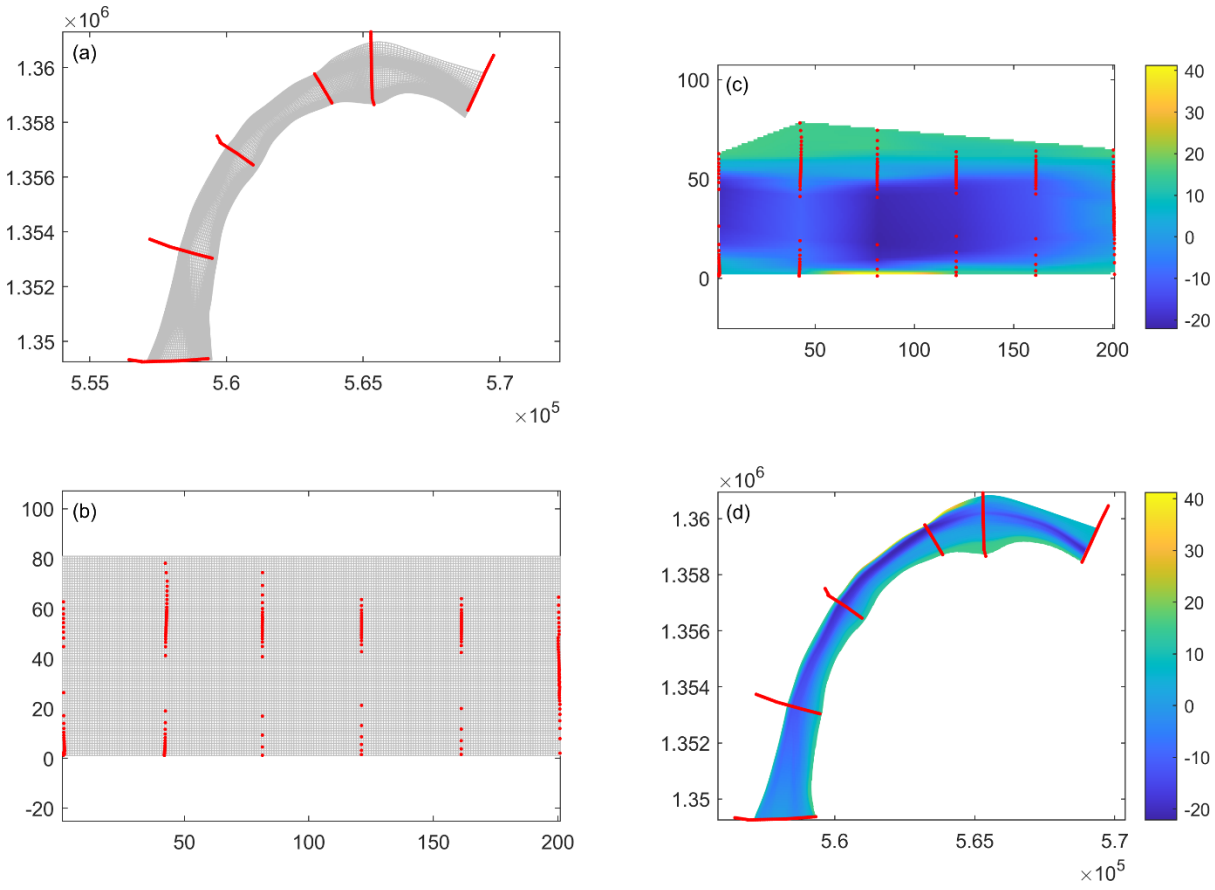

Figure 6.5 Bathymetry interpolation procedure for river reaches. (a) curvilinear grid and sample set in geographic space; (b) Sample set in curvilinear space; (c) Interpolated bathymetry in curvilinear space; (d) Back transformed bathymetry in geographic space. The channel now smoothly follows the correct thalweg even though only sparse cross-sections are given.

6.3 Hydrodynamic calibration: tidal propagation

The hydrodynamic calibration concentrated on the distribution of the tidal amplitudes throughout the lower Meghna delta and Sundarbans. It was carried out both for the stage 1 and stage 3 model setups and focused on a period of one month, January 2012, which was close to the date most of the bathymetric data was obtained and had a large number of functioning tide gauges.

6.3.1 Boundary conditions

The upstream boundary conditions varied little during the month of January 2012 and were hence taken as constant, with values of 8,340 m^3/s for the Padma and 1,440 m^3/s for the Meghna.

At the sea boundary, astronomical components of the water level were imposed, extracted from the global tidal model of (Egbert and Erofeeva, 2002) derived from the TOPEX-Poseidon laser altimetry data.

These components vary along the southern sea boundary; a typical set at the middle of this boundary is shown in Table 6.2. The component A0 represents the mean sea level and its value is consistent with the use of the BTM vertical datum.

Table 6.2 Astronomical components at centre of sea boundary

Component	Amplitude (m)	Phase (deg.)
A0	0.460	0
M2	0.523	76
S2	0.232	106
N2	0.112	70
K2	0.064	103
K1	0.114	245
O1	0.042	233
P1	0.035	239
Q1	0.002	307
MF	0.012	12
MM	0.006	5
M4	0.002	46
MS4	0.001	209
MN4	0.000	173

6.3.2 Tuning bathymetry and roughness

The two main variables determining the tidal propagation are the bathymetry and the roughness. In the bathymetry, especially for the narrower rivers it is important that the channel depth is well represented and narrow channels are connected even in a grid this is too coarse to resolve it. This has been achieve by taking the maximum sample depth in each cell instead of the average depth. This leads to good connectivity, although the average depth will be a bit overestimated.

As for the roughness, only very large-scale variations in roughness were allowed, which are specified per polygon, as shown below as an example.

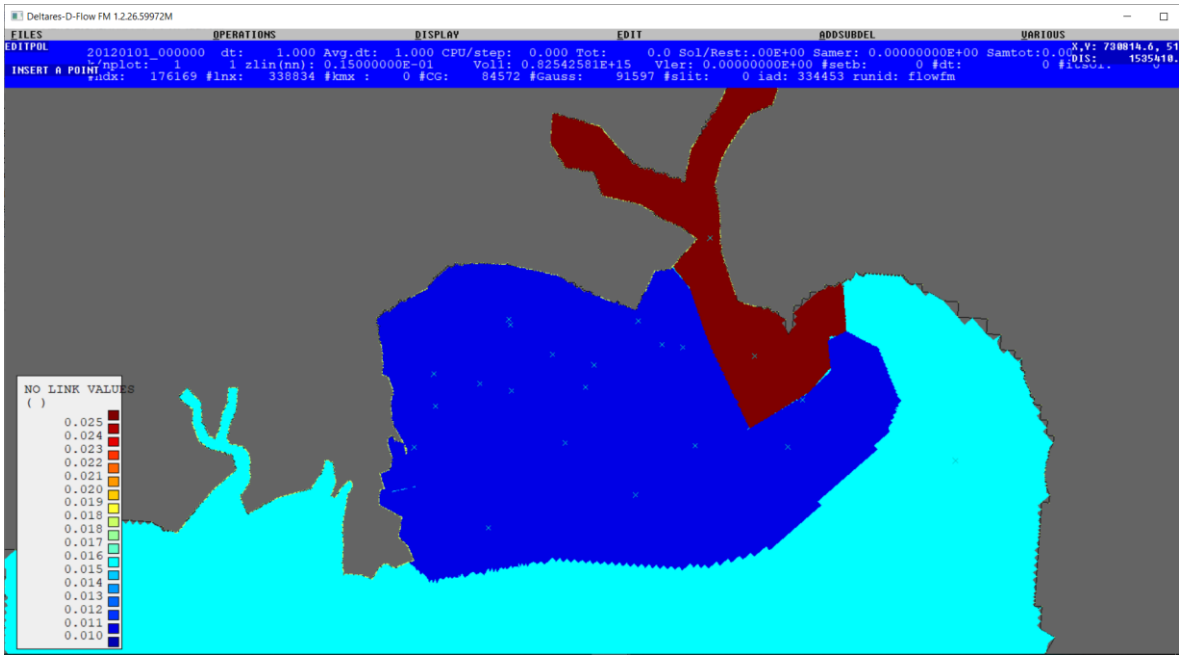

Figure 6.6 Example manning roughness map distinguishing sea (cyan), estuaries (blue) and Meghna//Padma (brown)

6.3.3 Results stage 1 model

The main variable that has been calibrated for in this coarse large-scale model is the distribution of the tidal amplitudes, and especially the M2 amplitude. The same tidal analysis procedure is applied to the simulation data as for the observations.

After a number of calibration runs, the following results were obtained, as shown in Figure 6.7 and Figure 6.8. In general, a reasonable distribution of the mean tidal range and the M2 amplitude is obtained, though there is some underestimation for the westernmost observation points, which are far up relatively narrow channels. Although further optimization may be possible, this situation was deemed acceptable to proceed to the sediment and morphology simulations.

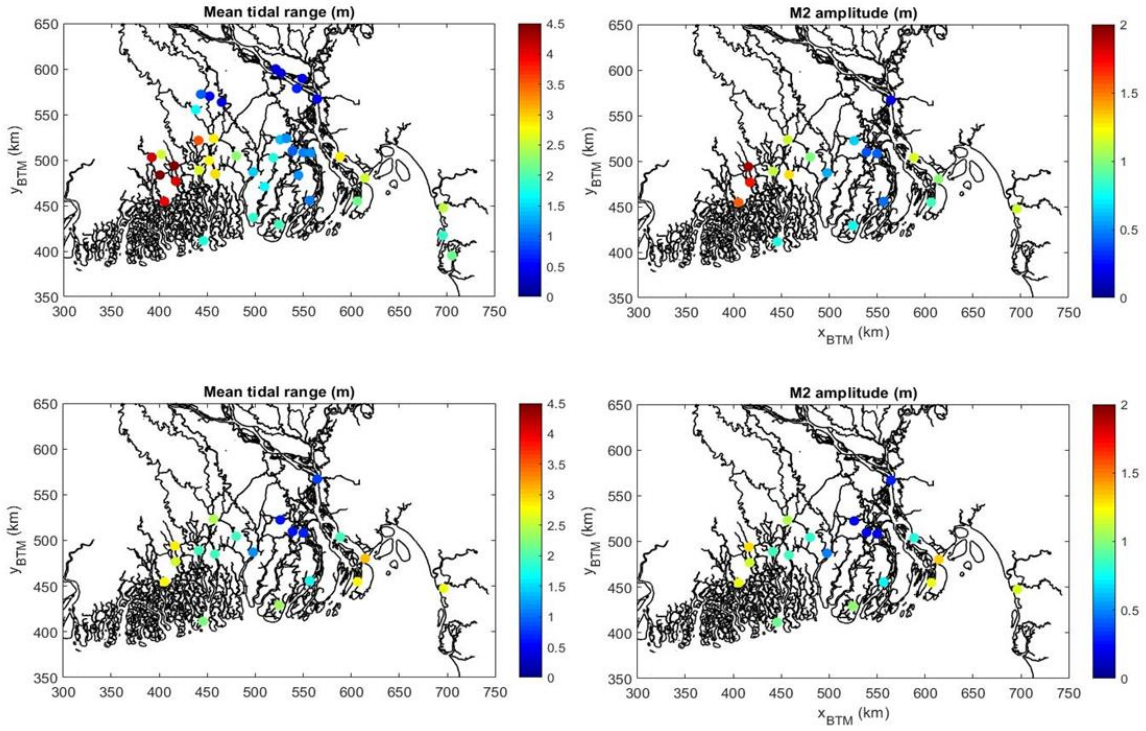

Figure 6.7 Observed (top panels) and simulated (bottom panels) mean tidal range (left panels) and M2 amplitude (right panels).

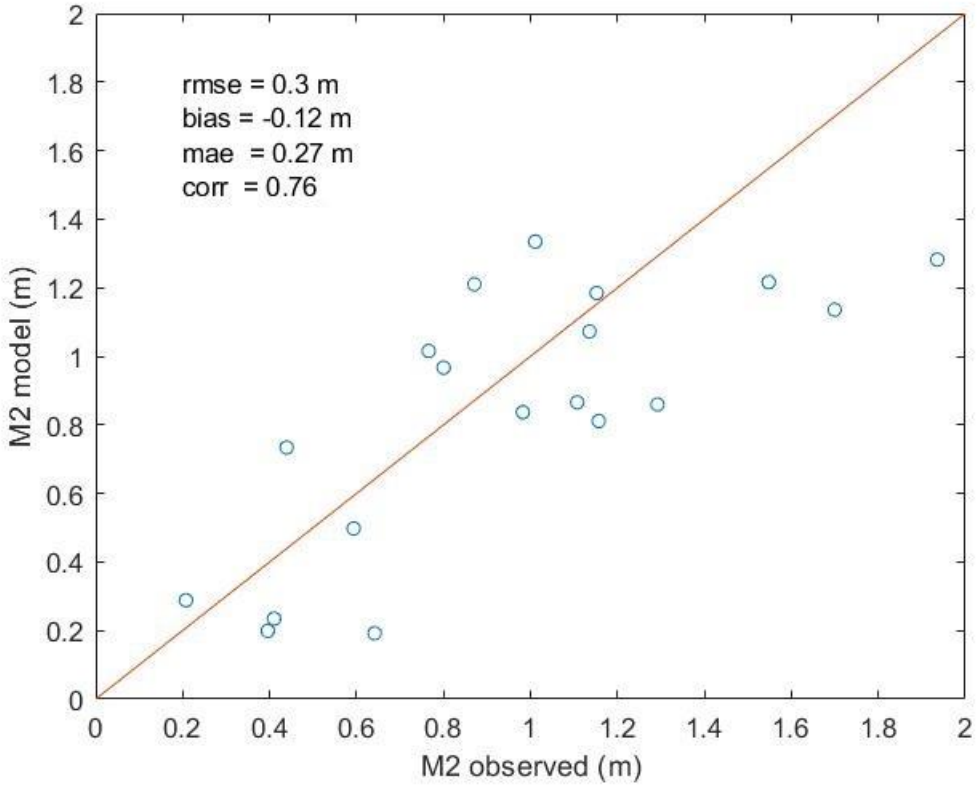

Figure 6.8 Simulated vs. observed M2 amplitude in points shown in Figure 6.7. (rmse = root mean square error, mae = mean average error, corr = correlation coefficient)

6.3.4 Results stage 3 model

After extending the model with the Ganges, Jamuna and Gorai rivers, it was recalibrated against the same dataset for the tidal propagation. The settings of run 13 showed a marked improvement going from the stage 1 model to the stage 3 model, particularly in the Pussur/Sibsa area. In the meantime, it was noticed that morphodynamic results were smoother and met with fewer problems when Chezy roughness was chosen rather than Manning formulation. An explanation for this fact is that with a constant Chezy, the roughness increases with depth, and therefore tidal flats are automatically smoother than channels which typically have large bedforms. In view of this several combinations of different Manning's and Chezy values were tried, as listed in Table 6.3. Although the differences are not enormous, a good fit was obtained with Chezy values of 120 in most of the area, with a bias of just 4 cm, an RMS error of 0.22 m and a correlation coefficient of 0.89 (see run 19). These Chezy values seem high and imply low roughness values. However, similar validation values were found in the Yangtze River with a similar model approach. Both systems consist mainly of high concentration, fine sediments. A possible explanation is that the presence of ample fine sediments leads to limited bed forms and form friction, while high sediment concentrations suppress turbulence limiting bed friction impact on the water flow.

Table 6.3 Overview of calibration tests and results.

Run	Manning/ Chezy	Uniform	Estuaries	West	Meghna/ Padma	Model stage	Bias	RMSE	corr
13	M	0,015	0,01	0,01	0,025	1	-0,12	0,30	0,76
13	M	0,015	0,01	0,01	0,025	3	0,11	0,23	0,88
14	C	65	100	100	65	3	-0,14	0,23	0,88
15	C	65	80	80	65	3	-0,21	0,24	0,88
16	C	65	100	150	65	3	-0,10	0,23	0,87
17	M	0,015	0,015	0,01	0,025	3	-0,04	0,23	0,87
18	M	0,015	0,015	0,015	0,015	3	-0,06	0,23	0,88
19	C	65	120	120	120	3	-0,04	0,22	0,89
20	C	120	120	120	120	3	0,04	0,24	0,86

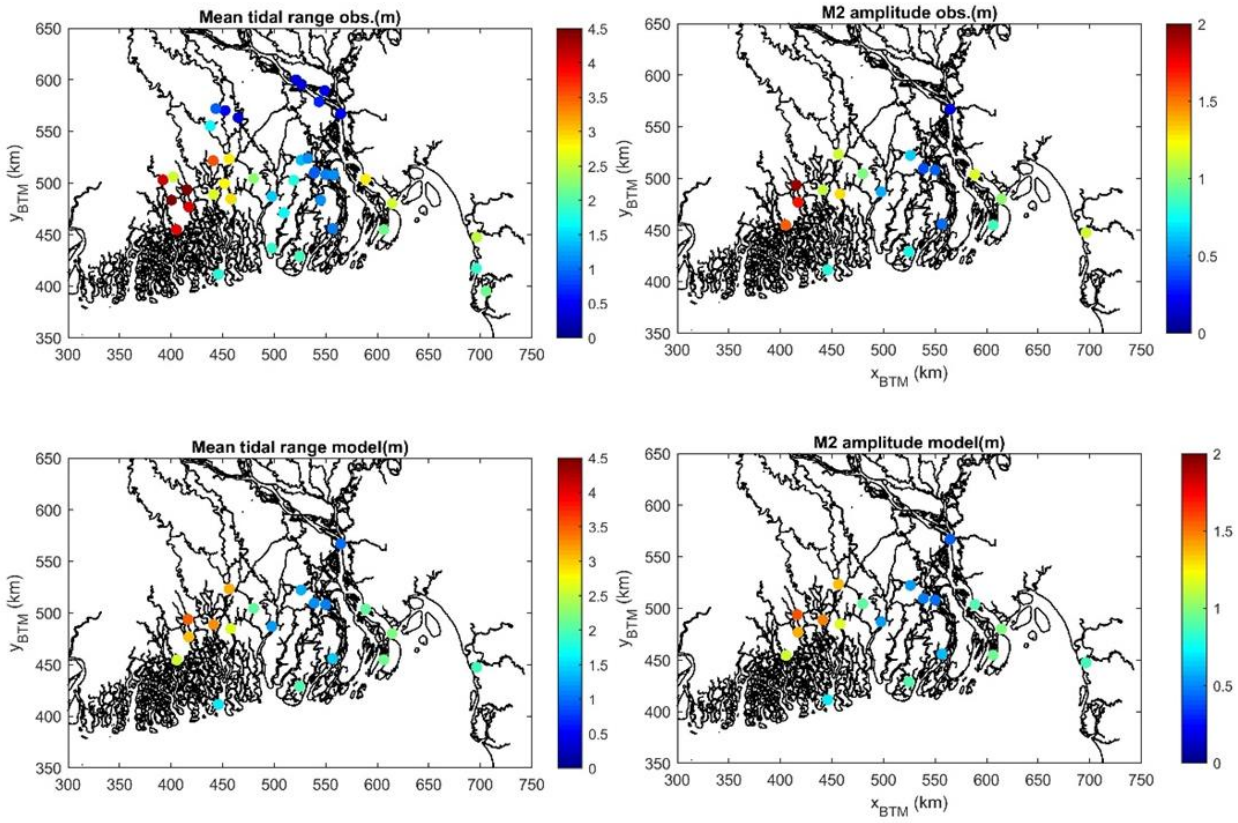

Figure 6.9 Observed and modelled mean tidal range (left panels) and M2 amplitude (right panels) for calibration run 19.

The distribution of observed and modelled mean tidal range and M2 tidal amplitude is quite similar as shown in Figure 6.9. The ratio between modelled and observed M2 tidal amplitude does not show a particular trend as shown in Figure 6.10.

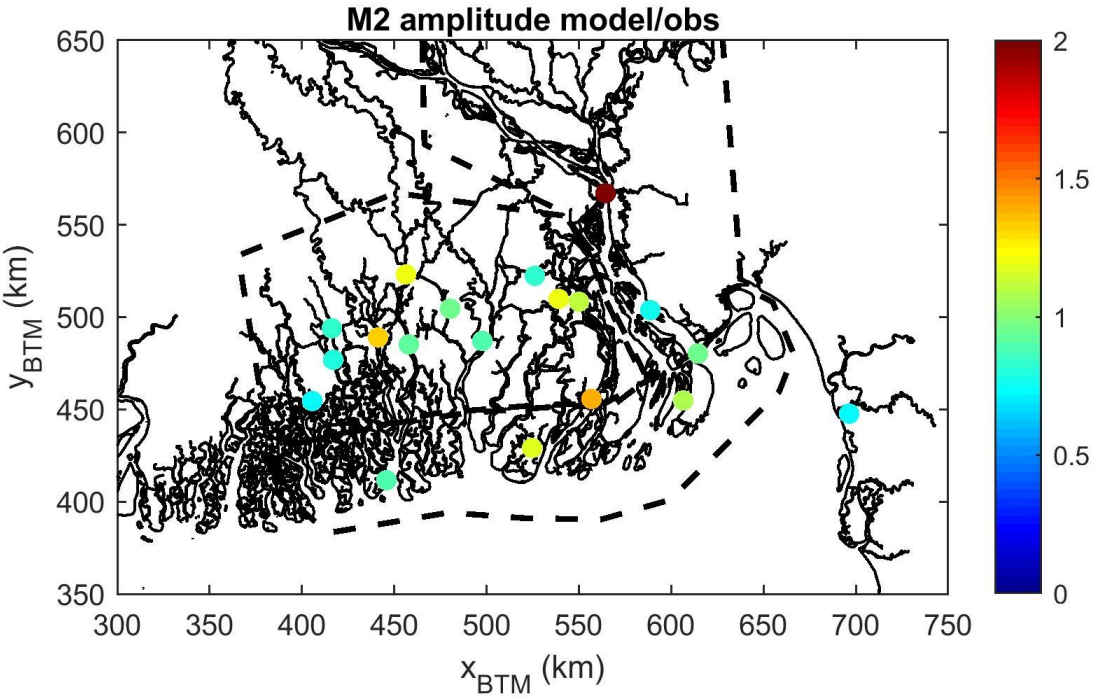

Figure 6.10 Ratio of modelled vs. observed M2 tidal amplitude, run 19.

Finally, the scatter plot in Figure 6.11 shows an acceptable correspondence between the observed and modelled M2 amplitudes.

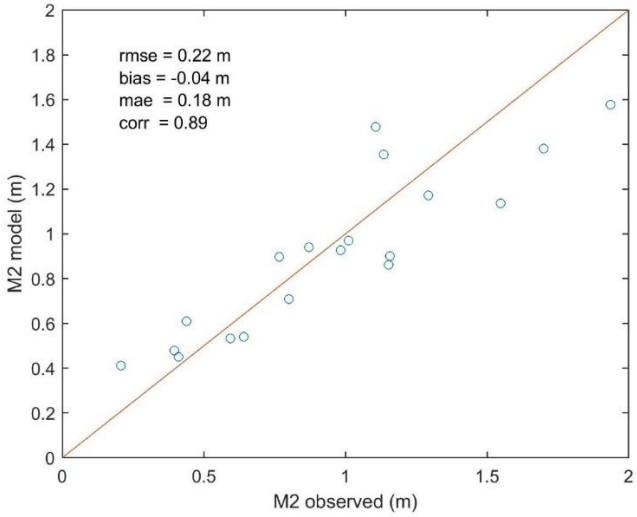

Figure 6.11 Modelled vs. observed M2 tidal amplitude, run 19.

A final modification to the roughness map was made based on a) morphological results that showed distinct patterns where the roughness changed abruptly, b) severe underestimation of discharges through section Hatiya North (see next Section) and c) an underestimation of water levels at Hardinge Bridge, in turn leading to too low discharges through the Gorai. The final roughness map for this report can be seen in Figure 6.12 as a spatial distribution.

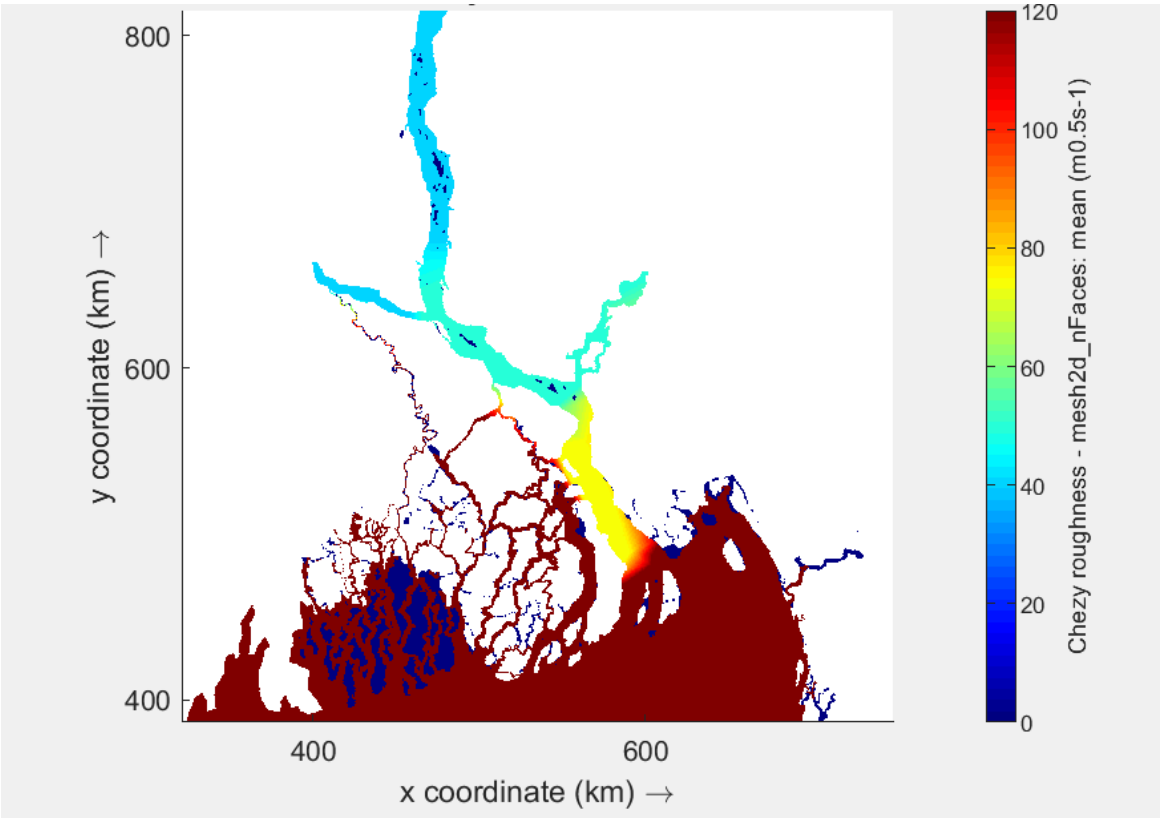

Figure 6.12 Spatial Chezy roughness distribution.

The comparison between the water level amplitudes and tidal range from observations and model in this final setup is shown in Figure 6.13 and Figure 6.14. The differences are small although there is a slight deterioration in the correlation coefficient, from 0.89 to 0.86. However, this leads to a more realistic distribution of flows as addressed in Section 6.4.

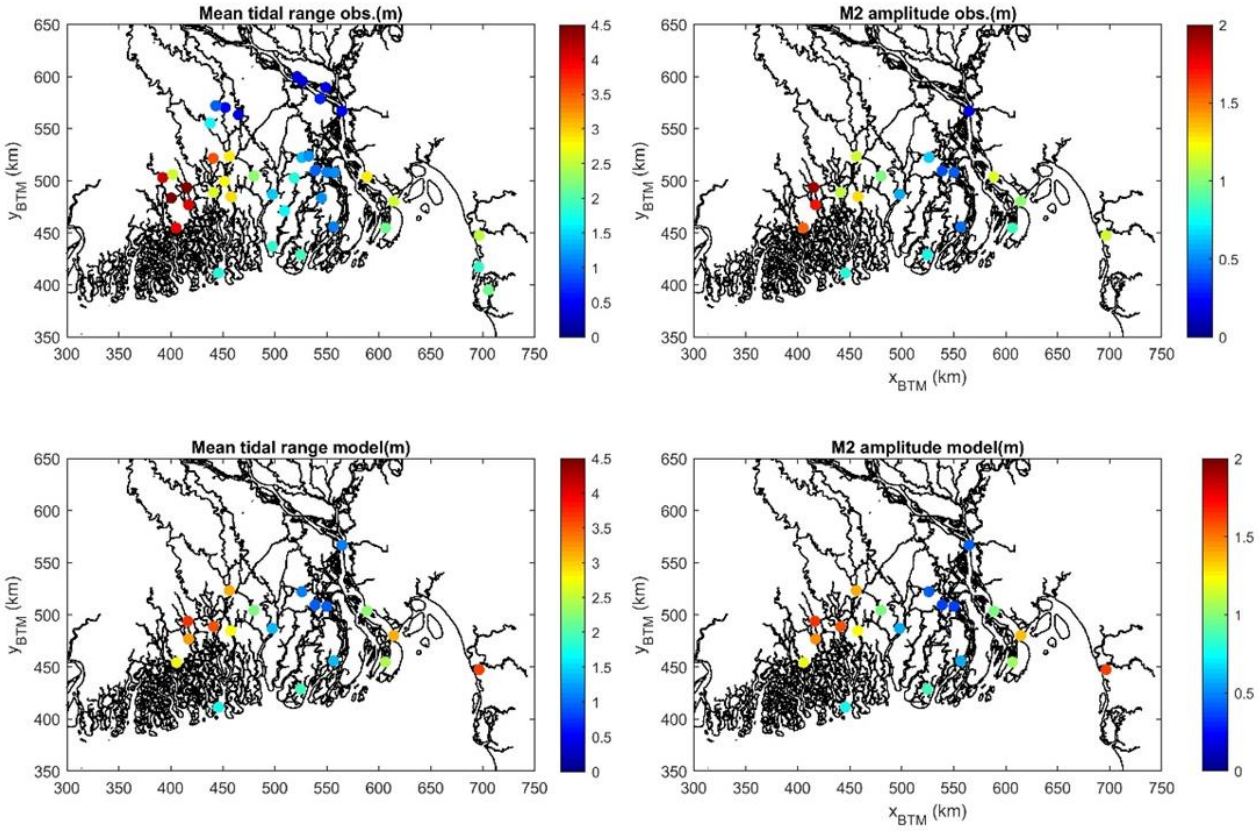

Figure 6.13 Observed and modelled mean tidal range (left panels) and M2 amplitude (right panels) for calibration run 20.

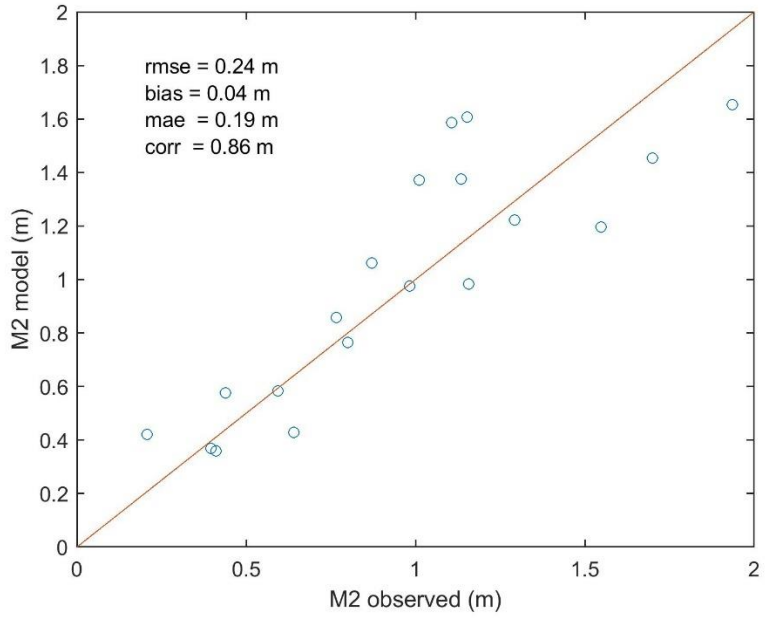

Figure 6.14 Modelled vs. observed M2 tidal amplitude, run 20

6.4 Hydrodynamic calibration: modelled vs. observed discharges

6.4.1 EDP 2009/2010

During the Estuary Development Programme in 2009/2010 several 13-hrs measurements were carried out in the Meghna estuary. These data were also used in the calibration of the meso-scale model of the lower Meghna and Tetulia. The location map is given below in Figure 6.15.

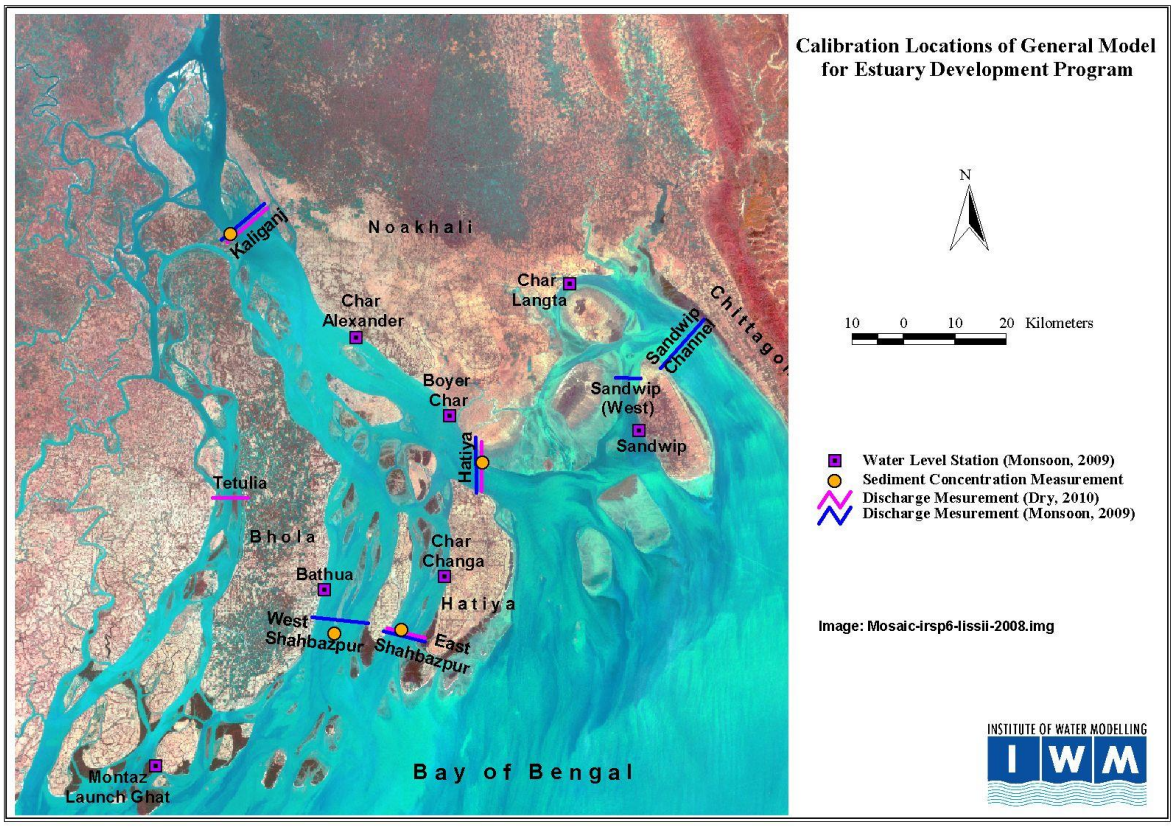

Figure 6.15 Location map of 13-hrs measurements during EDP programme

For the dry period the results are presented in Figure 6.16. The top panels show the comparison for the settings as in run 19; especially at Hatiya North the discharges are strongly underestimated; the main cause of this is the uneven roughness distribution in the area, forcing the flow more to the west. In run 20 this gradient in roughness has been removed, leading to much better agreement at Hatiya North. It is possible that a slight reduction of Chezy values in the whole area would improve the overall performance even further, but for now these results are acceptable, and further tuning has not been carried out at this stage.

The Tentulia -Nazpur cross-section and the Monpura-Jahipura section show a modest overestimation of the discharge amplitudes.

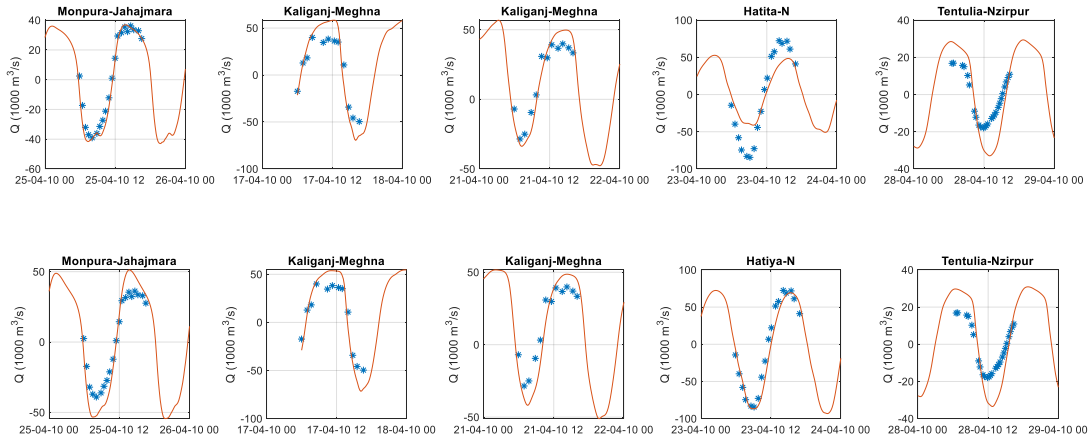

Figure 6.16 Calibration of discharges in Lower Meghna area. Top: with settings as in run 19; bottom: with roughness distribution as in Figure 6.12 (run 20). Dry period.

During the monsoon period most cross-sections show good agreement in amplitudes and phases, with the exception of Kaliganj and Tentulia cross-sections; in the first, the mean discharge seems to be overestimated whereas in the second, both amplitude and mean discharge are overestimated. This is likely due to the fact that the schematized annual hydrographs were used for the upstream boundary conditions.

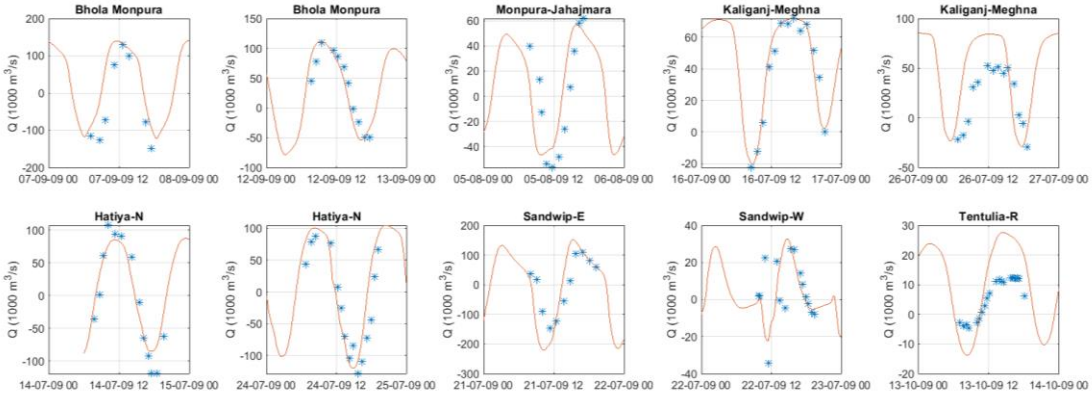

Figure 6.17 Calibration of discharges in Lower Meghna area. Top: with settings as in run 19; bottom: with roughness distribution as in Figure 6.12 (run 20). Monsoon season.

6.4.2 Pussur-Sibsa 2011

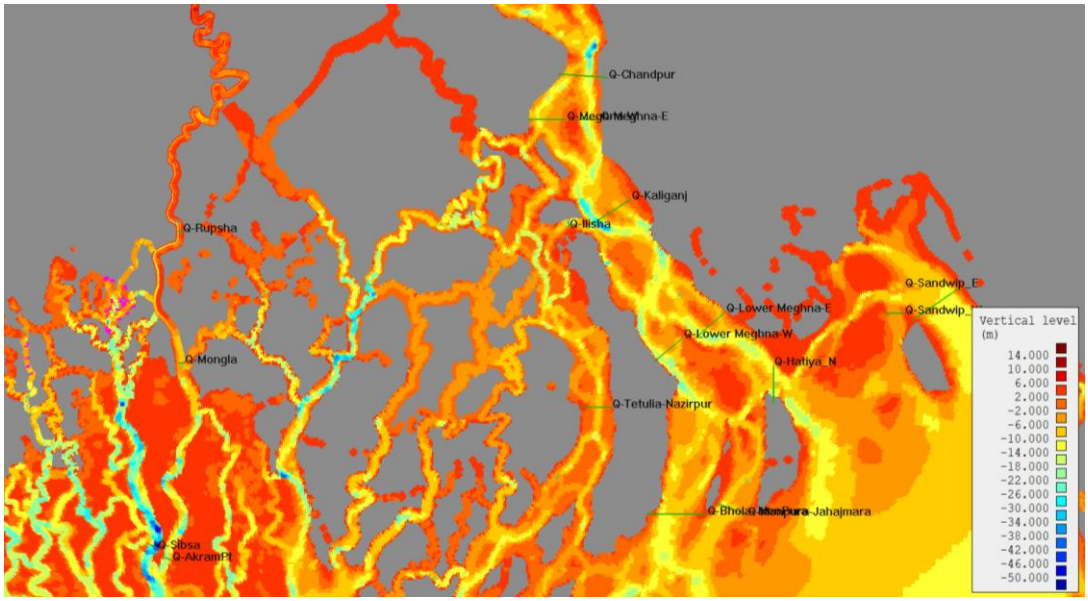

Figure 6.18 Representation of all 13-hrs measurements in stage 3 model

In the first stage model the upper reaches of the Pussur-Sibsa system were incompletely represented and the Gorai was not included. With the modifications in the stage 3 model the tidal amplitudes and discharges have much improved. The cross-sections considered are Akram Point, Mongla and Rupsha, see Figure 6.18. For the dry period (Figure 6.19), Akram Pt measurements are generally simulated well, as is Mongla on March 30, 2011; both underestimation and overestimation occur for the other two dates for Mongla. Rupsha data are followed closely on January 6 and 16, while there are unknown time shifts in the data around February 23 and March 1. Overall the agreement is acceptable given the scale of the model.

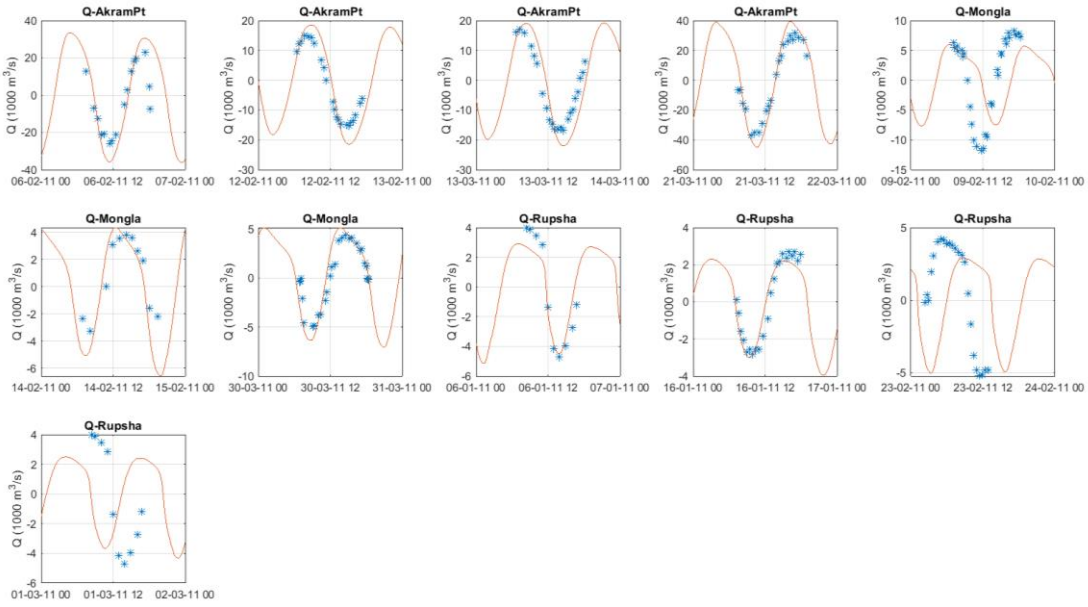

Figure 6.19 Comparison model – observations for Pussur-Sibsa area, dry period

For the monsoon period, as shown in Figure 6.20, the agreement is generally quite good. Extra attention was given to the Rupsha cross-section and as the bottom panel shows, some improvement is created by using the alternative roughness map given in Figure 6.12 and applying measured discharges at the upstream boundaries. A key factor in this is whether the water levels at Hardinge, which to a large extent drive the flow through the Gorai, are accurately represented. As Figure 6.21 shows, this is the case for the combination of roughness map and imposed discharges used in run 20. Earlier runs showed underestimation of the Hardinge Bridge water levels by up to metres.

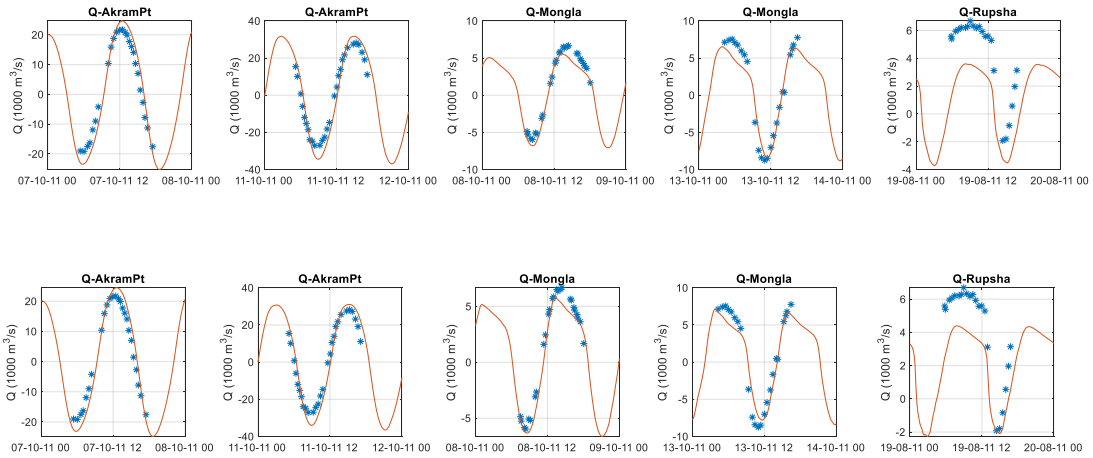

Figure 6.20 Comparison model – observations for Pussur-Sibsa area, monsoon period. Top panels: with schematized hydrograph; bottom panels: with measured discharges at upstream boundaries.

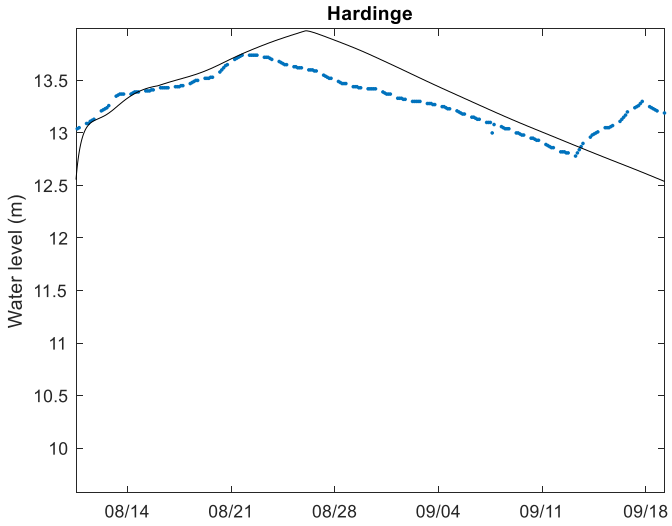

Figure 6.21 Comparison modelled (black) and observed (blue) water levels at Hardinge Bridge, monsoon period. Settings as in run 20.

6.5 Sediment model

6.5.1 Sediment Data

The literature review suggests that grain sizes of sediment of the GBM delta range from fine sands to clays, with seasonal variability in transport due to monsoons. Ganges bed sediment samples are 76% fine to very fine sands, with silt-sized grains making up the remaining bed layer (Datta and Subramanian, 1997). Downstream of the junction of the Ganges and Jamuna rivers, bed sediments are even finer with very coarse silts (Singh et al., 2007). In the coastal region, samples showed the dominant size class were also fine to very fine sands (Stummeyer et al., 2002). Sundarbans sediments are muddy, especially in the more inland located areas, while deeper portions of the Sundarbans estuaries may be sandier.

Suspended sediment in the main rivers of the GBM delta consists of fine silts and clays. Datta and Subramanian (1997) show fine silts and clays in the Ganges, Meghna, Jamuna and Padma Rivers, while the grain size of more than 95% of the suspended material is fine silt and clays (≤16 microns). Median grain sizes sampled in the Meghna estuary range from 13.8 to 25 microns, or fine to medium silts (Kuehl et al. 1989, Barua et al., 1994).

6.5.2 Model sediment settings

Following the data described in literature, the model includes both finer (mud) and coarser (sand) sediment fractions, each forced by its own sediment transport formula.

Mud transport will dominate suspended sediment concentrations, so that mud sediment settings play a major role in the calibration of concentrations and transports. The Krone-Partheniades transport formula describes the erosion and deposition of mud, while an advection-diffusion equation transports the mud (Krone 1962, 1993; Ariathurai 1974).

(10)

$$E = MS_e(\tau_{cw}, \tau_{cr,e})$$
$$D = w_s c_b S_d(\tau_{cw}, \tau_{cr,d})$$

With

E erosion flux, kg/m^2/s,

M erosion parameter,0.001 kg/m^2/s

D deposition flux, kg/m^2/s

w_s sediment fall velocity, 0.001 m/s

c_b near bed sediment concentration, kg/m^3

τ_{cw} maximum shear stress due to waves and current, N/m^2

$\tau_{cr,e}$ critical shear stress for erosion, 0.3 N/m^2

$\tau_{cr,d}$ critical shear stress for deposition, 1000 N/m^2

S_e erosion factor

S_d deposition factor

and

(11)
$$S_e(\tau_{cw},\tau_{cr,e}) = \left(\frac{\tau_{cw}}{\tau_{cr,e}} - 1\right) \quad for\ \tau_{cw} > \tau_{cr,e}$$
$$= 0 \qquad for\ \tau_{cw} \le \tau_{cr,e}$$

(12)
$$S_d(\tau_{cw},\tau_{cr,d}) = \left(1 - \frac{\tau_{cw}}{\tau_{cr,d}}\right) \quad for\ \tau_{cw} < \tau_{cr,d}$$
$$= 0 \qquad for\ \tau_{cw} \ge \tau_{cr,d}$$

Values for the different parameters applied in the standard settings of current study are given next to the parameter definitions. It was considered that mud deposition is not a function of shear stress ($\tau_{cr,d}$ >>1) and that, in our 2D model, mud is uniformly distributed over the water column. The near bed mud concentration is then given by a concentration constant over depth.

For the bed and suspended transport of non-cohesive sediment, Van Rijn et al. (2000) is followed as described in the D-morphology user manual (Deltares, 2020). Standard settings apply a sediment diameter of 150 µm, a bed slope factor (α_{bn}) of 200 and a maximum bed slope of 1:50. The latter parameters are explained in the next section.

6.5.3 Bed composition

In case of multiple sediment fractions, the model applies bed layering with an active layer concept to account for different bed sediment composition across the domain, over time and in the bed. Figure 6.22 shows the concept of the bed layer model. Initially, in the model setup, the bed consists of two underlayers (UL) of 0.25 m, and a layer that may vary in height depending on the initial sediment availability and erosion and deposition processes during a run. An active layer (AL) is present on top of the fixed layers. The active layer will rise during deposition and lower during erosion, respectively transferring and retrieving sediments and bed composition to/from underlying layers.

The initial bed composition consists of 15 m of sand and 15 m of mud that is equally distributed over a 30 m bed column. Then, during the first phase of a model run (e.g. a year), the model redistributes different sediment fractions throughout the domain, changing the bed composition based on prevailing shear stress and transport variations while bed level changes are not allowed. It is called the BCG (Bed Composition Generation) phase. Van der Wegen et al. (2011) further describe and validate the methodology. The BCG phase typically leads to sandier cells in higher energy environments. After this phase also bed level changes are allowed and the full morphodynamic runs starts.

Transport rates of different sediment fractions (sand, mud) will be proportional to their presence in the active layer. A larger percentage of sand in a cell will thus decrease mud erosion rates. The sand-mud interactions, where e.g. the presence of mud would influence the critical erosion shear stress of sand, has been classified as a second order effect.

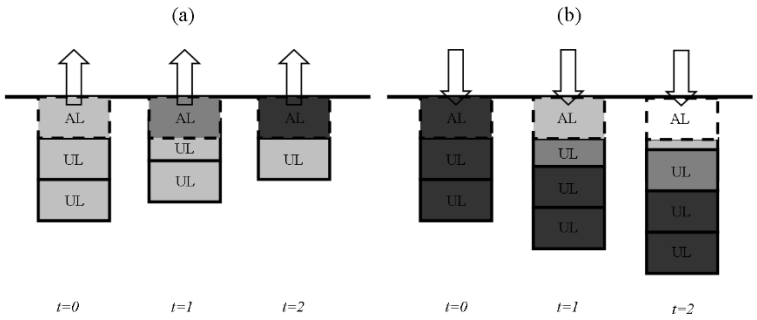

Figure 6.22 Conceptual multi-fraction bed layer model under conditions of (a) erosion of finer fractions (b) deposition of finer fractions. Darker colours indicate the presence of more, coarser fractions.

6.5.4 Morphology

Generally, in the model, sandy sediments will shape the morphology of the bed such as the meander length scale and cross-sectional profile of channels. Important parameters are the transverse bed slope parameter (α_{bn}) driving down-slope sediment transport, and the maximum bed slope parameter limiting the slope of the bed to a maximum value. If this bed slope is exceeded, numerical avalanching will redefine the bed until bed slopes are lower than the maximum bed slope. These model parameters are used to calibrate model results against observed channel-shoal patterns. Mud will generally settle in areas of limited shear stress, typically being shoals and wave sheltered areas. Mud transport is not affected by the transverse bed slope effect (α_{bn}) and the maximum bed slope factor. Entirely muddy environments will thus show relatively narrow, deep channels with steep banks.

6.6 Sediment transport boundary conditions

Based on the data analysis presented in Section 3.2 and given the wide variation in estimates of the sediment loads, the following simple conditions were taken, where the seasonal variation of the suspended load and wash load concentration was neglected. For both Ganges and Jamuna rivers a constant concentration of 0.9 kg/m^3 was assumed, well within the reported range of 0.75-1.25 kg/m^3; for the Meghna at Bhairab Bazar a much lower value of 0.1 kg/m^3. For the bed load transport equilibrium conditions were assumed. The total suspended load transport imposed on the upstream boundaries amounts to (20,200*0.9+11,300*0.9+4,600*0.1) kg/s = 28,810 kg/s = 913 Mt/yr, which is well within the range of estimates.

In order to produce the actual sediment fluxes mentioned in Akter (2014) it would be better to increase the mean concentration in the Ganges to 1.5 kg/m^3, as follows from the table below. However, for the runs reported in this report the earlier estimate of 0.9 kg/m^3 has been maintained.

Table 6.4 Flow and sediment characteristics for the Ganges, Brahmaputra, and Meghna rivers.

Rivers	Ganges	Brahmaputra	Meghna
Annual average discharge (m^3/s)	11,300	20,200	4,600
Sediment (million tonnes/y)	550	590	13
Annual average concentration (kg/m^3)	1.5	0.9	0.1
Average flood discharges (m^3/s)	52,000	70,000	13,700
D_{50} of the bed material (mm)	0.15	0.2	0.14

6.7 Sediment transport calibration

Since only infrequent and sparse concentration measurements are available, it was not considered useful to try and calibrate this large-scale model against individual measurements; rather, it was tried to reproduce the range and variability of sediment concentrations, based on the following approximate data, collected from various meso-scale reports:

Rupsha: 0.2-0.8 kg/m^3 for discharges between 0 and 6000 m^3/s;

Akram Pt: 0.2-1.5 kg/m^3 for discharges between 0 and 30,000 m^3/s;

Mongla: 0.4-1.0 kg/m^3 for discharges between 0 and 5,000 m^3/s;

Lower Meghna: in the range of 0.5-1.0 kg/m^3.

6.8 Morphodynamic model setup

6.8.1 Method

6.8.1.1 Real-time simulations vs. MorFac approach

The computational time for simulating a single year of hydrodynamics and morphology with a model such as this is in the order of 12-24 hours on a heavy computational cluster; therefore, 'brute-force' simulations of the morphological evolution over decades would be extremely cumbersome. Therefore, the well-established approach of 'morphological acceleration' or MorFac method (Roelvink 2006, Ranasinghe et al, 2011) has been applied. This works as follows: in Delft3D the model solves hydrodynamics, sediment transport and bottom updating at every timestep; however, the morphological changes are multiplied by the MorFac (the Morphological Acceleration Factor), effectively accelerating the morphological evolution. Thus, after one tidal cycle, the effect on the morphology is as if a number of cycles equal to MorFac had been run. This approach is acceptable as long as the changes within one tidal cycle, even accelerated, are small relative to the water depth.

The tidal cycle can be left unchanged or can be schematized to a single representative tide. However, the yearly discharge curve has a much longer timescale and has to be treated in a different way. As long as the discharge curve changes slowly, the flow distribution can be considered quasi-stationary. The hydrograph can then be accelerated, or 'squeezed' into a shorter time period, by the same MorFac. Squeezing the yearly hydrograph into two weeks does not fundamentally alter the flow distribution; after these two weeks all flow and transport events of a year have passed by. If now a MorFac of 26 (52 weeks divided by 2) is applied, then after one two-week cycle the morphological evolution of one year will have been simulated at the correct (morphological) speed; one hydrodynamic year with 26 such cycles thus represents 26 years of morphological change.

This methodology was tested by comparing a run forced by a 1-year hydrograph with a MorFac of 1 (run Sq1) to a run forced by a 14-days hydrograph (equal in shape, but different in duration) with a MorFac of 26 (run Sq26). Both runs applied a spin-up time of 14 days that allowed for suspension and transport of sediments but not for bed level updating and bed composition updating. Waves were included. Figure 6.23 shows that the differences are indeed minimal.

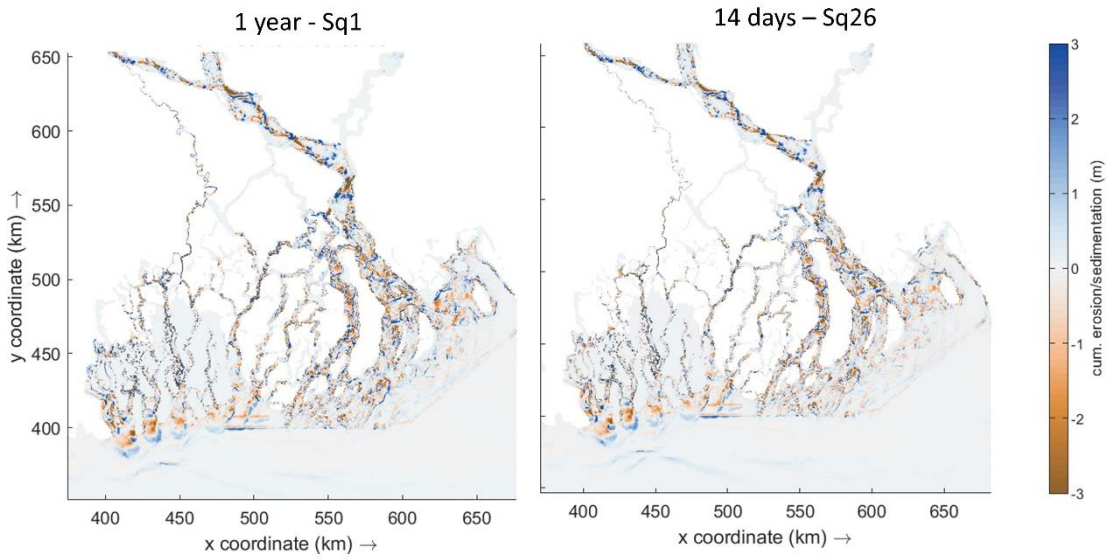

Figure 6.23 Erosion and sedimentation patterns for Run Sq1 after 1 year (upper panel) and Run Sq26 after 14 days (lower panel).

6.8.2 Domain and initial bathymetry

The domain of the morphodynamic model is the stage 3 model described in Section 7.2 and depicted in Figure 6.24. The model bathymetry sample sets were derived for two points in time, 2000 and 2012, using the datasets described in Section 3.2.1. Where multiple datasets were available, the one closest to the target date was used, in all other cases the available set was used. The initial bathymetry in the model runs is determined at runtime, by Delaunay triangulation. The depth is assigned to the grid cell centre using a tile approach.

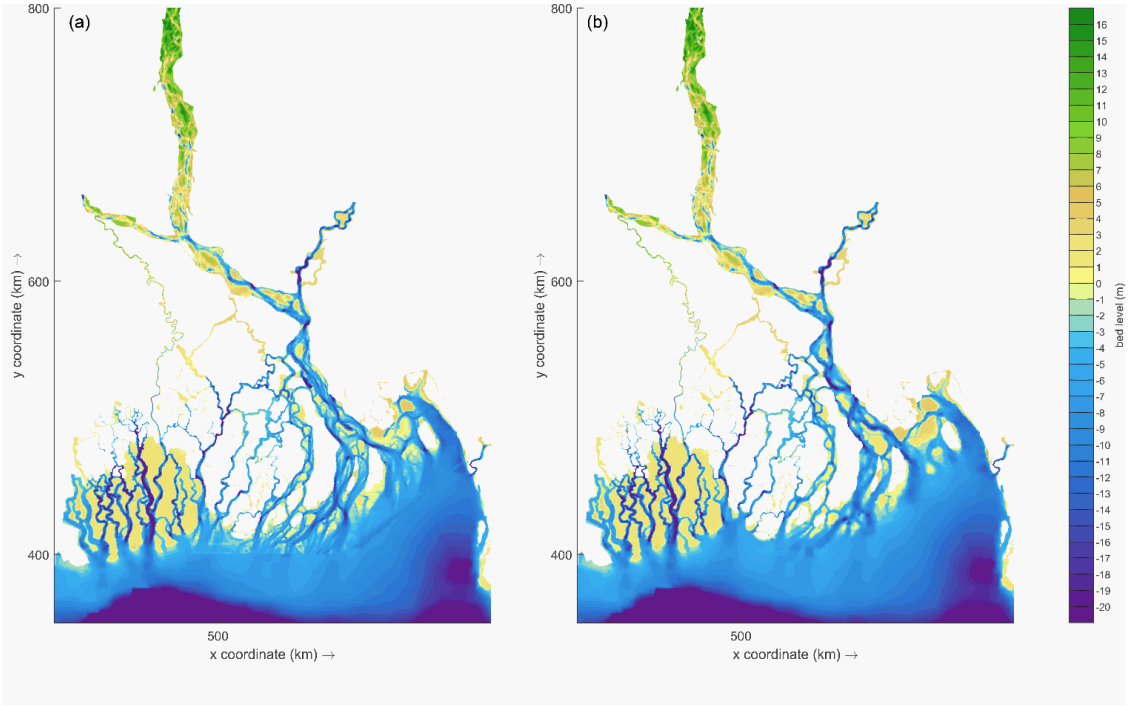

Figure 6.24 Morphodynamic model domain and bathymetry. (a) Bathymetry for runs starting in 2000; (b) Bathymetry for runs starting in 2012

6.8.3 Boundary conditions

River boundary conditions

River discharge boundary conditions are prescribed at Hardinge Bridge (Ganges), Bahadurabad (Jamuna) and Bhairab Bazar (Meghna). They are based on multi-year measurements by BWDB covering the period 1974-2012 as shown in Figure 6.25 (blue lines). A representative discharge curve was determined by determining the yearday of the peak discharge for each year and then taking the average of all discharges that are the same number of days before or after the peak. In this way smoothing out the discharge curve was avoided because of the variation in the peak discharge time. The result is shown in the yellow lines in the same figure. The variation in peak discharge and yearday of the peak discharge is shown in Figure 6.26. For the long-term simulations it is the intension to use one representative hydrograph as described above, but the variation shown here could later be used in more stochastic runs where the peak discharge is allowed to vary from year to year.

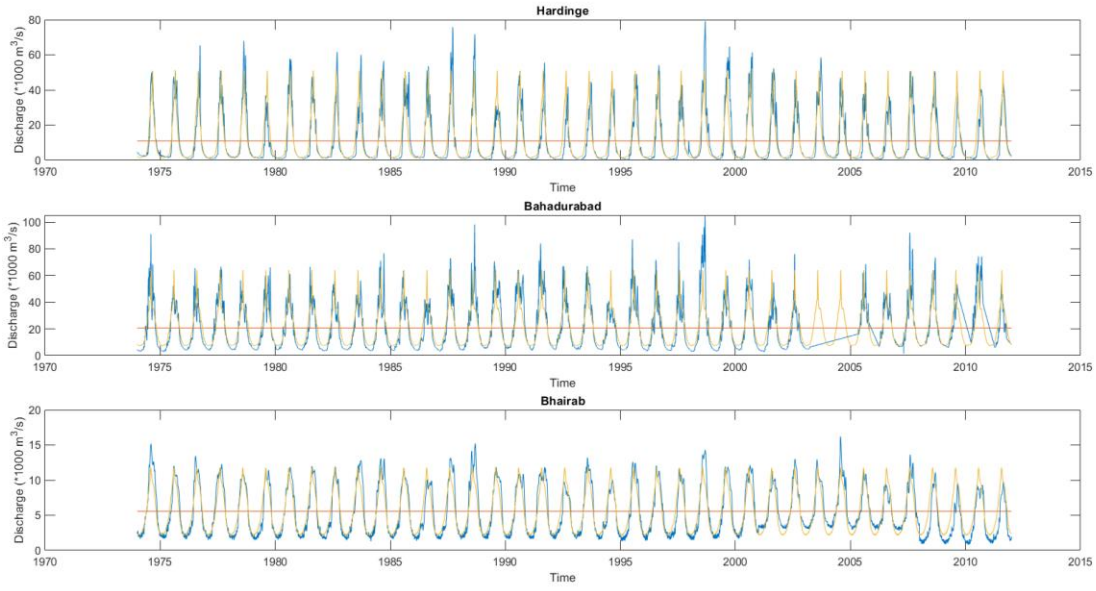

Figure 6.25 Observed river discharges of the main three rivers, 1974-2012. Blue lines: observed actual discharges. Yellow lines: multi-year average discharge curve based on days before/after peak.

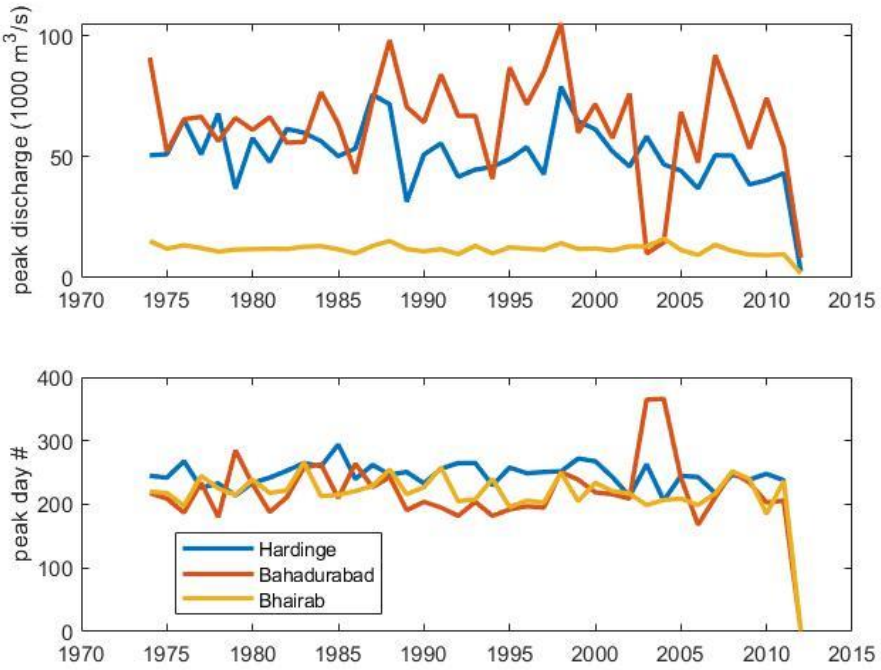

Figure 6.26 Observed peak discharges and yearday on which peak discharge took place, for Hardinge, Bahadurabad and Bhairab Bazar.

Wind fields

Wind fields are needed in the morphodynamic simulations to drive monsoon-related wind-driven circulation, and to generate local wind waves close to the coast, that add to the swell waves imposed on the boundaries. Spatial- and time-varying wind fields were sourced from the ECMWF ERA5 hindcast database (Hersbach et al., 2020), with the parameters listed in Table 6.5.

Table 6.5 Data parameters ERA5 wind fields.

Parameter	Time frame	Easting (deg)	Northing (deg)	Timestep (h)	Resolution (deg)
10m_u_component_of_wind	1979-2019	82-95	15-27	1	0.125
10m_v_component_of_wind	1979-2020	82-96	15-28	1	0.125
mean_sea_level_pressure	1979-2021	82-97	15-29	1	0.125

The hourly meteo fields were averaged over the period 1979-2019 for each month, in order to get a clean yearly wind climatology over the year (Figure 6.27). The resulting data was converted to Delft3D compatible files for spatially- and time-varying meteorological forcing.

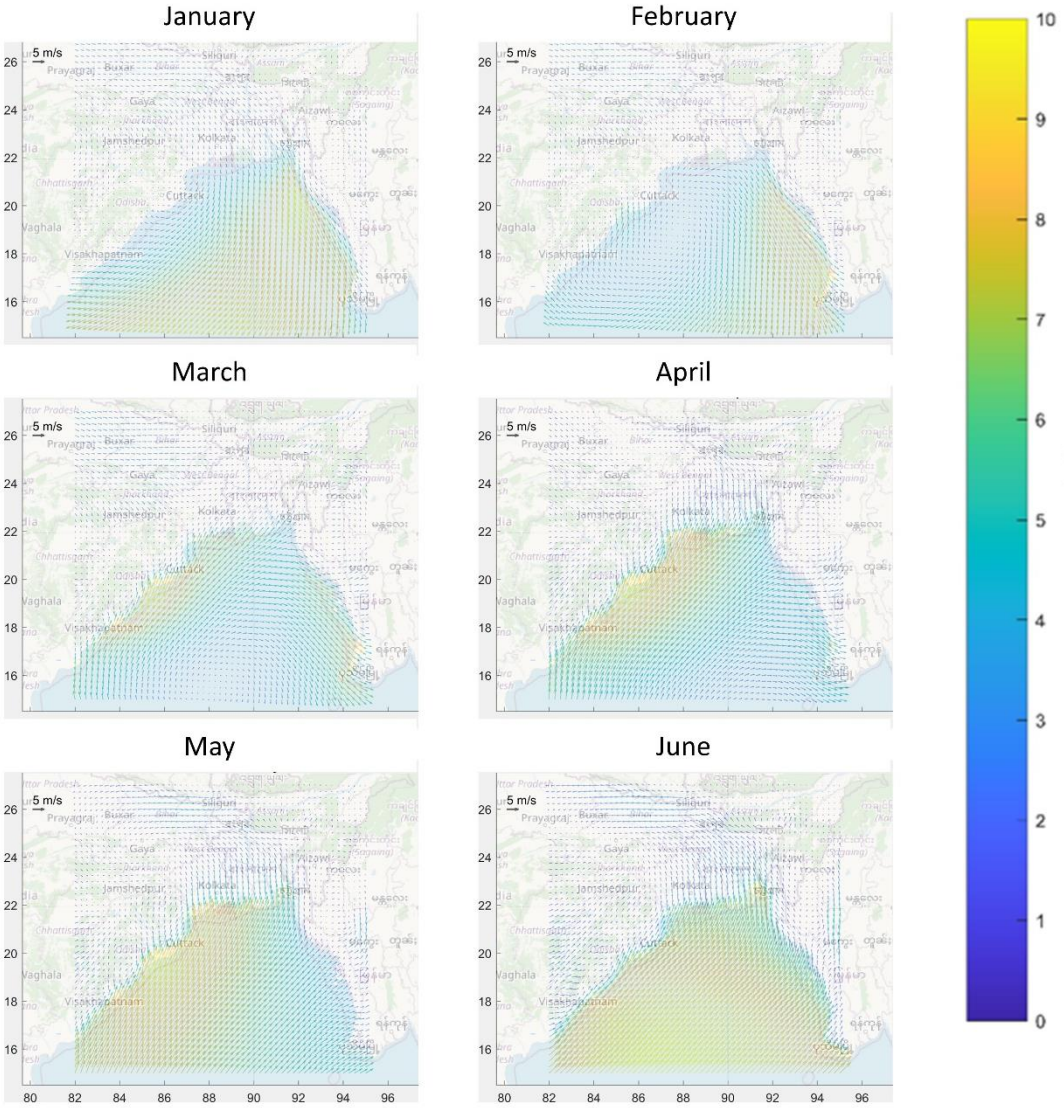
January
February
March
April
May
June
5 m/s
Siliguri
Prayagraj
Buxar
Gaya
Jamshedpur
Kolkata
Cuttack
Aizawl
Vaghala
Visakhapatnam
26
24
22
20
18
16
80
82
84
86
88
90
92
94
96
10
9
8
7
6
5
4
3
2
1
0

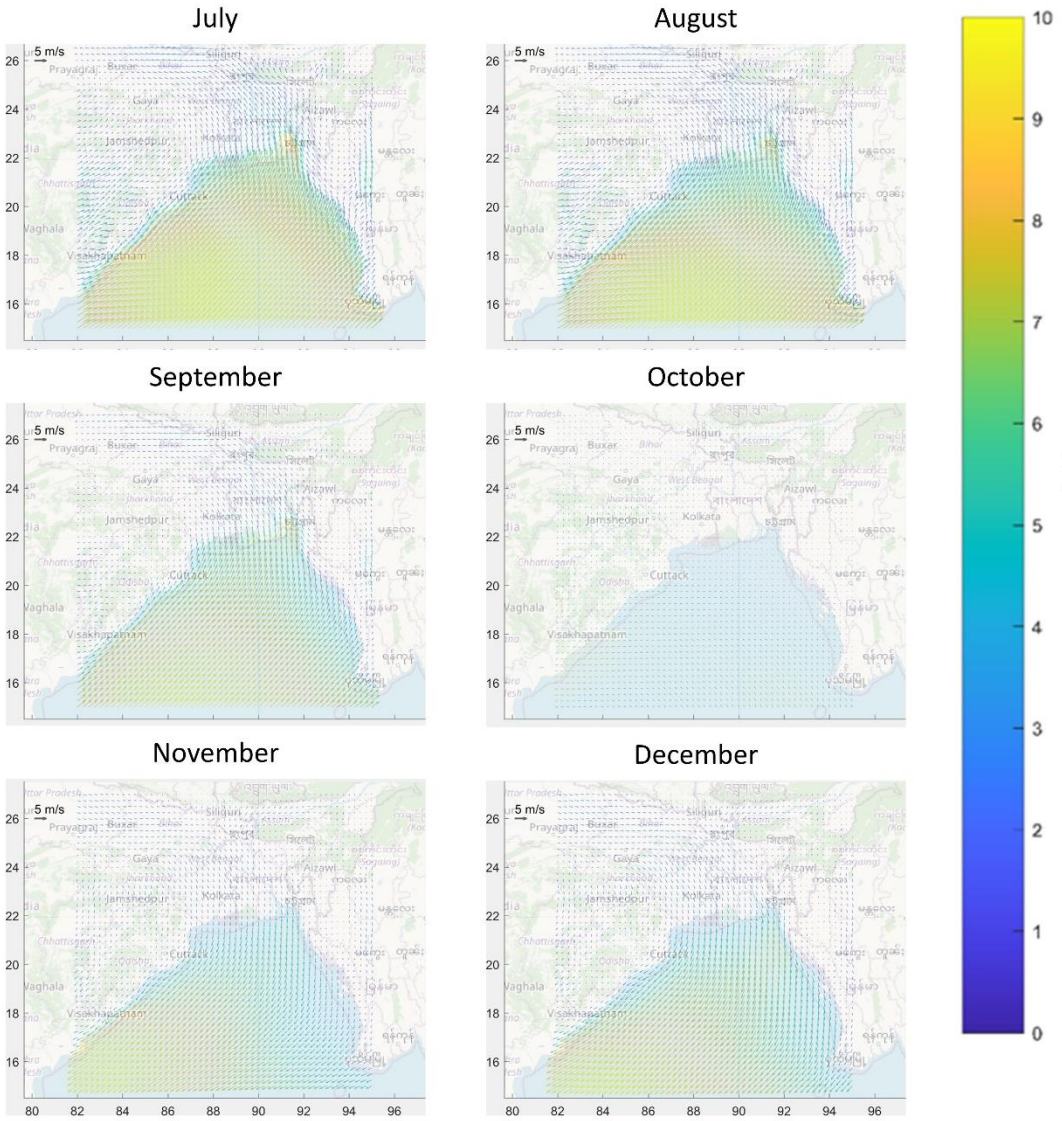

Figure 6.27 Monthly wind climatology for the Bay of Bengal, derived from 30 years of ERA5 data

Wave boundary conditions

Wave data was obtained for the same period as the wind fields at the following extraction point (20.5 ^{o}N, 91.0 ^{o}E), which has a water depth of 85m and is located due south of the Meghna estuary mouth. This location has been deemed representative for the area. From the same location, for the purpose of long-term simulations, monthly weighted average values of wave height period and direction were taken. These monthly weighted average values of wave height period and direction were applied as boundary conditions after 'squeezing' the time series by a MorFac of 26, resulting in time steps of variation of the wave conditions of a little over one day. The original time series is shown in Figure 6.28 for the period after 2000.

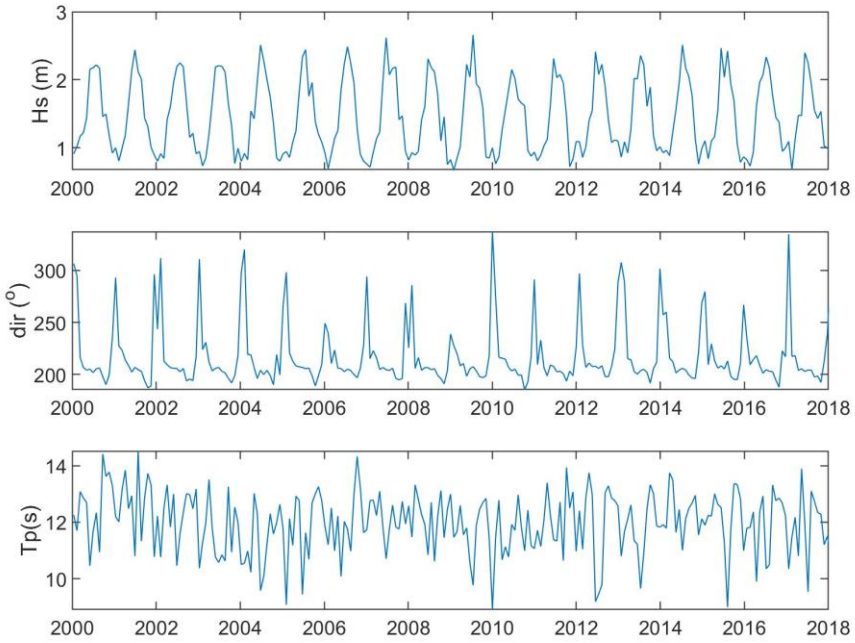

Figure 6.28 Monthly wave climatology at the 85m depth contour offshore of the Meghna estuary, derived from 30 years of ERA5 data

Assessing the effect of wind and waves

Because the effect of wind and waves on the large-scale sediment transport fluxes and erosion-sedimentation patterns was not known beforehand, as so far no existing models of the GBM delta had considered it, two base simulations were carried out, one without wind and waves and one with both. In the following sections, the results of both simulations will be compared with each other and with data, where possible.

6.8.4 Sediment settings

Given the enormous scale of the model domain sediment settings have to be a compromise between local knowledge and overall consistency. The modelling process starts from the simplest possible setup, whereby one sand fraction and one mud fraction are combined. Different initial distributions of the sand and mud have been tried and it was tested how these fractions interact in the bottom, where a layered bed composition model is applied. To avoid large morphological changes due to a wrong distribution of the sediments, so-called 'bed composition generation' (BCG) runs can be run, where the bed composition changes but the bathymetry is not updated. This provides a better starting point for morphological simulations. Alternatively or additionally an initial distribution of sediment thicknesses can be prescribed.

It is tried to adapt similar settings to those used in meso-scale models and in the 1D macro model, but this is not always possible, for instance because a meso model may be in a totally muddy area and hence have no sand fraction, which leads to different behaviour.

A simple tool can help us to assess the effect of sediment parameters on sediment concentration variations for a given area, under the assumption of spatially uniform conditions. It is focused on mud concentrations and uses the same input parameters as the Mike and Delft3D systems. Because different modelling practices exist at Deltares and DHI, it is useful to compare the effects of different settings, especially with respect to sedimentation and erosion thresholds. As shown below, this does not have to lead to very different outcomes. An example is given below:

Table 6.6 Typical parameter settings for sediment, comparison Deltares and DHI approaches.

Variable	Description	Typical Deltares setting (left panel)	Typical DHI setting (right panel)
u_{mean}	mean velocity (m/s)	0	0
u_{amp}	tidal velocity amplitude (m/s)	1.0	1.0
h	water depth (m)	10	10
frac	availability of mud fraction	1 6.6	1
M	Erosion parameter (kg/s/m2)	0.001	0.0002
w_s	fall velocity (m/s)	0.001	0.001
tau_{ce}	critical shear stress for erosion (N/m2)	0.3	0.2
tau_{cd}	critical shear stress for deposition (N/m2)	1000	0.1
C	Chezy value (m^1/2 /s)	120	120
cref	bed concentration (kg/m3)	700	700

The result for the case defined in Table 6.6 is a time series of velocity, shear stress, concentration and bottom variation over the tidal cycles. It can be seen that, for a fully muddy bottom (availability=1), and for these velocities of 1 m/s amplitude, a variation of the concentration between 0.5 and 1 g/l will be achieved, a typical value for the Pussur-Sibsa area. However, there are many combinations of parameters that can produce a similar time series of concentration. While Deltares practice is to apply continuous deposition (by setting a very high critical shear stress for deposition), DHI typically applies a low threshold for deposition; both approaches are well established in practice. In Table 6.6 and Figure 6.29 the values and results on the left are applying Deltares settings; on the right the DHI settings; both can clearly lead to similar results, though the DHI approach takes a little more time to reach an equilibrium response.

The fall velocity is the dominant parameter in determining how far the concentration falls back during slack tide.

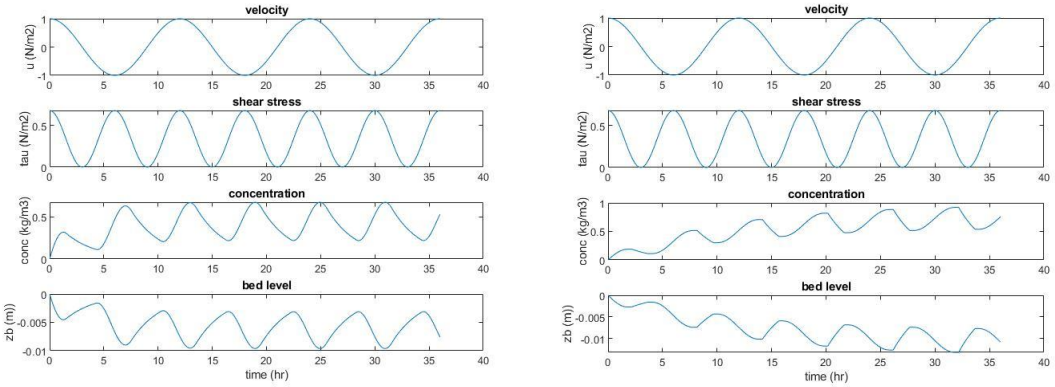

Figure 6.29 Behaviour of sediment concentration and bottom change as a function of sediment parameters; left panel: typical Deltares settings with no critical shear stress for deposition; right panel: typical DHI setting with critical shear stress for deposition

For the morphological simulations, settings of bed composition and sediment properties were varied until a satisfactory longer-term behaviour was achieved for both the morphological changes and the sediment concentration. Table 6.7 shows the sediment settings applied in the final setup.

Table 6.7 Overview of sediment parameters current model

Variable	Description	Current setting
D50	Sand median diameter (mm)	0.15
IniSedThick sand	Initial thickness of sand layer (m)	15
Cref, sand	Bed concentration sand (kg/m^3)	2650
IniSedThick sand	Initial thickness of mud layer (m)	15
frac	Availability of mud fraction	Depending on bed composition sand/mud, variable.
M	Erosion parameter (kg/s/m^2)	0.001
w_s	Fall velocity (m/s)	0.001
tau_{ce}	Critical shear stress for erosion (N/m^2)	0.3
tau_{cd}	Critical shear stress for deposition (N/m^2)	1000
C	Chezy value (m^1/2 /s)	120
Cref, mud	Bed concentration (kg/m^3)	700

With these settings, the sediment concentrations in the model range between 0.2 and 1.5 g/l. This is in line with observations both in the Pussur-Sibsa area and in the Meghna estuary mouth. These concentrations vary with the tide and throughout the monsoon.

In Figure 6.30 some time series of sediment concentration are shown from upstream at Hardinge to the Pussur-Sibsa estuary at Mongla. During the first (hydrodynamic) weeks the concentrations can be relatively high because of an initial availability of mud in the top layer of 50%. When the bed composition and morphology updating kicks in, the mud availability rapidly adapts to the local shear stresses and also the bottom profile, which can have local irregularities, tends to be smoothed by the morphodynamic updating. The evolution of the concentration with each (accelerated) hydrograph tends to a recurring pattern, and the concentrations level out at a range similar to the observations.

The spatial patterns of the time-averaged concentration are depicted in Figure 6.31, for both the simulation without and the one with wind and wave forcing. The overall pattern appears reasonable and the effect of the waves is reasonable, in that it mainly raises the level of sediment concentrations in the nearshore shelf areas.

A measure of the variability of the sediment concentration is the standard deviation in time of this concentration. As Figure 6.32 shows, the variability is substantial, almost of the same order of magnitude as the mean concentration, which is understandable due to the strong seasonal modulation and the intra-tidal and spring-neap variation. The wind and wave forcing does not add much to this variability, and in places it actually reduces it, as around Sandwip Island.

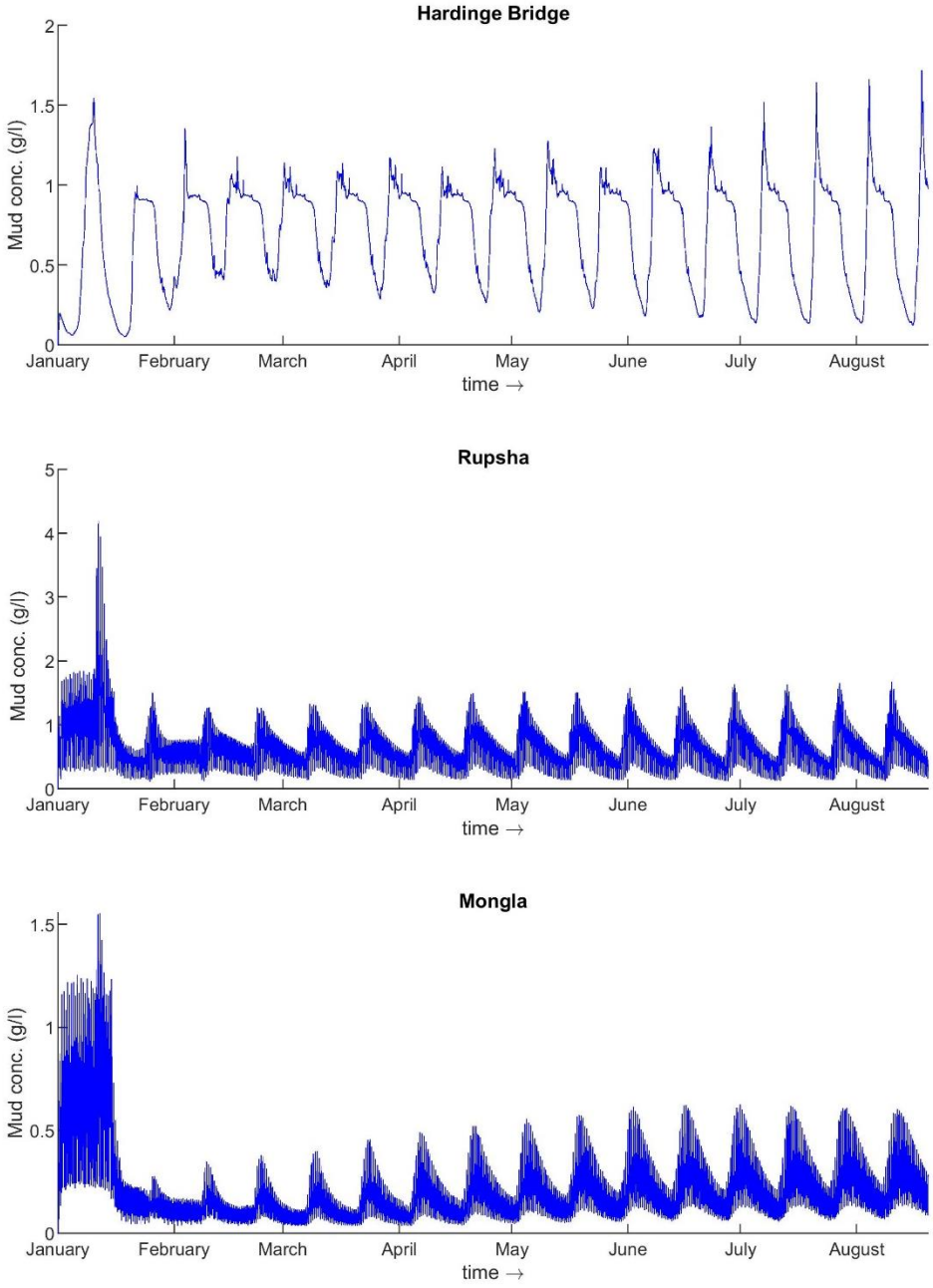

Figure 6.30 Time series of sediment concentration at Hardinge, Rupsha and Mongla.

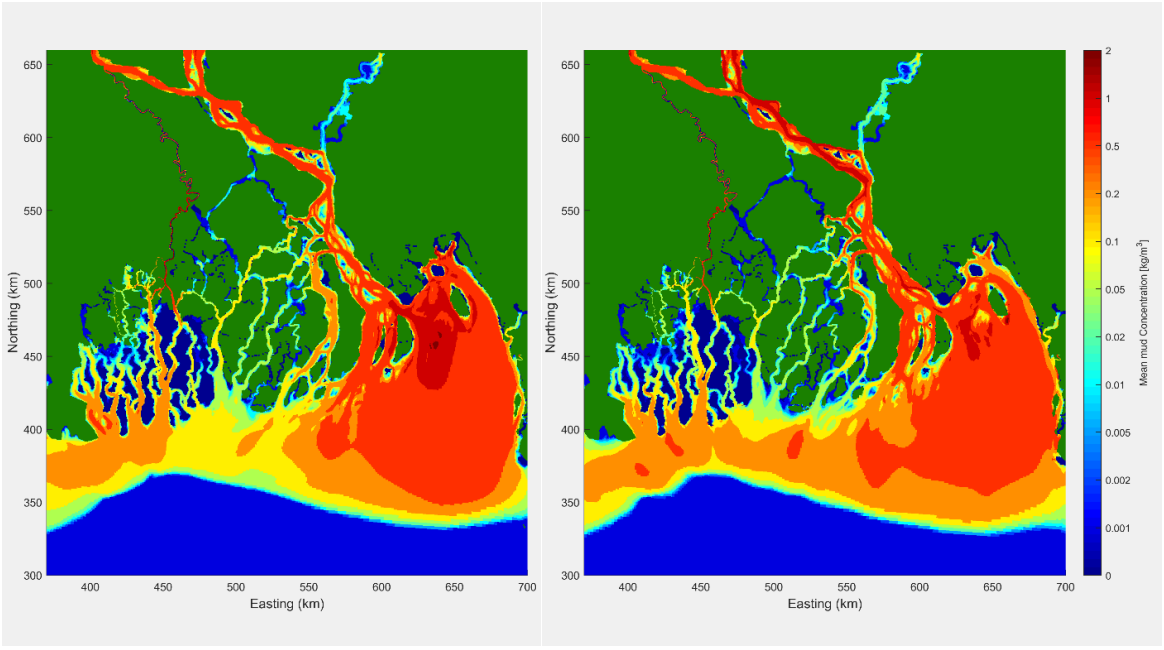

Figure 6.31 Time-averaged sediment concentration pattern in delta; left: without wind and wave forcing, right: with wind and wave forcing.

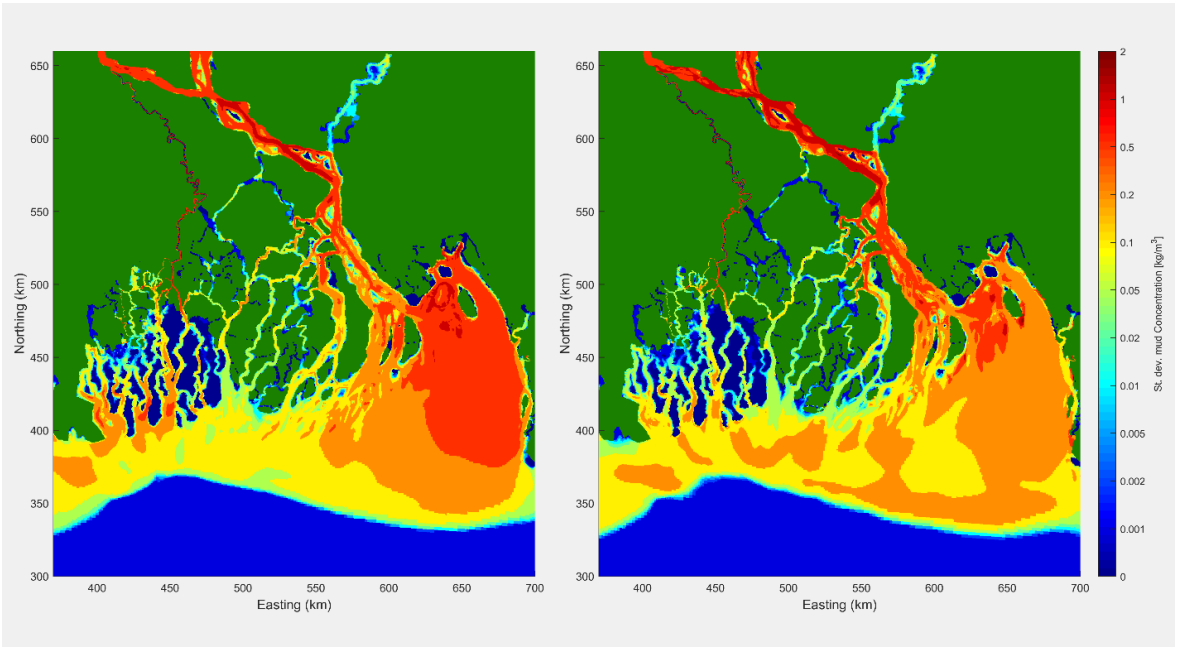

Figure 6.32 Standard deviation of sediment concentration pattern in delta; left: wind and wave forcing, right: with wind and wave forcing.

6.8.5 Morphological settings

In Table 6.8 the morphology model settings are summarized. Most parameters are set to default or have already been discussed, such as the MorFac and spin up interval MorStt; noteworthy are AlfaBn, a transverse bed slope gradient term that works only on the bedload part of the transport of the sand fraction. Since this is only a small part of the total sediment transport it needs to be set to relatively high values to have any effect and results in smoothing the bed evolution to a reasonable extent. Using the Wetslope keyword avalanching is activated when slopes get too high. As the grid is generally very coarse (500 m square cells in most cases) it is noted that a 1:50 slope still allows bed level differences of 10 m between neighbouring cells.

As was discussed before, the underlayer model (second part of Table 6.8) is essential to create a realistic spatial distribution of the sediment fractions in the top layer, which in turn greatly influences the sediment concentrations.

Table 6.8 Overview of morphological parameters current model

Morphology			
MorFac	26	[-]	Morphological scale factor
MorStt	1209600	[s]	Spin-up interval from TStart till start of morphological changes (14 d)
Thresh	0.05	[m]	Threshold sediment thickness for transport and erosion reduction
MorUpd	true	[-]	Update bathymetry during FLOW simulation
NeuBCMud	false	[-]	Neumann condition for upstream mud boundary
NeuBCSand	true	[-]	Neumann condition for upstream sand boundary
AksFac	1	[-]	van Rijn's reference height = AksFac* ks
RWave	2	[-]	Wave related roughness = RWAVE * estimated ripple height.
AlfaBs	1	[-]	Streamwise bed gradient factor for bed load transport
AlfaBn	200	[-]	Transverse bed gradient factor for bed load transport
Sus	1	[-]	Multiplication factor for suspended sediment reference concentration
Bed	1	[-]	Multiplication factor for bed-load transport vector magnitude
SusW	0	[-]	Wave-related suspended sed. transport factor
BedW	0	[-]	Wave-related bed load sed. transport factor
SedThr	0.2	[m]	Minimum water depth for sediment computations
ThetSD	0	[-]	Factor for erosion of adjacent dry cells
Wetslope	0.02	[-]	Threshold bed slope for avalanching
Underlayer			
IUnderLyr	2	[-]	Flag for underlayer concept 1 = one well mixed layer 2 = multiple layers
ExchLyr	false	[-]	True/false separate exchange layer
TTLForm	1	[-]	Transport layer thickness formulation
ThTrLyr	0.25	[m]	Thickness of the transport layer
MxNULyr	2	[-]	Number of underlayers (excluding final well mixed layer)
ThUnLyr	0.25	[m]	Thickness of each underlayer

6.8.6 Calibration

The most complete morphological calibration data available is the comparison of bathymetric surveys from 2000 and 2009, as described in the EDP report on updating of the morphological model of the EDP area (IWM, 2010). The areas used in the volume balance were converted to the BTM coordinate system and the same analysis was applied namely the rate of change of the erosion, deposition and net volumes per area. The areas are shown in Figure 6.33, along with the simulated erosion-sedimentation patterns over the same period of 2000 to 2009. In the left panel, as with the subsequent figures, the results without wind and wave effects are presented; in the right panel the erosion/sedimentation is shown for the simulation with the monthly averaged wind and wave time series.

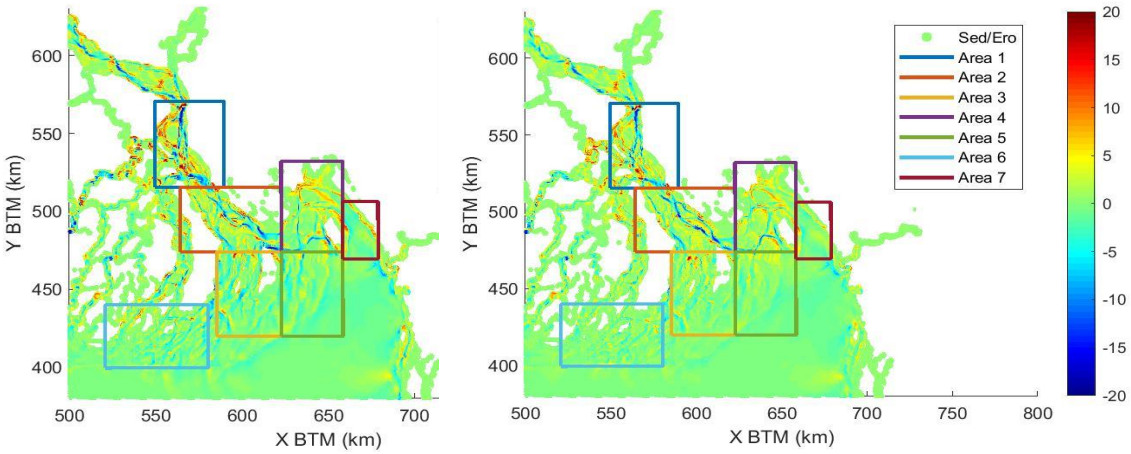

Figure 6.33 Sedimentation/erosion pattern over period 2000-2009 in lower Meghna area, and volume balance areas applied in EDP study (2009). Left panel: simulation without wind and waves; right panel: simulation with realistic time series of wind and waves.

In Figure 6.34 to Figure 6.40 the evolution of the erosion, sedimentation and net volumes is shown in time, clearly showing the effect of the seasonal variation on top of the trends. Also, the hypsometry change (the change in how the surface area is distributed as a function of bed level) is shown in the panel next to it. For each area, the trends are shown without (left) and with (right) wind and waves included. The effect is negligible in Area 1 and 2, as they are mostly sheltered from the waves, but for Area 3 the wind and waves are able to reverse the net erosion to net accretion especially leading to more sedimentation in shallow areas. In Area 4, which in the measurements showed the strongest accretion, an already positive net trend is enhanced; in Area 5 the negative net trend is reduced and then reversed to accretion. Area 6, southwest of Bhola, shows subtle differences with slightly more accretion with waves, and a hypsometry that is almost stable. Finally, Area 7 shows strong accretion in the shallow areas but a deepening of the channels, and a net positive trend.

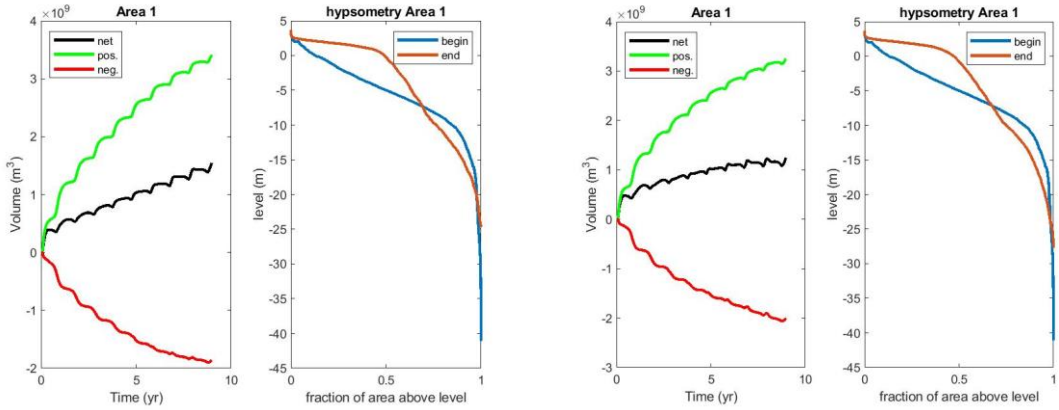

Figure 6.34 Volume and hypsometry change 2000- 2009; left: without and right: with wind and waves; Area 1.

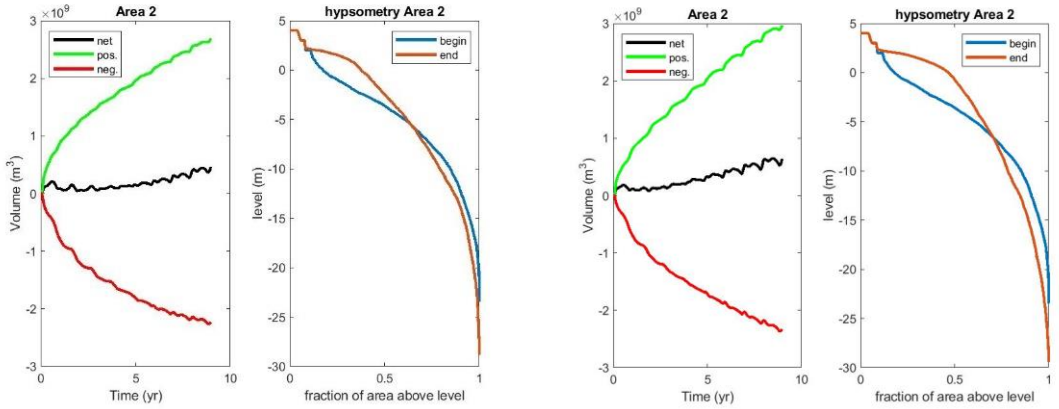

Figure 6.35 Volume and hypsometry change 2000- 2009; left: without and right: with wind and waves; Area 2.

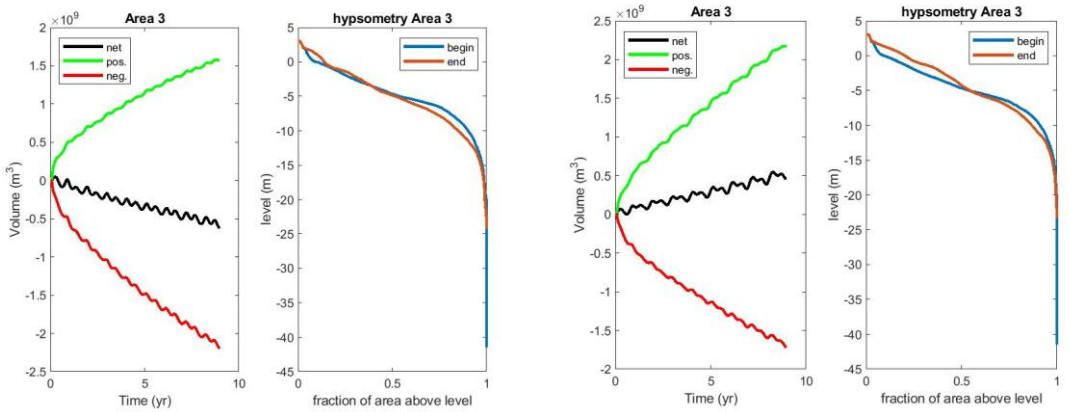

Figure 6.36 Volume and hypsometry change 2000- 2009; left: without and right: with wind and waves; Area 3.

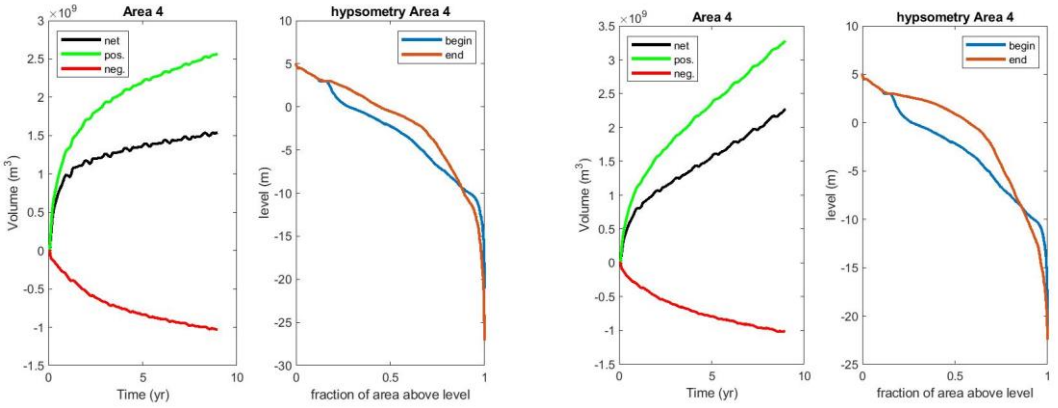

Figure 6.37 Volume and hypsometry change 2000- 2009; left: without and right: with wind and waves; Area 4.

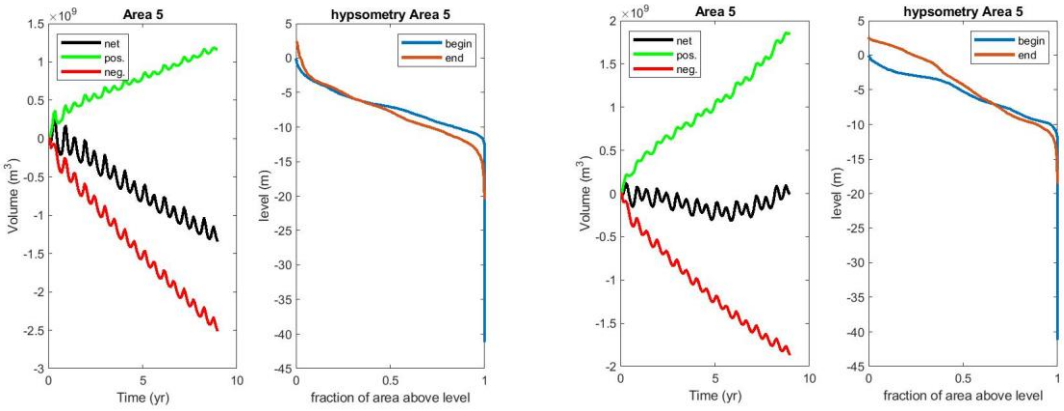

Figure 6.38 Volume and hypsometry change 2000- 2009; left: without and right: with wind and waves; Area 5.

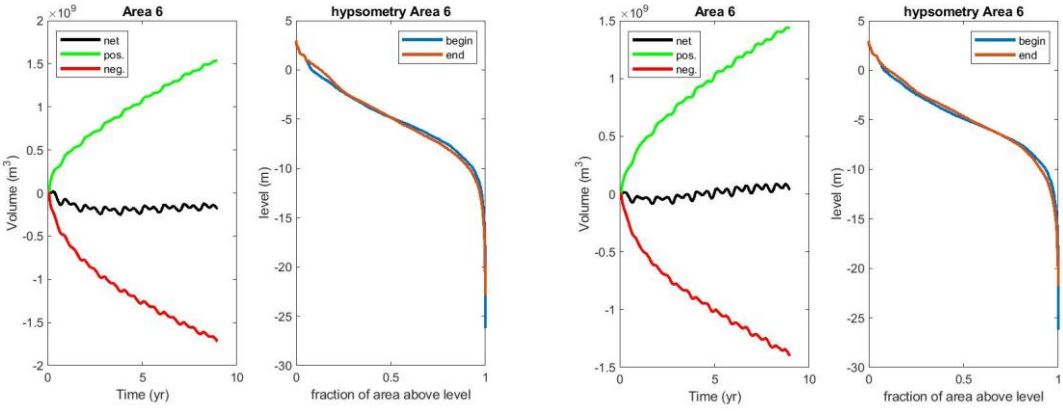

Figure 6.39 Volume and hypsometry change 2000- 2009; left: without and right: with wind and waves; Area 6.

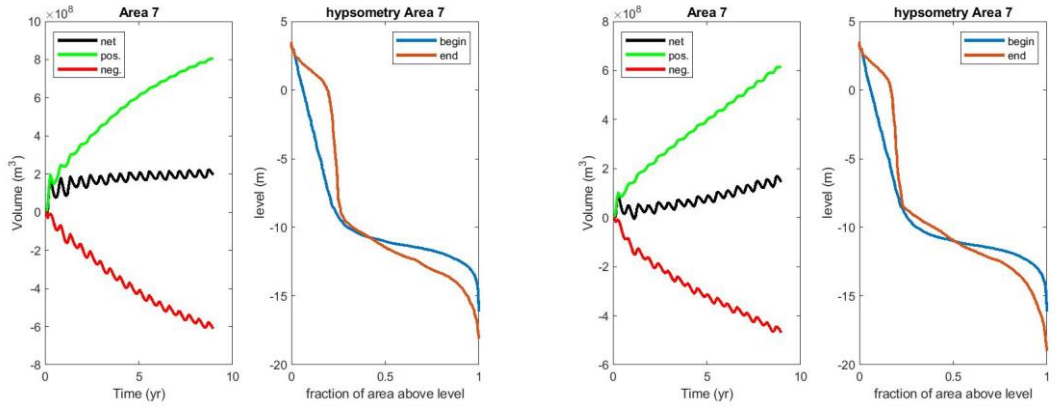

Figure 6.40 Volume and hypsometry change 2000- 2009; left: without and right: with wind and waves; Area 7.

The erosion, accretion and net volume change over the period from 2000 to 2009 as simulated is compared with the observed volumes in Figure 6.41. The results of the simulation without wind and wave effects show some agreement, albeit with a large scatter, for the gross volume changes but the net changes are uncorrelated or even negatively correlated. When the wind and waves were included the scatter in the gross changes reduces significantly and 5 out of the 7 areas show the correct sign of the net trend.

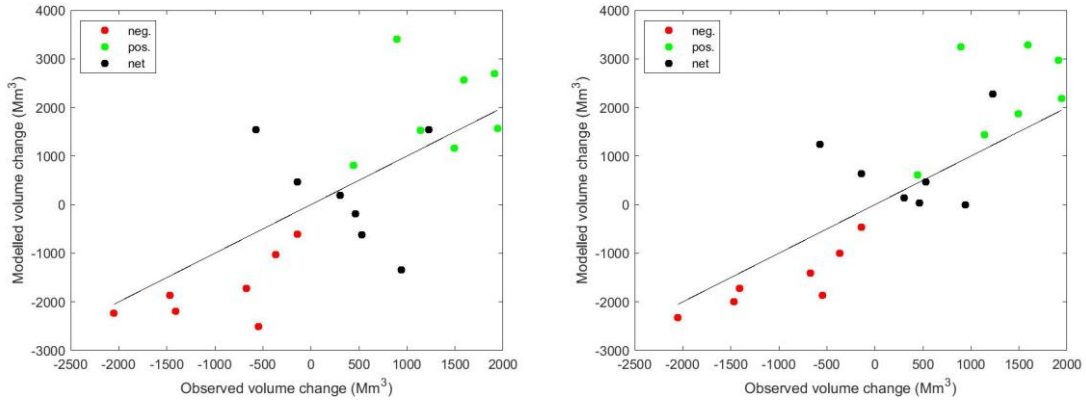

Figure 6.41 Computed vs. observed erosion (red), sedimentation (green) and net volume change (black) in the period 2000-2009, for a simulation without (left) and with (right) wind and waves.

The observed and modelled volume changes are also listed in the table below (Table 6.9). It is important to note that the overall trends are comparable, and erosion and sedimentation volume changes are highly to moderately correlated (0.85 resp. 0.53). Although the net volume change is the difference of two uncertain numbers, there is still a correlation of 0.13 and the total changes (negative, positive and net) are all overestimated by the same factor of approx. 1.6. Overall this result is as good as could be expected given the large uncertainties in the observed data, the boundary conditions and the model settings.

Table 6.9 Observed and modelled volumetric changes.

	Observed volume change (Mm3)			Modelled volume change (Mm3)		
	Neg.	Pos.	Net	Neg.	Pos.	Net
1	-1467	892	-574	-2003	3247	1245
2	-2050	1908	-142	-2325	2968	643
3	-1408	1941	533	-1721	2182	462
4	-366	1594	1228	-1005	3283	2278
5	-547	1492	944	-1871	1863	-7
6	-672	1138	465	-1403	1438	35
7	-139	444	305	-469	614	145
Total	*-6649*	*9409*	*2759*	*-10796*	*15596*	*4801*

Table 6.10 Statistics of the observed and modelled volumetric changes.

Parameter	Neg.	Pos.	Net
RMSE	367	854	962
BIAS	-592	884	292
MAE	592	884	752
SLOPE	1.62	1.66	1.74
CORR	0.85	0.53	0.13

6.8.7 Sensitivity analysis

Due to long computation times only a limited sensitivity analysis was carried out. The findings are summarized below:

- Excluding Coriolis' force has a very limited effect;
- Increasing the sand diameter from 150 µm (standard settings) to 250 µm has a very limited effect on morphodynamics. This is probably due to the fact that, for morphodynamic development, spatial sediment transport gradients are more important than actual transport magnitudes;
- Increasing the transverse bed transport parameter (α_{bm}) from 200 to 500 has a limited effect, whereas lower values (50,100) lead to much narrower and deeper channels;
- Applying a bed slope parameter of 1:200 instead of 1:50 (standard settings), leads to shallower and wider channels. For the Jamuna and Meghna estuary this looks reasonable. However, narrower estuaries like Pussur and Sibsa lose too much channel depth so that tidal intrusion is limited too much. Applying a muddier bed composition to the Pussur-Sibsa system (which is quite muddy) would lead to steeper slopes and deeper channels since the bed slope effect only applies to sand transports.

6.9 Present-day analysis

6.9.1 Distribution of surface sediment

Figure 6.42 shows the presence of mud as percentage of the upper bed layer volume. In the major rivers and estuaries, the mud is distributed towards the shoals, whereas mud is washed out in the

deeper channels that mainly consist of sand. Some mud deposits in the deeper coastal areas directly south of the Meghna mouth, while major mud deposition occurs in the area where the continental shelf rapidly deepens.

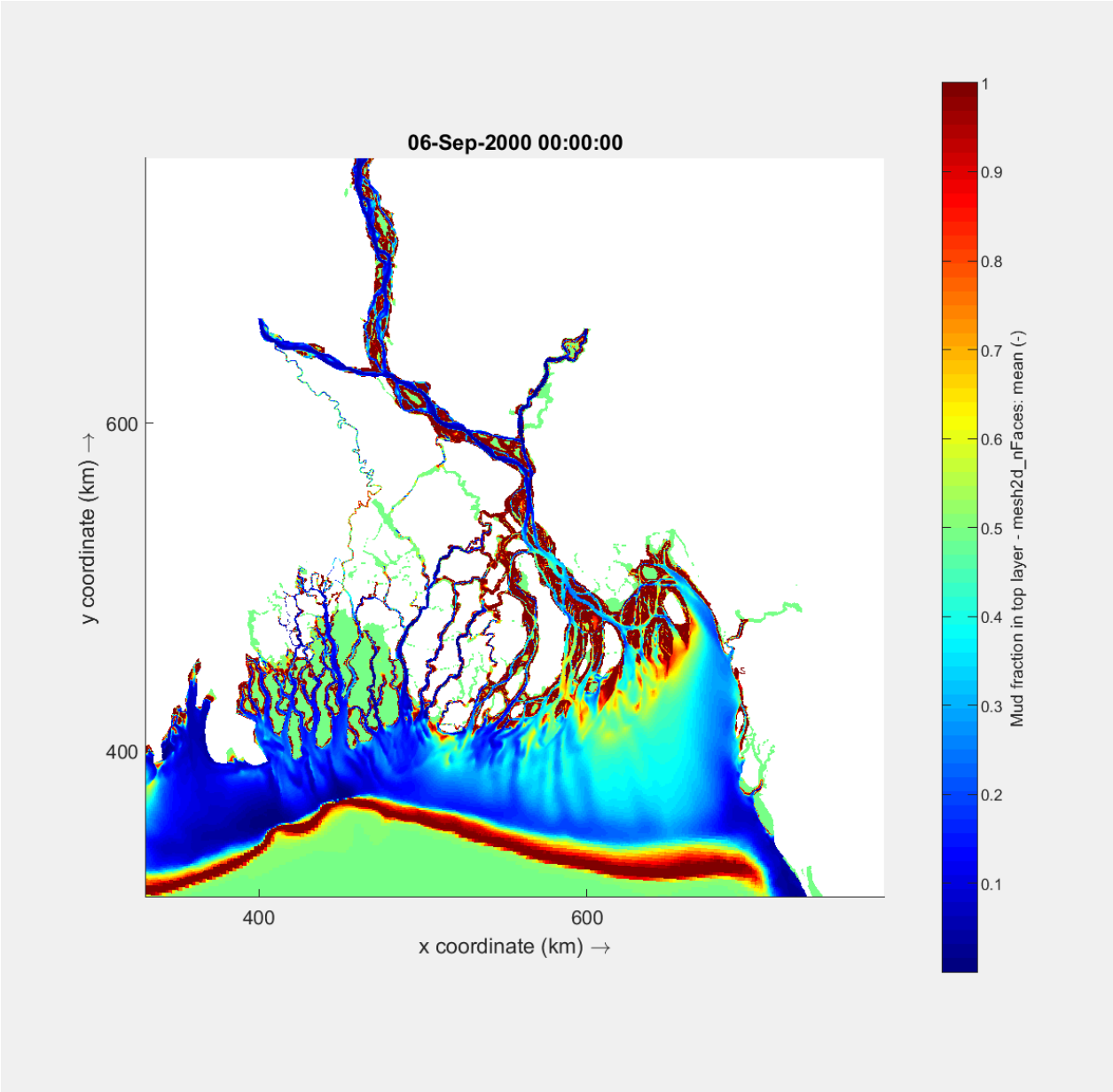

Figure 6.42 Mud volume percentage in upper bed layer after 15 years. The remaining percentage consists of sand

6.9.2 Sediment fluxes

Figure 6.43, Figure 6.44 and Figure 6.45 show significant spatial gradients in mud and sand transports. Sand transports are typically an order of magnitude smaller than mud transports. Combined sand and mud transport magnitudes amount to almost 900 Mt/year, which is similar to estimated values based on observations. The Ganges mud supply seems too low, since it should be similar to the supply by the Jamuna. This is probably due to the sediment concentration at the boundary that was defined too low. Cumulative sediment transport through the Gorai is about 20Mt. This is similar to estimated transports of 30 Mt (Table 2.1). Modelled transports through the Arial Khan

are very limited compared to estimated values of 25 Mt. Probably the bathymetry needs improvement in this region.

Largest mud transports are found in the Padma and upper Meghna, whereas, with decreasing cumulative transports, mud deposits in the lower Meghna and on the shelf topset. Largest sand transports are found in the lower Meghna and on the eastern shelf topset, probably due to enhanced shear stresses by wave action.

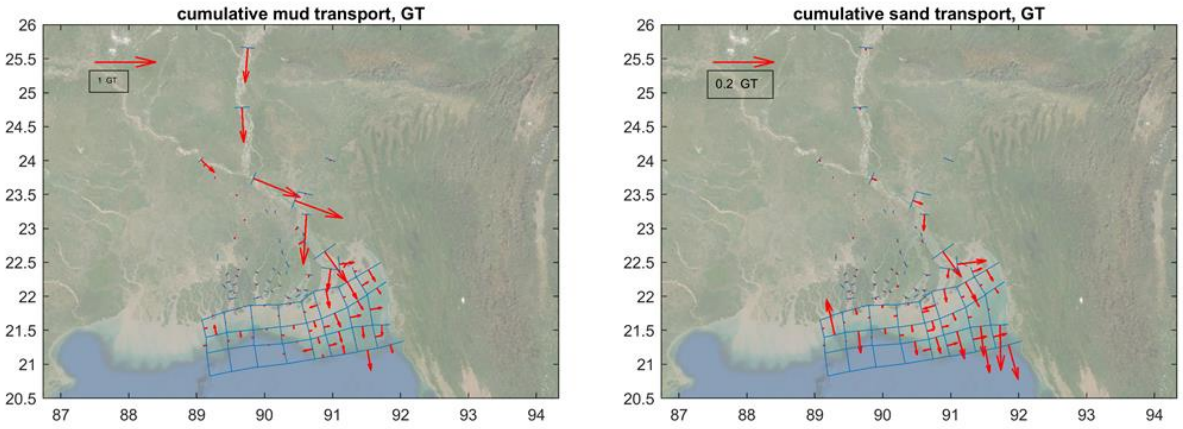

Figure 6.43 Yearly cumulative mud transports (left pane) and sand transports (right pane), mind the different vector scales

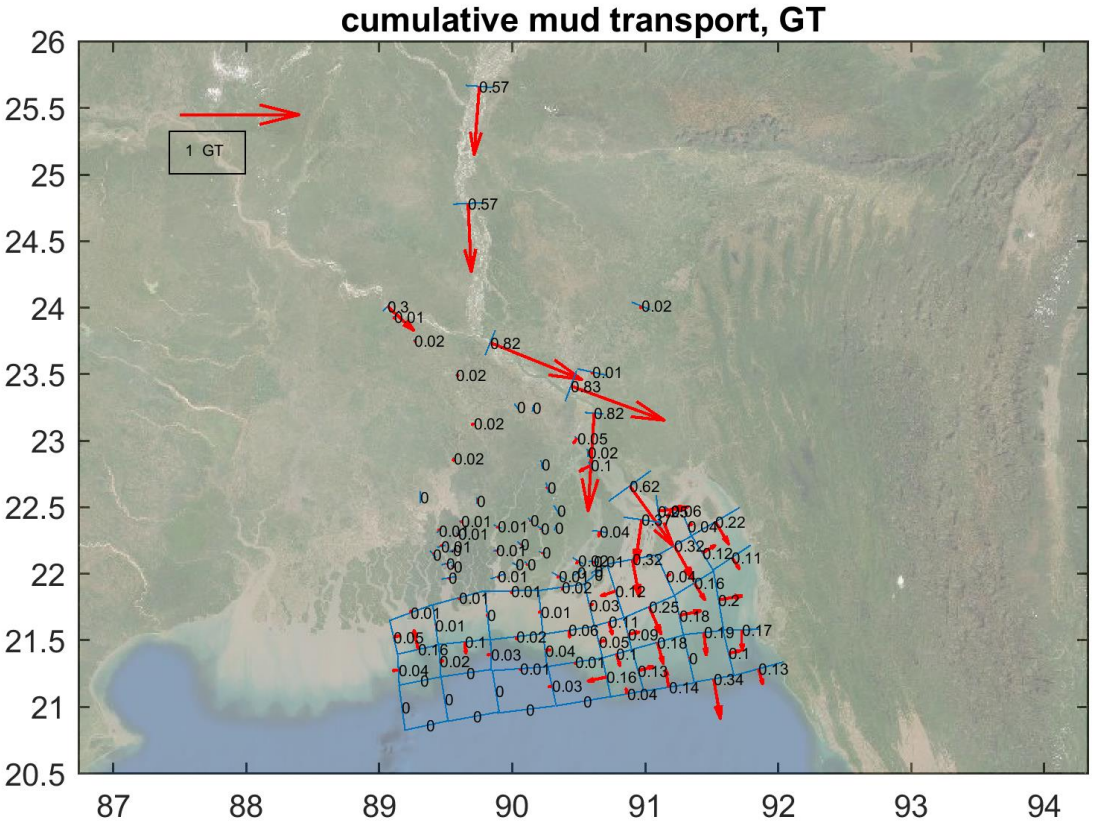

Figure 6.44 Yearly cumulative mud transports with amounts per cross-section

Figure 6.45 shows that wave action has the biggest impact on the magnitude of the sand transport. Mud transport is less affected, although transport magnitudes generally increase slightly towards the ocean due to wave action, except in the Meghna mouth, where they decrease slightly. Although most of the mud is transported towards the south, a small portion of mud transports along the shore. The smaller estuaries westward of the Meghna show a yearly net export of mud towards the ocean.

It is generally assumed that fine sediments discharging into the ocean from the Meghna estuary are transported along shore in westward direction and that a large part of these fine sediments will eventually be transported landward into the Sundarbans estuaries, where they potentially play a role in the siltation of channels. However, actual alongshore transports and associated sediment transport pathways have never been measured. The current project aims to carry out measurements of alongshore flows and concentrations to assess along shore sediment transport rates. Figure 6.45 also shows that the current model settings do not lead to significant along shore sediment transport rates. An extended sensitivity analysis on sediment properties could reveal potential other transport directions. Additionally, 3D processes due to interaction of the freshwater plume and (saline) ocean water could impact the along shore sediment dynamics as well.

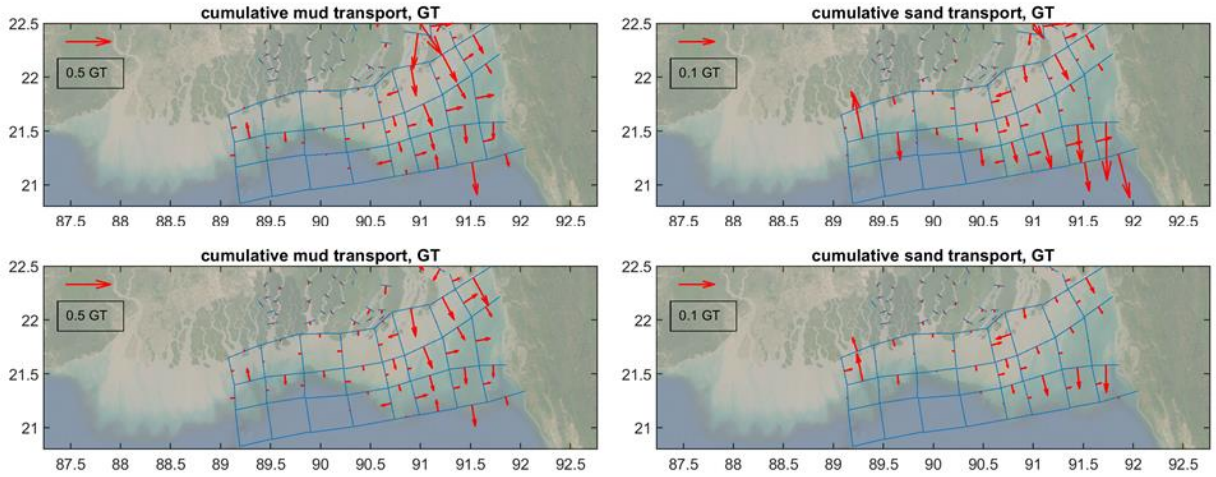

Figure 6.45 Yearly cumulative mud transports, details of Figure 6.44 (mind the different vector scales). Left panels are for mud. Top panels are with waves and wind. Lower panels are without waves and wind.

6.9.3 Volume balance

Sand and mud transport divergence will accrete and erode the bathymetry. The previous section made a sediment budget based on the cumulative transports through cross-sections in terms of sediment mass. Figure 6.46 shows the sediment budget based on the volumetric changes of predefined areas of the bathymetry. These include the different porosity values of mud and sand once deposited in the bed.

All upper reaches of the major rivers (except the Gorai River) and the area of the Tetulia and the eastern coastal area gain sediment. The Baleswar-Bishkali, the Pussur, the Sibsa and the Arpangasia areas gain volume. The western coastal area gains sediment while the eastern area loses sediment. Most of the ocean areas gain sediments.

Figure 6.47 and Figure 6.48 show that morphodynamic development is gradual with small fluctuations depending on the river flow variations, and to a much lesser extent on the varying wind and wave forcing. Many river and estuary areas (Figure 6.47) show decreasing morphodynamic activity, suggesting the development towards a (dynamic) equilibrium. This behaviour is less pronounced in coastal and ocean areas (Figure 6.48), with cumulative volume trends that are constant over time suggesting the gradual progradation of the (submerged) delta front and deposition around the eastern chars, whereas other areas with negative cumulative volumes reflect an eroding trend.

Adding the volumetric changes of Figure 6.46 leads to a nett sediment deposition of about 30 Gm^3 over 25 years. Considering an assumed dry bed density (averaged over sand and mud volumes) of 800 kg/m^3 this corresponds to 24 Gt over 25 years and 0.96 Gt per year. This is similar to the ~1Gt derived in the previous section based on cross-sectional cumulative sediment transports. This implies that almost all sediments supplied towards the GBM delta deposit in the domain defined in Figure 6.46.

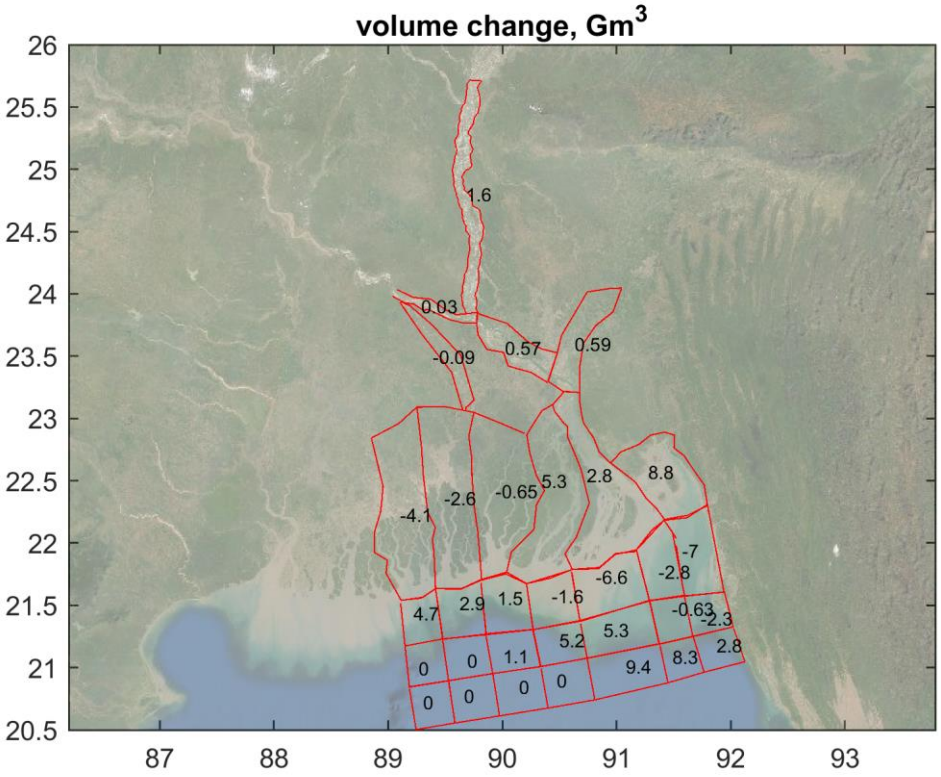

Figure 6.46 Bathymetry volume balance over 25 years, with waves and wind

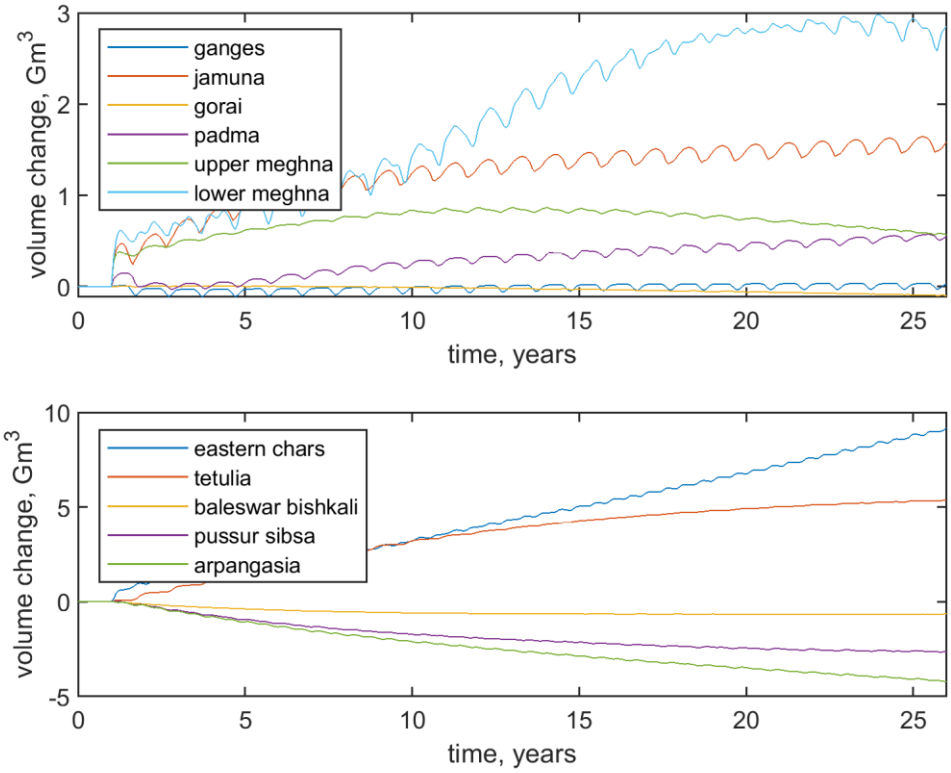

Figure 6.47 Cumulative sediment volume change over time for different areas. Without waves.

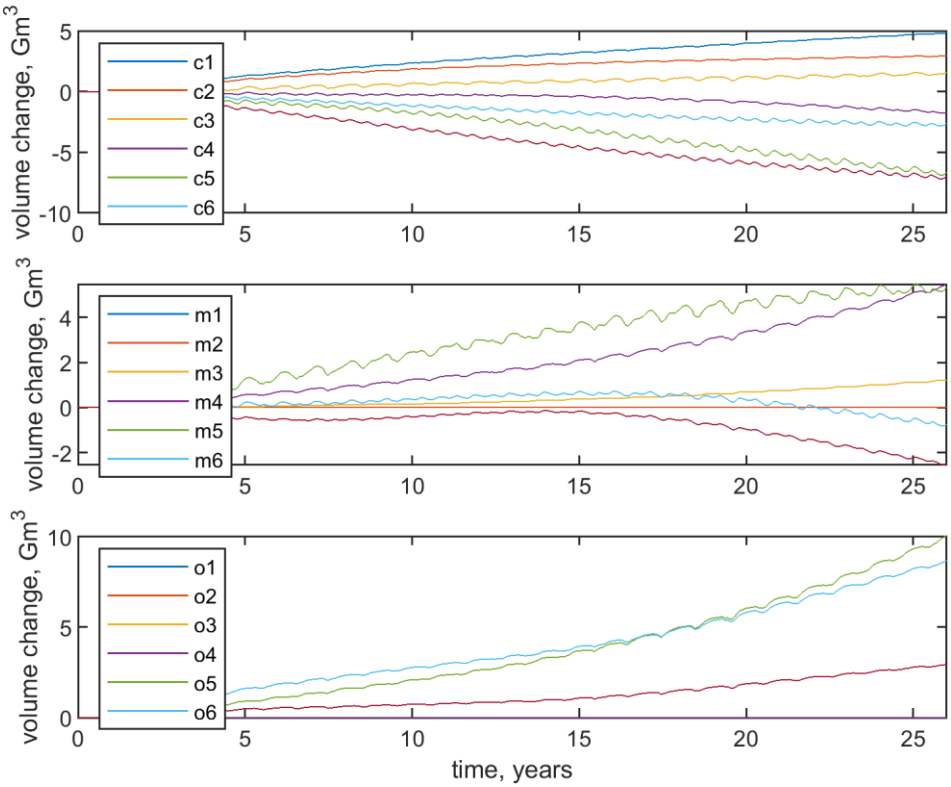

Figure 6.48 Cumulative sediment volume change over time for different areas, where 'c' refers to the coastal areas, 'm' to the middle range of ocean cells and 'o' refers to the most ocean directed areas. Numbers increase from west to east. Without waves.

6.9.4 Detailed sedimentation/erosion maps

In this section a closer look is given to the sedimentation-erosion patterns in the lower Meghna in comparison with the difference bathymetry maps from the EDP study (IWM, 2010), and to sedimentation/erosion patterns and bathymetry evolution in comparison with satellite-derived surface changes as provided by the Deltares Aqua Monitor.

Comparison 2000-2009 Meghna estuary

The sedimentation-erosion maps are shown in Figure 6.49 for the simulation and Figure 6.50 for the observed bed level change. Clearly, there is a good qualitative agreement in the general accretion trend and details such as the encroaching channels northeast of Hatiya island and middle-east of Bhola. The channels appear to be somewhat narrower in the simulation than in the observations, but not excessively so. The mild erosion east of Sandwip island is nicely reproduced.

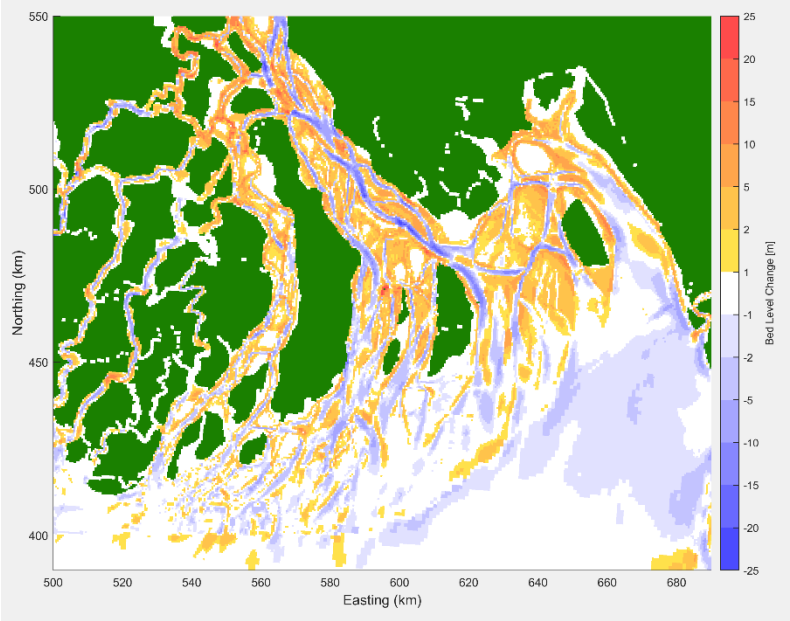

Figure 6.49 Simulated sedimentation-erosion pattern, Meghna estuary, 2000-2009

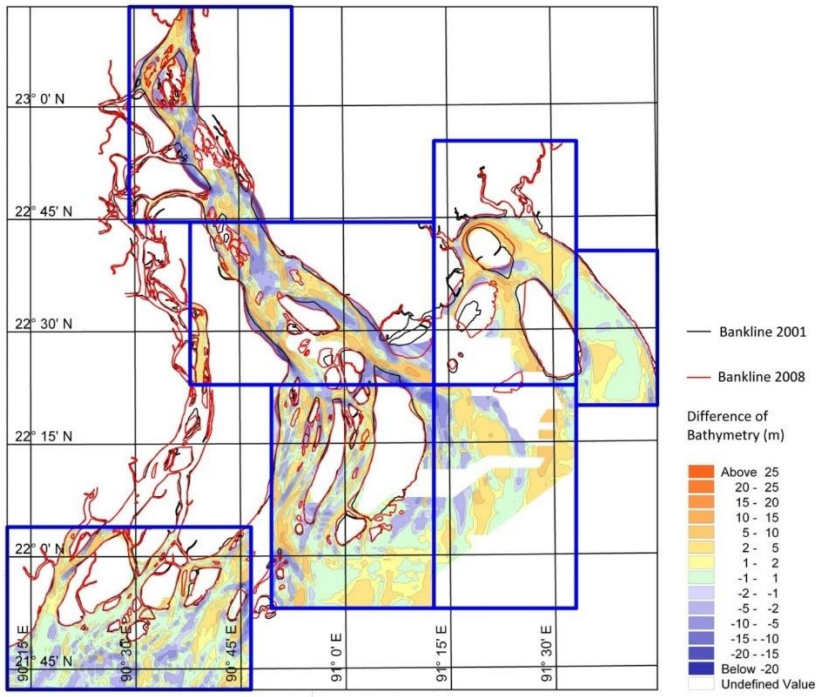

Figure 6.50 Observed sedimentation-erosion pattern, Meghna estuary, 2000-2009

Evolution of coastal areas 2000-2019

The simulated evolution over the period 2000-2019 is visualized in the sedimentation-erosion patterns in Figure 6.51 and in the initial and final bathymetric map in Figure 6.53. For evaluating whether these simulations agree with observations of changes in land and water area can be compared to the simulated evolution with the land/water surface area changes derived from satellite imagery and presented in the Aqua Monitor of Deltares, see Figure 6.52.

While there may be important quantitative differences, a rather striking qualitative agreement in these development can be seen; this may be illustrated by describing the evolution in 6areas denoted A through F in Figure 6.51 and Figure 6.52.

In A, in the Padma, the main channel is expanding while the rest of the river bed is strongly accreting; the pattern in simulation and satellite observations is strikingly similar. It is confirmed by the bed level evolution shown in Figure 6.53.

Similarly, around point B in the lower Meghna, the main channel is eroded close to the bank and adjacent areas show strong accretion, which coincides with bank erosion shown in the satellite imagery.

Point C is on the north side of Hatiya and shows an encroaching channel, where the imagery shows strong bank erosion.

Point D, between Hatiya and Sandwip islands, is in an area of strong accretion in the model and land creation in the satellite images.

Point E on the island of Bhola again shows an encroaching channel where the Aqua Monitor shows strong bank erosion.

Finally, F indicates the southern tips of the Sundarbans where there is a persistent coast line retreat according to the imagery, while the simulations show a generally erosive trend in this area.

It can be concluded that the model generally reproduces the trends in the satellite imagery, though in its present form it cannot directly predict bank erosion, given the relatively coarse grid. The model does seem to be capable of accreting areas up to the high water level, generally in areas where the satellite imagery shows water turned into land.

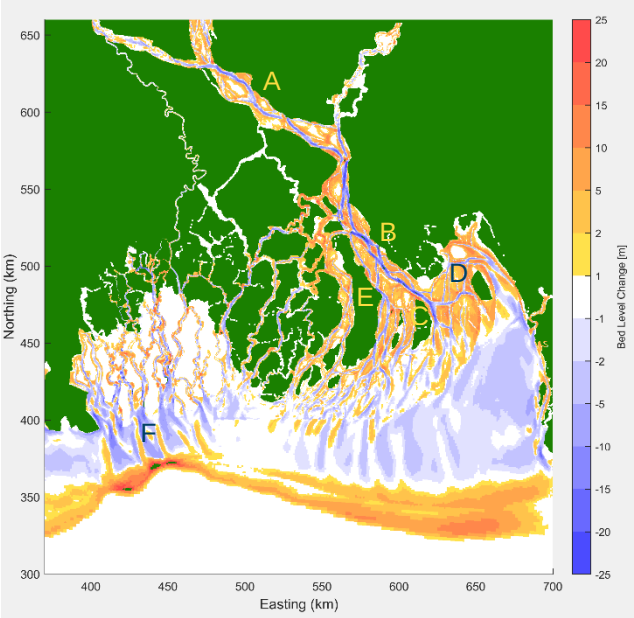

Figure 6.51 Simulated bed level changes, 2000-2019

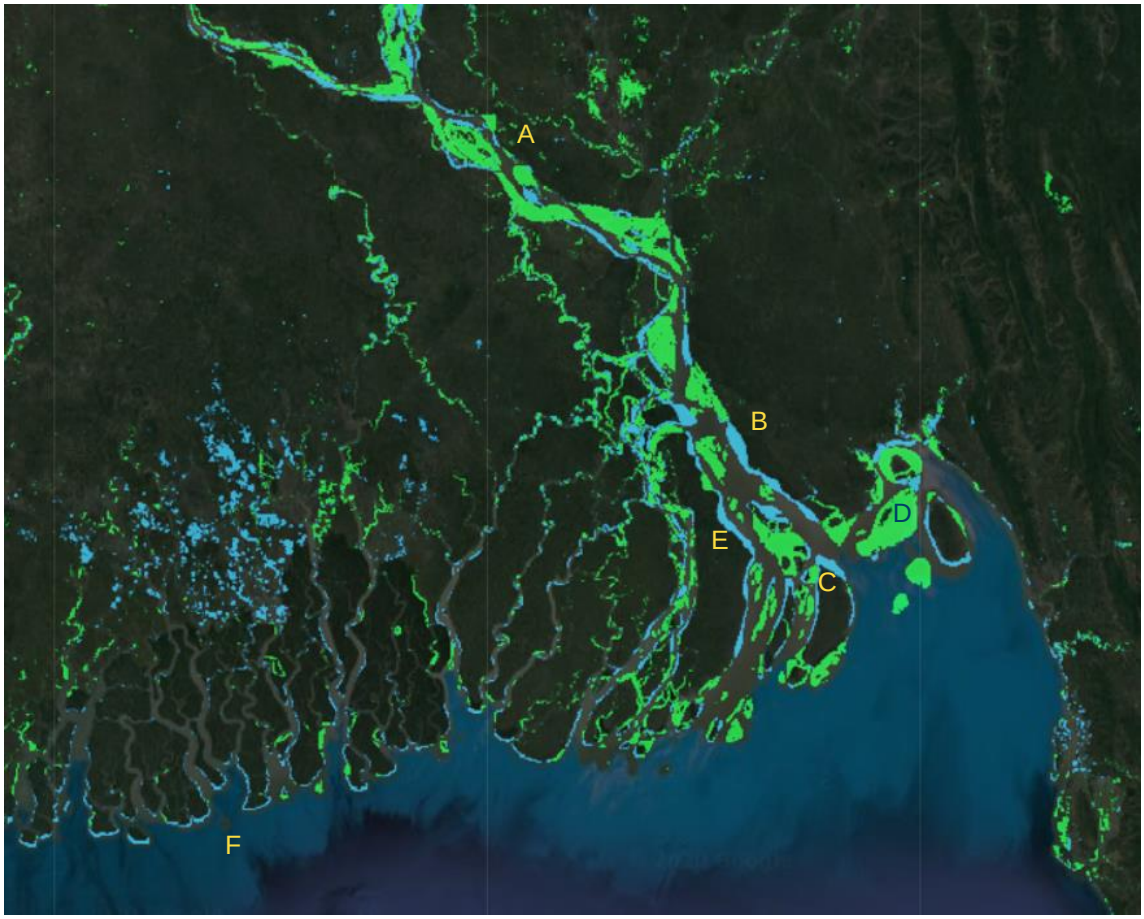

Figure 6.52 Observed land to water (blue) and water to land (green) changes, 2000-2019 (Source: Aqua Monitor)

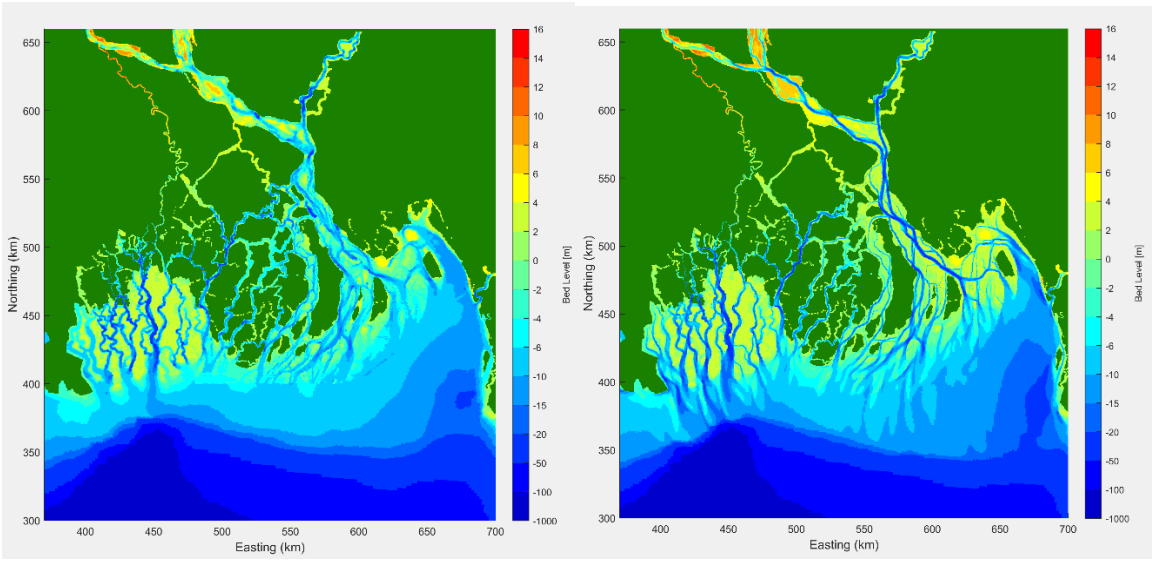

Figure 6.53 Simulated bed level changes, 2000-2019; left panel: bed level 2000; right panel: bed level 2019.

6.10 Conclusions

Based on the calibration results for hydrodynamics and morphology change over periods in the order of 10-20 years the following conclusions may be drawn:

- The macro scale morphodynamic model runs robustly on a 25-year timescale, with acceptable run times (in the order of days on a cluster)
- Some important parameters have been identified and a clear parameter setting has been arrived at.
- This setting leads to a physically reasonable distribution of bed sediment, concentration patterns, net sedimentation areas including delta top set, and erosion hotspots.
- The model shows a predictable behaviour as a function of processes and boundary conditions;
- A detailed validation over a ~9 year period shows reasonable agreement for gross and net volume changes and general patterns; there is an overestimation of overall sedimentation, erosion and net volume changes by factor 1.6, which is well within an acceptable range for morphodynamic models.
- Inclusion of wind and waves significantly improves the performance of the model in terms of reproduction of sedimentation, erosion and net volume changes.
- Straightforward boundary conditions can be applied that are easy to adjust to future scenarios.

In short, the macro-scale model has been developed to an acceptable level and can serve as a basis for future scenario runs.

6.11 Recommendations

Although this report presents a hindcast of the macro scale morphodynamics in the GBM Delta, the model is not perfect and adjustments in the model settings and formulations can be made. Based on the findings of this chapter the following recommendations may be formulated:

- Reconsider river boundary concentrations, e.g. increase Ganges from 0.9 to 1.6 g/l.
- Inspect the representation of smaller branches in the model and see if they can be improved without compromising the overall model performance; specifically, the Arial Khan and some branches between the Tetulia and the Sundarbans.
- Compare erosion/sedimentation patterns for other areas where bathymetry differences are available
- Correlate erosion hotspots with bank erosion locations and investigate if a bankline retreat model can be formulated at this scale.

The results of these recommendations will probably not fundamentally change the conclusions of this report, but will rather provide more detailed and validated insights at specific locations and areas.

7 Discussion

This study has focused on developing a series of models that vary in complexity (from empirical to process-based), spatial scales (basin wide to individual rivers and estuaries), and temporal scales (from annual hydrographs to single tides). The distinct different approaches used for modelling ensure a substantiated outcome on the integral study results, as different model approaches will always result in different outcomes. Using this approach, the (deterministic) outcomes of the study will be placed in a context of uncertainty and can be evaluated accordingly. Moreover, the validation exercises shown in this study give for each model an indication on model performance and uncertainty. The paragraphs below discuss the performance of the models and, if possible, the key components that can be improved to increase model performance and reduce uncertainty in model results.

7.1 Performance of the models

The **HydroTrend** hindcast model results for the reference scenario (1976-2006) capture the peak discharge in both the Ganges and Brahmaputra rivers well. Although the timing in the annual maximum (peak) discharge is modelled less accurate, the modelled hydrographs show close resemblance to the observed hydrographs. This is especially the case for the Brahmaputra river, and for a lesser extent for the Ganges river. The results show, however, that the performance of the model is largely determined on the climate change models used as boundary condition. Subsequently, the forecast results of water and sediment discharge show a large range in projected outcomes, depending on the climate change models used. This range should be narrowed down by omitting the results of HydroTrend models that show the least performance in the hindcast.

The **1D network model** for the GBM delta can simulate the river flow and suspended sediment transport distribution to the different river distributaries in the delta. However, due to the restrictions of the (1D) modelling approach and availability of field data, there are some limitations of the present version of the model. These limitations of the model are discussed in the following and recommendations are made on further improvement of the model.

Concerning the calibration of the model an obvious remaining shortcoming of the model is the mismatch between the model results and the field observations for the water level in the upstream rivers. The simulated water level at e.g. Hardinge is lower than observed during dry season, and higher during wet season. Further reduction of the mismatch by changing e.g. the roughness in the model is not attempted during the calibration for several reasons. First, the model simulates a good flow distribution to the Gorai river, for which the water level at Hardinge is a key influencing factor. Second, a good agreement between the modelled and observed water level variations would require a physically unrealistic spatial and temporal variation of the roughness. A temporal variation of the roughness, which is not possible within Delft3D-FM, would be required because of the opposite difference between model results and field observations. During wet season, a lower roughness in the upstream rivers than in the downstream boundaries would be required, although it is physically expected that it is the other way around. Third, as pointed out earlier, the mismatch is probably mainly due to the shortcomings in the used cross-sectional profiles in the model, for which the field data for the upper part (the flood plains) are too limited. Fourth, there is another possible data problem. As a matter of fact, the river discharges, prescribed at the upstream river boundaries, are not directly measured via flow velocity measurements, but derived from water level measurements using water stage-discharge relations. It is unknown how often the used relations are updated and how reliable they are. With these considerations it is recommended that further improvement of the model should be based on thorough analyses of the cross-sectional profiles and analyses of the water stage-discharge relations according to observations, 1D model results and 2D model results.

The downstream (seawards) boundaries of the model are located at the mouths of the estuaries in the delta. An unavoidable data availability problem concerns the downstream boundary conditions for the suspended sediment transport simulations. During flood, when inflow occurs at the boundaries, sediment concentration needs to be prescribed at the open boundaries. Information for these boundary conditions at the mouths of the estuaries is not available from field observations. The arbitrary conditions used in the present version of the model implies that the model results on sediment

transport in the most downstream part, i.e. within a distance in the order of the adaptation length for sediment concentration (flow velocity multiplied by water depth divided by settling velocity of sediment) from the boundaries, are not reliable. The model can further be improved by using information from the 2D model results for the downstream boundary conditions.

As for the **2D macro-scale Delft3D-FM** model, this has been developed to a sufficient extent to confidently simulate morphological developments in the delta over periods of up to decades. It is fed by relatively invariant tidal forcing far out in the Bay of Bengal, mean sea level and by the discharges and sediment concentrations upstream in the Ganges, Jamuna and Meghna. This means that it can be driven directly from outputs of the HydroTrend model, to simulate various future scenarios. Up to the level of detail of the model, which has around 500 m resolution, important developments in the delta can be simulated. The model can be applied to provide downstream water level and sediment concentration boundary conditions for the 1D Delft3D model and for meso-scale morphodynamic models that are developed for various systems: Pussur-Sibsa, Bishkali-Baleswar, Meghna-Tetulia and Sangu.

Application of the 2D model, as stated before, has been proven to be reliable at a time-scale of decades. Whether this will also be the case on time-scales up to a century remains to be established. A potential problem to be dealt with is that the shape of river and estuary cross-sections gradually deteriorate, a problem that 1D models do not have. For this time horizon it will therefore be an advantage to have the fast 1D approach at hand, to constrain the evolution.

In summary, it can be expected that the combination of the HydroTrend and Delft3D-FM 1D and 2D macro models will provide an optimal combination to tackle the long-term, macro-scale development of the GBM delta.

7.2 Lessons learned from the model results and future applications

The simulations carried out so far with the 1D Network model and the 2DH model with Delft3D-FM have been for calibration purposes. The existing knowledge on the GBM delta system is used to test if the models are able to correctly reproduce on hydrodynamics, sediment transport and morphological development in the delta. The simulations so far are less meant for generating new knowledge of the delta system. Nevertheless, the model results of the model simulations already provided us new insights in the GBM delta system, e.g. on the significance of the various processes for driving hydrodynamics, sediment transport and morphological changes. The models also provided more detailed quantitative information about the flow and sediment budgets of the delta.

According to both the 1D (Chapter 5) and 2D (Chapter 6) models, mud transport is more important than sand transport for the morphological changes in the delta, although the deeper parts of the channels have sandy bottoms. The field data concerning the sediment load from the upstream rivers already suggested this, but now the model results confirm that for the major part of the delta the morphological development is determined by mud transport. Based on the results of the 2D model it is concluded that wind and waves are important in addition to river flow and tide for the morphological development of the delta. Wind and waves are especially important for the sediment transport in the coastal zone and the morphological changes seawards of the estuaries.

The models also provide quantitative information about the water and sediment budget, i.e. water and sediment fluxes at various locations along the river branches and estuarine channels. Much more detailed information than the available field data can provide on how the water and sediment inputs from the upstream rivers are distributed over the delta via the river branches can be derived from the model results (see e.g. Figure 5.18 - 5.20 and Figure 6.43 - 6.46. Note that the model results also already give information concerning the uncertainties of e.g. the sediment transport through the river branches. For the river Gorai the 1D model calculates the sediment transport of 40 Mt/y and the 2D calculates 20 Mt/y. The results of both models are not far from the estimates in literature (30 Mt/y) but they indicate that there are considerable uncertainties concerning the sediment transport to this river. For the river branch Arial Khan the difference between the results of the two models is even bigger. The 1D model calculate the transport to this river as 31 Mt/y, which is close to the value reported in literature (25 Mt/y), whereas the 2D calculates the transport to be much lower.

In the remaining phase of the project the models will be applied, in combination with the meso-scale models, to evaluate how the future scenarios of river flow regime (discharge and sediment transport) and sea level rise will influence the large-scale water and sediment budget of the delta system. They will also be applied to evaluate management measures such as TRM. As an example, the models will help answering the question if future decline of river sediment input and/or sea level rise acceleration can cause certain parts of the delta to become sediment supply limited.

8 Conclusions

The modelling work within the project is carried out to improve our understanding of the long-term and large-scale dynamics of the Ganges-Brahmaputra-Meghna (GBM) delta. In this report there is focus on understanding and predicting the macro-scale (i.e. scale of the whole delta) morphodynamic processes. For this purpose, three types of models have been developed that cover the larger domain of the GBM catchment and delta (including the coastal zone):

- A basin scale hydrology model (HydroTrend). This model has been developed to simulate (future) sediment fluxes at the apex of the GBM delta. The model results of the annual mean and peak discharge (averaged over the period 1976-2000) compares well to observations. There are differences in the timing of hydrograph, which is inherent to the chosen model setup: simulations are calibrated to optimize to capture the peak discharge instead of the most accurate timing. The modelled sediment load compares well to literature values in the Ganges, but under estimates with respect to known values in the Brahmaputra. The reason for this is a large uncertainty in precipitation input for the model, and the fact that sediment discharge estimates for the Brahmaputra basin are not commonly found in the literature, and are highly variable. Future work will attempt to better constrain the sediment discharge in the Brahmaputra basin, both through detailed observations and modeling efforts.
- A 1D river branch model. This model has been developed as a computational efficient tool to estimate the distribution of discharge and suspended sediment load over the main tributaries of the GBM delta. The model compares well to observations of discharge in the Gorai and Padma and compares reasonably well to known values of sediment load in the Gorai and Arial Khan. Therefore, the model is considered appropriate to simulate the distribution of suspended sediment in the upstream part of the GBM delta. For the downstream part boundary conditions of incoming sediment fluxes need to be improved based on understanding gained in this project.
- A 2D large-scale coastal model. This model has been developed to simulate hydrodynamics, sediment transport (bed- and suspended load), and morphological change in the GBM delta. Using flexible mesh advantages and morphological acceleration techniques with schematized boundary conditions, the model can robustly run 25-year morphodynamics within acceptable computational times (order of days on a computational cluster). The model produces physically reasonable distributions of bed sediment composition, concentration patterns, net sedimentation areas, and agrees well to gross and net volumetric changes compared to observations. Therefore, the model is considered suitable to assess future morphodynamic trends forced by changes to the boundary conditions.

The models have been applied to simulate annual flow dynamics, sediment loads, and the volumetric changes as a result of historical and present boundary conditions (Deliverable D-4A-1: 2). The results of the models compare reasonably well to the general understanding of morphodynamics in the delta and to values known from literature. Therefore, the models are qualified as suitable to simulate trends in delta morphodynamics forced by boundary conditions that represent future scenarios (Deliverable D-4A-1: 3). With these abilities, the developed macro-scale models provide the tools to propagate the results from global climate change projections and anthropogenic changes in the catchment towards regional models in the delta.

9 References

Akter, J., Sarker, M. H., Popescu, I., & Roelvink, D. (2016a). Evolution of the Bengal Delta and Its Prevailing Processes. Journal of Coastal Research, 321, 1212–1226. https://doi.org/10.2112/jcoastres-d-14-00232.1

Allison, M., Khan, S. R., Goodbred, S., & Kuehl, S. (2003). Stratigraphic evolution of the late Holocene Ganges–Brahmaputra lower delta plain. Sedimentary Geology, 155, 317–342. https://doi.org/10.1016/S0037-0738(02)00185-9

Bangladesh Water Development Board (2012a). Coastal Embankment Improvement Project, Phase-I (CEIP-I). Volume I: Main Report.

Barua, D. K., Kuehl, S. A., Miller, R. L., and Moore, W. S. (1994). Suspended sediment distribution and residual transport in the coastal ocean off the Ganges-Brahmaputra river mouth. Marine Geology, 120(1-2), 41-61.

Chakrapani, G. J., Subramanian, V., Gibbs, R. J., and Jha, P. K. (1995). Size characteristics and mineralogy of suspended sediments of the Ganges River, India. Environmental Geology, 25(3), 192-196.

Coleman, J. M. (1969). Brahmaputra river: Channel processes and sedimentation. Sedimentary Geology, 3(2), 129–239. https://doi.org/10.1016/0037-0738(69)90010-4

Darby, S. E.; Dunn, F.E.; Nicholls, R. J.; Rahman, M.; Riddy, L., 2015. A first look at the influence of anthropogenic climate change on the future delivery of fluvial sediment to the Ganges–Brahmaputra–Meghna delta. Environmental Science: Processes & Impacts, 17, 1587–1600. 10.1039/C5EM00252D.

Datta, D. K., and Subramanian, V. (1997). Texture and mineralogy of sediments from the Ganges-Brahmaputra-Meghna river system in the Bengal Basin, Bangladesh and their environmental implications. Environmental Geology, 30(3-4), 181-188.

DHI, Deltares, UNESCO-IHE, IWM, Universtiy of Colorado, & Columbia University. (2019). Coastal Embankment Improvement Project, Phase-I (CEIP-I) Long - Long Term Monitoring, Research and Analysis of Bangladesh Coastal Zone (Sustainable Polders Adapted to Coastal Dynamics). Inception report. Retrieved from http://www.hydrology.bwdb.gov.bd/

Donchyts, G., Baart, F., Winsemius, H. et al. Earth's surface water change over the past 30 years. Nature Clim Change 6, 810–813 (2016). https://doi.org/10.1038/nclimate3111

Egbert, G. D., & Erofeeva, S. Y. (2002). Efficient inverse modeling of barotropic ocean tides. Journal of Atmospheric and Oceanic Technology, 19(2), 183–204. http://doi.org/10.1175/1520-0426(2002)019<0183:EIMOBO>2.0.CO;2

EGIS, 2001. Remote Sensing, GIS and Morphological Analyses of the Jamuna River: 2000, Part II. Dhaka, Bangladesh: EGIS for Water Resources Management, 66p.

Fergusson, J. (1863). On Recent Changes in the Delta of the Ganges. Quarterly Journal of the Geological Society, 19(1–2), 321 LP – 354. https://doi.org/10.1144/GSL.JGS.1863.019.01-02.35

Galappatti, R., Olesen, K. W., & Khan, A. S. (1996). Schematizing Large Active Rivers for Morphological Computations : Experience From Bangladesh.

Garzanti, E., Andò, S., France-Lanord, C., Vezzoli, G., Censi, P., Galy, V., and Najman, Y. (2010). Mineralogical and chemical variability of fluvial sediments: 1. Bedload sand (Ganga–Brahmaputra, Bangladesh). Earth and Planetary Science Letters, 299(3-4), 368-381.

Goodbred, S., & Kuehl, S. (2000a). Enormous Ganges–Brahmputra sediment discharge during strengthened early Holocene monsoon. Geology, 28, 1083–1086. https://doi.org/10.1130/0091-7613(2000)28<1083:EGSDDS>2.0.CO;2

Goodbred, S., & Kuehl, S. (2000b). The significance of large sediment supply, active tectonism, and eustasy on margin sequence development: Late Quaternary stratigraphy and evolution of the Ganges-Brahmaputra delta. Sedimentary Geology, 133, 227–248. https://doi.org/10.1016/S0037-0738(00)00041-5.

Hagenaars, G., de Vries, S., Luijendijk, A. P., de Boer, W. P., & Reniers, A. J. H. M. (2018). On the accuracy of automated shoreline detection derived from satellite imagery: A case study of the sand motor mega-scale nourishment. Coastal Engineering, 133(June 2017), 113–125. https://doi.org/10.1016/j.coastaleng.2017.12.011.

Hersbach, H., Bell, B., Berrisford, P., Hirahara, S., Horányi, A., Muñoz-Sabater, J., … Thépaut, J.-N. (n.d.). The ERA5 global reanalysis. *Quarterly Journal of the Royal Meteorological Society*, *n/a*(n/a). https://doi.org/10.1002/qj.3803

Higgins, S., Overeem, I., Rogers, K., Kalina, E., 2018. River linking in India: Downstream impacts on water discharge and suspended sediment transport to deltas. Elementa, 6, 1:20. DOI: 10.1525/elementa.269

Islam, M. R., Begum, S. F., Yamaguchi, Y., & Ogawa, K. (1999). The Ganges and Brahmaputra rivers in Bangladesh: Basin denudation and sedimentation. Hydrological Processes, 13(17), 2907–2923. https://doi.org/10.1002/(SICI)1099-1085(19991215)13:17<2907::AID-HYP906>3.0.CO;2-E

Islam, M. R., Yamaguchi, Y., and Ogawa, K. (2001). Suspended sediment in the Ganges and Brahmaputra Rivers in Bangladesh: observation from TM and AVHRR data. Hydrological Processes, 15(3), 493-509.Jansen et al., 1979

IWM; Institute for Water Modelling (2009) Use existing data on available digital elevation models to prepare useable Tsunami and storm surge inundation risk maps for the entire coastal region vol II. Institute of Water Modelling.

IWM; Institute for Water Modellng (2010). Estuary Development Programme – EDP. Updating of Hydrodynamic & Morphological Models to Investigate Land Accretion & Erosion in the Estuary Development Program (EDP) Area.

Kernkamp, H. W. J., Van Dam, A., Stelling, G. S., & De Goede, E. D. (2011). Efficient scheme for the shallow water equations on unstructured grids with application to the Continental Shelf. Ocean Dynamics, 61(8), 1175–1188. https://doi.org/10.1007/s10236-011-0423-6

Kettner, A. J. & Syvitski, J. P. M. HydroTrend v.3.0: A climate-driven hydrological transport model that simulates discharge and sediment load leaving a river system. Comput. Geosci. 34, 1170–1183 (2008).

Kettner, A.J.; Gomez, B.; Syvitski, J.P.M. 2007. Modeling suspended sediment discharge from the Waipaoa River system, New Zealand: The last 3000 years. Water Resources Research, 43, . 10.1029/2006WR005570

Kettner, A. J.; Restrepo, J. D.; Syvitski, J. P. M.; 2010. A Spatial Simulation Experiment to Replicate Fluvial Sediment Fluxes within the Magdalena River Basin, Colombia. The Journal of Geology, 118, 363–379. 10.1086/652659

Kuehl, S., Allison, M., Goodbred, S., & Kudrass, H. (2005). The Ganges–Brahmaputra Delta. In River Deltas - Concepts, Models and Examples (Vol. 83, pp. 413–434). https://doi.org/10.2110/pec.05.83.0413.

Kuehl, S. A., Hariu, T. M., and Moore, W. S. (1989). Shelf sedimentation off the Ganges-Brahmaputra river system: Evidence for sediment bypassing to the Bengal fan. Geology, 17(12), 1132-1135.

Lehner, B., Liermann, C.R., Revenga, C., Vorosmarty, C., Fekete, B., Crouzet, P., Doll, P., Endejan, M., Frenken, K., Magome, J., Nilsson, C., Robertson, J. C., Rodel, R., & Sindorf, N. (2001). Global Reservoir and Dam Database, Version 1 (GRanDv1): Dams, Revision 01 [Data set]. https://doi.org/10.7927/H4N877QK

Lehner, Bernhard, Liermann, C. R., Revenga, C., Vörösmarty, C., Fekete, B., Crouzet, P., Döll, P., Endejan, M., Frenken, K., Magome, J., Nilsson, C., Robertson, J. C., Rödel, R., Sindorf, N., & Wisser, D. (2011). High-resolution mapping of the world's reservoirs and dams for sustainable river-flow management. Frontiers in Ecology and the Environment, 9(9), 494–502. https://doi.org/10.1890/100125

MES II (Meghna Estuary Study), 2001. Hydro-Morphological Dynamics of the Meghna Estuary. Dhaka, Bangladesh: MES II, 80p.

Morehead, Mark D.; Syvitski, James P.; Hutton, Eric W.H.; Peckham, Scott D.; 2003. Modeling the temporal variability in the flux of sediment from ungauged river basins. Global and Planetary Change, 39, 95–110. 10.1016/S0921-8181(03)00019-5

Morgan, J.P. and McIntire, W.G., 1959. Quaternary geology of the Bengal Basin, East Pakistan and India. Bulletin of the Geological Society of America, 70, 319–342.

Partheniades, E., 1965. “Erosion and Deposition of Cohesive Soils.” Journal of the Hydraulics Division, ASCE 91 (HY 1): 105–139. January.

Payo, A., Mukhopadhyay, A., Hazra, S., Ghosh, T., Ghosh, S., Brown, S., … Haque, A. (2016). Projected changes in area of the Sundarban mangrove forest in Bangladesh due to SLR by 2100. Climatic Change, 139(2), 279–291. https://doi.org/10.1007/s10584-016-1769-z

Rahman, Munsur; Dustegir, Maruf; Karim, Rezaul; Haque, Anisul; Nicholls, Robert J.; Darby, Stephen E.; Nakagawa, Hajime; Hossain, Motahar; Dunn, Frances E.; Akter, Marin; 2018. Recent sediment flux to the Ganges-Brahmaputra-Meghna delta system. Science of The Total Environment, 643, 1054–1064. 10.1016/j.scitotenv.2018.06.147

Sarker, M. H., Akter, J., & Rahman, M. M. (2013). Century-Scale Dynamics of the Bengal Delta and Future Development. 4th International Conference on Water & Flood Management (ICWFM-2013), (August), 91–104.

Sarker, M. H., Thorne, C. R., Aktar, M. N., and Ferdous, M. R. (2014). Morpho-dynamics of the Brahmaputra–Jamuna River, Bangladesh. Geomorphology, 215, 45-59.

Singh, M., Singh, I. B., and Müller, G. (2007). Sediment characteristics and transportation dynamics of the Ganga River. Geomorphology, 86(1-2), 144-175.

Stummeyer, J., Marchig, V., and Knabe, W. (2002). The composition of suspended matter from Ganges–Brahmaputra sediment dispersal system during low sediment transport season. Chemical Geology, 185(1-2), 125-147.

Syvitski, J.P.M. and Milliman, J.D., 2007, Geology, geography and humans battle for dominance over the delivery of sediment to the coastal ocean. J. Geology 115, 1–19.

Uddin, M., Alam, J. Bin, Khan, Z. H., Jahid Hasan, G. M., & Rahman, T. (2014). Two Dimensional Hydrodynamic Modelling of Northern Bay of Bengal Coastal Waters. *Computational Water, Energy, and Environmental Engineering*, *03*(04), 140–151. https://doi.org/10.4236/cweee.2014.34015

Umitsu, M. (1985). Natural Levees and Landform Evolutions in the Bengal Lowland. 58(2), 149–164.

Umitsu, M. (1993). Late quaternary sedimentary environments and landforms in the Ganges Delta. Sedimentary Geology, 83(3–4), 177–186. https://doi.org/10.1016/0037-0738(93)90011-S

VanRijn,L.C.(2007a).Unifiedviewofsedimenttransportbycurrentsandwaves.I:Initiationofmotion,bedroughness,andbed-load

transport.JournalofHydraulicEngineering,133(6),649–667.https://doi.org/10.1061/(ASCE)0733-9429(2007)133:6(649)

VanRijn,L.C.(2007b).Unifiedviewofsedimenttransportbycurrentsandwaves.II:Suspendedtransport.JournalofHydraulicEngineering, 133(6),668–689.https://doi.org/10.1061/(ASCE)0733-9429(2007)133:6(668).

Wang, Z. B., Winterwerp, J. C., & He, Q. (2014). Interaction between suspended sediment and tidal amplification in the Guadalquivir Estuary. *Ocean Dynamics*, *64*(10), 1487–1498. https://doi.org/10.1007/s10236-014-0758-x.

Wang, Z.B.; Elias, E.P.L.; Van der Spek, A.J.F.; Lodder, Q.J. Sediment budget and morphological development of the Dutch Wadden Sea-impact of accelerated sea-level rise and subsidence until 2100. Neth. J. Geosci. 2018, 97, 183–214.

Williams, C. A. (1919). History of the Rivers in the Gangetic Delta, 1750-1918. Retrieved from https://books.google.com.bd/books?id=tLfgOwAACAAJ.

Wilson, C. A., & Goodbred, S. L. (2015). Construction and Maintenance of the Ganges-Brahmaputra-Meghna Delta: Linking Process, Morphology, and Stratigraphy. *Annual Review of Marine Science*, *7*(1), 67–88. https://doi.org/10.1146/annurev-marine-010213-135032

Winterwerp, J. C., Lely, M., & He, Q. (2009). Sediment-induced buoyancy destruction and drag reduction in estuaries. *Ocean Dynamics*, *59*(5), 781–791. https://doi.org/10.1007/s10236-009-0237-y

Ya-feng, S., Tze-chu, H., Pen-hsing, C., & Chi-chun, L. (1980). Distribution, features and variations of glaciers in China. World Glacier Inventory: Proceedings of the Riederalp Workshop, 126, 111–116.

A Summary statistics Hydrotrend results

TableApx A.1 Summary statistics from HydroTrend simulations of the Ganges basin for the reference, RCP4.5, and RCP8.5 scenarios. Reference scenario statistics are averaged over the time period 1976-2006. RCP4.5 and RCP8.5 emission scenario values are averaged over the time periods representative of the years 2020, 2040, 2060, and 2080 (see model setup section for more details). Statistics from the reference scenario (2000) are included within each climate model section in the RCP4.5 and RCP8.5 portions of the table for ease of analysis.

Ganges Basin Summary Statistics					
Reference Scenario (1976 – 2006)					
Unit/description:		**Mean Qw**	**Mean Qs**	**Mean SSC**	**Mean Qb**
		m^3/s	kg/s	kg/m^3	kg/s
Climate model:	GFDL-ESM2M	13018	15823	0.276	273
	HadGEM2	13184	15894	0.162	277
	IPSL_CM5A	14399	16752	0.087	302
	MIROC-ESM-CHEM	11315	14827	0.296	237
	NORESM-M	12311	15310	0.272	258
RCP4.5 (2006 – 2099)					
Unit/description:		**Mean Qw**	**Mean Qs**	**Mean SSC**	**Mean Qb**
		m^3/s	kg/s	kg/m^3	kg/s
Climate Model	**Representative Climate of Year and Averaging Interval**				
GFDL-ESM2M	2000 (1976-2006)	13018	15823	0.276	273
	2020 (2006-2035)	11783	15916	0.270	247
	2040 (2026-2055)	11587	15990	0.286	243
	2060 (2046-2075)	12649	17069	0.267	265
	2080 (2066-2095)	12979	17423	0.254	272
HadGEM2	2000 (1976-2006)	13184	15894	0.162	277
	2020 (2006-2035)	17622	18810	0.164	370
	2040 (2026-2055)	18804	19984	0.182	395
	2060 (2046-2075)	18938	20907	0.129	397
	2080 (2066-2095)	20620	22374	0.194	433
IPSL_CM5A	2000 (1976-2006)	14399	16752	0.087	302
	2020 (2006-2035)	15319	18078	0.114	322
	2040 (2026-2055)	17060	19725	0.117	358
	2060 (2046-2075)	21737	22828	0.124	456
	2080 (2066-2095)	21826	23308	0.170	458
MIROC-ESM-CHEM	2000 (1976-2006)	11315	14827	0.296	237
	2020 (2006-2035)	11450	15571	0.310	240
	2040 (2026-2055)	12270	16281	0.262	258
	2060 (2046-2075)	13686	17793	0.261	287
	2080 (2066-2095)	14304	18454	0.270	300

NORESM-M	2000 (1976-2006)	12311	15310	0.272	258
	2020 (2006-2035)	15427	17733	0.247	324
	2040 (2026-2055)	16369	18729	0.254	344
	2060 (2046-2075)	17807	19679	0.235	374
	2080 (2066-2095)	18538	20114	0.240	389
RCP8.5 (2006 – 2099)					
Unit/description:		**Mean Qw**	**Mean Qs**	**Mean SSC**	**Mean Qb**
		m^3/s	kg/s	kg/m^3	kg/s
Climate Model	**Representative Climate of Year and Averaging Interval**				
GFDL-ESM2M	2000 (1976-2006)	13018	15823	0.276	273
	2020 (2006-2035)	12280	16160	0.264	258
	2040 (2026-2055)	13070	17149	0.259	274
	2060 (2046-2075)	12245	17388	0.286	257
	2080 (2066-2095)	13393	19016	0.276	281
HadGEM2	2000 (1976-2006)	13184	15894	0.162	277
	2020 (2006-2035)	19412	19703	0.164	407
	2040 (2026-2055)	17972	19823	0.171	377
	2060 (2046-2075)	20669	22528	0.152	434
	2080 (2066-2095)	24853	26049	0.165	522
IPSL_CM5A	2000 (1976-2006)	14399	16752	0.087	302
	2020 (2006-2035)	16281	18634	0.166	342
	2040 (2026-2055)	19343	21345	0.144	406
	2060 (2046-2075)	23447	24920	0.148	492
	2080 (2066-2095)	22993	26353	0.120	483
MIROC-ESM-CHEM	2000 (1976-2006)	11315	14827	0.296	237
	2020 (2006-2035)	11312	15588	0.272	237
	2040 (2026-2055)	13450	17565	0.198	282
	2060 (2046-2075)	16012	20128	0.267	336
	2080 (2066-2095)	16429	21662	0.263	345
NORESM-M	2000 (1976-2006)	12311	15310	0.272	258
	2020 (2006-2035)	14312	17059	0.250	300
	2040 (2026-2055)	14274	17753	0.279	300
	2060 (2046-2075)	15755	19275	0.273	331
	2080 (2066-2095)	16488	20706	0.235	346

TableApx A.2 Summary statistics from HydroTrend simulations of the Brahmaputra basin for the reference, RCP4.5, and RCP8.5 scenarios. Reference scenario statistics are averaged over the time period 1976-2006. RCP4.5 and RCP8.5 emission scenario values are averaged over the time periods representative of the years 2020, 2040, 2060, and 2080 (see model setup for more details). Statistics from the reference scenario (2000) are included within each climate model section in the RCP4.5 and RCP8.5 portions of the table for ease of analysis.

Brahmaputra Basin Summary Statistics					
Reference Scenario (1976 – 2006)					
Unit/description:		**Mean Qw**	**Mean Qs**	**Mean SSC**	**Mean Qb**
		m^3/s	kg/s	kg/m^3	kg/s
Climate model:	GFDL-ESM2M	18916	7501	0.164	879
	HadGEM2	18172	7795	0.181	844
	IPSL_CM5A	18990	8159	0.141	882
	MIROC-ESM-CHEM	19284	8291	0.186	896
	NORESM-M	18947	8061	0.168	880
RCP4.5 Emission Scenario (2006 – 2099)					
Unit/description:		**Mean Qw**	**Mean Qs**	**Mean SSC**	**Mean Qb**
		m^3/s	kg/s	kg/m^3	kg/s
Climate Model	**Representative Climate of Year and Averaging Interval**				
GFDL-ESM2M	2000 (1976-2006)	18916	7501	0.164	879
	2020 (2006-2035)	20164	9243	0.152	936
	2040 (2026-2055)	21088	9943	0.169	979
	2060 (2046-2075)	21374	10438	0.150	993
	2080 (2066-2095)	21807	10803	0.174	1013
HadGEM2	2000 (1976-2006)	18172	7795	0.181	844
	2020 (2006-2035)	18521	8779	0.204	860
	2040 (2026-2055)	19928	9455	0.199	926
	2060 (2046-2075)	21477	11303	0.223	997
	2080 (2066-2095)	22938	12455	0.225	1065
IPSL_CM5A	2000 (1976-2006)	18990	8159	0.141	882
	2020 (2006-2035)	21038	9925	0.093	977
	2040 (2026-2055)	22416	11379	0.170	1041
	2060 (2046-2075)	24762	13144	0.114	1150
	2080 (2066-2095)	24749	13638	0.155	1149
MIROC-ESM-CHEM	2000 (1976-2006)	19284	8291	0.186	896
	2020 (2006-2035)	19378	9167	0.178	900
	2040 (2026-2055)	19407	9975	0.181	901
	2060 (2046-2075)	22269	11885	0.213	1034
	2080 (2066-2095)	22926	12748	0.216	1065
NORESM-M	2000 (1976-2006)	18947	8061	0.168	880

	2020 (2006-2035)	20406	9356	0.172	948
	2040 (2026-2055)	21436	10388	0.179	996
	2060 (2046-2075)	21882	10834	0.183	1016
	2080 (2066-2095)	21696	10966	0.196	1008
RCP8.5 Emission Scenario (2006 – 2099)					
Unit/description:		**Mean Qw**	**Mean Qs**	**Mean SSC**	**Mean Qb**
		m^3/s	kg/s	kg/m^3	kg/s
Climate Model	**Representative Climate of Year and Averaging Interval**				
GFDL-ESM2M	2000 (1976-2006)	18916	7501	0.164	879
	2020 (2006-2035)	19751	9230	0.180	917
	2040 (2026-2055)	21107	10337	0.163	980
	2060 (2046-2075)	23647	11594	0.163	1098
	2080 (2066-2095)	24724	13589	0.128	1148
HadGEM2	2000 (1976-2006)	18172	7795	0.181	844
	2020 (2006-2035)	18919	8881	0.204	879
	2040 (2026-2055)	19622	9509	0.213	911
	2060 (2046-2075)	21047	11762	0.233	977
	2080 (2066-2095)	22947	14025	0.255	1066
IPSL_CM5A	2000 (1976-2006)	18990	8159	0.141	882
	2020 (2006-2035)	22339	10480	0.155	1037
	2040 (2026-2055)	23002	12188	0.061	1068
	2060 (2046-2075)	25384	14907	0.199	1179
	2080 (2066-2095)	26780	17452	0.127	1244
MIROC-ESM-CHEM	2000 (1976-2006)	19284	8291	0.186	896
	2020 (2006-2035)	19595	9435	0.210	910
	2040 (2026-2055)	21262	11403	0.203	987
	2060 (2046-2075)	23598	14090	0.238	1096
	2080 (2066-2095)	24683	16555	0.252	1146
NORESM-M	2000 (1976-2006)	18947	8061	0.168	880
	2020 (2006-2035)	19639	8975	0.180	912
	2040 (2026-2055)	19756	9871	0.186	918
	2060 (2046-2075)	20697	11222	0.213	961
	2080 (2066-2095)	22887	13203	0.224	1063

B Hypsometric curves of schematized profiles

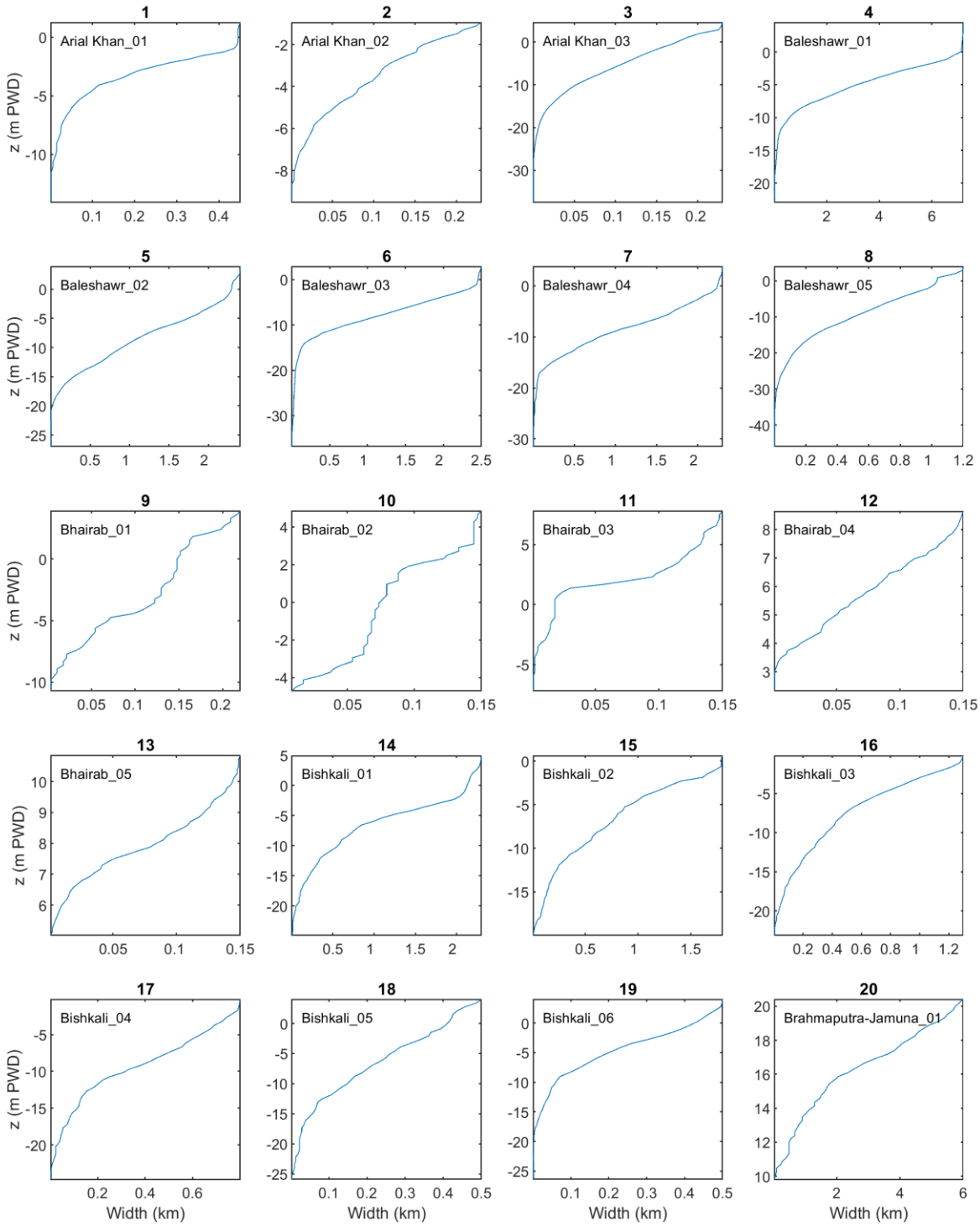

FigureApx B.1 Hypsometric curves based on the subset of topo-bathymetric observations enclosed by the polygon.

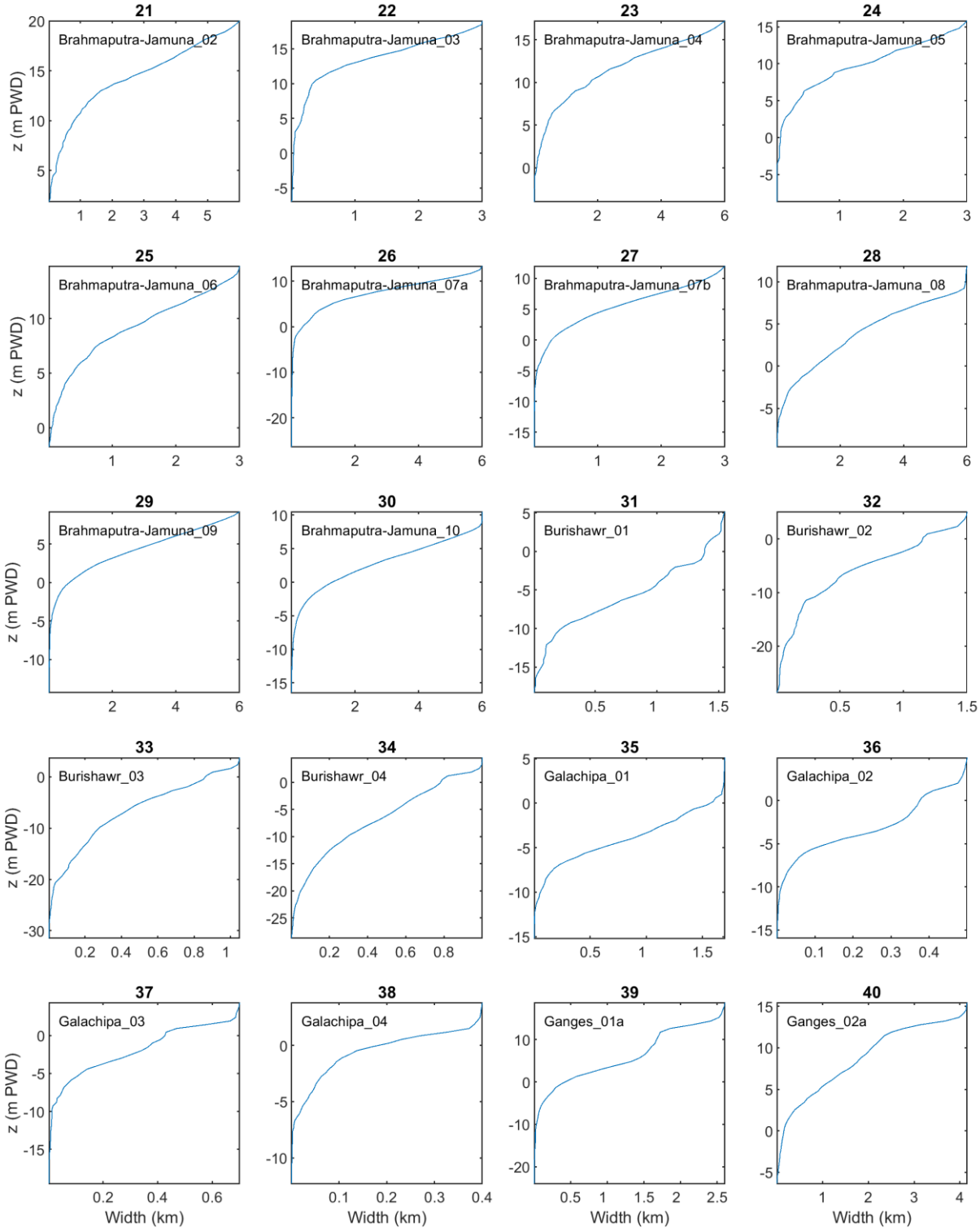

FigureApx B.2 Hypsometric curves based on the subset of topo-bathymetric observations enclosed by the polygon.

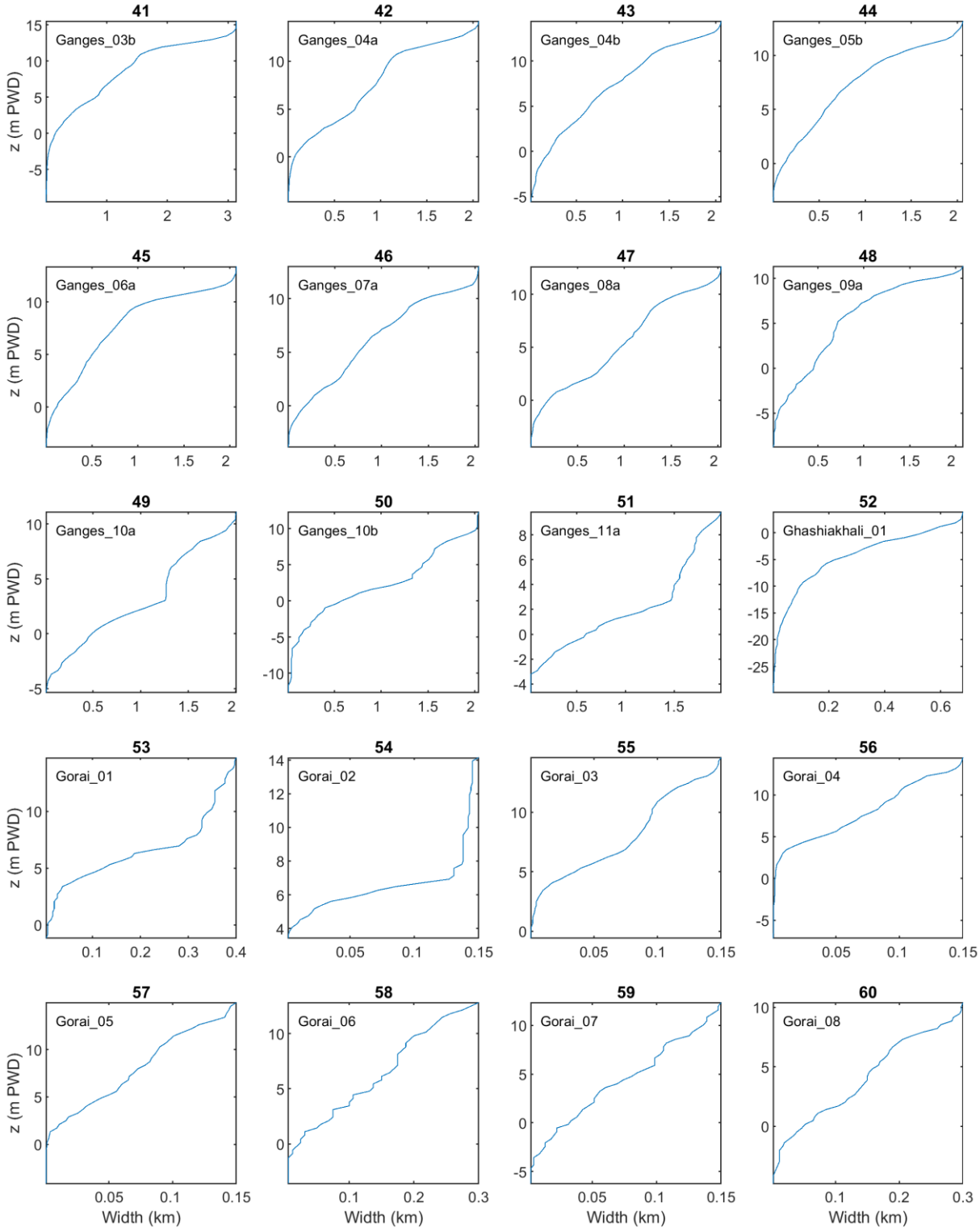

FigureApx B.3 Hypsometric curves based on the subset of topo-bathymetric observations enclosed by the polygon.

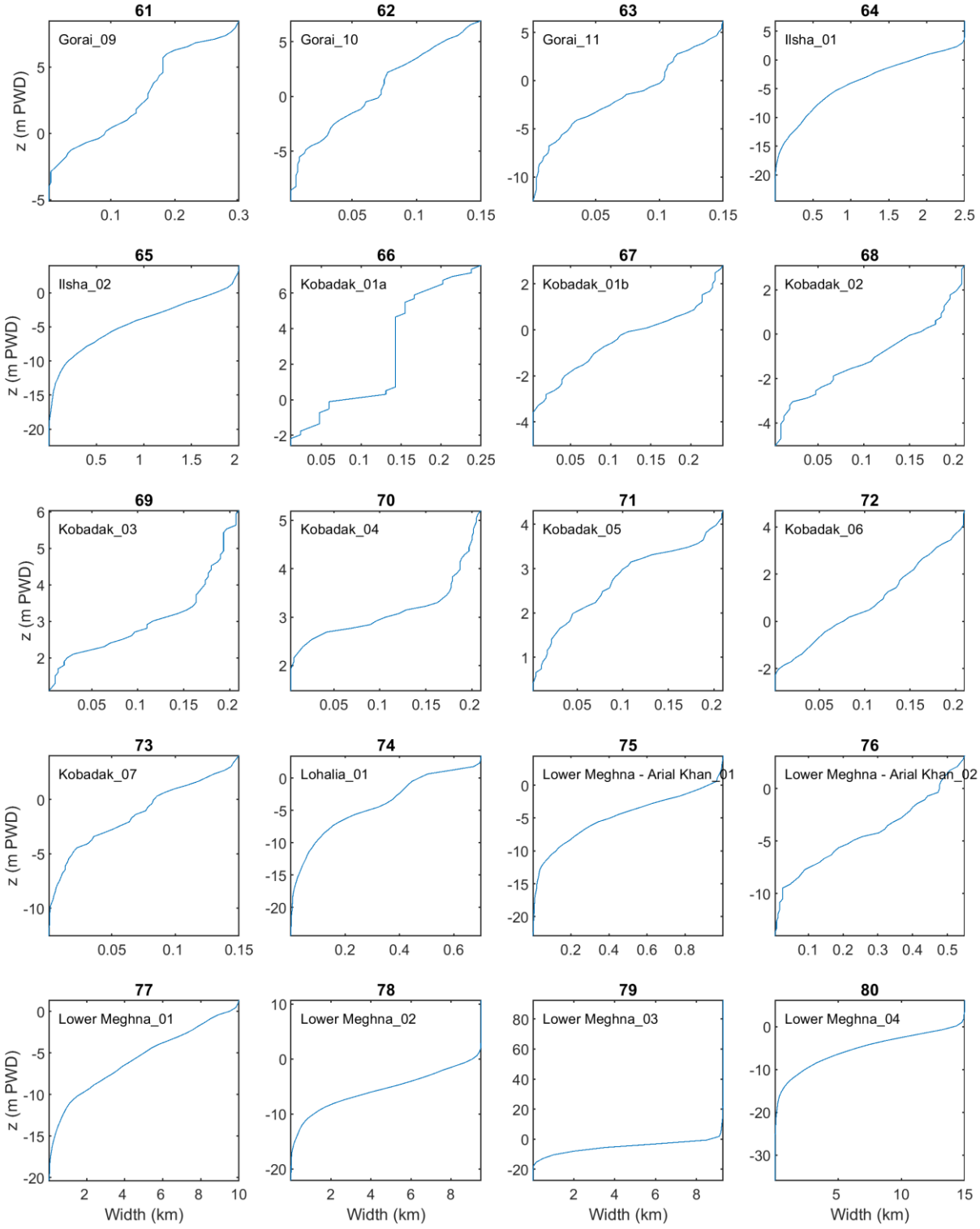

FigureApx B.4 Hypsometric curves based on the subset of topo-bathymetric observations enclosed by the polygon.

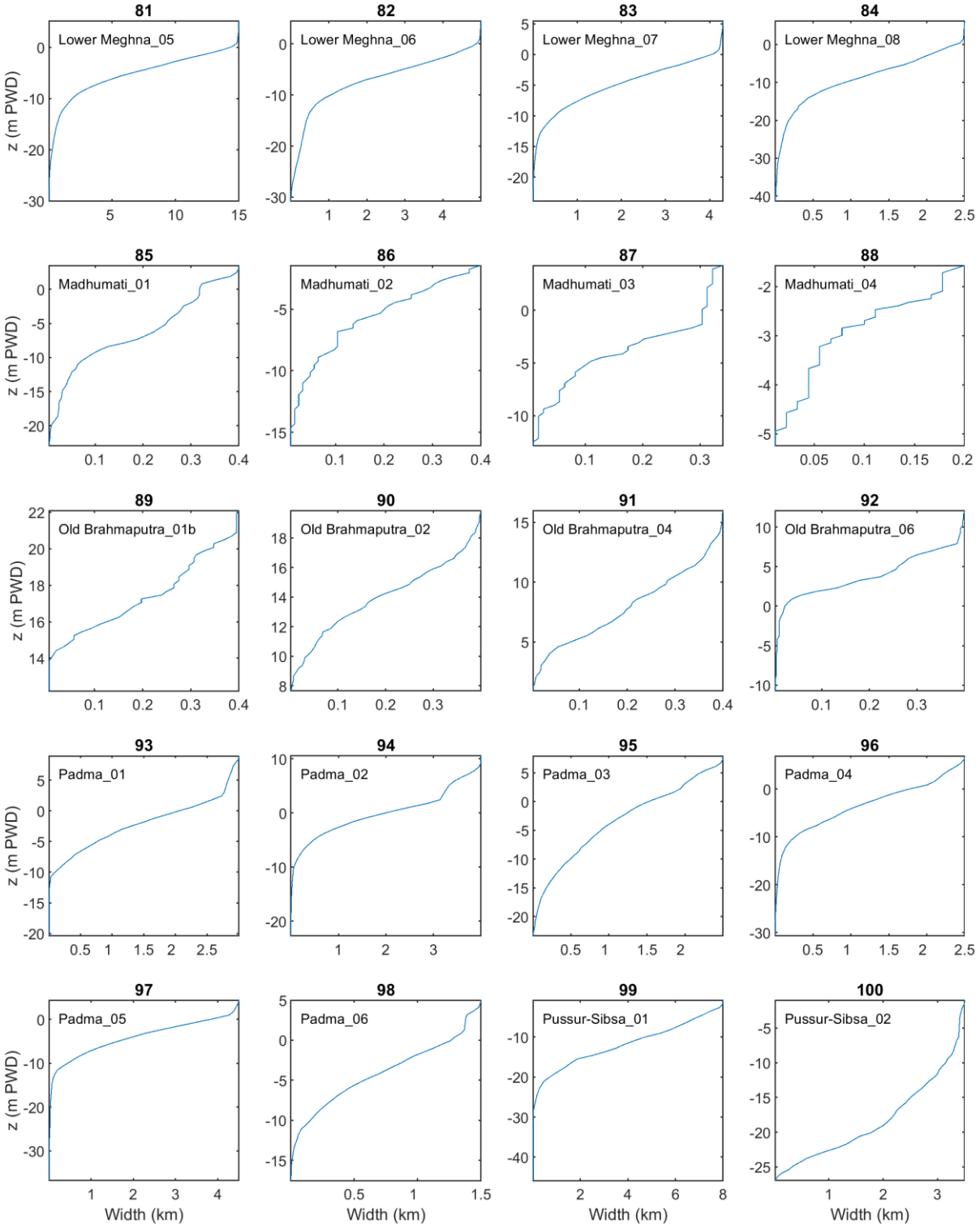

FigureApx B.5 Hypsometric curves based on the subset of topo-bathymetric observations enclosed by the polygon.

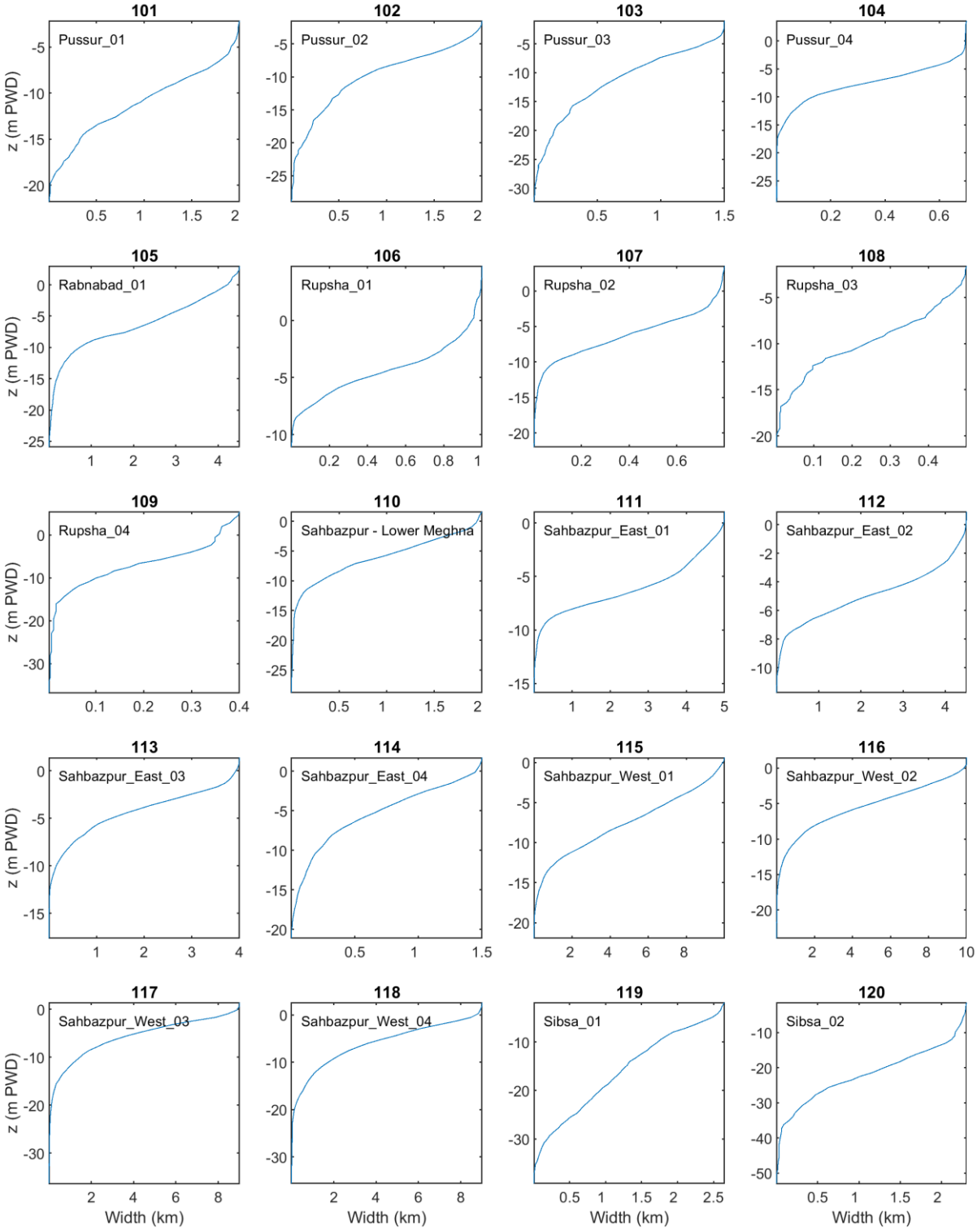

FigureApx B.6 Hypsometric curves based on the subset of topo-bathymetric observations enclosed by the polygon.

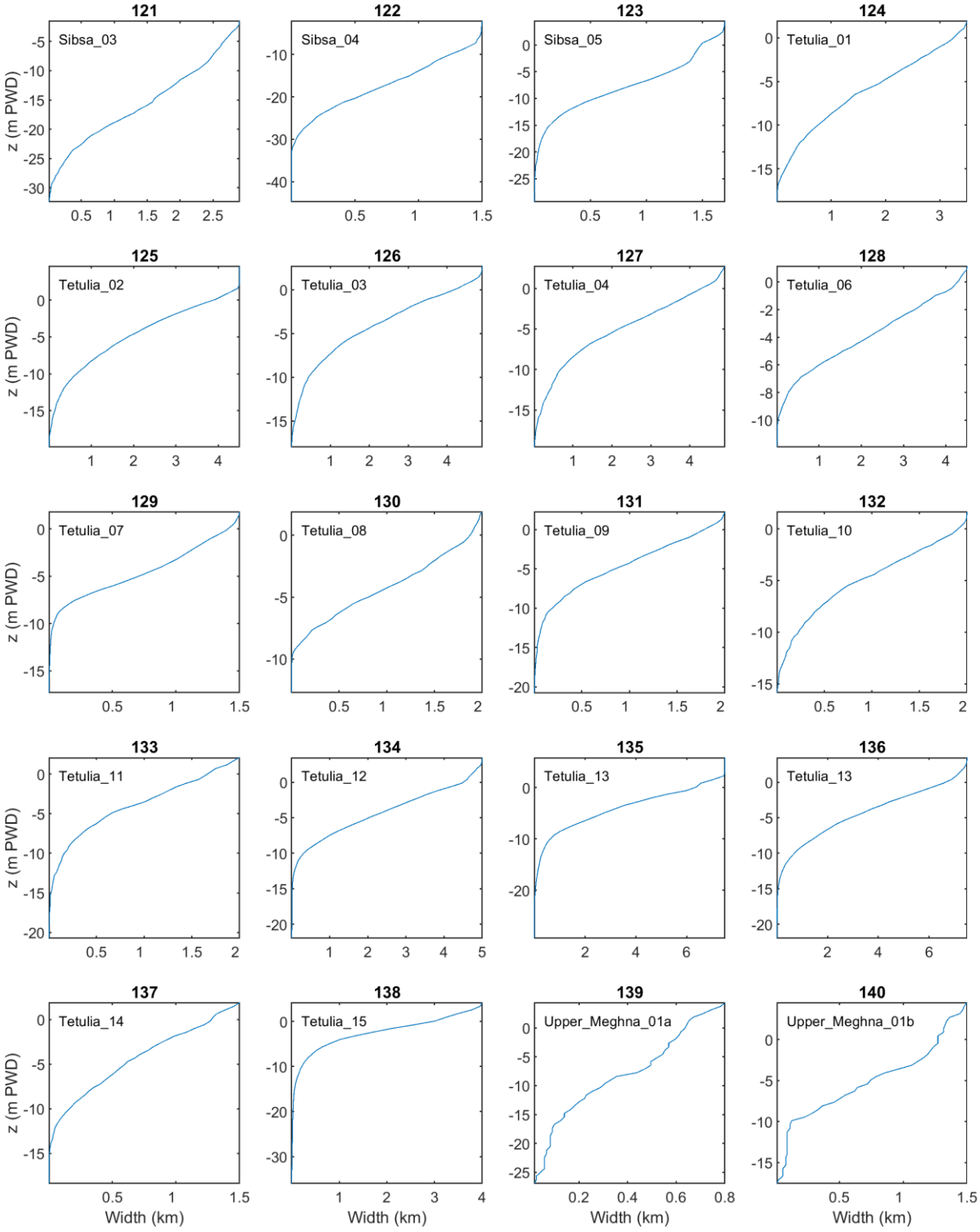

FigureApx B.7 Hypsometric curves based on the subset of topo-bathymetric observations enclosed by the polygon.

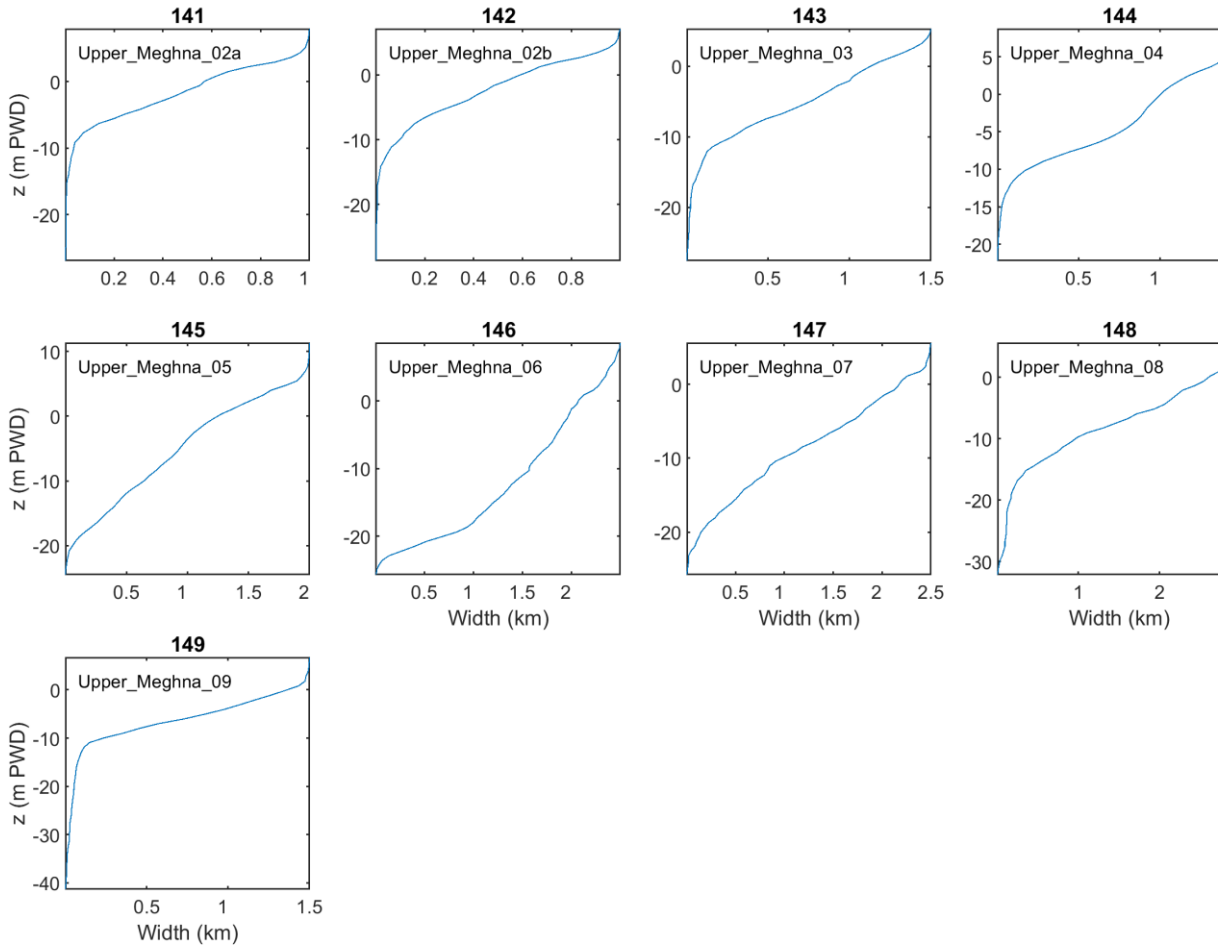

FigureApx B.8 Hypsometric curves based on the subset of topo-bathymetric observations enclosed by the polygon.

C Automatic grid generation based on distance to bank lines

Procedure to create an automatically refined grid for Bangladesh rivers

- Landboundary Rivers_Bangladesh, remove points in deep water -> landboundary_nosea.ldb; use this ldb to determine distances to shorelines
- In makescatter.m
  - Read the landboundary file landboundary_nosea.ldb
  - Extend with extracoastline.ldb for the coasts of India and east coast of BD
  - Create a sample grid based on xg=[150:1:800]*1e3;yg=[250:1:900]*1e3;
  - For each sample point compute distance to nearest ldb point
  - Use this distance to determine grid size according to dx=min(max(dist/4,dxmin),dxmax); here dxmin=500 and dxmax=16000
  - Convert map of dx to fake map of depth using h=dx.^2/9.81/dtmin^2;
  - Write fakedepth.xyz
- Run runcli.bat, containing:
  copy fakedepth.xyz + fakedepth_largescale.xyz test.xyz
  copy BOBrect16km_net.nc TMP_net.nc
  "c:\Program Files (x86)\Deltares\Delft3D FM Suite 2019 HMWQ (1.5.0.40944)\plugins\DeltaShell.Dimr\kernels\x64\dflowfm\bin\dflowfm-cli.exe" --refine:hmin=500:dtmax=240:directional=0:outsidecell=1:connect=1:maxlevel=5 TMP_net.nc test.xyz
  pause
- Define a polygon to exclude permanently dry areas: landmask.pol
- Load the grid out_net.nc in RGFGRID
- Load the polygon landmask.pol
- Select the polygon
- Under operations – delete – grid select ‘delete cells’
- Save ugrid